Node Selection, Synchronization and Power Allocation in Cooperative Wireless Networks

Mohammed W. Baidas

Dissertation submitted to the Faculty of the
Virginia Polytechnic Institute and State University
in partial fulfillment of the requirements for the degree of

Doctor of Philosophy
in
Electrical and Computer Engineering

Allen B. MacKenzie, Chair
Richard M. Buehrer
Claudio da Silva
Michael R. Taaffe
Sedki Mohamed Riad

March 21, 2012
Blacksburg, Virginia

Keywords: Cooperation, Game Theory, Network Coding, Node Selection, Optimization, Power Allocation, Synchronization

Node Selection, Synchronization and Power Allocation in Cooperative Wireless Networks

Mohammed W. Baidas

ABSTRACT

Recently, there has been an increasing demand for reliable, robust and high data rate communication systems that can counteract the limitations imposed by the scarcity of two fundamental resources for communications: bandwidth and power. In turn, cooperative communications has emerged as a new communication paradigm in which network nodes share their antennas and transmission resources for distributed data exchange and processing. Recent studies have shown that cooperative communications can achieve significant performance gains in terms of signal reliability, coverage area, and power savings when compared with conventional communication schemes. However, the merits of cooperative communications can only be exploited with efficient resource allocation in terms of bandwidth utilization and power control.

Additionally, the limited network resources in wireless environments can lead rational network nodes to be selfish and aim at maximizing their own benefits. Therefore, assuming fully cooperative behaviors such as unconditionally sharing of one's resources to relay for other nodes is unjustified. On the other hand, a particular network node may try to utilize resources from other nodes and also share its own resources so as to improve its own performance, which in turn may prompt other nodes to behave similarly and thus promote cooperation.

This dissertation aims to answer the following three questions: "How can bandwidth-efficient multinode cooperative communications be achieved?", "How can optimal power allocation be achieved in a distributed fashion?", and finally, "How can network nodes dynamically interact with each other so as to promote cooperation?". In turn, this dissertation focuses on three main problems of cooperation in ad-hoc wireless networks: (i) optimal node selection in network-coded cooperative communications, (ii) auction-based distributed power allocation in single- and multi-relay cooperative networks, and finally (iii) coalitional game-theoretic analysis and modeling of the dynamic interactions among the network nodes and their coalition formations.

Bi-directional relay networks are first studied in a scenario where two source nodes are communicating with each other via a set of intermediate relay nodes. The symbol error rate performance and achievable cooperative diversity orders are studied. Additionally, the effect of timing synchronization errors on the symbol error rate performance is investigated. Moreover, a sum-of-rates maximizing optimal power allocation is proposed. Relay selection is also proposed to improve the total achievable rate and mitigate the effect of timing synchronization errors.

Multinode cooperative communications are then studied through the novel concept of many-to-many space-time network coding. The symbol error rate performance under perfect and imperfect timing synchronization and channel state information is theoretically analyzed and the optimal power allocation that maximizes the total network rate is derived. Optimal node selection is also proposed to fully exploit cooperative diversity and mitigate timing offsets and channel estimation errors.

Further, this dissertation investigates distributed power allocation for single-relay cooperative networks. The distributed power allocation algorithm is conceived as an ascending-clock auction where multiple source nodes submit their power demands based on an announced relay price and are efficiently allocated cooperative transmit power. It is analytically and numerically shown that the proposed ascending-clock auction-based distributed algorithm leads to efficient power allocation, enforces truth-telling, and maximizes the social welfare.

A distributed ascending-clock auction-based power allocation algorithm is also proposed for multi-relay cooperative networks. The proposed algorithm is shown to converge to the unique Walrasian Equilibrium allocation which maximizes the social welfare when source nodes truthfully report their cooperative power demands. The proposed algorithm achieves the same performance as could be achieved by centralized control while eliminating the need for complete channel state information and signaling overheads.

Finally, the last part of the dissertation studies altruistic coalition formation and stability in cooperative wireless networks. Specifically, the aim is to study the interaction between network nodes and design a distributed coalition formation algorithm so as to promote cooperation while accounting for cooperation costs. This involves an analysis of coalitions' merge-and-split processes as well as the impact of different cooperative power allocation criteria and mobility on coalition formation and stability. A comparison with centralized power allocation and coalition formation is also considered, where the proposed distributed algorithm is shown to provide reasonable tradeoff between network sum-rate and computational complexity.

Dedication

To my family, my beloved wife, Amal, and my dear son, Abdulrahman.

Acknowledgements

First and foremost, all praise is due to Allah for his blessings and for giving the strength to achieve this important step in my life.

I would like to express my deepest gratitude to my advisor, Prof. Allen B. MacKenzie for his continuous guidance and support during my Ph.D. study and research. Prof. MacKenzie accepted me into his research group and gave me a second chance to pursue the Ph.D. degree and make this great achievement. It has been a pleasure to work with and learn from him.

I would also like to thank the other dissertation committee members. Special thanks are due to Prof. R. M. Buehrer for his guidance, enlightening comments and collaboration. His knowledge and insights were extremely valuable and greatly enriched my work. My sincere gratitude also goes to Prof. C. da Silva, Prof. M. Taaffe and Prof. S. Riad for agreeing to serve on my dissertation committee and for devoting the time to reviewing the manuscript.

I am deeply indebted to my parents and my family for all their prayers and support throughout the past years. I would also like to thank my dearest lifelong friend and brother, Mohammed Al-Yaqoub for standing by my side all these years. My deepest thanks are also given to my wife, Amal, for her endless love and support. She has always believed in me, shared with me hopes and dreams, and endlessly encouraged me in my work. Amal has always been there for me and without her sacrifice, especially during the last year of my research work, it would have been hard for me to complete and defend my dissertation.

Finally, I would like to acknowledge the financial support from Kuwait University for my graduate study. Without their support and scholarship extensions, it would have been difficult for me to pursue my Ph.D. studies and complete this dissertation.

Contents

List of Figures

List of Tables

Chapter 1

Introduction

The explosive demand for reliable, robust and high data rate wireless communication systems has attracted attention to the study of resource allocation and utilization. Wireless communication channels suffer from several impairments such as fading, shadowing and interference which can severely degrade system performance. Thus, researchers are currently pursuing new communications and networking paradigms that can efficiently utilize scarce bandwidth and power resources as well as counteract the adverse effects of wireless channel impairments. Multi-antenna wireless transmitters and receivers can yield dramatic gains in rate and reliability, however size and form restrictions largely limit their practical applications. In turn, cooperative communications has emerged as an effective means to utilize the broadcast nature of wireless networks and exploit the inherent spatial and multiuser diversities. In cooperative communication systems, several nodes form a virtual antenna array to exchange information between one another and towards other destination nodes.

This chapter motivates the research problems studied in this dissertation and encourages future work in the area of distributed resource allocation in network-coded cooperative wireless networks. In addition, the significant references from a broad array of relevant literature are reviewed. In particular, our objective is to highlight the latest contributions in cooperative diversity in wireless networks and wireless network coding and provide the reader with the necessary background on game-theoretic tools and techniques used in different parts of the dissertation.

In the remainder of this chapter, the motivation of this dissertation is discussed in Section 1.1. Section 1.2 summarizes the relevant literature on cooperative diversity and wireless network coding. An overview of game theory is given in Section 1.3. Two Motivating examples on the use of network coding in cooperative relay networks and exploitation of diversity and coding gains are presented in Sections 1.4 and 1.5, respectively. Finally, the outline of the dissertation is given in Section 1.6.

1.1 Motivation

Cooperation in wireless communication networks results when network nodes use their bandwidth and power resources to mutually enhance their transmissions. More precisely, cooperation can be promoted in many ways that entail different tradeoffs between bandwidth, power, and complexity costs for greater benefits achieved by exploiting spatial diversity gains in wireless networks. Conventional communication networks employ "direct" transmissions only and hence forego these benefits.

Although cooperative communications can exploit diversity gains, they inadvertently lead to low bandwidth utilization. In addition, conventional relay networks are not directly applicable for multinode communications. In turn, this work contributes to the advancement of multinode cooperative communications by studying network-coded relay networks. Specifically, the first question this dissertation aims to answer is "How can bandwidth-efficient multinode cooperative communications be achieved?", and thus investigates the use of wireless network coding to combine data transmissions from different network nodes in time-division and multiple-access based communication schemes. Optimal node selection is also proposed to improve bandwidth efficiency and mitigate the impact of imperfect timing synchronization of network nodes' simultaneous transmissions.

Most existing works on power control in cooperative communication networks mainly focus on optimal power allocation by means of a centralized controller. This in turn requires complete and accurate channel state information to be available at the central controller for optimal power allocation, which is generally neither scalable nor robust to channel estimation errors. Additionally, most works ignore situations in which selfish users falsely reveal their private information and report their demands for communication resources in order to achieve higher payoffs. In turn, enforcing truth-telling is necessary to guarantee fairness and efficiency in transmission resources allocation. Furthermore, pricing and payment mechanisms are necessarily needed to incentivize relay nodes to share their transmission resources in forwarding other nodes' data. Therefore, the second question that this dissertation aims to answer is "How can optimal power allocation be achieved in a distributed fashion?". This dissertation proposes the use of game-theoretic distributed power allocation in single- and multi-relay cooperative networks using auction theory.

The significance of studying cooperative communications from a game-theoretic perspective comprises multiple factors. First, by modeling the distributed power allocation problem as an auction game, network users' behaviors and power demands can be analyzed in a formalized game structure. This in turn allows the use of game theory tools and facilitates the theoretical analysis. Second, in game theory, several optimality criteria for the power allocation problem exist that have counterparts in communications and optimization theories. Additionally, game theory encompasses well-defined equilibrium criteria to measure game optimality under various operational conditions. Such tools are highly desirable when centralized control and computational approaches are formidable.

Finally, in ad-hoc wireless networks, network nodes do not necessarily serve a common goal or belong to the same authority. Consequently, fully cooperative behaviors cannot be assumed as users will selfishly aim at maximizing their own payoffs. However, if a network node tries to utilize transmission resources from other nodes and also share its own resources so as to improve its own performance, then this may prompt other nodes to behave similarly and thus promote cooperation. Motivated by the potential selfishness of network nodes, the aim here is to answer the fundamental question of "How can network nodes dynamically interact with each other so as to promote cooperation?" In particular, our interest is in studying the existence of cooperation in ad-hoc wireless networks with selfish nodes using coalitional game theory. Moreover, scenarios in which nodes can form cooperative coalitions for efficient bandwidth utilization and optimal power allocation are studied.

In summary, cooperative communications is a promising communications paradigm that allows more efficient utilization of the transmission resources of single antenna network users. However, successful deployment is threatened by the uncooperative behaviors of selfish users and further restrained by the distributed nature of ad-hoc wireless networks. Thus, this dissertation aims to investigate optimal node selection schemes in network-coded cooperative relay networks, develop game-theoretic efficient distributed power allocation mechanisms to enforce truth-telling, and study distributed coalition formation to suppress selfish users and promote cooperation.

1.2 Literature Review

Recently, there has been an increased interest in transmission techniques that can exploit transmit diversity motivated by the increased capacity of multiple-input multiple-output (MIMO) systems. To exploit transmit diversity and achieve high coding gains, the transmitter conventionally is required to be equipped with multiple antenna which are required to be well-separated to avoid correlated channel fading among the different antennas. Although it may be feasible to equip base-stations with multiple antennas, it may not be feasible for small mobile and wireless devices as the correlation and spatial domain propagation are both antenna dependent. This in turn suggests that transmit diversity might instead be achieved through user-cooperation or *cooperative diversity*. On a different note, single transmissions from different users using time-division multiple-access (TDMA) cause large transmission delays and lead to inefficient bandwidth utilization. In addition, simultaneous transmissions from multiple distributed users using frequency-division multiple access (FDMA), code-division multiple-access (CDMA), or TDMA are associated with issues of imperfect frequency and/or timing synchronization which are practically challenging due to the asynchronous nature of cooperation. In turn, wireless network coding has emerged as an attractive means by which multiple transmissions from different users can be efficiently combined.

In the following subsections, related research works on cooperative diversity and wireless network coding is presented.

1.2.1 Cooperative Diversity in Wireless Networks

The study of cooperative diversity in this dissertation is centered around relay channels and their multi-terminal extensions. The classical relay channel first introduced and examined by van der Meulen and later studied by researchers in the information theory community models a three terminal communication channel [1]. Specifically, a terminal called a "relay" receives and then re-transmits a processed information-bearing signal to improve system performance. In many scenarios, several network nodes—without any information to transmit or receive—could act as relays and help transmit and/or receive signals to/from other nodes. Subsequently, Cover and El Gamal derived lower and upper bounds on the channel capacity of specific non-faded relay channel models [2]. Later, several works considered the capacity of relay channels with coding strategies that can achieve the ergodic capacity of the relay channel. Furthermore, capacity theorems for multiple-access relay channels were developed in [3] while transmitter and receiver cooperation was studied in [4].

User cooperation was first introduced in [5] and [6]. In particular, a CDMA cooperative system was studied with two users using orthogonal codes to exchange their information. It was demonstrated that with channel phases knowledge at the transmitter sides, user cooperation can lead to high data rate for both users as they are less sensitive to channel variations. In fast-fading channels, the achievable region of a two-user cooperative system was shown to include the capacity region of the two-user multiple-access system (i.e. no cooperation between the two users). For slow-fading channels, the outage probability of the cooperative system was demonstrated to be less than that of the non-cooperative system.

Cooperation Protocols

Cooperative diversity was formally introduced in [7]. Specifically, several protocols over half-duplex relays were analyzed along with their outage capacity. Moreover, two main categories of cooperation protocols were proposed: (1) fixed relaying and (2) adaptive relaying.

In fixed relaying, channel resources are split between the source and the relay in a deterministic manner and generally over two phases. In the first "broadcasting" phase, the source broadcasts its information signal and both the relay and the destination try to receive it. In the second "cooperation" phase, the relay re-transmits a processed version of its received signal to the destination. The processing at the relay is governed by the type of cooperation protocol employed. In the amplify-and-forward (AF) protocol, the relay scales the received signal and forwards its amplified version to the destination. It is noteworthy that the AF protocol suffers from noise amplification and propagation; however it has been shown to still achieve a full diversity order of two [7]. Another type of processing is where the relay decodes its received signal, re-encodes it, and then forwards it to the destination. This type of fixed relaying is known as decode-and-forward (DF). For this protocol to achieve a diversity order of two, correct decoding at the relay must be ensured, otherwise only diversity order one can be achieved. Although fixed relaying has the advantage of easy implementation, it is

bandwidth inefficient. This is attributed to the fact that the channel resources are split in half between the source and the relay while the source-destination channel is not necessarily in bad condition. This in turn motivates the use adaptive relaying protocols which comprise two main protocols, namely the selective relaying and the incremental relaying.

For selective relaying, if the signal-to-noise ratio (SNR) of the signal received at the relay exceeds a certain threshold, then it decodes-and-forwards it to the destination; otherwise, the relay remains idle. Such a relaying protocol improves upon the DF protocol and has been shown to achieve full diversity of two if the SNR threshold is carefully designed to overcome the DF protocol's inherent deficiency in correctly decoding its received signal [7]. On the other hand, the incremental relaying is based on a feedback channel from the destination to the relay through which the former informs the latter whether it has decoded the source's signal correctly. It was illustrated in [7] that incremental relaying results in the best spectral efficiency among the other cooperation protocols and also achieves full diversity order of two.

Distributed Space-Time Coding

Distributed space-time codes have also been proposed as another form of cooperative diversity to achieve high bandwidth efficiency while achieving full diversity order [8]. Specifically, a cooperative scheme has been proposed in which relays decode their received signals from the source and re-transmit them—if decoded correctly—using a distributed space-time code column that is drawn from a space-time code matrix. Furthermore, it has been illustrated that distributed space-time codes employed by decode-and-forward relays can achieve full diversity order equal to the number of cooperative relays, over only two transmission phases. However, the main challenge in implementing distributed space-time coding is the stringent requirement for perfect timing synchronization among the cooperating relays. Distributed space-time coding for amplify-and-forward and decode-and-forward cooperation protocols have been studied in [9], and several other works have considered the practical implementation and performance of distributed space-time coding [10, 11, 12].

Related Work

Several works have analyzed the performance of single- and multi-relay cooperative networks. For instance, in [13, 14], the symbol-error-rate performance of single-relay amplify-and-forward and decode-and-forward cooperative networks was studied under Rayleigh fading channels. In particular, exact as well as asymptotic upper-bound expressions for the symbol-error-rate performance were derived. Moreover, optimal source and relay power allocation was studied, and it was shown that if the source-relay channel is in good condition, then equal power allocation is near-optimal. In [15], the symbol error rate performance of multiuser single amplify-and-forward relay networks in Nakagami$-m$ channels was studied. Exact symbol error rate performance for multi-relay amplify-and-forward cooperative networks in Rayleigh fading channels was studied in [16] and [17], where it was shown that full diversity order is achieved. Multi-relay decode-and-forward cooperative networks were

studied in [18], where it was shown that full diversity order is achieved if each relay combines the received signals from a previous relay's transmission as well as the source's transmission. Furthermore, multi-relay optimal power allocation was also provided in [18]. Outage probability analysis and optimal power allocation for multi-relay amplify-and-forward networks were studied in [19].

In another line of work, the authors in [20] propose a new cooperative communication protocol for multi-relay decode-and-forward networks, which achieves higher bandwidth efficiency than the conventional DF cooperative protocol while guaranteeing the same diversity order by alternating between direct and cooperative transmissions through a single optimally selected relay. In addition, optimal relay selection for decode-and-forward cooperative networks has also been studied in [21]. Relay selection for amplify-and-forward cooperative networks was investigated in [22], where closed-form expressions for the symbol error rate, outage probability, and average end-to-end SNR gain are derived. In [23], the outage probability of optimum cooperation protocol selection is analyzed and compared against conventional cooperative networks. In particular, the relay may choose either amplify-and-forward, decode-and-forward, or direct transmission (DT) to forward the source's signal. Particularly, two relay selection schemes were verified to be superior: selection between AF and DF protocols or selecting between DF and DT. In [24, 25], single amplify-and-forward relay selection and power allocation are analyzed to minimize system outage probability while achieving full diversity order. Many single-relay and multi-relay selection schemes and their achievable diversity orders are also studied in [26, 27]. Different power allocation criteria for multi-relay cooperative networks are investigated in [28].

1.2.2 Wireless Network Coding

Network coding has recently attracted much attention due to its ability to efficiently distribute data and improve network throughput [29] [30]. Conventionally, network coding has emerged as a technique by which intermediate nodes combine several data symbols/packets from different sources for transmission towards one or more destinations. In conventional multi-relay cooperative networks with N nodes out of which a source node wishes to transmit its data to a destination node through the other $N-2$ nodes, the channel resources are split into $N-1$ orthogonal channels using TDMA. Clearly, with the increase in the number of nodes in the network, conventional cooperative communication protocols become bandwidth inefficient. In addition, conventional cooperative networks are not suited for simultaneous data distribution and exchange between multiple nodes. This in turn motivates the use of physical-layer or "wireless" network coding for data exchange over multiple cooperative nodes in wireless networks.

There have been many works aiming at utilizing wireless network coding in cooperative relay networks [31]. For example, in [32], bi-directional traffic flows by wireless network coding are proposed to increase the achievable throughput in amplify-and-forward relay networks (as illustrated in Fig. 1.1). Specifically in Fig. 1.1, the conventional bi-directional

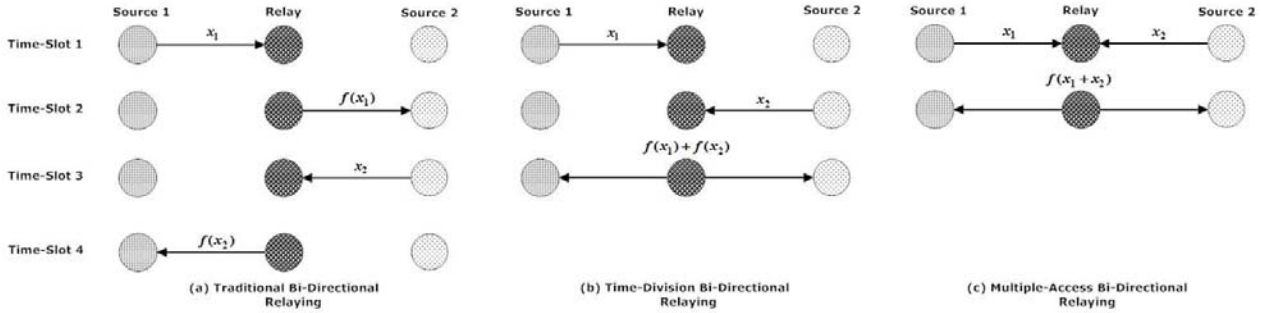

Figure 1.1: Bi-Directional Relaying Using Wireless Network Coding

relaying takes four time-slots while the time-division bi-directional relaying using wireless network coding requires only three time-slots. However, using a multiple-access channel and wireless network coding, only two time-slots are required. In [33], it was shown that the two time-slots bi-directional relaying offers the highest maximum sum-rate but the worst error rate performance, while the three time-slots bi-directional relaying offers a good trade-off between the maximum achievable sum-rate and error performance. In [34], the wireless transmission from two sources to two destinations over a single relay is studied to evaluate the throughout and error performance of amplify-and-forward and decode-and-forward cooperation protocols with linear network coding. Multi-relay bi-directional amplify-and-forward relaying with adaptive modulation has been proposed in [35] to improve spectral efficiency. A relay selection scheme has been proposed in [36] which selects the relay that is best suited for wireless network coding. The proposed scheme has been proven to lead to a more robust performance and higher system throughput than conventional bi-directional and direct transmission schemes. Finally, linear network coding has been proposed in [37] for location-aware cooperative communications so as to offer incremental diversity, even power distribution, and significant reduction in aggregate transmit power and transmission delays.

1.3 An Overview of Game Theory

Game theory is a promising approach to the analysis and modeling of players' conflicting objectives and decision-makers' interactions [38][39]. Primarily, game theory has been proposed as an extensive set of modeling tools and techniques to model strategic decision problems in economics or analyze the rational behavior of different organisms in biology and social sciences. This section presents an overview of the most fundamental and relevant concepts of game theory and briefly outlines how such concepts can be leveraged in designing distributed algorithms for node selection, multinode cooperation, and power allocation in cooperative wireless networks.

Recently, game theory has emerged as an indispensable tool for studying, modeling, and analyzing the dynamic interactions of network users as well as designing self-enforcing distributed algorithms for efficient resource allocation in wireless networks [40, 41, 42, 43, 44]. A game model consists of a set of players, a set of actions (or strategies) available to each

player, and a set of payoffs for each combination of the players' actions. In particular, the players are network nodes, which may be source nodes that generate data or relay nodes that forward other nodes' data to certain destinations in the network. The strategy space may include data forwarding decisions, channel and/or power allocation, or route participation. Specifically, source nodes can decide how much of the relay nodes' transmission resources (e.g. channel and power allocation) are required and agree to pay a price to the relay nodes in return for their transmission resource utilization in forwarding their data. Also, relay nodes decide what channel resources and how much power to allocate to each source node for forwarding their data and how much they charge for sharing their transmission resources. As for payoffs, they can take several forms depending on the system parameters, such as transmission rate, bandwidth utilization, power consumption or lifetime. Such payoffs are necessary in the design of a distributed algorithm so as to faithfully represent each selfish node's desired share of the available transmission resources.

1.3.1 Non-Cooperative and Cooperative Games

In decentralized ad-hoc wireless networks, nodes act selfishly and autonomously, and aim to maximize their share of transmission resources. Thus, the game-theoretical study in this dissertation comprises two types of games, namely non-cooperative and cooperative games. In non-cooperative games, individually "rational" network nodes make decisions independently so as to maximize their own utility without caring about the effects of their choices on the other players in the game. Without centralized control, selfish network nodes do not cooperate and any cooperation must be self-enforcing. Clearly, non-cooperative games are particularly suited for modeling nodes' selfish behavior in ad-hoc wireless networks, which motivates the design of distributed resource allocation algorithms derived from game theory.

For efficient resource allocation in ad-hoc wireless networks with selfish nodes, a designed algorithm may incorporate a multi-objective optimization problem, the solution of which is shared by the different network nodes in a distributed fashion. Luckily, non-cooperative game theory includes well-defined optimization criteria to measure and quantify optimality under a variety of scenarios. More specifically, Nash Equilibrium is a key concept to determine the outcome of a game in which two or more nodes interactively make decisions and select their best strategy [38]. In turn, the selected strategies are such that no selfish node has an incentive to unilaterally change its action. Although the existence of Nash Equilibrium is quite general, uniqueness is a desired property and must be analyzed case-by-case. For instance, by optimally tuning the design of a resource allocation algorithm, it is possible to manipulate the behavior of the rational network nodes towards an efficient allocation at the equilibrium. In addition, uniqueness of an equilibrium can be proven under special cases such as the payoff function of each player and the feasible region being strictly convex. In the case of multiple equilibria, it is highly desirable to determine those equilibria that are superior to others. An outcome of a game is Pareto-optimal if there is no outcome that makes every node at least as well off and at least one player strictly better off [38].

In cooperative games, network nodes are able to form binding commitments and the joint actions of groups of nodes can be analyzed. In such games, communication among network nodes is allowed. In addition, the outcomes that result when the players come together in different combinations can be defined. There are two important types of cooperative games, namely bargaining games and coalitional games. In bargaining games, network nodes have the opportunity to reach a mutually beneficial agreement. Nash bargaining solution (NBS) plays an important role in cooperative games as it determines a unique Pareto optimal solution to the game and models the bargaining interactions based on six intuitive axioms [45]. In coalitional games, network nodes can cooperate with each other by forming cooperative groups with the aim of improving their payoffs in a game. Such groups are named coalitions and often defined in terms of a characteristic function, which specifies the outcomes that each coalition can achieve for itself when its nodes coordinate their actions.

Since auction theory and coalitional games are extensively studied in this dissertation, a more detailed elaboration of their main principles is given in the following subsections.

1.3.2 Auction Theory

An auction is a mechanism—conducted by an auctioneer—by which resources are bought and sold by eliciting bids from potential buyers (i.e. bidders). In particular, a group of bidders submit their bids for the resources at the announced price(s) and then resources are appropriately allocated to bidders based on the bids and auction rules. In general, an auction model is comprised of three major parts: (1) a description of potential bidders, (2) the set of possible resource allocations (i.e. quantity and type of each resource, whether resources are divisible and whether there are any restrictions on how resources are allocated), and (3) the values of the various resource allocations to each bidder [46].

In many cases, auctions are precisely used to achieve price discovery. Specifically, a seller (or buyers) does (do) not exactly know what an item or resource is worth and how much it should be sold or bought for. In turn, auctions can be used as a market test to explore and determine what the prevailing prices are. This process can also achieve "winner determination" by determining who wins the auction and gets the resource. Moreover, auctions are used to determine how much each winning bidder should pay, based on its allocated resource [47]. In auctions with multiple bidders, each resource being auctioned off has a value to each bidder. In turn, each bidder wishes to win that resource and make a payment that is below that value so that the difference between the valuation and payment (price paid) leaves the bidders with some profit/surplus. Therefore, a valuation is the maximum bid that any bidder is willing to place. Additionally, bidders do not know with certainty how the other bidders value the resource being auctioned off. Depending on the information available to bidders, the valuations of different bidders to the same resource may be independent (i.e. private value model) or dependent (i.e. interdependent values model).

Evaluating Auctions

There are various auction designs to choose from. In particular, an auction design can be chosen based on the one or more of the following criteria:

- Revenue: In this criterion, auctioneers select the auction design that results in the maximum revenue for each sold item.
- Efficiency: An auction is said to be efficient if the bidder who values the item the most *ex-post*, actually wins it.
- Social welfare maximization: This criterion in an auction design aims at maximizing the sum of the seller(s) and bidders revenues.
- Simplicity: The time and effort (i.e. complexity) involved in an auction mechanism is also considered as an important design criterion.
- Collusion-resistance: Some auction designs prevent bidders from controlling the auction. In particular, an auction design is collusion-resistant if it prevents "special deals" between certain buyers and sellers, market manipulation, and wins by favorite bidders.
- Truth-telling: An auction design that makes a rational buyer's best interest is to bid truthfully is said to enforce truth-telling. This is because a buyer's ex-post payoff from a truthful bid is at least as high as from any other bid.

Auction Classification

There are several ways by which auctions can be classified. In particular, open and closed bid auctions are based on whether the bids of each bidder are disclosed to the other bidders. Specifically, in open bid auctions, bids are revealed, and bidders take turns in submitting their bids until the winners are determined. Two commonly used open auctions are [47]

- English auction: an ascending price auction where the price increases round by round from a low price in small increments until there is only one interested bidder who wins the resource, and pays his/her final bid.
- Dutch auction: a descending price auction where the price progressively decreases round by round from a high price until a single bidder accepts the price, wins the resource, and pays that price.

It should be noted that open ascending bid auctions help bidders in early in the auction process to recognize each other which gives rise to the possibility of collusion. On the other hand, in closed (or sealed-bid) auctions, bids/strategies are not revealed to the bidders and kept secret. Only the auctioneer knows the bids submitted by each participant and allocates the resource accordingly. The two most commonly used closed auctions are [47]

- First-price (sealed-bid) auction: an auction in which each bidder submits its bid in a sealed envelope simultaneously and the bidder with the highest bid wins the resource and makes a payment equivalent to his/her own bid.

- Second-price (sealed-bid) auction: an auction where each bidder submits its bid in a sealed envelope simultaneously and the bidder with the highest bid wins the resource and makes a payment equal to the second highest bid. This auction type is also known as the Vickrey auction.

It is noteworthy that closed bid auctions do not promote collusion. Although the described four auctions seem to be different at the outset, they can be shown to be equivalent under certain conditions. More specifically, the Dutch open descending price auction is strategically equivalent to the first-price sealed-bid auction. When bidders have private values, the English open ascending price auction is equivalent to the second-price sealed-bid auction. Furthermore, William Vickrey, a Nobel laureate in Economics, proved that the English and Dutch auctions yield the same expected revenue under the assumptions of risk-neutrality and privately known values drawn from a common distribution [48].

The previously discussed auction types are used for auctioning a single unit. Auction mechanisms and rules become more involved when multiple indistinguishable/identical units of the same resource (also units of divisible resources) are auctioned off simultaneously. Auctioning multiple indistinguishable units of a resource can be achieved in a closed auction format either using the discriminatory auction, the uniform price auction, or the Vickrey auction, which are detailed as follows.

- Discriminatory (or pay-as-bid) auction: auction in which each bidder pays an amount equal to the sum of his/her bids that are deemed to be winning. This auction type is the natural extension to the first-price sealed-bid auction (of a single unit resource).
- Uniform-price auction: auction where all the units are sold at a "market-clearing" price such that the total amount demanded is equal to the total amount supplied. In particular, at any price between the highest losing bid and the lowest winning bid, the demand and supply are equal [47]. The uniform-price auction is the natural extension of the second-price auction for the multi-unit case.
- Vickrey auction: auction in which the bidder who wins a number of units (say k), pays the k highest losing bids of the other bids. Therefore, for a bidder to win the k^{th} unit, its k^{th} highest bid must defeat the k^{th} lowest competing bid. Similar to the uniform-price auction, the Vickrey auction also reduces to a second-price sealed-bid auction for a single unit.

There are several open auction types for the multi-unit case:

- Multi-unit Dutch auction: this auction type is similar to its single unit counterpart in that the price is gradually lowered until a bidder indicates that he/she is willing to buy a unit at the current price and the process continues until all the units have been sold. It can be shown that the multi-unit Dutch auction is outcome-equivalent but not strategically-equivalent to the discriminatory auction.

- Multi-unit English auction: auction in which the auctioneer starts with a low price and then gradually raises it. As the price rises, bidders reduce the number of demanded units until the market clears and all the units are sold at the market-clearing price.
- Ausubel auction: auction type that is like the English auction as the auctioneer starts with a low price which is gradually raised [49]. Each bidder indicates its demand at the current price and the quantity demanded is reduced as the price rises. In particular, each unit of demand is thought of as a "claim" on that unit. When the price is low, the number of claimed units exceeds the total number of units available, so no units are awarded. As the price increases, the total number of units claimed decreases until the number of units claimed by other bidders is less than the supply. In this case, a bidder is said to have "clinched" a unit, irrespective of what happens later in the auction, as there is at least one unit that is not claimed by the other bidders [49]. The Ausubel auction is an alternative ascending-price auction type that is outcome-equivalent to the Vickrey auction.

When auctioning multiple items that are distinguishable, such items can be sold as bundles or packages instead of individual units of a resource. This is achieved using combinatorial auctions in which each bidder submits bids for groups of units of different resources and the auctioneer allocates the units such that the aggregate total of their values to the bidders are maximized. In turn, each bidder who wins a subset of the available items from the different resources pays the opportunity cost imposed on the other bidders [50].

1.3.3 Coalitional Games

Coalitional games are a fundamental class of cooperative games, which are used to model coalition formation, resource allocation and decision making within the domain of game theory and social choice. In coalitional games, players may act together—possibly sharing some cost—and form coalitions in order to accomplish a joint task. Also, they may act together to achieve their private goals. The players are still selfish in the sense that they will cooperate only if it benefits them. In coalitional games, a basic question is to determine which coalition structures are stable in the sense that no player or coalition has incentive to deviate. The importance of this question lies in the fact that the stable coalition structures are those that will be formed in the course of the cooperation. Moreover, for a set $\mathcal{S}$ of N players, the coalition value, denoted as $v(C)$, quantifies the utility or worth of a coalition C in a game. In turn, any coalitional game can be uniquely defined by the pair $(\mathcal{S}, v)$ and a coalition value can take a characteristic, partition or graph form [51]. In the characteristic form, the value of a coalition $C \subseteq \mathcal{S}$ is independent of the coalitions formed among the players outside of C (i.e. it solely depends on the members of coalition C and not in $\mathcal{S} \setminus C$). A game in partition form is one where for any coalition $C \subseteq \mathcal{S}$, the coalition value depends not only on the members of C but also on the coalitions formed by the members in $\mathcal{S} \setminus C$ [52]. On the other hand, games in graph form are concerned with the connection between the players—through a graph structure—in the coalitions, which in turn affects the value of the game [53].

For some games, outcomes can be specified in terms of a utility that a coalition can achieve. Depending on how the value of a coalition is mapped into payoffs, a coalitional game can be either with transferable utility (TU) or with non-transferable utility (NTU). In coalitional games with transferable utility, the total value of a coalition C can be arbitrarily divided among its members according to some division scheme, while in NTU games, the division of the coalition value is restricted as the payoff each user in a coalition C receives is dependent on the joint actions of the players in C. Also, each payoff division scheme in a TU game can be interpreted as an action in the NTU game. Thus, a TU game can be seen as a special case of the NTU game. Moreover, if $\upsilon(C \cup C') \geq \upsilon(C) + \upsilon(C')$ for all $C \cap C' = \phi$, then the game is called superadditive (i.e. the formation of a large coalition out of disjoint coalitions guarantees at least the value that is obtained by the disjoint coalitions separately). In such a game, cooperation is always beneficial and forming the grand coalition is mutually beneficial to all the players. In such a case, finding a coalition structure that yields the maximal social welfare is trivial. If superadditivity does not hold, the grand coalition may seldom form and the resulting coalition structure is not necessarily optimal [54].

In general, for a coalition game with N players, there are $2^N - 1$ coalitions (i.e. exponential in the number of players). In addition, the number of coalition structures that can be obtained by partitioning the set of N players into non-empty subsets corresponds to the Bell number [55]. For example, a coalition game with $N = 8$ players has 4140 possible coalition structures. In turn, finding stable outcomes among all possible outcomes of a coalitional game is a challenging combinatorial task. Furthermore, the limited execution times and computational complexity may prevent the ability to find stable/optimal solutions. Hence, the design of distributed resource allocation algorithms in wireless networks must incentivize nodes to form coalitions that result in maximum benefits, maintain such coalitions, and also pose good tradeoff between optimally and complexity.

1.4 Motivating Example 1: Network Coding

In this section, a motivating example of an amplify-and-forward relay network with and without wireless network coding is presented. The aim of this example is to illustrate the achievable rate improvement with wireless network coding when compared with conventional—without network coding—amplify-and-forward relay networks.

1.4.1 Network Model

Consider a network of two source nodes and a relay node, denoted as S_1, S_2 and R, respectively. In particular, consider the case where source node S_j for $j \in \{1, 2\}$ wishes to communicate its data symbol x_j to the destination D through the intermediate relay (as shown in Fig. 1.2). Data transmission between the source nodes and the destination is performed in a TDMA fashion and consists of two phases: (1) the broadcasting phase, and (2) the cooperation phase.

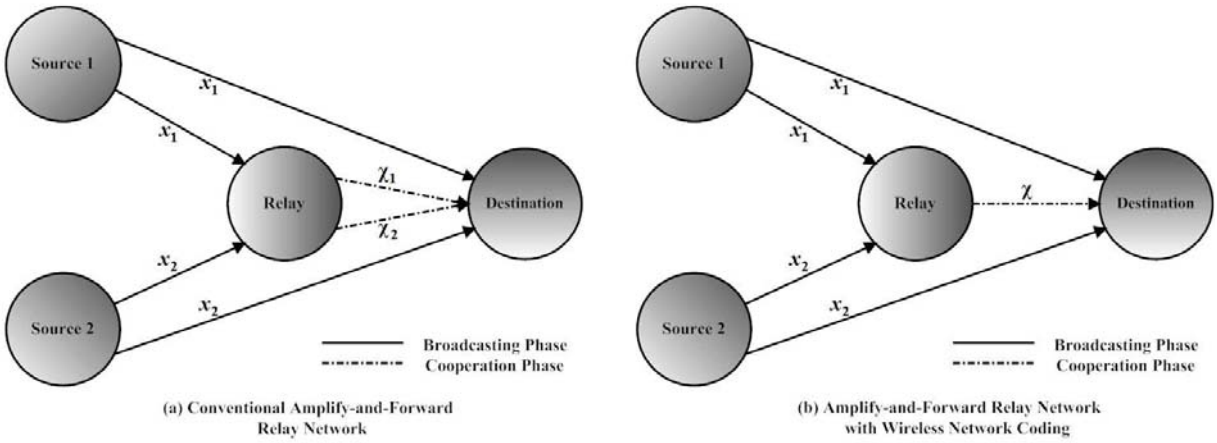

Figure 1.2: Amplify-and-Forward Relay Network Models

Broadcasting Phase

In the broadcasting phase, source node S_j broadcasts its symbol and the signals received at the relay node and the destination are given by

$$y_{j,r} = \sqrt{P_{B_j}} h_{j,r} x_j + n_{j,r}, \tag{1.1}$$

and

$$y_{j,d} = \sqrt{P_{B_j}} h_{j,d} x_j + n_{j,d}, \tag{1.2}$$

respectively, where P_{B_j} is node S_j's broadcast transmit power and $n_{j,r}$ and $n_{j,d}$ are the zero-mean additive white Gaussian noise (AWGN) samples with variance N_0 at relay node R and destination D, respectively. Moreover, $h_{j,r}$ and $h_{j,d}$ are the statistically independent channel fading coefficients between node S_j and nodes R and D, respectively. In total, the broadcasting phase is performed over two time-slots.

Cooperation Phase

The signal analysis under the two amplify-and-forward relay network models illustrated in Fig. 1.2 are detailed as follows.

- Conventional Amplify-and-Forward (C-AF): Under this cooperative scheme, the cooperation phase is performed over two time-slots, where in time-slot T_{2+j} the relay forwards source node S_j's signal, for $j \in \{1, 2\}$. The received signal at the destination corresponding to each source node S_j is expressed as

  $$y_{j,r,d} = \mathcal{X}_j h_{r,d} + n_{j,r,d}, \tag{1.3}$$

  where $\mathcal{X}_j = \beta_{j,r} y_{j,r}$ and

$$\beta_{j,r} = \sqrt{\frac{P_{C_j}}{P_{B_j}|h_{j,r}|^2 + N_0}}, \tag{1.4}$$

with P_{C_j} being the cooperative transmit power to relay symbol x_j. The total power constraint P for each source node S_j is given by $P = P_{B_j} + P_{C_j}$, where $P_{B_j} = \delta_{B_j} P$ such that $0 < \delta_{B_j} \leq 1$. Moreover $P_{C_j} = \delta_{C_j} P$ with $\delta_{C_j} = 1 - \delta_{B_j}$.

The destination performs a maximum-ratio-combining (MRC) operation on the received signals as follows

$$y_j = \alpha_{j,d} y_{r,d} + \alpha_{j,r,d} y_{j,r,d} \tag{1.5}$$

where

$$\alpha_{j,d} = \frac{\sqrt{P_{B_j}} h_{j,d}^*}{N_0} \quad \text{and} \quad \alpha_{j,r,d} = \frac{\beta_{j,r}\sqrt{P_{B_j}} h_{j,r}^* h_{r,d}^*}{(\beta_{j,r}^2 + 1) N_0}, \tag{1.6}$$

with $(\cdot)^*$ denoting complex conjugation. Hence, the SNR at the output of the MRC is written as

$$\gamma_j = \gamma_{j,d} + \gamma_{j,r,d} \tag{1.7}$$

where $\gamma_{j,d} = P_{B_j}|h_{j,d}|^2/N_0$ and

$$\gamma_{j,r,d} = \frac{1}{N_0} \frac{P_{B_j} P_{C_j} |h_{j,r}|^2 |h_{r,d}|^2}{P_{B_j}|h_{j,r}|^2 + P_{C_j}|h_{r,d}|^2 + N_0}. \tag{1.8}$$

The channel coefficients $h_{j,d}$, $h_{j,r}$ and $h_{r,d}, \forall j \in \{1, 2\}$ are modeled as zero-mean complex Gaussian random variables with variances $\sigma_{j,d}^2, \sigma_{j,r}^2$ and $\sigma_{r,d}^2$, respectively.

The cooperative diversity is rigorously defined as the rate of decay of the symbol error rate (SER) P_{SER} with the SNR on a log-log scale as [56] [57]

$$\Gamma = -\lim_{SNR \to \infty} \frac{\log P_{SER}}{\log SNR}, \tag{1.9}$$

where $SNR = P/N_0$. At high enough SNR, the SER of M-ary phase shift keying (M-PSK) signals can be approximated as [56]

$$P_{SER}^{C-AF} \lesssim \left(\frac{N_0}{P}\right)^2 \frac{\Theta(2)}{\delta_{B_j}\sigma_{j,d}^2 b_{psk}^2} \frac{\delta_{B_j}\sigma_{j,r}^2 + \delta_{C_j}\sigma_{r,d}^2}{\delta_{B_j}\delta_{C_j}\sigma_{j,r}^2\sigma_{r,d}^2}, \tag{1.10}$$

where $b_{psk} = \sin^2(\pi/M)$ and

$$\Theta(2) = \frac{1}{\pi} \int_0^{(M-1)\pi/M} \left(\left(\sin^2\theta\right)\right)^2 \, d\theta. \tag{1.11}$$

Thus, it is clear from (1.10) that a full diversity order of $\Gamma = 2$ is achieved. Finally, since four time-slots are required under this cooperative scheme, the achievable rate of node S_j at the destination is given by[1]

$$R_{j,d}^{C-AF} = \frac{1}{4}\log_2\left(1 + \frac{P_{B_j}|h_{j,d}|^2}{N_0} + \frac{P_{B_j}P_{C_j}|h_{j,r}|^2|h_{r,d}|^2}{N_0(P_{B_j}|h_{j,r}|^2 + P_{C_j}|h_{r,d}|^2 + N_0)}\right). \tag{1.12}$$

- Amplify-and-Forward with Wireless Network Coding (AF-WNC): Under this scheme, the relay node forms a linear network code $\mathcal{X}$ from the received signals in the broadcasting phase in the form of

$$\mathcal{X}(t) = \sum_{i=1}^{2} \beta_{i,r} y_{i,r} c_i(t), \tag{1.13}$$

where $y_{i,r}$ and $\beta_{i,r}$ are defined in (1.1) and (1.4), respectively. Moreover, $c_i(t)$ is the signature waveform assigned to source node S_i which is assumed to be known by the destination. The cross-correlation of $c_i(t)$ and $c_j(t)$ is $\rho_{i,j} = \langle c_i(t), c_j(t)\rangle \triangleq (1/T)\int_0^T c_i(t)c_j^*(t)dt$ for $i \neq j$ with $\rho_{j,j} = 1$ and T is the symbol duration. The received signal at the destination is given by

$$\mathcal{Y}_{r,d}(t) = h_{r,d}\mathcal{X}(t) + n_{r,d}(t), \tag{1.14}$$

where $n_{r,d}$ is the AWGN noise sample at the destination. The received signal at the destination is passed through a matched filter bank and the output is given by

$$\mathcal{Y}_{r,d} = \langle \mathcal{Y}_{r,d}(t), c_j(t)\rangle = \sum_{i=1}^{2} \beta_{i,r}\sqrt{P_{B_i}} h_{i,r}h_{r,d}x_i\rho_{i,j} + n_{j,r,d}. \tag{1.15}$$

Without loss of generality, it is assumed that $\rho_{i,j} = \rho$ for $i \neq j$. Hence, the destination performs multi-source signal detection and the decorrelated signal can be shown to be

$$\tilde{\mathcal{Y}}_{j,r,d} = \beta_{j,r}\sqrt{P_{B_j}} h_{j,r}h_{r,d}x_j + \tilde{n}_{j,r,d} \tag{1.16}$$

where $\tilde{n}_{j,r,d} \sim \mathcal{CN}(0, N_0\varrho_2(\beta_{j,r}^2|h_{r,d}|^2+1))$ and $\varrho_2 = \frac{1}{1-\rho^2}$ is the decorrelation coefficient. Following the signal analysis in (1.5 - 1.8), the SER at high SNR is approximated as

$$P_{SER}^{AF-WNC} \lesssim \left(\frac{N_0}{P}\right)^2 \frac{\varrho_2\Theta(2)}{\delta_{B_j}\sigma_{j,d}^2 b_{psk}^2} \frac{\delta_{B_j}\sigma_{j,r}^2 + \delta_{C_j}\sigma_{r,d}^2}{\delta_{B_j}\delta_{C_j}\sigma_{j,r}^2\sigma_{r,d}^2}. \tag{1.17}$$

Clearly, a diversity order of two is also achieved for the AF-WNC scheme. Now, since only three time-slots are required under the AF-WNC scheme, the achievable rate is

[1]The maximum achievable rate (capacity) in bits/s is given by $C = W\log_2\left(1 + \frac{P|h|^2}{N_0 W}\right)$, where h is the channel fading coefficient and W is the network bandwidth. In this dissertation, network bandwidth is normalized, leading to normalized achievable rate of $R = \log_2\left(1 + P|h|^2/N_0\right)$ which has the units of bits/s/Hz.

$$R_{j,d}^{AF-WNC} = \frac{1}{3}\log_2\left(1 + \frac{P_{B_j}|h_{j,d}|^2}{N_0} + \frac{P_{B_j}P_{C_j}|h_{j,r}|^2|h_{r,d}|^2}{N_0\varrho_2(P_{B_j}|h_{j,r}|^2 + P_{C_j}|h_{r,d}|^2 + N_0)}\right). \quad (1.18)$$

Comparing (1.12) and (1.18), it is clear that the AF-WNC network scheme achieves a higher rate than the C-AF scheme at the expense of a degradation of at most $10\log_{10}\varrho_2$ dB which is due to decorrelation coefficient.

1.4.2 Performance Evaluation

In this subsection, the BPSK SER performance of the conventional amplify-and-forward relay network and its counterpart relay network with wireless network coding is simulated and evaluated. For simplicity, the total power P is equally allocated between the broadcasting and cooperation phases as $P_{B_j} = P_{C_j} = P/2, \forall j \in \{1,2\}$. In addition, the channel coefficients are assumed to have unity variance (i.e. $\sigma_{j,d}^2 = \sigma_{j,r}^2 = 1, \forall j \in \{1,2\}$ and $\sigma_{r,d}^2 = 1$). Moreover, under the AF-WNC scheme, the decorrelation coefficient is set to $\varrho_2 = 1.6$.

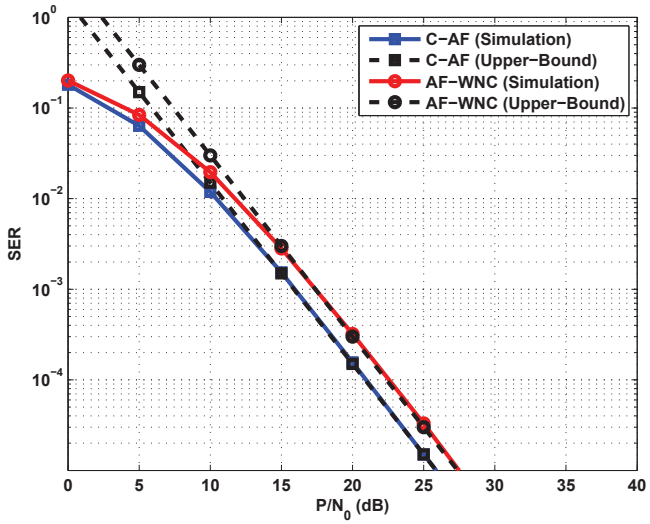

Figure 1.3: BPSK SER Performance of the Multinode Amplify-and-Forward Relay Networks

In Fig. 1.3, it can be seen that the SER performance of the C-AF network scheme is better than of the AF-WNC scheme by about 1 dB and this is attributed the noise decorrelation coefficient resulting from using non-orthogonal signature waveforms. In addition, the theoretical upper-bound derivations happen to be asymptotic at high SNR for both schemes, which confirms the diversity order of two. The achievable rate for the C-AF and AF-WNC schemes is illustrated in Fig. 1.4. Clearly, the AF-WNC scheme results in a higher rate than the C-AF scheme. In turn, the AF-WNC scheme offers a good tradeoff in terms of a significant improvement in the achievable rate at the expense of a slight degradation in the SER performance.

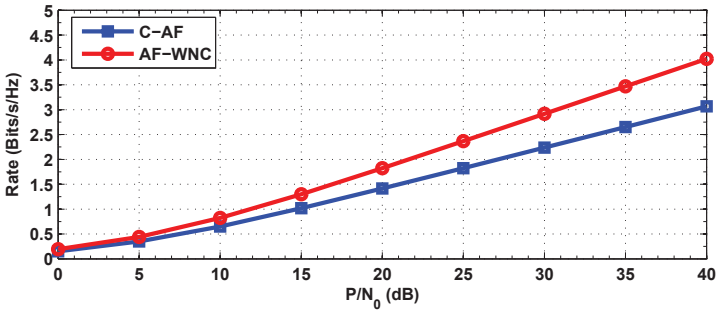

Figure 1.4: Achievable Rate of the Multinode Amplify-and-Forward Relay Networks

In all, this example has illustrated the merit of using wireless network coding in relay networks which is particularly attractive for multinode cooperative communications to overcome the problems of low bandwidth efficiency and large transmission delays.

1.5 Motivating Example 2: Coding and Diversity Gains

In this section, the impact of forward error correction (FEC) on the performance of relay networks is considered in the form of convolutional coding. This is to verify the exploitable coding gain in addition to cooperative diversity gain.

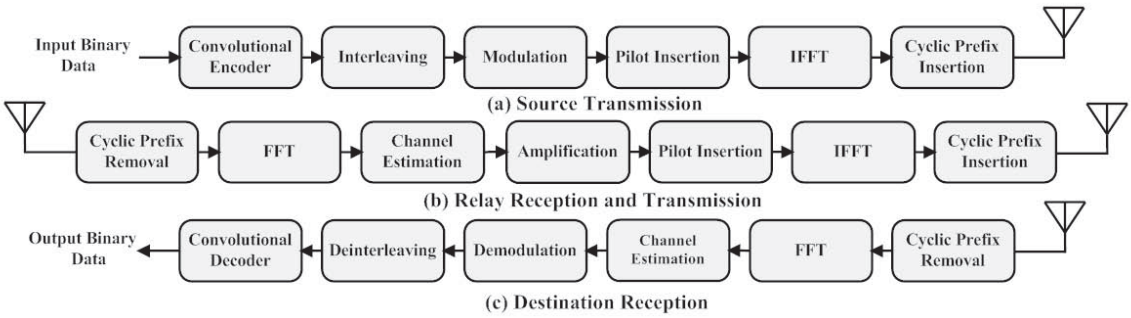

Figure 1.5: Coded OFDM System Model: (a) Source Transmission, (b) Relay Reception and Transmission, and (c) Destination Reception

1.5.1 System Model and Operation

The system model is based on an orthogonal frequency division multiplexing (OFDM) dual-hop amplify-and-forward relay network with a source node S, a half-duplex relay node R and a destination node D, all equipped with a single antenna [58] [59]. Perfect timing and frequency synchronization between all the communicating nodes is assumed.

The operation of the cooperative OFDM-based relay network is as follows [60]. In the broadcasting phase, the source node transmits its data in blocks of size N_d, which are received by both the relay and the destination. In the cooperation phase, the relay forwards its

received signal to the destination which maximum-ratio-combines and recovers the sources' symbols on each subcarrier from the signals received in both transmission phases.

At the source node, the binary data is first grouped and then convolutionally coded, typically with rate of 1/2, octal polynomials $(171, 133)$, and a constraint length of 7 [61][62]. A pseudorandom frequency interleaver is then employed such that adjacent subcarriers become approximately uncorrelated after interleaving. The encoded-interleaved bits are modulated into data symbols X_k for $k = 0, 1, \ldots, N_s$, and then pilot symbols are inserted. After that, inverse fast Fourier transform (IFFT) of size N_s is performed. A cyclic prefix of length N_{CP} (that is longer than the channel's delay spread) is introduced so as to convert frequency-selective fading at each subcarrier into frequency-flat fading. The source signal is then transmitted through a wireless channel with additive white Gaussian noise. The channel between any two nodes j and i is modeled as a multipath fading channel with L paths, as

$$h_{j,i}(\tau) = \sum_{l=1}^{L} \alpha_{j,i}(l)\delta(\tau - \tau_l), \tag{1.19}$$

where τ_l is the delay of the l^{th} path, $\delta(\cdot)$ is the Dirac delta function, and $\alpha_{j,i}(l)$ is the complex amplitude of the l^{th} path. Specifically, the $\alpha_{j,i}(l)$'s are modeled as zero-mean complex Gaussian random variables and for simplicity, the channels are normalized such that the channel variance is $\sum_{l=1}^{L} \alpha_{j,i}(l) = 1$.

In the cooperation phase, the received signal at the relay is amplified and forwarded to the destination, where the cyclic prefix is removed from the received signal and then the fast Fourier transform (FFT) is applied. The post-FFT signals on the k^{th} subcarrier received from the source and the relay nodes for $k = 0, 1, \ldots, N_s$, are expressed as

$$Y_{s,k,d} = \sqrt{P_{B_{s,k}}} H_{s,k,d} X_k + N_{s,k,d}, \tag{1.20}$$

and

$$\begin{aligned} Y_{r,k,d} &= H_{r,k,d} B_{s,k,r} \sqrt{P_{B_{s,k}}} H_{s,k,r} X_k + H_{r,k,d} B_{s,k,r} N_{s,k,r} + N_{r,k,d} \\ &= H_{r,k,d} B_{s,k,r} \sqrt{P_{B_{s,k}}} H_{s,k,r} X_k + \bar{N}_{r,k,d}, \end{aligned} \tag{1.21}$$

where $\bar{N}_{r,k,d} = H_{r,k,d} B_{s,k,r} N_{s,k,r} + N_{r,k,d}$. In addition, $H_{s,k,d}$, $H_{s,k,r}$, and $H_{r,k,d}$ are the frequency domain channel coefficients of the $S - D$, $S - R$ and $R - D$ links, respectively. Also, $N_{s,k,d}$, $N_{s,k,r}$, and $N_{r,k,d}$ are the zero-mean complex AWGN samples with variance N_0. Moreover, $B_{s,k,r} = \sqrt{\frac{P_{C_{s,k}}}{P_{B_{s,k}} |H_{s,k,r}|^2 + N_0}}$ is a normalization factor with $P_{B_{s,k}}$ and $P_{C_{s,k}}$ being the broadcasting and cooperative powers allocated at the k^{th} subcarrier, respectively. The known pilot symbols are then extracted and channel estimation is performed[2]. After that, the maximum-ratio-combined signal is demodulated and then deinterleaved. Finally, the destination uses a soft-decision Viterbi decoder for error correction and outputs binary data [63].

[2]It is assumed that the relay and destination nodes have perfect channel knowledge.

1.5.2 Simulation Results

The following simulation illustrates a SER performance comparison between coded and uncoded OFDM-based systems with direct and cooperative transmissions. In particular, BPSK modulation is employed along with the IEEE802.11g standard parameters. Accordingly, a channel bandwidth of 20 MHz is used with a $N_s = 64$-point FFT size, a cyclic prefix equivalent to 25% of the OFDM symbol duration (i.e. $N_{CP} = 16$ samples) and a data symbol duration of 50 ns[3]. The total power is equally split between the broadcasting and cooperation phases (i.e. $P_{s,k} = P_{r,k}$ with $P = P_{s,k} + P_{r,k}$ being the transmitted power per source symbol at the k^{th} subcarrier). The incoming data consists of 128 bytes. The fading channel model assumes a quasi-static exponentially decaying power delay profile with root mean square (RMS) delay spread of $\tau_{\text{rms}} = 50$ ns and $L = 10$ paths [64]. The path gains are zero-mean complex Gaussian random variables, where all the paths are statistically independent and the maximum delay spread of the channel is less than the cyclic prefix length.

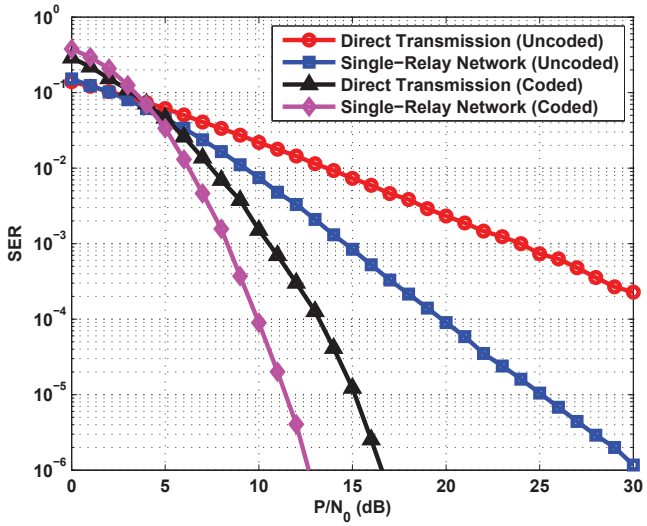

Figure 1.6: BPSK SER Performance of the OFDM-Based Single-Relay Networks

As can be seen in Fig. 1.6, the SER performance of the single-relay network for uncoded OFDM significantly outperforms that of the direct transmission by about 10 dB at SER of 10^{-4}. This is due to the diversity gain achievable through cooperation. Obviously, the performance of the coded OFDM system for direct transmission is better than that of the uncoded system. In addition, the coded OFDM-based single-relay network outperforms that of direct transmission by about 4 dB at SER of 10^{-4}. Clearly, the diversity gain under the coded system is less than that of its uncoded counterpart. By comparing the performance of the uncoded direct transmission with the coded single-relay network, coding and diversity gains result in a saving of about 20 dB for a SER of 10^{-4}. This establishes the significance of exploiting cooperative diversity gains in addition to coding gains.

[3]All the N_s subcarriers are utilized for data transmission.

1.6 Dissertation Outline

In this section, the contents of each chapter are outlined.

- **Bi-Directional Relaying (Chapter 2):**
  In this chapter, a comparative performance analysis of network-coded multi-relay bi-directional amplify-and-forward (BD-AF) networks is presented. In such networks, communication is performed over two phases, the broadcasting phase and the cooperation phase. In the broadcasting phase, both source nodes broadcast their signals simultaneously to the N intermediate relay nodes, while in the cooperation phase, transmission is based on one of two modes: (1) time-division (TD), and (2) multiple-access (MA). In the TD-BD-AF scheme, each relay node is allocated a time-slot to transmit its processed signal, while in the MA-BD-AF scheme, all the N relay nodes simultaneously transmit linearly coded signals to both source nodes, in a single time-slot. Moreover, a suboptimal relay selection (i.e. SRS-BD-AF) that approximately maximizes the sum-of-rates is proposed such that only one relay out of the N relays transmits its network-coded signal to both source nodes. Optimal and suboptimal sum-of-rates maximizing power allocations are studied under the TD-BD-AF and MA-BD-AF schemes, respectively, where it is shown that the MA-BD-AF scheme reduces to the SRS-BD-AF scheme. Symbol error rate performance analysis is provided, where it is shown that both the TD-BD-AF and SRS-BD-AF schemes achieve full diversity. Imperfect timing synchronization is analyzed and it is demonstrated that the SRS-BD-AF outperforms the other schemes in terms of the achievable rate. Simulation results are provided to complement the theoretical analysis.

- **Space-Time Network Coding (Chapter 3):**
  Chapter 3 treats the multinode amplify-and-forward cooperative communications via the novel concept of many-to-many space-time network coding (M2M-STNC) for a network of N nodes. The communication under the M2M-STNC scheme is split into two phases: (1) the broadcasting phase, in which each node in its allocated time-slot broadcasts its data symbol to all the other nodes in the network, and (2) the cooperation phase in which simultaneous transmissions from $N-1$ nodes to a destination node take place in every time-slot. To improve the achievable sum-rate of each node, optimal power allocation is proposed. Moreover, the M2M-STNC scheme with optimal node selection (i.e. M2M-STNC-ONS) is proposed where the optimal node is selected based on the maximum harmonic mean value of the source, intermediate, and destination nodes' scaled instantaneous channel gains. Theoretical symbol-error-rate analysis for M-ary phase shift keying (M-PSK) modulation is derived for both the M2M-STNC and M2M-STNC-ONS schemes. In addition, the effect of timing synchronization errors and imperfect channel state information on the SER performance and achievable rate is also analytically studied. It is shown that the proposed M2M-STNC-ONS scheme outperforms its counterpart scheme in terms of the SER performance as well as the total achievable rate.

- **Auction-Based Power Allocation for Single-Relay Cooperative Networks (Chapter 4):**
  In this chapter, a distributed efficient power allocation game-theoretic framework in ad-hoc wireless networks is proposed where multiple source nodes communicate with a single destination node via a relay node. The distributed power allocation among the source nodes is formulated as an ascending-clock auction. Specifically, two distributed auction algorithms are proposed, namely the conventional ascending-clock auction (C-ACA) and the alternative ascending-clock auction (A-ACA). Both the C-ACA and A-ACA algorithms are proven to converge in a finite number of time-steps to the optimal power allocation that maximizes the social welfare. In addition, the A-ACA algorithm distributively enforces truthful power demands while the C-ACA algorithm does not. Analytical and numerical results are presented to verify the convergence, truth-telling, and social welfare maximization properties of the proposed algorithms.

- **Auction-Based Power Allocation for Multi-Relay Cooperative Networks (Chapter 5):**
  The multi-relay power allocation in cooperative wireless networks is considered in Chapter 5. An ascending-clock auction is proposed to efficiently allocate cooperative relay power among multiple source nodes in a distributed fashion. In particular, each source node reports its power demand to each relay node based on the relays' announced prices. It is proven that the proposed auction algorithm enforces truthful power demands and converges in a finite number of time-steps to the unique Walrasian Equilibrium allocation that maximizes the social welfare. Numerical results are presented to supplement the theoretical analysis and demonstrate the efficiency of the proposed distributed relay power allocation algorithm.

- **A Coalitional Game-Theoretic Analysis of Cooperative Networks (Chapter 6):**
  In this Chapter, distributed altruistic coalition formation for decode-and-forward cooperative relay networks is studied. The communication is performed over two phases, the broadcasting phase and the cooperation phase. In the broadcasting phase, each node broadcasts its signal in its time-slot, while in the cooperation phase, all the nodes within their coalitions simultaneously relay each others' signals. A distributed merge-and-split algorithm is proposed to allow nodes to form coalitions and improve their achievable sum-rate. Moreover, the impact of different power allocation criteria as well as mobility on coalition formations is studied. The proposed algorithm is compared with that of centralized control obtained and shown to yield a good tradeoff between network sum-rate and computational complexity.

- **Summary, Conclusions and Future Work (Chapter 7):**
  In Chapter 7, the research work of the dissertation is summarized along with the contributions and publications. In addition, potential future research directions and problems are discussed in this chapter.

Chapter 2

Bi-Directional Relaying

2.1 Introduction

As discussed in Chapter 1, cooperative relay networks have been studied extensively in the wireless research literature in recent years due to their ability to combat fading and increase network capacity [7] [56]. In a variety of applications in cooperative relay networks, such as multi-hop networks [65] [66], two different source nodes—between which there is no direct link—may need to exchange data through a set of intermediate relays. In turn, bi-directional relaying combined with wireless network coding has recently attracted attention in the wireless literature as a means to improve bandwidth efficiency and increase network throughput (e.g. see [67, 68, 69] and references therein). In particular, the bi-directional amplify-and-forward (BD-AF) communication is split into two phases: the broadcasting phase and the cooperation phase. In the broadcasting phase, both source nodes simultaneously broadcast their information while in the cooperation phase, a single relay (or multiple relays) retransmits a processed version of its received signal. In the wireless literature, several works considered single relay bi-directional transmission. For instance, the authors in [32] demonstrated that two source nodes that wish to exchange information with each other—and between which there is no direct link—can communicate through a single amplify-and-forward relay node such that the received simultaneous transmissions from both source nodes are combined and relayed over only two time-slots. In [70], analog network coding with differential modulation for single relay bi-directional networks is proposed along with bit error rate performance analysis.

For the multi-relay case, transmission in the cooperation phase takes one of two modes: (1) time-division (TD) or (2) multiple-access (MA). Under the TD-BD-AF scheme, each relay is assigned a time-slot to transmit its processed signal while in the MA-BD-AF scheme, all the relays simultaneously transmit their signals over a single time-slot. Consequently, the former scheme leads to bandwidth inefficiency while the latter scheme requires stringent timing synchronization and/or beamforming between the distributed relay nodes, which are practically challenging. To fully exploit diversity gains while achieving bandwidth efficiency

in multi-relay bi-directional networks, relay selection and optimal power allocation are essential[1]. For example, a relay selection scheme that maximizes the worst received signal-to-noise ratio (SNR) of the source nodes is proposed in [71]. Joint relay-selection and analog-network coding using differential modulation is proposed in [72]. Specifically, a suboptimal min-max symbol error rate (SER) criterion for relay selection is utilized. Different optimal distributed beamforming criteria based on second-order convex cone programming are studied in [73], where the authors consider the scenario of two source nodes—with no direct link between them—transmitting their information simultaneously to a set of relays which amplify-and-forward their received signals over a total of 2 time-slots. In [74], an optimal joint relay selection and power allocation scheme to achieve SNR balancing and rate fairness between the source nodes is proposed. The previous works and most of the literature on bi-directional relaying assume perfect timing synchronization in either source broadcasting and/or relay cooperation phases [72, 73, 74, 75, 76]. Such stringent requirement is practically prohibitive and thus should not be overlooked when evaluating the performance of such networks.

The discussed research studies motivate and shed light on the significance of relay selection (RS) in multi-relay bi-directional networks—with N relay nodes deployed between the two source nodes—without further degrading network throughput. In this chapter, a suboptimal relay selection scheme that requires only two time-slots and approximately maximizes the sum-of-rates between the two source nodes is proposed and denoted as suboptimal-relay-selection bi-directional amplify-and-forward (SRS-BD-AF). The proposed scheme is compared with the TD-BD-AF and MA-BD-AF schemes which require a total of $N+1$ and two time-slots, respectively, in terms of the SER and achievable rate performance. Sum-of-rates maximizing optimal and suboptimal power allocations are studied under the TD-BD-AF and MA-BD-AF schemes, respectively, where the MA-BD-AF scheme under suboptimal power allocation is shown to reduce to the SRS-BD-AF scheme. Furthermore, a symbol error rate analysis for M-ary phase shift keying (M-PSK) modulation of the different bi-directional relaying schemes is also presented, and the TD-BD-AF and SRS-BD-AF schemes are proven to achieve full diversity. Imperfect timing synchronization is also analyzed and it is shown that the SRS-BD-AF scheme outperforms the other two schemes in terms of the achievable rate. To the best of the author's knowledge, there is no research analyzing the SER performance and achievable rate of the sum-of-rates maximizing relay selection under perfect and imperfect timing synchronization due to its mathematically intractability.

In the remainder of this chapter, the network models of the different bi-directional relaying schemes are presented in Section 2.2 while the approximate probability of relay selection is theoretically analyzed in Section 2.3. The SER performance analysis of the different bi-directional schemes is presented in Section 2.4 while the sum-of-rates maximizing relay power allocation is formulated in Section 2.5. The timing synchronization analysis is discussed in Section 2.6 while the simulation results and performance comparisons are presented in Section 2.7. The chapter conclusions and final remarks are outlined in Section 2.8.

[1]Relay selection in conventional "unidirectional" relay networks for single and multi-relay networks has extensively been studied in the wireless literature (e.g. see [24] and [26]).

2.2 Network Models

The amplify-and-forward bi-directional network models assume two source nodes S_1 and S_2 exchange information with each other through a set of $N \geq 2$ relay nodes R_k (for $k \in \{1, 2, \ldots, N\}$) deployed in between. Moreover, half-duplex single antenna nodes and no direct link between the two source nodes are assumed. The channel fading coefficients h_{s_j,r_k} between source node S_j for $j \in \{1, 2\}$ and relay node R_k are modeled as $h_{s_j,r_k} \sim \mathcal{CN}(0, \sigma^2_{s_j,r_k})$. In addition, $\sigma^2_{s_j,r_k} = d^{-\nu}_{s_j,r_k}$ is the channel variance with d_{s_j,r_k} being the distance between source node S_j and relay node R_k, and ν is the path-loss exponent. Perfect channel estimation is assumed at every source and relay node, and both the forward h_{s_j,r_k} and backward h_{r_k,s_j} channel fading coefficients are reciprocal (i.e. $h_{s_j,r_k} = h_{r_k,s_j}$), as in time division duplexing (TDD) systems. It should also be noted that the channel gain squared $|h_{s_j,r_k}|^2, \forall j \in \{1, 2\}, \forall k \in \{1, 2, \ldots, N\}$ is an exponential random variable with rate $1/\sigma^2_{s_j,r_k}$.

The communication between the two source nodes under the different network models is performed in a TDMA fashion over two phases, namely the broadcasting phase and the cooperation phase, as detailed in the following subsections.

2.2.1 TD-BD-AF

The time-division bi-directional amplify-and-forward (TD-BD-AF) multi-relay network model is illustrated in Fig. 2.1.

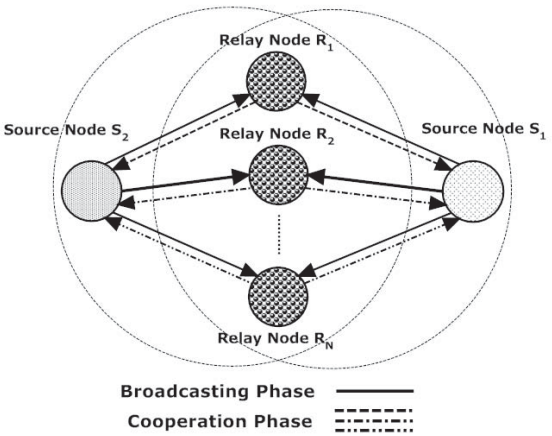

Figure 2.1: Time-Division Bi-Directional Amplify-and-Forward Network Model

Broadcasting Phase

In the broadcasting phase, both source node S_1 and source node S_2 broadcast their symbols simultaneously to the N relay nodes in between. For source separation at each relay node, each transmitted signal by each source node S_j for $j \in \{1, 2\}$ is spread using a signature waveform $c_j(t)$, where it is assumed that each relay node knows the signature waveforms of the two source nodes. Also, the cross-correlation of $c_i(t)$ and $c_j(t)$ is $\rho_{i,j} = \langle c_i(t), c_j(t) \rangle \triangleq$

$(1/T_s)\int_0^{T_s} c_i(t)c_j^*(t)dt$ for $i \neq j$ with $\rho_{j,j} = 1$ and T_s being the symbol duration. Assuming perfect timing synchronization, relay node R_k for $k \in \{1, 2, \ldots, N\}$ receives a signal $y_{r_k}(t)$, which contains both symbols from both source nodes as follows

$$y_{r_k}(t) = \sqrt{P_{s_1}} h_{s_1,r_k} x_1 c_1(t) + \sqrt{P_{s_2}} h_{s_2,r_k} x_2 c_2(t) + n_{r_k}(t), \tag{2.1}$$

where x_1 and x_2 are the transmitted data symbols from source nodes S_1 and S_2, respectively. Moreover, $n_{r_k}(t)$ is the additive noise process at relay node R_k which is modeled as a zero-mean complex Gaussian random variable with variance N_0. In addition, P_{s_1} and P_{s_2} are the transmit powers at source nodes S_1 and S_2, respectively. The received signal at relay node R_k is passed through a matched filter bank (MFB) of two branches, giving

$$\mathcal{Y}_{r_k,s_j} = \langle y_{r_k}(t), c_j(t) \rangle = \sum_{i=1}^{2} \sqrt{P_{s_i}} h_{s_i,r_k} x_i \rho_{i,j} + n_{r_k,s_j}. \tag{2.2}$$

The output of the MFB can be expressed in vector form as follows

$$\boldsymbol{\mathcal{Y}}_{r_k} = \boldsymbol{R}\boldsymbol{A}_{r_k}\boldsymbol{x} + \boldsymbol{n}_{r_k}, \tag{2.3}$$

where $\boldsymbol{\mathcal{Y}}_{r_k} = [\mathcal{Y}_{r_k,s_1}, \mathcal{Y}_{r_k,s_2}]^T$, $\boldsymbol{x} = [x_1, x_2]^T$, $\boldsymbol{n}_{r_k} = [n_{r_k,s_1}, n_{r_k,s_2}]^T \sim \mathcal{CN}(\boldsymbol{0}, N_0\boldsymbol{R})$. Moreover, $\boldsymbol{R}$, and $\boldsymbol{A}_{r_k}$ are 2×2 matrices with $\boldsymbol{R}$ being defined as

$$\boldsymbol{R} = \begin{bmatrix} 1 & \rho_{1,2} \\ \rho_{2,1} & 1 \end{bmatrix}, \tag{2.4}$$

and matrix $\boldsymbol{A}_{r_k}$ is expressed as

$$\boldsymbol{A}_{r_k} = \begin{bmatrix} \sqrt{P_{s_1}} h_{s_1,r_k} & 0 \\ 0 & \sqrt{P_{s_2}} h_{s_2,r_k} \end{bmatrix}. \tag{2.5}$$

The received signal vector $\boldsymbol{\mathcal{Y}}_{r_k}$ is then decorrelated (assuming matrix $\boldsymbol{R}$ is nonsingular) as

$$\bar{\boldsymbol{\mathcal{Y}}}_{r_k} = \boldsymbol{R}^{-1}\boldsymbol{\mathcal{Y}}_{r_k} = \boldsymbol{A}_{r_k}\boldsymbol{x} + \bar{\boldsymbol{n}}_{r_k}, \tag{2.6}$$

where $\bar{\boldsymbol{n}}_{r_k} = \boldsymbol{R}^{-1}\boldsymbol{n}_{r_k}$ and $\bar{\boldsymbol{n}}_{r_k} \sim \mathcal{CN}(\boldsymbol{0}, N_0\boldsymbol{R}^{-1})$. Hence, the decorrelated received signal corresponding to symbol x_j for $j \in \{1, 2\}$ is expressed as

$$\bar{\mathcal{Y}}_{r_k,s_j} = \sqrt{P_{s_j}} h_{s_j,r_k} x_j + \bar{n}_{r_k,s_j}, \tag{2.7}$$

where $\bar{n}_{r_k,s_j} \sim \mathcal{CN}(0, N_0\varrho_j)$ and ϱ_j is the j^{th} diagonal element of matrix $\boldsymbol{R}^{-1}$. Without loss of generality, it is assumed that $\rho_{1,2} = \rho_{2,1} = \rho$. Thus, $\varrho_j = \frac{1}{1-\rho^2} \triangleq \varrho, \forall j \in \{1, 2\}$.

Cooperation Phase

In the cooperation phase, relay node R_k forms a linear combination $\mathcal{X}_{r_k}(t)$ of its decorrelated signals and broadcasts it in its assigned time-slot. Particularly, $\mathcal{X}_{r_k}(t)$ is written as

$$\mathcal{X}_{r_k}(t) = \sum_{i=1}^{2} \beta_{r_k,s_i} \bar{\mathcal{Y}}_{r_k,s_i} c_i(t), \tag{2.8}$$

where β_{r_k,s_i} is the normalization factor, given by

$$\beta_{r_k,s_i} = \sqrt{\frac{1}{P_{s_i}|h_{s_i,r_k}|^2 + N_0\varrho}}. \tag{2.9}$$

Without loss of generality and due to the symmetry of the bi-directional transmission, the received signal at source node S_1 will be analyzed. Thus, the received signal at source node S_1 transmitted by relay node R_k is written as

$$y_{s_1,r_k}(t) = \sqrt{P_{r_k}} h_{s_1,r_k} \mathcal{X}_{r_k}(t) + w_{s_1,r_k}(t), \tag{2.10}$$

where P_{r_k} is relay R_k's transmit power while $w_{s_1,r_k}(t)$ is the zero-mean additive noise process with variance N_0 at source node S_1 due to relay node R_k's transmission. As before, the received signal is passed through the MFB, yielding

$$Y_{s_1,r_k,s_j} = \langle y_{s_1,r_k}(t), c_j(t) \rangle = \sqrt{P_{r_k}} h_{s_1,r_k} \sum_{i=1}^{2} \beta_{r_k,s_i} \bar{\mathcal{Y}}_{r_k,s_i} \rho_{i,j} + w_{s_1,r_k,s_j}. \tag{2.11}$$

The received signal in vector form is expressed as

$$\boldsymbol{Y}_{s_1,r_k} = \boldsymbol{R}\boldsymbol{B}_{s_1,r_k} \bar{\boldsymbol{\mathcal{Y}}}_{r_k} + \boldsymbol{w}_{s_1,r_k}, \tag{2.12}$$

where $\bar{\boldsymbol{\mathcal{Y}}}_{r_k} = \left[\bar{\mathcal{Y}}_{r_k,s_1}, \bar{\mathcal{Y}}_{r_k,s_2}\right]^T$, $\boldsymbol{Y}_{s_1,r_k} = [Y_{s_1,r_k,s_1}, Y_{s_1,r_k,s_2}]^T$, $\boldsymbol{w}_{s_1,r_k} = [w_{s_1,r_k,s_1}, w_{s_1,r_k,s_2}]^T \sim \mathcal{CN}(\boldsymbol{0}, N_0\boldsymbol{R})$, and $\boldsymbol{B}_{s_1,r_k} = \sqrt{P_{r_k}} h_{s_1,r_k} \boldsymbol{B}_{r_k}$. Also, the 2×2 diagonal matrix $\boldsymbol{B}_{r_k}$ is defined as

$$\boldsymbol{B}_{r_k} = \begin{bmatrix} \beta_{r_k,s_1} & 0 \\ 0 & \beta_{r_k,s_2} \end{bmatrix}. \tag{2.13}$$

The received signal is decorrelated as $\bar{\boldsymbol{Y}}_{s_1,r_k} = \boldsymbol{R}^{-1}\boldsymbol{Y}_{s_1,r_k}$, where $\bar{\boldsymbol{Y}}_{s_1,r_k} = \left[\bar{Y}_{s_1,r_k,s_1}, \bar{Y}_{s_1,r_k,s_2}\right]^T$. Hence, the signal corresponding to symbol x_2 at the output of the MFB is expressed as

$$\bar{Y}_{s_1,r_k,s_2} = \sqrt{P_{r_k}} h_{s_1,r_k} \beta_{r_k,s_2} \bar{\mathcal{Y}}_{r_k,s_2} + \bar{w}_{s_1,r_k,s_2}, \tag{2.14}$$

where $\bar{w}_{s_1,r_k,s_2} \sim \mathcal{CN}(0, N_0\varrho)$. Substituting (2.7) into (2.14) yields

$$\bar{Y}_{s_1,r_k,s_2} = \sqrt{P_{r_k}P_{s_2}} h_{s_1,r_k} h_{s_2,r_k} \beta_{r_k,s_2} x_2 + \eta_{s_1,r_k,s_2}, \tag{2.15}$$

where $\eta_{s_1,r_k,s_2} = \sqrt{P_{r_k}} h_{s_1,r_k} \beta_{r_k,s_2} \bar{n}_{r_k,s_2} + \bar{w}_{s_1,r_k,s_2}$ is the equivalent noise term and $\eta_{s_1,r_k,s_2} \sim \mathcal{CN}(0, (P_{r_k}|h_{s_1,r_k}|^2 \beta_{r_k,s_2}^2 + 1)N_0\varrho)$. By applying a matched filter to its received decorrelated signal $\bar{Y}_{s_1,r_k,s_2}$, the instantaneous SNR value γ_{r_k,s_2} of the received signal $\bar{Y}_{s_1,r_k,s_2}$ is given by

$$\gamma_{r_k,s_2} = \frac{1}{N_0\varrho} \frac{P_{s_2}P_{r_k}|h_{s_1,r_k}|^2|h_{s_2,r_k}|^2}{P_{r_k}|h_{s_1,r_k}|^2 + P_{s_2}|h_{s_2,r_k}|^2 + N_0\varrho}, \tag{2.16}$$

which at high SNR can be tightly upper-bounded as [77]

$$\bar{\gamma}_{r_k,s_2} \approx \frac{1}{N_0\varrho} \frac{P_{s_2}P_{r_k}|h_{s_1,r_k}|^2|h_{s_2,r_k}|^2}{P_{r_k}|h_{s_1,r_k}|^2 + P_{s_2}|h_{s_2,r_k}|^2}. \tag{2.17}$$

which is easily shown to be the scaled harmonic mean of two exponential random variables[2]

$$X_{s_2,r_k} = \frac{P_{s_2}|h_{s_2,r_k}|^2}{N_0\varrho} \quad \text{and} \quad X_{r_k,s_1} = \frac{P_{r_k}|h_{s_1,r_k}|^2}{N_0\varrho}, \tag{2.18}$$

with rates $\lambda_{s_2,r_k} = N_0\varrho/(P_{s_2}\sigma^2_{s_2,r_k})$, $\lambda_{r_k,s_1} = N_0\varrho/(P_{r_k}\sigma^2_{s_1,r_k})$, respectively. Similarly, the upper-bounded instantaneous SNR at source node S_2 due to relay node R_k's transmission is

$$\bar{\gamma}_{r_k,s_1} \approx \frac{1}{N_0\varrho}\frac{P_{s_1}P_{r_k}|h_{s_1,r_k}|^2|h_{s_2,r_k}|^2}{P_{s_1}|h_{s_1,r_k}|^2 + P_{r_k}|h_{s_2,r_k}|^2}, \tag{2.19}$$

which is the scaled harmonic mean of

$$X_{s_1,r_k} = \frac{P_{s_1}|h_{s_1,r_k}|^2}{N_0\varrho} \quad \text{and} \quad X_{r_k,s_2} = \frac{P_{r_k}|h_{s_2,r_k}|^2}{N_0\varrho}. \tag{2.20}$$

Based on the above system description, all N relay nodes participate in the transmission of signals between the two source nodes, resulting in a cumulative SNR at source node S_1 of

$$\gamma_{s_2} = \sum_{k=1}^{N}\gamma_{r_k,s_2} = \sum_{k=1}^{N}\frac{1}{N_0\varrho}\frac{P_{s_2}P_{r_k}|h_{s_1,r_k}|^2|h_{s_2,r_k}|^2}{P_{r_k}|h_{s_1,r_k}|^2 + P_{s_2}|h_{s_2,r_k}|^2 + N_0\varrho}. \tag{2.21}$$

Since each relay node is allocated a dedicated time-slot, this scheme requires a total of $N+1$ time-slots. Thus, the achievable transmission rate of source node S_2 is

$$\mathcal{R}_{s_2}^{\text{TD-BD-AF}}(\gamma_{s_2}) = \frac{1}{N+1}\log_2\left(1 + \sum_{k=1}^{N}\frac{1}{N_0\varrho}\frac{P_{s_2}P_{r_k}|h_{s_1,r_k}|^2|h_{s_2,r_k}|^2}{P_{r_k}|h_{s_1,r_k}|^2 + P_{s_2}|h_{s_2,r_k}|^2 + N_0\varrho}\right). \tag{2.22}$$

It should be noted that the total transmit power constraint P is set to $P = P_S + P_R$, where $P_S = P_{s_1} + P_{s_2} = \delta_S P$ is the total source nodes transmit power with $0 < \delta_S \leq 1$ being the source nodes power allocation factor. Furthermore, $P_{s_j} = \delta_{s_j}\delta_S P$ where $0 < \delta_{s_j} \leq 1$ for $j \in \{1, 2\}$ is source node S_j's power allocation factor, and $\delta_{s_1} + \delta_{s_2} = 1$. Similarly, $P_R = \sum_{k=1}^{N} P_{r_k} = \delta_R P$ is the total relay transmit power and $0 \leq \delta_R < 1$ is the relay power allocation factor. Also, $P_{r_k} = \delta_{r_k}\delta_R P$, where $0 \leq \delta_{r_k} \leq 1$ for $k \in \{1, 2, \ldots, N\}$ is relay node R_k's power allocation factor, and $\sum_{k=1}^{N}\delta_{r_k} = 1$.

2.2.2 MA-BD-AF

To overcome the bandwidth inefficiency of the TD-BD-AF scheme, the MA-BD-AF scheme is considered, as shown in Fig. 2.2. As in the TD-BD-AF scheme, both source nodes simultaneously transmit their symbols in the broadcasting phase. However, in the cooperation phase, all the N relay nodes—assuming perfect timing synchronization—simultaneously broadcast their signals $\mathcal{X}_{r_k}(t)$ to both source nodes in the same time-slot. The received signal at source node S_1 is written as

[2]The scaled harmonic mean of two random variables X_1 and X_2 is given by $Z = \frac{X_1X_2}{X_1+X_2}$.

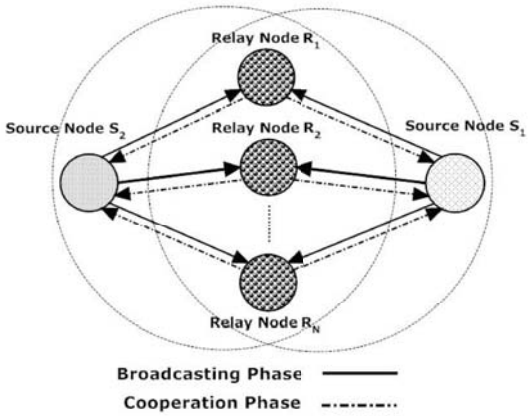

Figure 2.2: Multiple-Access Bi-Directional Amplify-and-Forward Network Model

$$y_{s_1}(t) = \sum_{k=1}^{N} \sqrt{P_{r_k}} h_{s_1,r_k} \mathcal{X}_{r_k}(t) + w_{s_1}(t), \tag{2.23}$$

which is when cross-correlated with signature waveform $c_j(t)$ yields

$$Y_{s_1,s_j} = \langle y_{s_1}(t), c_j(t) \rangle = \sum_{k=1}^{N} \sqrt{P_{r_k}} h_{s_1,r_k} \sum_{i=1}^{2} \beta_{r_k,s_i} \bar{\mathcal{Y}}_{r_k,s_i} \rho_{i,j} + w_{s_1,s_j}. \tag{2.24}$$

In vector form, the received signal at the output of the MFB is shown to be

$$\boldsymbol{Y}_{s_1} = \boldsymbol{R} \left(\sum_{k=1}^{N} \boldsymbol{B}_{s_1,r_k} \bar{\boldsymbol{\mathcal{Y}}}_{r_k} \right) + \boldsymbol{w}_{s_1}, \tag{2.25}$$

where $\boldsymbol{Y}_{s_1} = [Y_{s_1,s_1}, Y_{s_1,s_2}]^T$ and $\boldsymbol{w}_{s_1} = [w_{s_1,s_1}, w_{s_1,s_2}]^T \sim \mathcal{CN}(\boldsymbol{0}, N_0 \boldsymbol{R})$, while $\bar{\boldsymbol{\mathcal{Y}}}_{r_k}$ is defined in (2.6). Following similar steps to those in the previous section, the decorrelated received signal corresponding to symbol x_2 at the output of the MFB is obtained as

$$\bar{Y}_{s_1,s_2} = \sum_{k=1}^{N} \sqrt{P_{r_k}} h_{s_1,r_k} \beta_{r_k,s_2} \bar{\mathcal{Y}}_{r_k,s_2} + \bar{w}_{s_1,s_2}, \tag{2.26}$$

where $\bar{w}_{s_1,s_2} \sim \mathcal{CN}(0, N_0 \varrho)$. As before, the decorrelated signal at S_1 is further expanded as

$$\bar{Y}_{s_1,s_2} = \sum_{k=1}^{N} \left(\sqrt{P_{r_k} P_{s_2}} h_{s_1,r_k} h_{s_2,r_k} \beta_{r_k,s_2} \right) x_2 + \eta_{s_1,s_2}, \tag{2.27}$$

where $\eta_{s_1,s_2} = \sum_{k=1}^{N} \sqrt{P_{r_k}} h_{s_1,r_k} \beta_{r_k,s_2} \bar{n}_{r_k,s_2} + \bar{w}_{s_1,s_2}$ is the total zero-mean noise term with variance $(\sum_{k=1}^{N} P_{r_k} |h_{s_1,r_k}|^2 \beta_{r_k,s_2}^2 + 1) N_0 \varrho$. When $\bar{Y}_{s_1,s_2}$ is passed through a matched-filter, the instantaneous SNR is obtained as

$$\gamma_{s_2} = \frac{P_{s_2} \left(\sum_{k=1}^{N} \frac{P_{r_k} |h_{s_1,r_k}|^2 |h_{s_2,r_k}|^2}{P_{s_2} |h_{s_2,r_k}|^2 + N_0 \varrho} \right)}{N_0 \varrho \left(1 + \sum_{k=1}^{N} \frac{P_{r_k} |h_{s_1,r_k}|^2}{P_{s_2} |h_{s_2,r_k}|^2 + N_0 \varrho} \right)}. \tag{2.28}$$

Notice in (2.28) that the MA-BD-AF scheme is degraded by noise amplification due to the simultaneous transmissions of the N relay nodes. Since only two time-slots are required for symbols exchange between source nodes S_1 and S_2, the achievable transmission rate of source S_2 is given by [28]

$$\mathcal{R}_{s_2}^{\text{MA-BD-AF}}(\gamma_{s_2}) = \frac{1}{2}\log_2\left(1 + \frac{P_{s_2}\left(\sum_{k=1}^{N}\frac{P_{r_k}|h_{s_1,r_k}|^2|h_{s_2,r_k}|^2}{P_{s_2}|h_{s_2,r_k}|^2+N_0\varrho}\right)}{N_0\varrho\left(1+\sum_{k=1}^{N}\frac{P_{r_k}|h_{s_1,r_k}|^2}{P_{s_2}|h_{s_2,r_k}|^2+N_0\varrho}\right)}\right). \tag{2.29}$$

In comparison with the TD-BD-AF scheme, the MA-BD-AF scheme poses a tradeoff between the improvement in the number of time-slots (i.e. bandwidth utilization) and the degradation in the received SNR due to the noise amplification, in addition to the stringent timing synchronization requirement, as will be studied later in this chapter.

2.2.3 RS-BD-AF

Under this scheme (see Fig. 2.3), the broadcasting phase is identical to that of the TD-BD-AF scheme. However, in the cooperation phase, a single relay node transmits its linearly coded signal to both source nodes, based on one of the following criteria.

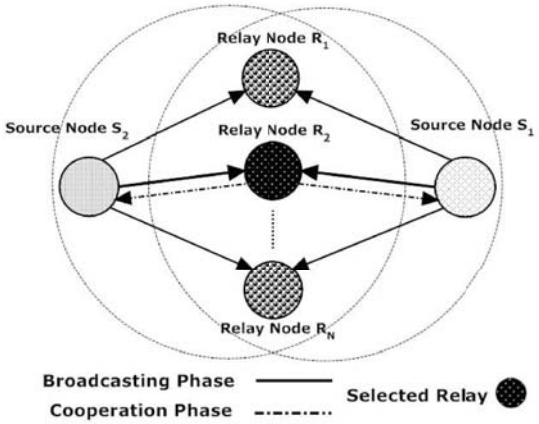

Figure 2.3: Relay Selection Bi-Directional Amplify-and-Forward Network Model

Optimal Relay Selection (ORS):

Under the ORS-BD-AF scheme, the relay node that maximizes the sum-of-rates of source nodes S_1 and S_2—when it is allocated the total relay power $P_R = \delta_R P$—is selected for bi-directional relaying. That is,

$$r_{\text{ors}} = \arg\max_{k=1,2,\ldots,N}\{\mathcal{R}_{s_1}(\gamma_{r_k,s_1}) + \mathcal{R}_{s_2}(\gamma_{r_k,s_2})\}, \tag{2.30}$$

where $\mathcal{R}_{s_1}(\gamma_{r_k,s_1})$ and $\mathcal{R}_{s_2}(\gamma_{r_k,s_2})$ are the achievable rates of nodes S_1 and S_2 due to relay node R_k's transmission. Such a scheme is analytically difficult to analyze [72][78].

Suboptimal Relay Selection (SRS):

By noting that the $\log_2(\cdot)$ function is concave and strictly monotonically increasing in its parameter, then by using the arithmetic-geometric means inequality, the sum-rate selection metric in (2.30) at high SNR is tightly upper-bounded as [79]

$$\frac{1}{2}\log_2\left(1+\gamma_{r_k,s_1}\right)+\frac{1}{2}\log_2\left(1+\gamma_{r_k,s_2}\right)\lesssim\log_2\left(1+\frac{1}{2}(\gamma_{r_k,s_1}+\gamma_{r_k,s_2})\right). \tag{2.31}$$

The suboptimal relay selection metric is $r_{\text{srs}}=\arg\max_{k=1,2,\ldots,N}\{\log_2\left(1+\frac{1}{2}(\gamma_{r_k,s_1}+\gamma_{r_k,s_2})\right)\}$, and due to the monotonicity of the $\log_2(\cdot)$ function, it is equivalent to

$$r_{\text{srs}}=\arg\max_{k=1,2,\ldots,N}\{\gamma_{r_k,s_1}+\gamma_{r_k,s_2}\}. \tag{2.32}$$

The achievable rate of source node S_2 under the ORS-BD-AF and SRS-BD-AF schemes is

$$\mathcal{R}_{s_2}^{\text{RS-BD-AF}}(\gamma_{r_{rs},s_2})=\frac{1}{2}\log_2\left(1+\frac{1}{N_0\varrho}\frac{P_{s_2}P_R|h_{s_1,r_{\text{rs}}}|^2|h_{s_2,r_{\text{rs}}}|^2}{P_R|h_{s_1,r_{\text{rs}}}|^2+P_{s_2}|h_{s_2,r_{\text{rs}}}|^2+N_0\varrho}\right). \tag{2.33}$$

where $\gamma_{r_{\text{rs}},s_2}=\gamma_{r_{\text{ors}},s_2}$ under the former scheme and $\gamma_{r_{\text{rs}},s_2}=\gamma_{r_{\text{srs}},s_2}$ under the latter scheme. In general, $\gamma_{r_{\text{rs}},s_2}$ is the SNR of symbol x_2 due to the transmission of the selected relay node.

Finally, for the case of $N=1$, the MA-BD-AF, ORS-BD-AF and SRS-BD-AF schemes reduce to the TD-BD-AF scheme.

2.3 Approximate Probability of Relay Selection

In this section, the approximate probability of selecting each relay node under the proposed SRS-BD-AF scheme is determined analytically. Based on the suboptimal relay selection scheme presented in Section 2.2.3, it is noted that the sum of the upper-bounded instantaneous SNR values $\bar{\gamma}_{r_k}=\bar{\gamma}_{r_k,s_1}+\bar{\gamma}_{r_k,s_2}$ for $k\in\{1,2,\ldots,N\}$ is the sum of two *correlated* not necessarily identically distributed scaled harmonic mean random variables. Each sum term $\bar{\gamma}_{r_k}$ is expressed as

$$\bar{\gamma}_{r_k}=\bar{\gamma}_{r_k,s_1}+\bar{\gamma}_{r_k,s_2}=\frac{X_{s_1,r_k}X_{r_k,s_2}}{X_{s_1,r_k}+X_{r_k,s_2}}+\frac{X_{s_2,r_k}X_{r_k,s_1}}{X_{s_2,r_k}+X_{r_k,s_1}}, \tag{2.34}$$

where the cumulative distribution function (CDF) of $\bar{\gamma}_{r_k,s_2}$ (and similarly of $\bar{\gamma}_{r_k,s_1}$) is given by

$$P_{\bar{\gamma}_{r_k,s_2}}(\gamma)=1-2\gamma\sqrt{\lambda_{s_2,r_k}\lambda_{r_k,s_1}}e^{-\gamma(\lambda_{s_2,r_k}+\lambda_{r_k,s_1})}K_1\left(2\gamma\sqrt{\lambda_{s_2,r_k}\lambda_{r_k,s_1}}\right), \tag{2.35}$$

where $K_1(\cdot)$ is the first-order modified Bessel function of the second kind [80]. At high SNR, $K_1(\cdot)$ can be approximated for small enough x as $K_1(x)\approx 1/x$. Thus, the CDF at high SNR is approximated as $P_{\bar{\gamma}_{r_k,s_2}}(\gamma)\approx 1-e^{-\gamma(\lambda_{s_2,r_k}+\lambda_{r_k,s_1})}$ with the probability density function (PDF) being defined as $p_{\bar{\gamma}_{r_k,s_2}}(\gamma)=(\lambda_{s_2,r_k}+\lambda_{r_k,s_1})e^{-\gamma(\lambda_{s_2,r_k}+\lambda_{r_k,s_1})}$. Notice that the approximate CDF and PDF of $\bar{\gamma}_{r_k,s_2}$ pertain to an exponential random variable with rate

$$\lambda_{s_2,r_k,s_1} \triangleq \lambda_{s_2,r_k} + \lambda_{r_k,s_1} = \left(\frac{N_0\varrho}{P}\right) \frac{\delta_{s_2}\delta_S\sigma^2_{s_2,r_k} + \delta_R\sigma^2_{s_1,r_k}}{\delta_{s_2}\delta_S\delta_R\sigma^2_{s_1,r_k}\sigma^2_{s_2,r_k}}. \tag{2.36}$$

Similarly, the rate of the exponential random variable $\tilde{\gamma}_{r_k,s_1}$ is given by

$$\lambda_{s_1,r_k,s_2} \triangleq \lambda_{s_1,r_k} + \lambda_{r_k,s_2} = \left(\frac{N_0\varrho}{P}\right) \frac{\delta_{s_1}\delta_S\sigma^2_{s_1,r_k} + \delta_R\sigma^2_{s_2,r_k}}{\delta_{s_1}\delta_S\delta_R\sigma^2_{s_1,r_k}\sigma^2_{s_2,r_k}}. \tag{2.37}$$

Let $\rho_{1,k,2}$ be the correlation coefficient between $\bar{\gamma}_{r_k,s_1}$ and $\bar{\gamma}_{r_k,s_2}$, as determined by

$$\rho_{1,k,2} = \rho_{2,k,1} = \frac{\mathrm{Cov}(\bar{\gamma}_{r_k,s_1}, \bar{\gamma}_{r_k,s_2})}{\sqrt{\mathrm{Var}(\bar{\gamma}_{r_k,s_1})\mathrm{Var}(\bar{\gamma}_{r_k,s_2})}}, \quad 0 \leq \rho_{1,k,2}, \rho_{2,k,1} \leq 1, \tag{2.38}$$

where $\mathrm{Cov}(\bar{\gamma}_{r_k,s_1}, \bar{\gamma}_{r_k,s_2})$ is the covariance of $\bar{\gamma}_{r_k,s_1}$ and $\bar{\gamma}_{r_k,s_2}$. The moment generating function (MGF) of $\bar{\gamma}_{r_k}$ is given by [81]

$$\mathcal{M}_{\bar{\gamma}_{r_k}}(s) = \left(\frac{1}{1+s\chi_{k,1}}\right)\left(\frac{1}{1+s\chi_{k,2}}\right), \tag{2.39}$$

where $\chi_{k,1}$ and $\chi_{k,2}$ are the eigenvalues of matrix $A_k = D_kC_k$, where matrix D_k is given by

$$D_k = \begin{bmatrix} 1/\lambda_{s_1,r_k,s_2} & 0 \\ 0 & 1/\lambda_{s_2,r_k,s_1} \end{bmatrix}, \tag{2.40}$$

while matrix C_k is given by

$$C_k = \begin{bmatrix} 1 & \sqrt{\rho_{1,k,2}} \\ \sqrt{\rho_{2,k,1}} & 1 \end{bmatrix}. \tag{2.41}$$

It can be verified that the eigenvalues are given by

$$\chi_{k,1} = \frac{\lambda_{s_1,r_k,s_2} + \lambda_{s_2,r_k,s_1}}{2\lambda_{s_1,r_k,s_2}\lambda_{s_2,r_k,s_1}} - \sqrt{\left(\frac{\lambda_{s_1,r_k,s_2} + \lambda_{s_2,r_k,s_1}}{2\lambda_{s_1,r_k,s_2}\lambda_{s_2,r_k,s_1}}\right)^2 - \frac{(1-\rho_{1,k,2})}{\lambda_{s_1,r_k,s_2}\lambda_{s_2,r_k,s_1}}}, \tag{2.42a}$$

$$\chi_{k,2} = \frac{\lambda_{s_1,r_k,s_2} + \lambda_{s_2,r_k,s_1}}{2\lambda_{s_1,r_k,s_2}\lambda_{s_2,r_k,s_1}} + \sqrt{\left(\frac{\lambda_{s_1,r_k,s_2} + \lambda_{s_2,r_k,s_1}}{2\lambda_{s_1,r_k,s_2}\lambda_{s_2,r_k,s_1}}\right)^2 - \frac{(1-\rho_{1,k,2})}{\lambda_{s_1,r_k,s_2}\lambda_{s_2,r_k,s_1}}}. \tag{2.42b}$$

Using $\mathcal{M}_{\bar{\gamma}_{r_k}}(s) = s\mathcal{L}\{P_{\bar{\gamma}_{r_k}}\}$, the CDF of $\bar{\gamma}_{r_k}$ can be shown to be

$$P_{\bar{\gamma}_{r_k}}(\gamma) = 1 - \frac{\mu_{k,1}e^{-\gamma\mu_{k,2}} - \mu_{k,2}e^{-\gamma\mu_{k,1}}}{\mu_{k,1} - \mu_{k,2}}, \quad \gamma \geq 0, \tag{2.43}$$

where $\bar{\gamma}_{r_k}(\gamma)$ is verified to be a hypo-exponential random variable of two exponential random variables with rates $\mu_{k,1} = 1/\chi_{k,1}$ and $\mu_{k,2} = 1/\chi_{k,2}$ [82]. The PDF of $\bar{\gamma}_{r_k}$ is given by

$$p_{\bar{\gamma}_{r_k}}(\gamma) = \frac{\mu_{k,1}\mu_{k,2}}{\mu_{k,1} - \mu_{k,2}}\left(e^{-\gamma\mu_{k,2}} - e^{-\gamma\mu_{k,1}}\right), \quad \gamma \geq 0. \tag{2.44}$$

For the case of $N = 2$ relay nodes, the probability that relay node R_k has a greater sum SNR $\bar{\gamma}_{r_k}$ than node R_l for $k, l \in \{1, 2\}$ and $k \neq l$ is determined as

$$\begin{aligned}\Pr\left[\bar{\gamma}_{r_l} < \bar{\gamma}_{r_k}\right] &= \frac{\mu_{l,1}\mu_{l,2}}{\mu_{l,1}-\mu_{l,2}} \int_0^\infty \left(e^{-\gamma\mu_{2,l}} - e^{-\gamma\mu_{1,l}}\right) \Pr\left(\bar{\gamma}_{r_l} < \bar{\gamma}_{r_k} | \bar{\gamma}_{r_l} = \gamma\right)\, d\gamma \\ &= \left(\frac{\mu_{l,1}\mu_{l,2}}{\mu_{l,1}-\mu_{l,2}}\right)\left(\frac{\mu_{k,1}\mu_{k,2}}{\mu_{k,1}-\mu_{k,2}}\right)\left[\sum_{i=1}^{2} \frac{(-1)^i}{\mu_{k,i}}\left(\frac{\mu_{l,1}-\mu_{l,2}}{(\mu_{k,i}+\mu_{l,1})(\mu_{k,i}+\mu_{l,2})}\right)\right].\end{aligned} \tag{2.45}$$

In general, the probability that relay node R_l has the smallest SNR sum $\bar{\gamma}_{r_l}$ among the N relay nodes is obtained as

$$\Pr\left[\bar{\gamma}_{r_l} = \min_{k=1,\ldots,N} \bar{\gamma}_{r_k}\right] = \prod_{k=1}^{N}\left(\frac{\mu_{k,1}\mu_{k,2}}{\mu_{k,1}-\mu_{k,2}}\right) \int_0^\infty \left(e^{-\gamma\mu_{l,2}} - e^{-\gamma\mu_{l,1}}\right) \prod_{k=1,k\neq l}^{N}\left[\frac{e^{-\gamma\mu_{k,2}}}{\mu_{k,2}} - \frac{e^{-\gamma\mu_{k,1}}}{\mu_{k,1}}\right]\, d\gamma. \tag{2.46}$$

Thus, for $N = 3$, the approximate probability of relay node R_k to be selected is

$$\Pr\left[\bar{\gamma}_{r_k} = \max_{q=1,2,3} \bar{\gamma}_{r_q}\right] = \Pr\left[\bar{\gamma}_{r_k} > \bar{\gamma}_{r_q} > \bar{\gamma}_{r_l}\right] + \Pr\left[\bar{\gamma}_{r_k} > \bar{\gamma}_{r_l} > \bar{\gamma}_{r_q}\right], \tag{2.47}$$

for $k, q, l \in \{1, 2, 3\}$, and $k \neq q \neq l$. Also,

$$\begin{aligned}\Pr\left[\bar{\gamma}_{r_k} > \bar{\gamma}_{r_q} > \bar{\gamma}_{r_l}\right] &= \Pr\left[\bar{\gamma}_{r_k} > \bar{\gamma}_{r_q} | \bar{\gamma}_{r_l} = \min\{\bar{\gamma}_{r_k}, \bar{\gamma}_{r_q}, \bar{\gamma}_{r_l}\}\right] \cdot \Pr\left[\bar{\gamma}_{r_l} = \min\{\bar{\gamma}_{r_k}, \bar{\gamma}_{r_q}, \bar{\gamma}_{r_l}\}\right] \\ &= \Pr\left[\bar{\gamma}_{r_k} > \bar{\gamma}_{r_q}\right] \cdot \Pr\left[\bar{\gamma}_{r_l} = \min\{\bar{\gamma}_{r_k}, \bar{\gamma}_{r_q}, \bar{\gamma}_{r_l}\}\right],\end{aligned} \tag{2.48}$$

where $\Pr\left[\bar{\gamma}_{r_k} > \bar{\gamma}_{r_q}\right]$ and $\Pr\left[\bar{\gamma}_{r_l} = \min\{\bar{\gamma}_{r_k}, \bar{\gamma}_{r_q}, \bar{\gamma}_{r_l}\}\right]$ are defined in (2.45) and (2.46), respectively. Similarly,

$$\Pr\left[\bar{\gamma}_{r_k} > \bar{\gamma}_{r_l} > \bar{\gamma}_{r_q}\right] = \Pr\left[\bar{\gamma}_{r_k} > \bar{\gamma}_{r_l}\right] \cdot \Pr\left[\bar{\gamma}_{r_q} = \min\{\bar{\gamma}_{r_k}, \bar{\gamma}_{r_q}, \bar{\gamma}_{r_l}\}\right]. \tag{2.49}$$

For $N \geq 4$, the approximate probability of optimal node selection can be determined recursively as $\Pr\left[\bar{\gamma}_{r_k} = \max_{q=1,2,\ldots,N} \bar{\gamma}_{r_q}\right]$ for all the different inequality permutations. Notice that the eigenvalues derived in (2.42) can be written as

$$\chi_{k,1} = \left(\frac{P}{N_0\varrho}\right)(\psi_k - \zeta_k), \tag{2.50a}$$

$$\chi_{k,2} = \left(\frac{P}{N_0\varrho}\right)(\psi_k + \zeta_k). \tag{2.50b}$$

where

$$\psi_k = \frac{\Phi_{s_1,r_k,s_2} + \Phi_{s_2,r_k,s_1}}{2\Phi_{s_1,r_k,s_2}\Phi_{s_2,r_k,s_1}}, \tag{2.51}$$

and

$$\zeta_k = \sqrt{\psi_k^2 - \frac{(1-\rho_{1,k,2})}{\Phi_{s_1,r_k,s_2}\Phi_{s_2,r_k,s_1}}}. \tag{2.52}$$

It can be shown that

$$\Pr\left[\bar{\gamma}_{r_l} < \bar{\gamma}_{r_k}\right] = \frac{1}{\zeta_k}\left[\frac{\psi_k+\zeta_k}{(\psi_l^2-\zeta_l^2)+2\psi_l(\psi_k+\zeta_k)+(\psi_k+\zeta_k)^2}+\frac{\psi_k-\zeta_k}{(\psi_l^2-\zeta_l^2)+2\psi_l(\psi_k-\zeta_k)+(\psi_k-\zeta_k)^2}\right], \tag{2.53}$$

which is independent of P/N_0. The same result can be obtained for $\Pr\left[\bar{\gamma}_{r_l} = \min_{k=1,\ldots,N} \bar{\gamma}_{r_k}\right]$ in (2.46) and thus for $\Pr\left[\bar{\gamma}_{r_k} = \max_{q=1,2,\ldots,N} \bar{\gamma}_{r_q}\right]$, for $N \geq 3$.

2.4 Symbol Error Rate Analysis

The SER of the M-PSK modulation conditional on the channel statistics is given by [83]

$$P_{SER|\{h\}} = \frac{1}{\pi}\int_0^{(M-1)\pi/M} \exp\left(-\frac{b_{psk}\gamma}{\sin^2\theta}\right) d\theta, \tag{2.54}$$

where $b_{psk} = \sin^2(\pi/M)$ and γ is the SNR in terms of the channel coefficients. The moment generating function of γ is determined using

$$\mathcal{M}_\gamma(s) = \int_{-\infty}^{\infty} e^{-s\gamma} p_\gamma(\gamma)\, d\gamma, \tag{2.55}$$

where $p_\gamma(\gamma)$ is the PDF of γ. Therefore, the SER performance is obtained as

$$P_{SER} = \frac{1}{\pi}\int_0^{(M-1)\pi/M} \mathcal{M}_\gamma\left(\frac{b_{psk}}{\sin^2\theta}\right) d\theta. \tag{2.56}$$

2.4.1 TD-BD-AF Scheme

Approximate SER Performance

With the knowledge of the channel coefficients, source node S_1 combines all the received signals from each relay node with maximal-ratio-combining (MRC). Thus, the approximate instantaneous SNR at the output of the MRC detector at source node S_1 corresponding to symbol x_2 is given by [84]

$$\bar{\gamma}_{s_2} = \sum_{k=1}^{N} \bar{\gamma}_{r_k,s_2}, \tag{2.57}$$

where $\bar{\gamma}_{r_k,s_2}$ is defined in (2.17). The PDF of $\bar{\gamma}_{r_k,s_2}$ is given by [77]

$$p_{\bar{\gamma}_{r_k,s_2}}(\gamma) = 2\lambda_{s_2,r_k}\lambda_{r_k,s_1} e^{-\gamma(\lambda_{s_2,r_k}+\lambda_{r_k,s_1})} \times \left[\frac{\lambda_{s_2,r_k}+\lambda_{r_k,s_1}}{\sqrt{\lambda_{s_2,r_k}\lambda_{r_k,s_1}}} K_1\left(2\gamma\sqrt{\lambda_{s_2,r_k}\lambda_{r_k,s_1}}\right) + 2K_0\left(2\gamma\sqrt{\lambda_{s_2,r_k}\lambda_{r_k,s_1}}\right)\right], \quad \gamma \geq 0, \tag{2.58}$$

where $K_0(\cdot)$ and $K_1(\cdot)$ are the zeroth- and first-order modified Bessel functions of the second kind, respectively [80]. The MGF of $\bar{\gamma}_{r_k,s_2}$ has been determined in [77] as

$$\mathcal{M}_{\bar{\gamma}_{r_k,s_2}}(s) = \frac{16\lambda_{s_1,r_k}\lambda_{r_k,s_2}}{3(\lambda_{s_1,r_k}+\lambda_{r_k,s_2}+2\sqrt{\lambda_{s_1,r_k}\lambda_{r_k,s_2}}+s)^2}\times \left[\frac{4(\lambda_{s_1,r_k}+\lambda_{r_k,s_2}}{\lambda_{s_1,r_k}+\lambda_{r_k,s_2}+2\sqrt{\lambda_{s_1,r_k}\lambda_{r_k,s_2}}+s} + {}_2F_1\left(3,\frac{3}{2};\frac{5}{2};\frac{\lambda_{s_1,r_k}+\lambda_{r_k,s_2}-2\sqrt{\lambda_{s_1,r_k}\lambda_{r_k,s_2}}+s}{\lambda_{s_1,r_k}+\lambda_{r_k,s_2}+2\sqrt{\lambda_{s_1,r_k}\lambda_{r_k,s_2}}+s}\right)\times \right. \\ \left. {}_2F_1\left(2,\frac{1}{2};\frac{5}{2};\frac{\lambda_{s_1,r_k}+\lambda_{r_k,s_2}-2\sqrt{\lambda_{s_1,r_k}\lambda_{r_k,s_2}}+s}{\lambda_{s_1,r_k}+\lambda_{r_k,s_2}+2\sqrt{\lambda_{s_1,r_k}\lambda_{r_k,s_2}}+s}\right)\right], \tag{2.59}$$

where ${}_2F_1(\cdot,\cdot;\cdot;\cdot)$ is the hypergeometric function [80]. By substituting (2.59) into (2.56), the approximate SER of source node S_2 under the TD-BD-AF scheme is obtained as

$$\tilde{P}_{SER_2}^{\text{TD-BD-AF}} \approx \frac{1}{\pi}\int_0^{(M-1)\pi/M}\prod_{k=1}^{N}\mathcal{M}_{\bar{\gamma}_{r_k,s_2}}\left(\frac{b_{psk}}{\sin^2\theta}\right)d\theta. \tag{2.60}$$

2.4.2 Upper-Bound and Diversity Order Analysis

The expression for $\mathcal{M}_{\bar{\gamma}_{r_k,s_2}}(s)$ shown in (2.59) is difficult to manipulate, however, a simple closed-form MGF exists and is given by [56]

$$\mathcal{M}_{\bar{\gamma}_{r_k,s_2}}(s) = \frac{(\lambda_{s_1,r_k}-\lambda_{r_k,s_2})^2+(\lambda_{s_1,r_k}+\lambda_{r_k,s_2})s}{\omega^2} + \frac{2\lambda_{s_1,r_k}\lambda_{r_k,s_2}s}{\omega^3}\ln\frac{(\lambda_{s_1,r_k}+\lambda_{r_k,s_2}+s+\omega)^2}{4\lambda_{s_1,r_k}\lambda_{r_k,s_2}}, \tag{2.61}$$

where $\omega = \sqrt{(\lambda_{s_1,r_k}-\lambda_{r_k,s_2})^2+2(\lambda_{s_1,r_k}+\lambda_{r_k,s_2})s+s^2}$. At high SNR, the MGF in (2.61) can be approximated as [56]

$$\mathcal{M}_{\bar{\gamma}_{r_k,s_2}}(s) \approx \frac{\lambda_{s_1,r_k}+\lambda_{r_k,s_2}}{s} = \varrho\left(\frac{N_0}{P}\right)\frac{\delta_{r_k}\delta_R\sigma_{s_1,r_k}^2+\delta_{s_2}\delta_S\sigma_{s_2,r_k}^2}{s\delta_{s_2}\delta_S\delta_{r_k}\delta_R\sigma_{s_1,r_k}^2\sigma_{s_2,r_k}^2}. \tag{2.62}$$

Therefore, upon substitution of (2.62) for $k \in \{1,2,\ldots,N\}$ into (2.56), the upper-bound SER of source node S_2 under the TD-BD-AF scheme at high SNR can be approximated as

$$\bar{P}_{UB-SER_2}^{\text{TD-BD-AF}} \approx \Theta(N)\left(\frac{N_0}{P}\right)^N\prod_{k=1}^{N}\varrho\frac{\delta_{r_k}\delta_R\sigma_{s_1,r_k}^2+\delta_{s_2}\delta_S\sigma_{s_2,r_k}^2}{b_{psk}\delta_{s_2}\delta_S\delta_{r_k}\delta_R\sigma_{s_1,r_k}^2\sigma_{s_2,r_k}^2}, \tag{2.63}$$

where,

$$\Theta(N) = \frac{1}{\pi}\int_0^{(M-1)\pi/M}\left(\sin^2(\theta)\right)^N d\theta. \tag{2.64}$$

The diversity order is determined as $\Gamma_2^{\text{TD-BD-AF}} = -\lim_{SNR\to\infty}\frac{\log(\bar{P}_{UB-SER_2}^{\text{TD-BD-AF}})}{\log(SNR)}$, where $SNR = P/N_0$ [56]. It is evident that under the TD-BD-AF scheme, source node S_2 achieves a full diversity order of $\Gamma_2^{\text{TD-BD-AF}} = N$.

2.4.3 MA-BD-AF

With respect to the MA-BD-AF scheme, the derived instantaneous SNR γ_{s_2} in (2.28) is extremely difficult to manipulate and thus in this work, only the SER of source node S_2 conditional on the channel state information is presented in the form of

$$P^{\text{MA-BD-AF}}_{SER_2|\{h_{s_1,r_k},h_{s_2,r_k}\}_{k=1}^{N}}(\gamma_{s_2}) = \frac{1}{\pi}\int_0^{(M-1)\pi/M} \exp\left(-\frac{b_{psk}\gamma_{s_2}}{\sin^2\theta}\right) d\theta, \tag{2.65}$$

which can be numerically evaluated and averaged.

2.4.4 ORS-BD-AF

As the SER performance of the ORS-BD-AF scheme is also analytically untractable, the SER performance of node S_2 is obtained by substituting $\gamma_{r_{\text{ors},s_2}}$ in (2.33) into (2.56) and then numerically evaluating it.

2.4.5 SRS-BD-AF

Finding an approximate SER expression for the performance of the SRS-BD-AF is difficult due to the correlation between the scaled harmonic mean random variables $\bar{\gamma}_{r_k,s_1}$ and $\bar{\gamma}_{r_k,s_2}$, $\forall k \in \{1,2,\ldots,N\}$ [72][78]. In addition, the selected relay node might not necessarily result in the maximum SNR value $\bar{\gamma}_{r_{\text{srs}},s_j}$ to source node S_j. Alternatively, the SER performance of source node S_2 (and similarly of node S_1) is bounded as

$$P^{\text{SRS-BD-AF}}_{LB-SER_2} \leq P^{\text{SRS-BD-AF}}_{SER_2} \leq P^{\text{SRS-BD-AF}}_{UB-SER_2}, \tag{2.66}$$

where $P^{\text{SRS-BD-AF}}_{LB-SER_2}$ and $P^{\text{SRS-BD-AF}}_{UB-SER_2}$ are lower- and upper-bound SER performances.

Lower-Bound SER Performance

A lower-bound (LB) SER performance of node S_2 is obtained by considering a best-case scenario on relay selection. This happens when the relay selection scheme always selects the relay node with the highest received SNR value for source node S_2. Considering source node S_2, the LB relay selection is

$$r_{LB_2} = \arg\max_{k=1,2,\ldots,N}\{\mathcal{R}_{s_2}(\gamma_{r_k,s_2})\} = \arg\max_{k=1,2,\ldots,N}\gamma_{r_k,s_2}, \tag{2.67}$$

where γ_{r_k,s_2} is defined in (2.16) with $P_{r_k} = P_R$. Approximating γ_{r_k,s_2} as $\bar{\gamma}_{r_k,s_2}$ (see (2.17)), the MGF of $\bar{\gamma}_{r_{LB_2}}$ can be determined using $\mathcal{M}_{\bar{\gamma}_{r_{LB_2}}}(s) = s\mathcal{L}\{P_{\bar{\gamma}_{r_{LB_2}}}(\gamma)\}$, where the CDF of $\bar{\gamma}_{r_{LB_2}}$ is obtained as

$$P_{\bar{\gamma}_{r_{LB_2}}}(\gamma) = \Pr\left[\max_{k=1,\ldots,N}\bar{\gamma}_{r_k,s_2} < \gamma\right] = \prod_{k=1}^{N} P_{\bar{\gamma}_{r_k,s_2}}(\gamma) = \prod_{k=1}^{N}\left(1 - e^{-\gamma\lambda_{s_2,r_k,s_1}}\right). \tag{2.68}$$

Thus, by expanding the product term in (2.68), the MGF is shown to be

$$\mathcal{M}_{\bar{\gamma}_{r_{LB_2}}}(s) = 1 - \sum_{k=1}^{N} \frac{s}{s + \lambda_{s_2,r_k,s_1}} + \cdots + \frac{(-1)^N s}{s + \sum_{k=1}^{N} \lambda_{s_2,r_k,s_1}}. \tag{2.69}$$

Thus, the approximate lower-bound SER performance is given by

$$\tilde{P}_{LB-SER_2}^{\text{SRS-BD-AF}} \approx \frac{1}{\pi} \int_0^{(M-1)\pi/M} \left(1 - \sum_{k=1}^{N} \frac{\frac{Pb_{PSK}}{\sin^2(\theta) N_0 \varrho}}{\frac{Pb_{PSK}}{\sin^2(\theta) N_0 \varrho} + \Phi_{s_2,r_k,s_1}} + \cdots + \frac{(-1)^N \frac{Pb_{PSK}}{\sin^2(\theta) N_0 \varrho}}{\frac{Pb_{PSK}}{\sin^2(\theta) N_0 \varrho} + \sum_{k=1}^{N} \Phi_{s_2,r_k,s_1}} \right) d\theta, \tag{2.70}$$

where

$$\Phi_{s_2,r_k,s_1} = \frac{\delta_{s_2} \delta_S \sigma_{s_2,r_k}^2 + \delta_R \sigma_{s_1,r_k}^2}{\delta_{s_2} \delta_S \delta_R \sigma_{s_1,r_k}^2 \sigma_{s_2,r_k}^2}. \tag{2.71}$$

Diversity Order Analysis of Lower-Bound SER Performance

The PDF of $\bar{\gamma}_{r_{LB_2}}$ is obtained by differentiating $P_{\bar{\gamma}_{r_{LB_2}}}(\gamma)$ in (2.68), yielding

$$p_{\bar{\gamma}_{r_{LB_2}}}(\gamma) = \sum_{m=1}^{N} p_{\bar{\gamma}_{r_m,s_2}}(\gamma) \prod_{k=1,k\neq m}^{N} \left(1 - e^{-\gamma \lambda_{s_2,r_k,s_1}} \right). \tag{2.72}$$

At high SNR, the approximation $e^x \simeq (1 + x)$ when $x \to 0$ is used in the PDF of $\bar{\gamma}_{r_{LB_2}}$, giving

$$p_{\bar{\gamma}_{r_{LB_2}}}(\gamma) \approx \sum_{m=1}^{N} \lambda_{s_2,r_m,s_1} (1 - \gamma \lambda_{s_2,r_m,s_1}) \gamma^{N-1} \prod_{k=1,k\neq m}^{N} \lambda_{s_2,r_k,s_1}. \tag{2.73}$$

Therefore, the MGF of $\bar{\gamma}_{r_{LB_2}}$ can be approximated as

$$\bar{\mathcal{M}}_{\bar{\gamma}_{r_{LB_2}}}(s) \approx N! \left(\frac{N_0 \varrho}{sP} \right)^N \prod_{k=1}^{N} \Phi_{s_2,r_k,s_1}. \tag{2.74}$$

Hence, the approximation of the lower-bound SER performance at high SNR is shown to be

$$\bar{P}_{LB-SER_2}^{\text{SRS-BD-AF}} \approx \left(\frac{N_0}{P} \right)^N \frac{N! \Theta(N) \varrho^N}{b_{PSK}^N} \prod_{k=1}^{N} \Phi_{s_2,r_k,s_1}, \tag{2.75}$$

where $\Theta(N)$ is defined in (2.64). The diversity order is determined as $\Gamma_{LB_2}^{\text{SRS-BD-AF}} = N$. A similar result can be derived for node S_1.

Upper-Bound SER Performance

To derive an upper-bound (UB) SER performance relative to source node S_2, consider the scenario where the—exponentially distributed—SNR terms, $\bar{\gamma}_{r_k,s_2}$ for $k \in \{1, 2, \ldots, N\}$ are independent and identically distributed with rate defined by $\lambda_{s_2,r_{\max},s_2} = \max_{k=1,\ldots,N} \lambda_{s_2,r_k,s_1}$, which corresponds to the relay with the minimum SNR value. Thus, the CDF of $\bar{\gamma}_{s_2,r_{\max},s_1}$ is given by $P_{\bar{\gamma}_{s_2,r_{\max},s_1}}(\gamma) = 1 - e^{\gamma\lambda_{s_2,r_{\max},s_1}}$, where $\lambda_{s_2,r_{\max},s_1} = \left(\frac{N_0\varrho}{P}\right)\Phi_{s_2,r_{\max},s_1}$. Also, the CDF of the selected relay with respect to source node S_2 is obtained as

$$P_{\bar{\gamma}_{UB_2}}(\gamma) = \left(P_{\bar{\gamma}_{s_2,r_{\max},s_1}}(\gamma)\right)^N, \tag{2.76}$$

while the MGF is given by

$$\mathcal{M}_{\bar{\gamma}_{UB_2}}(s) = 1 + \sum_{k=1}^{N} \binom{N}{k} \frac{(-1)^k s}{s + k \cdot \lambda_{s_2,r_{\max},s_1}}. \tag{2.77}$$

The approximate upper-bound SER performance of source node S_2 is obtained by substituting (2.77) into (2.56), yielding

$$\tilde{P}_{UB-SER_2}^{\text{SRS-BD-AF}} \approx \frac{1}{\pi}\int_0^{(M-1)\pi/M} \left(1 + \sum_{k=1}^{N} \binom{N}{k} \frac{(-1)^k \frac{Pb_{PSK}}{\sin^2(\theta)N_0\varrho}}{\frac{Pb_{PSK}}{\sin^2(\theta)N_0\varrho} + k \cdot \Phi_{s_2,r_{\max},s_1}}\right) d\theta. \tag{2.78}$$

Diversity Order Analysis of Upper-Bound SER Performance

The PDF of the selected relay relative to source node S_2 is obtained by differentiating the CDF in (2.76), yielding

$$p_{\bar{\gamma}_{UB_2}}(\gamma) = N\left(P_{\bar{\gamma}_{s_2,r_{\max},s_1}}(\gamma)\right)^{N-1} p_{\bar{\gamma}_{s_2,r_{\max},s_1}}(\gamma), \tag{2.79}$$

where $p_{\bar{\gamma}_{UB_2}}(\gamma) = \lambda_{s_2,r_{\max},s_1} e^{-\gamma\lambda_{s_2,r_{\max},s_1}}$. At high SNR, $p_{\bar{\gamma}_{UB_2}}(\gamma)$ is approximated as

$$p_{\bar{\gamma}_{UB_2}}(\gamma) \approx N \cdot \lambda_{s_2,r_{\max},s_1}(\gamma\lambda_{s_2,r_{\max},s_1})^{N-1}(1 - \gamma\lambda_{s_2,r_{\max},s_1}). \tag{2.80}$$

with MGF given by

$$\bar{\mathcal{M}}_{\bar{\gamma}_{UB_2}}(s) \approx N! \left(\frac{N_0\varrho}{sP}\right)^N \left(\Phi_{s_2,r_{\max},s_1}\right)^N. \tag{2.81}$$

Hence, the approximate upper-bound SER performance at high SNR is determined as

$$\bar{P}_{UB-SER_2}^{\text{SRS-BD-AF}} \approx \left(\frac{N_0}{P}\right)^N \frac{N!\Theta(N)\varrho^N}{b_{PSK}^N} \left(\Phi_{s_2,r_{\max},s_1}\right)^N. \tag{2.82}$$

Clearly, the diversity order is obtained as $\Gamma_{UB_2}^{\text{SRS-BD-AF}} = N$. It is noteworthy that the derived SER upper- and lower-bounds apply to both the ORS-BD-AF and SRS-BD-AF schemes, as the upper-bound represents the worst-case scenario on relay selection, while the lower-bound represents the best-case scenario for node S_2.

2.5 Power Allocation

In this section, the sum-of-rates maximizing relay power allocation for the TD-BD-AF and MA-BD-AF schemes is studied.

2.5.1 TD-BD-AF

Notice that the achievable rate in (2.22) can be re-expressed as

$$\mathcal{R}_{s_2}^{\text{TD-BD-AF}}(\gamma_{s_2}) = \frac{1}{N+1}\log_2\left(1+\sum_{k=1}^{N}\frac{P_{r_k}\Lambda_{s_2,r_k}}{P_{r_k}+\Upsilon_{s_{2,1},r_k}}\right), \tag{2.83}$$

where

$$\Lambda_{s_2,r_k} = \frac{P_{s_2}|h_{s_2,r_k}|^2}{N_0\varrho}, \tag{2.84}$$

and

$$\Upsilon_{s_{2,1},r_k} = \frac{P_{s_2}|h_{s_2,r_k}|^2+N_0\varrho}{|h_{s_1,r_k}|^2}. \tag{2.85}$$

The rate function in (2.83) can be verified to be a strictly concave and increasing function in $P_{r_k}, \forall k \in \{1,2,\ldots,N\}$. Thus, the sum-of-rates maximizing optimal relay power allocation is formulated as

$$\begin{aligned} \max_{P_{r_k}\geq 0} \quad & \mathcal{R}_{s_1}^{\text{TD-BD-AF}} + \mathcal{R}_{s_2}^{\text{TD-BD-AF}} \\ \text{s.t.} \quad & \sum_{k=1}^{N} P_{r_k} \leq P_R, \end{aligned} \tag{2.86}$$

which is a convex optimization problem that is efficiently solved using any standard convex optimization algorithm [85].

2.5.2 MA-BD-AF

The achievable rate of source node S_j for $j \in \{1,2\}$ under the MA-BD-AF scheme is re-expressed as

$$\mathcal{R}_{s_j}^{\text{MA-BD-AF}}(\gamma_{s_j}) = \frac{1}{2}\log_2\left(1+\frac{\sum_{k=1}^{N}P_{r_k}\xi_{s_j,r_k}}{1+\sum_{k=1}^{N}P_{r_k}\zeta_{s_j,r_k}}\right), \tag{2.87}$$

where

$$\xi_{s_j,r_k} = \frac{P_{s_j}|h_{s_1,r_k}|^2|h_{s_2,r_k}|^2}{N_0\varrho(P_{s_j}|h_{s_j,r_k}|^2+N_0\varrho)}, \tag{2.88}$$

and ζ_{s_j,r_k} for $j \in \{1,2\}$ is given by

$$\zeta_{s_1,r_k} = \frac{|h_{s_2,r_k}|^2}{P_{s_1}|h_{s_1,r_k}|^2 + N_0\varrho}, \text{ and } \zeta_{s_2,r_k} = \frac{|h_{s_1,r_k}|^2}{P_{s_2}|h_{s_2,r_k}|^2 + N_0\varrho}. \tag{2.89}$$

Now, let $\boldsymbol{\xi}_{s_j} = \left[\xi_{s_j,r_1}, \ldots, \xi_{s_j,r_N}\right]^T$, $\boldsymbol{\zeta}_{s_j} = \left[\zeta_{s_j,r_1}, \ldots, \zeta_{s_j,r_N}\right]^T$, and $\boldsymbol{P}_r = [P_{r_1}, \ldots, P_{r_N}]^T$, for $N \geq 2$. In turn, the instantaneous SNR of each source node S_j is given by

$$\gamma_{s_j} = \frac{\boldsymbol{\xi}_{s_j}^T \boldsymbol{P}_r}{1 + \boldsymbol{\zeta}_{s_j}^T \boldsymbol{P}_r}, \tag{2.90}$$

which is a ratio of two linear functions in continuous decision variables (i.e. the relay powers P_{r_k}'s for $k \in \{1,2,\ldots,N\}$). It should also be clear that $1 + \boldsymbol{\zeta}_{s_j}^T \boldsymbol{P}_r > 0, \forall j \in \{1,2\}$.

The sum-of-rates maximizing optimal relay power allocation problem under the MA-BD-AF scheme is formulated as

$$\begin{aligned} \text{(OPT):} \qquad \max_{P_{r_k} \geq 0} \quad & \sum_{j=1}^{2} \frac{1}{2} \log_2 \left(1 + \frac{\boldsymbol{\xi}_{s_j}^T \boldsymbol{P}_r}{1 + \boldsymbol{\zeta}_{s_j}^T \boldsymbol{P}_r}\right) \\ \text{s.t.} \quad & \sum_{k=1}^{N} P_{r_k} \leq P_R, \end{aligned} \tag{2.91}$$

Such an optimization problem is non-convex [86], although the feasible region is a nonempty, compact convex set. Thus, problem (2.91) generally has one or more local optimal solutions that are not globally optimal. However, by using the inequality in (2.31), a suboptimal solution to problem (2.91) is obtained by alternatively solving

$$\begin{aligned} \text{(S-OPT):} \qquad \max_{P_{r_k} \geq 0} \quad & \frac{\boldsymbol{\xi}_{s_1}^T \boldsymbol{P}_r}{1 + \boldsymbol{\zeta}_{s_1}^T \boldsymbol{P}_r} + \frac{\boldsymbol{\xi}_{s_2}^T \boldsymbol{P}_r}{1 + \boldsymbol{\zeta}_{s_2}^T \boldsymbol{P}_r} \\ \text{s.t.} \quad & \sum_{k=1}^{N} P_{r_k} \leq P_R, \end{aligned} \tag{2.92}$$

and then substituting the solution back into (2.87). In (2.92), the objective function is the sum of two linear fractional functions. The SNR term γ_{s_j} when defined over a convex set is both pseudoconvex and pseudoconcave (or quasimonotonic [87]) [88]. Moreover, the sum of quasimonotonic functions is, in general, neither quasiconvex nor quasiconcave [89] [90]. In addition, the maximization of the sum of linear fractional functions is in general known to be NP-complete [91]. Therefore, a simplified, yet accurate formulation that lends problem (2.92) to feasible implementation in convex optimization packages is highly desirable. To do so, each fraction (or equivalently SNR term) γ_{s_j} can be transformed into [92]

$$\gamma_{s_j}(\boldsymbol{P}_r) = \left(\boldsymbol{\xi}_{s_j}^T - \gamma_{s_j}(\boldsymbol{P}_r)\boldsymbol{\zeta}_{s_j}^T\right)\boldsymbol{P}_r. \tag{2.93}$$

Such a transformation allows us to treat each function $\gamma_{s_j}(\boldsymbol{P}_r)$ as a parameter γ_{s_j} that is varied and thus, globally solve problem (2.92) by convex parametric programming techniques. Also, the objective function in (2.92) is formulated as a bi-parameter linear function

$$\sum_{j=1}^{2} \frac{\boldsymbol{\xi}_{s_j}^T \boldsymbol{P}_r}{1+\boldsymbol{\zeta}_{s_j}^T \boldsymbol{P}_r} = \sum_{j=1}^{2} \left(\boldsymbol{\xi}_{s_j}^T - \gamma_{s_j} \boldsymbol{\zeta}_{s_j}^T\right) \boldsymbol{P}_r. \tag{2.94}$$

Now, let $\boldsymbol{\gamma} = [\gamma_{s_1}, \gamma_{s_2}]^T$ be a parameter vector and also define

$$\mathcal{G}(\boldsymbol{\gamma}) = \max_{P_{r_k} \geq 0} \left[\sum_{j=1}^{2} \left(\boldsymbol{\xi}_{s_j}^T - \gamma_{s_j} \boldsymbol{\zeta}_{s_j}^T\right) \boldsymbol{P}_r \right], \tag{2.95}$$

which is a convex, monotone non-increasing function in $\boldsymbol{\gamma}$. Therefore, solving problem (2.92) corresponds to finding the vector $\boldsymbol{\gamma}$ that satisfies

$$\mathcal{E}(\boldsymbol{\gamma}) = \mathcal{G}(\boldsymbol{\gamma}) - \mathbf{1}^T \boldsymbol{\gamma} = 0, \tag{2.96}$$

where $\mathbf{1}$ is the 2×1 all-ones vector. Combining (2.95) and (2.96), the optimization problem in (2.92) is reformulated into the following linear programming problem

$$\begin{aligned} \max_{\boldsymbol{\gamma}, \boldsymbol{P}_r} \quad & \sum_{j=1}^{2} \left(\boldsymbol{\xi}_{s_j}^T - \gamma_{s_j} \boldsymbol{\zeta}_{s_j}^T\right) \boldsymbol{P}_r \\ \text{s.t.} \quad & \sum_{k=1}^{N} P_{r_k} \leq P_R, \\ & \gamma_{s_j} \geq \left(\boldsymbol{\xi}_{s_j}^T - \gamma_{s_j} \boldsymbol{\zeta}_{s_j}^T\right) \boldsymbol{P}_r, \quad j \in \{1,2\}, \\ & P_{r_k} \geq 0, \qquad\qquad\qquad\quad k \in \{1,2,\ldots,N\}. \end{aligned} \tag{2.97}$$

Hence, parameterizing problem (2.92) has led to a linearization of the non-linear objective function about the optimal solution, and thus problem (2.97) is solved efficiently (i.e. in polynomial-time).

Due to the convexity of the feasible region of the reformulated problem, the optimal solution must exist on the edge of the feasible region and hence, maximum and minimum values at the extreme points exist [88] [93]. It is straightforward to verify that when $\boldsymbol{P}_r = [0, \ldots, 0]^T$, then the objective function in (2.97) attains its minimum value. It can be further verified that the objective function is continuous and strictly monotonically increasing in P_R. Therefore, the total relay power constraint is always met (i.e. $\sum_{k=1}^{N} P_{r_k} = P_R$). Based on the discussion thus far, the following theorem is established.

Theorem 2.1: The suboptimal sum-of-rates maximizing relay power allocation under the MA-BD-AF scheme is equivalent to the suboptimal relay selection under the SRS-BD-AF scheme, i.e.

$$\max_{\sum_{k=1}^{N} P_{r_k} = P_R} \sum_{j=1}^{2} \frac{\boldsymbol{\xi}_{s_j}^T \boldsymbol{P}_r}{1+\boldsymbol{\zeta}_{s_j}^T \boldsymbol{P}_r} = \max_{k=1,2,\ldots,N} \left(\frac{P_R \xi_{s_1,r_k}}{1+P_R \zeta_{s_1,r_k}} + \frac{P_R \xi_{s_2,r_k}}{1+P_R \zeta_{s_2,r_k}} \right). \tag{2.98}$$

Proof: Define the following Lagrangian problem

$$\mathcal{L}\left(\lambda,\{\upsilon_{r_k}\}_{k=1}^{N}\right)=-\sum_{j=1}^{2}\frac{\boldsymbol{\xi}_{s_j}^{T}\boldsymbol{P}_r}{1+\boldsymbol{\zeta}_{s_j}^{T}\boldsymbol{P}_r}+\lambda\left(\sum_{k=1}^{N}P_{r_k}-P_R\right)-\sum_{k=1}^{N}\upsilon_{r_k}P_{r_k}. \tag{2.99}$$

The Karush-Kuhn-Tucker (KKT) conditions can be determined as [94]

$$\begin{aligned}-\sum_{j=1}^{2}\frac{\xi_{s_j,r_l}+\sum_{k=1}^{N}P_{r_k}\left(\xi_{s_j,r_l}\zeta_{s_j,r_k}-\xi_{s_j,r_k}\zeta_{s_j,r_l}\right)}{\left(1+\sum_{k=1}^{N}P_{r_k}\zeta_{s_j,r_k}\right)^2}+\lambda&=\upsilon_{r_l},\\ \lambda\left(\sum_{k=1}^{N}P_{r_k}-P_R\right)&=0,\\ \upsilon_{r_l}P_{r_l}&=0,\quad\forall l\in\{1,2,\ldots,N\},\end{aligned} \tag{2.100}$$

where $\lambda\geq 0$ and $\upsilon_{r_l}\geq 0,\forall l\in\{1,2,\ldots,N\}$ are the dual variables associated with the total power constraint and relay powers' positivity, respectively. As discussed earlier, $\sum_{k=1}^{N}P_{r_k}=P_R$, and thus, $\lambda>0$. If $P_{r_l}>0$ for $l\in\{1,2,\ldots,N\}$, then

$$\sum_{j=1}^{2}\frac{\xi_{s_j,r_l}+\sum_{k=1}^{N}P_{r_k}\left(\xi_{s_j,r_l}\zeta_{s_j,r_k}-\xi_{s_j,r_k}\zeta_{s_j,r_l}\right)}{\left(1+\sum_{k=1}^{N}P_{r_k}\zeta_{s_j,r_k}\right)^2}=\lambda. \tag{2.101}$$

Thus,

$$\sum_{j=1}^{2}\frac{\xi_{s_j,r_l}+\sum_{k=1}^{N}P_{r_k}\left(\xi_{s_j,r_l}\zeta_{s_j,r_k}-\xi_{s_j,r_k}\zeta_{s_j,r_l}\right)}{\left(1+\sum_{k=1}^{N}P_{r_k}\zeta_{s_j,r_k}\right)^2}=\sum_{j=1}^{2}\frac{\xi_{s_j,r_q}+\sum_{k=1}^{N}P_{r_k}\left(\xi_{s_j,r_q}\zeta_{s_j,r_k}-\xi_{s_j,r_k}\zeta_{s_j,r_q}\right)}{\left(1+\sum_{k=1}^{N}P_{r_k}\zeta_{s_j,r_k}\right)^2}, \tag{2.102}$$

for $q\in\{1,2,\ldots,N\}$ and $q\neq l$. Rearranging (2.102), yields

$$\frac{\left(1+\sum_{k=1}^{N}P_{r_k}\zeta_{s_1,r_k}\right)^2}{\left(1+\sum_{k=1}^{N}P_{r_k}\zeta_{s_2,r_k}\right)^2}=-\frac{\left(\xi_{s_1,r_l}-\xi_{s_1,r_q}\right)+\sum_{k=1}^{N}P_{r_k}\left(\left(\xi_{s_1,r_l}-\xi_{s_1,r_q}\right)\zeta_{s_1,r_k}-\left(\zeta_{s_1,r_l}-\zeta_{s_1,r_q}\right)\xi_{s_1,r_k}\right)}{\left(\xi_{s_2,r_l}-\xi_{s_2,r_q}\right)+\sum_{k=1}^{N}P_{r_k}\left(\left(\xi_{s_2,r_l}-\xi_{s_2,r_q}\right)\zeta_{s_2,r_k}-\left(\zeta_{s_2,r_l}-\zeta_{s_2,r_q}\right)\xi_{s_2,r_k}\right)}. \tag{2.103}$$

Since the left-hand-side term is a positive constant, then the right-hand-side expression cannot simultaneously be satisfied for any two relay powers R_l and R_q for $l,q\in\{1,2,\ldots,N\}$ and $l\neq q$. Hence, (2.103) is satisfied for only one relay and that relay is allocated the total relay power P_R. □

Based on Theorem 2.1, the MA-BD-AF scheme reduces to the SRD-BD-AF scheme by allocating the total relay power P_R to the selected relay node. This means that the proposed suboptimal relay selection can be achieved by enumerating all the N approximate sum SNR values alternatively (i.e. setting $P_{r_1}=P_R$, then $P_{r_2}=P_R$ and so on) and then selecting the one with the maximum approximate sum SNR value.

2.6 Timing Synchronization Analysis

So far, the analysis of the different bi-directional relaying schemes assumed perfect timing synchronization of signal transmissions. In practice, perfect timing synchronization for geographically distributed nodes is challenging. Hence, in this section, the effect of timing synchronization errors on the SER performance as well as the achievable rate of the TD-BD-AF, MA-BD-AF and RS-BD-AF schemes is evaluated. With respect to the TD-BD-AF and RS-BD-AF schemes, synchronization in the cooperation phase is not of major issue as only one relay node is transmitting at any given time-slot. This in turn implies that these two schemes are mainly affected by the timing synchronization errors in the broadcasting phase, which propagate to the cooperation phase, affecting the SNR at the receiving ends and resulting in intersymbol interference (ISI) and SNR loss. On the other hand, timing synchronization errors in the MA-BD-AF scheme could also occur in the cooperation phase and this is due to the simultaneous transmissions of the intermediate relay nodes. In what follows, it is assumed that nodes within the network are synchronized in frequency.

2.6.1 Signal Model for TD-BD-AF

The received signal at relay node R_k during the broadcasting phase is given by

$$\tilde{y}_{r_k}(t) = \sum_{l=-\infty}^{\infty} \left(\sum_{i=1}^{2} \sqrt{P_{s_i}} h_{s_i,r_k} x_i(l) c_i(t - lT_s - \tau_{s_i,r_k}) \right) + n_{r_k}(t), \tag{2.104}$$

where $\tau_{s_i,r_k} \in [0, T_s)$ for $i \in \{1, 2\}$ is the normalized timing offset between source S_i and relay node R_k. In this work, only the first-order ISI terms are considered as higher-order side-lobes are assumed to have negligible effect, yielding

$$\tilde{y}_{r_k}(t) = \sum_{l=-1}^{1} \left(\sum_{i=1}^{2} \sqrt{P_{s_i}} h_{s_i,r_k} x_i(l) c_i(t - lT_s - \tau_{s_i,r_k}) \right) + n_{r_k}(t), \tag{2.105}$$

where the propagation delays and oscillator mismatches are assumed to remain constant during each time-slot but vary from one time-slot to another [95]. Relay node R_k employs a matched-filter bank with each filter being matched to each source node's symbol time, sampled at $t = lT_s + \tau_{s_j,r_k}$ for $j \in \{1, 2\}$. Since each source node transmits asynchronously with respect to the other, the sampled received signal at end of the l^{th} symbol interval at relay node R_k is expressed as [96] [97]

$$\tilde{y}_{r_k,s_j}(l) = \int_{-\infty}^{\infty} \tilde{y}_{r_k}(t) c_j^*(t - lT_s - \tau_{s_j,r_k}) dt. \tag{2.106}$$

Without loss of generality, the random time delays between the source nodes and relay node R_k are ordered such that $0 \leq \tau_{s_1,r_k} \leq \tau_{s_2,r_k} < T_s$. The observation window of relay node R_k spans from the most recently received $(l-1)st$ symbol of source node S_2 to the end of the first received $(l+1)$ symbol of source node S_1 (i.e. $[(l-1)T_s + \tau_{s_1,r_k}, (l+1)T_s + \tau_{s_2,r_k}]$).

Let $\tilde{\boldsymbol{R}}_{r_k}(l)$ be the 2×2 matrix whose partial correlation entries are modeled for $l = 1$, $l = 0$, and $l = -1$ as [98] [99]

$$\tilde{\rho}^{(1)}_{i,r_k,j} = \begin{cases} \frac{1}{T_s}\int_{\tau_{s_j,r_k}}^{\tau_{s_i,r_k}} c_i(t-\tau_{s_i,r_k})c_j^*(t-\tau_{s_j,r_k})\,dt = \rho_{i,j}\left(\frac{\tau_{s_i,r_k}-\tau_{s_j,r_k}}{T_s}\right), & \tau_{s_i,r_k} > \tau_{s_j,r_k} \\ 0, & \text{otherwise} \end{cases}, \tag{2.107}$$

$$\begin{aligned} \tilde{\rho}^{(0)}_{i,r_k,j} &= \frac{1}{T_s}\int_{\max(\tau_{s_i,r_k},\tau_{s_j,r_k})}^{\min(\tau_{s_i,r_k},\tau_{s_j,r_k})+T_s} c_i(t-\tau_{s_i,r_k})c_j^*(t-\tau_{s_j,r_k})\,dt \\ &= \begin{cases} \rho_{i,j}\left(1-\frac{\tau_{s_i,r_k}-\tau_{s_j,r_k}}{T_s}\right), & \tau_{s_i,r_k} \geq \tau_{s_j,r_k} \\ \rho_{i,j}\left(1-\frac{\tau_{s_j,r_k}-\tau_{s_i,r_k}}{T_s}\right), & \tau_{s_i,r_k} < \tau_{s_j,r_k} \end{cases}, \end{aligned} \tag{2.108}$$

and

$$\tilde{\rho}^{(-1)}_{i,r_k,j} = \begin{cases} \frac{1}{T_s}\int_{\tau_{s_i,r_k}}^{\tau_{s_j,r_k}} c_i(t-\tau_{s_i,r_k})c_j^*(t-\tau_{s_j,r_k})\,dt = \rho_{i,j}\left(\frac{\tau_{s_j,r_k}-\tau_{s_i,r_k}}{T_s}\right), & \tau_{s_i,r_k} < \tau_{s_j,r_k} \\ 0, & \text{otherwise} \end{cases}, \tag{2.109}$$

where $\rho_{i,j} = \rho, \forall i \neq j$. Furthermore, the time-offsets are uniformly distributed as $(\tau_{s_i,r_k} - \tau_{s_j,r_k}) \sim U\left[-\Delta T_s/2, \Delta T_s/2\right]$, where $\Delta T_s \in [0, T_s)$. Thus, the correlation matrix $\tilde{\boldsymbol{R}}_{r_k}(0)$ is expressed as

$$\tilde{\boldsymbol{R}}_{r_k}(0) = \begin{bmatrix} \tilde{\rho}^{(0)}_{1,r_k,1} & \tilde{\rho}^{(0)}_{1,r_k,2} \\ \tilde{\rho}^{(0)}_{2,r_k,1} & \tilde{\rho}^{(0)}_{2,r_k,2} \end{bmatrix}, \tag{2.110}$$

where it should be noted that $\tilde{\rho}^{(0)}_{j,r_k,j} = 1, \forall j \in \{1,2\}$. Moreover, matrix $\tilde{\boldsymbol{R}}_{r_k}(1)$ is given by

$$\tilde{\boldsymbol{R}}_{r_k}(1) = \begin{bmatrix} 0 & \tilde{\rho}^{(1)}_{1,r_k,2} \\ 0 & 0 \end{bmatrix}, \tag{2.111}$$

and $\tilde{\boldsymbol{R}}_{r_k}(1) = \tilde{\boldsymbol{R}}^T_{r_k}(-1)$. For the synchronous case where all the source nodes's symbols are perfectly aligned (i.e. $\tau_{s_j,r_k} - \tau_{s_j,r_k} = 0, \forall j \in \{1,2\}$), then $\tilde{\boldsymbol{R}}_{r_k}(l)$ for $l \in \{-1,1\}$ simplifies to the all-zeros matrix and $\tilde{\boldsymbol{R}}_{r_k}(0) = \boldsymbol{R}$. Now, the received signal in vector form is expressed as

$$\tilde{\boldsymbol{\mathcal{Y}}}_{r_k}(l) = \tilde{\boldsymbol{R}}_{r_k}(1)\boldsymbol{A}_{r_k}\boldsymbol{x}(l-1) + \tilde{\boldsymbol{R}}_{r_k}(0)\boldsymbol{A}_{r_k}\boldsymbol{x}(l) + \tilde{\boldsymbol{R}}_{r_k}(-1)\boldsymbol{A}_{r_k}\boldsymbol{x}(l+1) + \tilde{\boldsymbol{n}}_{r_k}(l), \tag{2.112}$$

where $\tilde{\boldsymbol{\mathcal{Y}}}_{r_k}(l) = \left[\tilde{\mathcal{Y}}_{r_k,s_1}(l), \tilde{\mathcal{Y}}_{r_k,s_2}(l)\right]^T$, $\boldsymbol{x}(l+\varsigma) = [x_1(l+\varsigma), x_2(l+\varsigma)]^T$ for $\varsigma \in \{-1,0,1\}$, and $\tilde{\boldsymbol{n}}_{r_k}(l) = [\tilde{n}_{r_k,s_1}(l), \tilde{n}_{r_k,s_2}(l)]^T$ with variance obtained as

$$E\left[\tilde{\boldsymbol{n}}_{r_k}(l)\tilde{\boldsymbol{n}}^H_{r_k}(l-\varsigma)\right] = \begin{cases} N_0\tilde{\boldsymbol{R}}_{r_k}(-1), & \text{if } \varsigma = -1 \\ N_0\tilde{\boldsymbol{R}}_{r_k}(0), & \text{if } \varsigma = 0 \\ N_0\tilde{\boldsymbol{R}}_{r_k}(1), & \text{if } \varsigma = 1 \\ 0, & \text{otherwise} \end{cases}, \tag{2.113}$$

where $E[\cdot]$ the expectation operator. Now, the decorrelated received signal is determined as

$$\tilde{\tilde{\boldsymbol{\mathcal{Y}}}}_{r_k}(l) = \boldsymbol{R}^{-1}\tilde{\boldsymbol{\mathcal{Y}}}_{r_k}(l) = \tilde{\tilde{\boldsymbol{R}}}_{r_k}(1)\boldsymbol{A}_{r_k}\boldsymbol{x}(l-1) + \tilde{\tilde{\boldsymbol{R}}}_{r_k}(0)\boldsymbol{A}_{r_k}\boldsymbol{x}(l) + \tilde{\tilde{\boldsymbol{R}}}_{r_k}(-1)\boldsymbol{A}_{r_k}\boldsymbol{x}(l+1) + \tilde{\tilde{\boldsymbol{n}}}_{r_k}(l), \quad (2.114)$$

where $\tilde{\tilde{\boldsymbol{R}}}_{r_k}(1) = \boldsymbol{R}^{-1}\tilde{\boldsymbol{R}}_{r_k}(1)$, $\tilde{\tilde{\boldsymbol{R}}}_{r_k}(0) = \boldsymbol{R}^{-1}\tilde{\boldsymbol{R}}_{r_k}(0)$, and $\tilde{\tilde{\boldsymbol{R}}}_{r_k}(-1) = \boldsymbol{R}^{-1}\tilde{\boldsymbol{R}}_{r_k}(-1)$. In addition,

$$E\left[\tilde{\tilde{\boldsymbol{n}}}_{r_k}(l)\tilde{\tilde{\boldsymbol{n}}}^H_{r_k}(l-\varsigma)\right] = \begin{cases} N_0\boldsymbol{R}^{-1}\tilde{\boldsymbol{R}}_{r_k}(-1)\boldsymbol{R}^{-T}, & \text{if } \varsigma = -1 \\ N_0\boldsymbol{R}^{-1}\tilde{\boldsymbol{R}}_{r_k}(0)\boldsymbol{R}^{-T}, & \text{if } \varsigma = 0 \\ N_0\boldsymbol{R}^{-1}\tilde{\boldsymbol{R}}_{r_k}(1)\boldsymbol{R}^{-T}, & \text{if } \varsigma = 1 \\ 0, & \text{otherwise} \end{cases}. \quad (2.115)$$

Hence, the decorrelated received signal of source node S_j with timing offsets for $j \in \{1,2\}$ is written as

$$\begin{aligned} \tilde{\tilde{\mathcal{Y}}}_{r_k,s_j}(l) &= \sqrt{P_{s_1}}h_{s_1,r_k}\sum_{\varsigma=-1}^{0}\tilde{\tilde{\rho}}^{(\varsigma)}_{j,r_k,1}x_1(l-\varsigma) + \sqrt{P_{s_2}}h_{s_2,r_k}\sum_{\varsigma=0}^{1}\tilde{\tilde{\rho}}^{(\varsigma)}_{j,r_k,2}x_2(l-\varsigma) + \tilde{\tilde{n}}_{r_k,s_j}(l) \\ &= \sum_{i=1}^{2}\sqrt{P_{s_i}}h_{s_i,r_k}\sum_{\varsigma=i-2}^{i-1}\tilde{\tilde{\rho}}^{(\varsigma)}_{j,r_k,i}x_i(l-\varsigma) + \tilde{\tilde{n}}_{r_k,s_j}(l), \end{aligned} \quad (2.116)$$

where $\tilde{\tilde{n}}_{r_k,s_j}(l) \sim \mathcal{CN}\left(0, N_0\tilde{\varrho}^{(0)}_{r_k,s_{j,j}}\right)$, and in general

$$\tilde{\varrho}^{(\varsigma)}_{r_k,s_{i,j}} = E\left[\tilde{\tilde{n}}_{r_k,s_i}(l)\tilde{\tilde{n}}^*_{r_k,s_j}(l-\varsigma)\right] \quad (2.117)$$

for $\varsigma \in \{-1,0,1\}$, and according to (2.115).

In the cooperation phase, as each relay transmits its linearly coded signal in its dedicated time-slot with no simultaneous transmissions, the perfect timing synchronization requirement is bypassed since the receiving source nodes can maintain slot synchronization, which in turn implies that coarse slot synchronization is available [9]. In turn, any synchronization scheme employed in conventional TDMA systems can be used to achieve timing synchronization at the source nodes. Thus, the received signal by source node S_1 is expressed as

$$\tilde{y}^{(l)}_{s_1,r_k}(t) = \sqrt{P_{r_k}}h_{s_1,r_k}\tilde{\mathcal{X}}^{(l)}_{r_k}(t) + w^{(l)}_{s_1,r_k}(t), \quad (2.118)$$

where $\tilde{\mathcal{X}}^{(l)}_{r_k}(t) = \sum_{i=1}^{2}\tilde{\beta}_{r_k,s_i}\tilde{\tilde{\mathcal{Y}}}_{r_k,s_i}(l)c_i(t)$, and $\tilde{\beta}_{r_k,s_i}$ for $i \in \{1,2\}$ is given by

$$\tilde{\beta}_{r_k,s_i} = \sqrt{\frac{1}{P_{s_1}|h_{s_1,r_k}|^2\sum_{\varsigma=-1}^{0}\left(\tilde{\tilde{\rho}}^{(\varsigma)}_{i,r_k,1}\right)^2 + P_{s_2}|h_{s_2,r_k}|^2\sum_{\varsigma=0}^{1}\left(\tilde{\tilde{\rho}}^{(\varsigma)}_{i,r_k,2}\right)^2 + N_0\tilde{\varrho}^{(0)}_{r_k,s_{i,i}}}}. \quad (2.119)$$

The received signal at the output of the MFB is written as

$$\tilde{Y}_{s_1,r_k,s_j}(l) = \langle\tilde{y}^{(l)}_{s_1,r_k}(t), c_j(t)\rangle = \sqrt{P_{r_k}}h_{s_1,r_k}\sum_{i=1}^{N}\tilde{\beta}_{r_k,s_i}\tilde{\tilde{\mathcal{Y}}}_{s_i,r_k}(l)\rho_{i,j} + w_{s_1,r_k,s_j}(l). \quad (2.120)$$

In vector form, the received cross-correlated signal is written as $\tilde{\boldsymbol{Y}}_{s_1,r_k}(l) = \boldsymbol{R}\boldsymbol{B}_{s_1,r_k}\tilde{\tilde{\boldsymbol{\mathcal{Y}}}}_{r_k}(l) + \boldsymbol{w}_{s_1,r_k}(l)$, where $\tilde{\tilde{\boldsymbol{\mathcal{Y}}}}_{r_k}(l) = \left[\tilde{\tilde{\mathcal{Y}}}_{r_k,s_1}(l), \tilde{\tilde{\mathcal{Y}}}_{r_k,s_2}(l)\right]^T$, $\tilde{\boldsymbol{Y}}_{s_1,r_k}(l) = \left[\tilde{Y}_{s_1,r_k,s_1}(l), \tilde{Y}_{s_1,r_k,s_2}(l)\right]^T$, $\boldsymbol{w}_{s_1,r_k}(l) = [w_{s_1,r_k,s_1}(l), w_{s_1,r_k,s_2}(l)]^T \sim \mathcal{CN}(\boldsymbol{0}, N_0\boldsymbol{R})$, and matrices $\boldsymbol{R}$ and $\boldsymbol{B}_{s_1,r_k}$ is defined in (2.4) and (2.13), respectively. In this case, the decorrelated signal is determined as $\tilde{\tilde{\boldsymbol{Y}}}_{s_1,r_k}(l) = \boldsymbol{R}^{-1}\tilde{\boldsymbol{Y}}_{s_1,r_k}(l)$, with $\tilde{\tilde{\boldsymbol{Y}}}_{s_1,r_k}(l) = \left[\tilde{\tilde{Y}}_{s_1,r_k,s_1}(l), \tilde{\tilde{Y}}_{s_1,r_k,s_2}(l)\right]^T$, and the decorrelated signal corresponding to symbol x_2 is expressed as

$$\begin{aligned}\tilde{\tilde{Y}}_{s_1,r_k,s_2}(l) &= \sqrt{P_{r_k}}h_{s_1,r_k}\tilde{\beta}_{r_k,s_2}\tilde{\tilde{\mathcal{Y}}}_{s_2,r_k}(l) + \tilde{w}_{s_1,r_k,s_2}(l) \\ &= \tilde{\tilde{Y}}^{\text{Desired}}_{s_1,r_k,s_2}(l) + \tilde{\tilde{Y}}^{\text{ISI}}_{s_1,r_k,s_2}(l) + \tilde{\eta}_{s_1,r_k,s_2}(l),\end{aligned} \tag{2.121}$$

where $\tilde{w}_{s_1,r_k,s_2}(l) \sim \mathcal{CN}(0, N_0\varrho)$, and $\tilde{\eta}_{s_1,r_k,s_2}(l) = \sqrt{P_{r_k}}h_{s_1,r_k}\tilde{\beta}_{r_k,s_2}\tilde{\tilde{n}}_{r_k,s_2}(l) + \tilde{w}_{s_1,r_k,s_2}(l)$ is the equivalent zero-mean additive noise term. Moreover, $\tilde{\tilde{Y}}^{\text{Desired}}_{s_1,r_k,s_2}(l)$ is defined as

$$\tilde{\tilde{Y}}^{\text{Desired}}_{s_1,r_k,s_2}(l) = \tilde{\tilde{\rho}}^{(0)}_{2,r_k,2}\sqrt{P_{r_k}P_{s_2}}h_{s_1,r_k}h_{s_2,r_k}\tilde{\beta}_{r_k,s_2}x_2(l), \tag{2.122}$$

while $\tilde{\tilde{Y}}^{\text{ISI}}_{s_1,r_k,s_2}(l)$ is given by

$$\tilde{\tilde{Y}}^{\text{ISI}}_{s_1,r_k,s_2}(l) = \sqrt{P_{r_k}}h_{s_1,r_k}\tilde{\beta}_{r_k,s_2}\left(\sqrt{P_{s_2}}h_{s_2,r_k}\tilde{\tilde{\rho}}^{(1)}_{2,r_k,2}x_2(l-1) + \sqrt{P_{s_1}}h_{s_1,r_k}\sum_{\varsigma=-1}^{0}\tilde{\tilde{\rho}}^{(\varsigma)}_{2,r_k,1}x_1(l-\varsigma)\right). \tag{2.123}$$

Finally, passing $\tilde{\tilde{Y}}_{s_1,r_k,s_2}(l), \forall k \in \{1,2,\ldots,N\}$ through a matched filter, the conditional signal-to-interference-plus-noise ratio (SINR) corresponding to symbol x_2 received at source node S_1 is shown to be[3]

$$\tilde{\gamma}_{s_2} = \sum_{k=1}^{N}\frac{\tilde{\mathcal{S}}_{s_1,r_k,s_2}}{\tilde{\mathcal{I}}_{s_1,r_k,s_2} + \tilde{\mathcal{N}}_{s_1,r_k,s_2}}, \tag{2.124}$$

where

$$\tilde{\mathcal{S}}_{s_1,r_k,s_2} = \left(\tilde{\tilde{\rho}}^{(0)}_{2,r_k,2}\right)^2\tilde{\beta}^2_{r_k,s_2}P_{r_k}P_{s_2}|h_{s_1,r_k}|^2|h_{s_2,r_k}|^2 \tag{2.125}$$

is the variance of the desired signal term in (2.122), and $\tilde{\mathcal{I}}_{s_1,r_k,s_2}$ is the variance of the ISI term, as given by

$$\tilde{\mathcal{I}}_{s_1,r_k,s_2} = P_{r_k}|h_{s_1,r_k}|^2\tilde{\beta}^2_{r_k,s_2}\left(P_{s_2}|h_{s_2,r_k}|^2\left(\tilde{\tilde{\rho}}^{(1)}_{2,r_k,2}\right)^2 + P_{s_1}|h_{s_1,r_k}|^2\sum_{\varsigma=-1}^{0}\left(\tilde{\tilde{\rho}}^{(\varsigma)}_{2,r_k,1}\right)^2\right). \tag{2.126}$$

Finally, $\tilde{\mathcal{N}}_{s_1,r_k,s_2}$ is the noise variance of $\tilde{\eta}_{s_1,r_k,s_2}(l)$ in (2.121), which is written as

$$\tilde{\mathcal{N}}_{s_1,r_k,s_2} = \left(P_{r_k}|h_{s_1,r_k}|^2\tilde{\beta}^2_{r_k,s_2}\tilde{\varrho}^{(0)}_{r_k,s_{2,2}} + \varrho\right)N_0. \tag{2.127}$$

[3]Since all the transmitted symbols are assumed to be statistically independent, the symbol index l is dropped.

It can be verified that each SINR term in (2.124) reduces to that of the SNR in (2.16) under perfect timing synchronization.

2.6.2 Signal Model for MA-BD-AF

Under the MA-BD-AF scheme, the broadcasting phase is as in the TD-BD-AF scheme, however in the cooperation phase, the received signal corresponding to the l^{th} symbol interval at node S_1 is expressed as

$$\begin{aligned}\tilde{y}_{s_1}^{(l)}(t) &= \sum_{l=-1}^{1}\left(\sum_{k=1}^{N}\sqrt{P_{r_k}}h_{s_1,r_k}\tilde{\mathcal{X}}_{r_k}^{(l)}(t-lT_s-\tau_{r_k,s_1})\right)+w_{s_1}^{(l)}(t)\\ &= \sum_{l=-1}^{1}\left(\sum_{k=1}^{N}\sqrt{P_{r_k}}h_{s_1,r_k}\sum_{i=1}^{2}\tilde{\beta}_{r_k,s_i}\tilde{\tilde{\mathcal{Y}}}_{r_k,s_i}(l)c_i(t-lT_s-\tau_{r_k,s_1})\right)+w_{s_1}^{(l)}(t),\end{aligned} \tag{2.128}$$

where $w_{s_1}^{(l)}(t)$ is the zero-mean additive noise process of the l^{th} symbol received at source node S_1 with variance N_0, and τ_{r_k,s_1} is the time-shift between relay node R_k and source node S_1. It is noteworthy that τ_{s_j,r_k} in (2.104) is not necessarily equal to τ_{r_k,s_j} for $j\in\{1,2\}$. Since there are $N\geq 2$ relaying nodes then source node S_1 samples its received signal at $t=lT_s+\Delta_{s_1}$, which as given by

$$\tilde{y}_{s_1,s_j}(l)=\int_{-\infty}^{\infty}\tilde{y}_{s_1}^{(l)}(t)c_j^*(t-lT_s-\Delta_{s_1})dt, \tag{2.129}$$

where Δ_{s_1} is the time-shift chosen by node S_1 to compensate for the average transmission delay of the relay nodes. The cross-correlated received signal is expressed in vector form as

$$\tilde{\boldsymbol{Y}}_{s_1}(l)=\sum_{k=1}^{N}\Big(\tilde{\boldsymbol{R}}_{r_k,s_1}(1)\tilde{\boldsymbol{B}}_{s_1,r_k}\tilde{\tilde{\boldsymbol{\mathcal{Y}}}}_{r_k}(l-1)+\tilde{\boldsymbol{R}}_{r_k,s_1}(0)\tilde{\boldsymbol{B}}_{s_1,r_k}\tilde{\tilde{\boldsymbol{\mathcal{Y}}}}_{r_k}(l)+\tilde{\boldsymbol{R}}_{r_k,s_1}(-1)\tilde{\boldsymbol{B}}_{s_1,r_k}\tilde{\tilde{\boldsymbol{\mathcal{Y}}}}_{r_k}(l+1)\Big)+\boldsymbol{w}_{s_1}(l), \tag{2.130}$$

where $\tilde{\boldsymbol{Y}}_{s_1}(l)=\left[\tilde{Y}_{s_1,s_1}(l),\tilde{Y}_{s_1,s_2}(l)\right]^T$ and $\boldsymbol{w}_{s_1}(l)=[w_{s_1,s_1}(l),w_{s_1,s_2}(l)]^T\sim\mathcal{CN}(\boldsymbol{0},N_0\boldsymbol{R})$. Also, $\tilde{\tilde{\boldsymbol{\mathcal{Y}}}}_{r_k}$ is defined in (2.114) and $\tilde{\boldsymbol{B}}_{s_1,r_k}=\sqrt{P_{r_k}}h_{s_1,r_k}\tilde{\boldsymbol{B}}_{r_k}$, with matrix $\tilde{\boldsymbol{B}}_{r_k}$ begin expressed as

$$\tilde{\boldsymbol{B}}_{r_k}=\begin{bmatrix}\tilde{\beta}_{r_k,s_1} & 0\\ 0 & \tilde{\beta}_{r_k,s_2}\end{bmatrix}. \tag{2.131}$$

In addition, matrix $\tilde{\boldsymbol{R}}_{r_k,s_1}(0)$ is written as

$$\tilde{\boldsymbol{R}}_{r_k,s_1}(0)=\begin{bmatrix}\tilde{\rho}_{1,r_k,s_1,1}^{(0)} & \tilde{\rho}_{1,r_k,s_1,2}^{(0)}\\ \tilde{\rho}_{2,r_k,s_1,1}^{(0)} & \tilde{\rho}_{2,r_k,s_1,2}^{(0)}\end{bmatrix}, \tag{2.132}$$

where $\tilde{\rho}_{j,r_k,s_1,j}^{(0)}=1,\forall j\in\{1,2\}$ and in general

$$\tilde{\rho}^{(0)}_{i,r_k,s_1,j} = \frac{1}{T_s}\int_{\Delta_{s_1}}^{T_s+\Delta_{s_1}} c_i(t-\tau_{r_k,s_i})c_j^*(t-\Delta_{s_1})\,dt = \begin{cases} \rho_{i,j}\left(1-\frac{\Delta_{s_1}-\tau_{r_k,s_1}}{T_s}\right), & \Delta_{s_1}\geq\tau_{r_k,s_1} \\ \rho_{i,j}\left(1-\frac{\tau_{r_k,s_1}-\Delta_{s_1}}{T_s}\right), & \Delta_{s_1}<\tau_{r_k,s_1} \end{cases}. \quad (2.133)$$

On the other hand, matrix $\tilde{\boldsymbol{R}}_{r_k,s_1}(1)$ is expressed as [97]

$$\tilde{\boldsymbol{R}}_{r_k,s_1}(1) = \begin{bmatrix} 0 & \tilde{\rho}^{(1)}_{1,r_k,s_1,2} \\ 0 & 0 \end{bmatrix}, \quad (2.134)$$

with

$$\tilde{\rho}^{(1)}_{i,r_k,s_1,j} = \begin{cases} \frac{1}{T_s}\int_0^{T_s} c_i(t+T_s-\tau_{r_k,s_i}+\Delta_{s_1})c_j^*(t)\,dt = \rho_{i,j}\left(\frac{\tau_{r_k,s_1}-\Delta_{s_1}}{T_s}\right), & \tau_{r_k,s_1}>\Delta_{s_1} \\ 0, & \text{otherwise} \end{cases}, \quad (2.135)$$

and

$$\tilde{\rho}^{(-1)}_{i,r_k,s_1,j} = \begin{cases} \frac{1}{T_s}\int_0^{T_s} c_i(t)c_j^*(t-T_s-\tau_{r_k,s_j}+\Delta_{s_1})\,dt = \rho_{i,j}\left(\frac{\Delta_{s_1}-\tau_{r_k,s_1}}{T_s}\right), & \Delta_{s_1}>\tau_{r_k,s_1} \\ 0, & \text{otherwise} \end{cases}. \quad (2.136)$$

As before, $(\Delta_{s_1}-\tau_{r_k,s_1})\sim U\left[-\Delta T_s/2,\Delta T_s/2\right]$, where $\Delta T_s\in[0,T_s)$. Now, the received signal is decorrelated as $\tilde{\tilde{\boldsymbol{Y}}}_{s_1}(l)=\boldsymbol{R}^{-1}\tilde{\boldsymbol{Y}}_{s_1}(l)$, yielding

$$\tilde{\tilde{\boldsymbol{Y}}}_{s_1}(l)=\sum_{k=1}^{N}\left(\tilde{\tilde{\boldsymbol{R}}}_{r_k,s_1}(1)\tilde{\boldsymbol{B}}_{s_1,r_k}\tilde{\tilde{\boldsymbol{y}}}_{r_k}(l-1)+\tilde{\tilde{\boldsymbol{R}}}_{r_k,s_1}(0)\tilde{\boldsymbol{B}}_{s_1,r_k}\tilde{\tilde{\boldsymbol{y}}}_{r_k}(l)+\tilde{\tilde{\boldsymbol{R}}}_{r_k,s_1}(-1)\tilde{\boldsymbol{B}}_{s_1,r_k}\tilde{\tilde{\boldsymbol{y}}}_{r_k}(l+1)\right)+\tilde{\boldsymbol{w}}_{s_1}(l), \quad (2.137)$$

where $\tilde{\tilde{\boldsymbol{Y}}}_{s_1}(l)=\left[\tilde{\tilde{Y}}_{s_1,s_1}(l),\tilde{\tilde{Y}}_{s_1,s_2}(l)\right]^T$, $\tilde{\boldsymbol{w}}_{s_1}(l)=[\tilde{w}_{s_1,s_1}(l),\tilde{w}_{s_1,s_2}(l)]^T\sim\mathcal{CN}\left(\boldsymbol{0},N_0\boldsymbol{R}^{-1}\right)$, $\tilde{\tilde{\boldsymbol{R}}}_{r_k,s_1}(1)=\boldsymbol{R}^{-1}\tilde{\boldsymbol{R}}_{r_k,s_1}(1)$, $\tilde{\tilde{\boldsymbol{R}}}_{r_k,s_1}(0)=\boldsymbol{R}^{-1}\tilde{\boldsymbol{R}}_{r_k,s_1}(0)$, and $\tilde{\tilde{\boldsymbol{R}}}_{r_k,s_1}(-1)=\boldsymbol{R}^{-1}\tilde{\boldsymbol{R}}_{r_k,s_1}(-1)$. Therefore, the received decorrelated signal corresponding to symbol x_2 is obtained as

$$\begin{aligned}\tilde{\tilde{Y}}_{s_1,s_2}(l)&=\sum_{k=1}^{N}\sqrt{P_{r_k}}h_{s_1,r_k}\left(\tilde{\beta}_{r_k,s_1}\sum_{\varsigma=-1}^{0}\tilde{\tilde{\rho}}^{(\varsigma)}_{2,r_k,s_1,1}\tilde{\tilde{y}}_{r_k,s_1}(l-\varsigma)+\tilde{\beta}_{r_k,s_2}\sum_{\varsigma=0}^{1}\tilde{\tilde{\rho}}^{(\varsigma)}_{2,r_k,s_1,2}\tilde{\tilde{y}}_{r_k,s_2}(l-\varsigma)\right)+\tilde{w}_{s_1,s_2}(l)\\&=\sum_{k=1}^{N}\sqrt{P_{r_k}}h_{s_1,r_k}\left(\sum_{i=1}^{2}\tilde{\beta}_{r_k,s_i}\sum_{\varsigma=i-2}^{i-1}\tilde{\tilde{\rho}}^{(\varsigma)}_{2,r_k,s_1,i}\left(\sum_{j=1}^{2}\sqrt{P_{s_j}}h_{s_j,r_k}\sum_{\varepsilon=j-2}^{j-1}\tilde{\tilde{\rho}}^{(\varepsilon)}_{i,r_k,j}x_j(l-\varsigma-\varepsilon)\right)\right)+\tilde{\eta}_{s_1,s_2}(l),\end{aligned} \quad (2.138)$$

where

$$\tilde{\eta}_{s_1,s_2}(l)=\sum_{k=1}^{N}\sqrt{P_{r_k}}h_{s_1,r_k}\left(\sum_{i=1}^{2}\tilde{\beta}_{r_k,s_i}\sum_{\varsigma=i-2}^{i-1}\tilde{\tilde{\rho}}^{(\varsigma)}_{2,r_k,s_1,i}\tilde{\tilde{n}}_{r_k,s_i}(l-\varsigma)\right)+\tilde{w}_{s_1,s_2}(l). \quad (2.139)$$

Finally, the SINR obtained at the output of the matched filter after a series of manipulations is obtained as

$$\tilde{\gamma}_{s_2} = \frac{\tilde{\mathcal{S}}_{s_2}}{\tilde{\mathcal{I}}_{s_2} + \tilde{\mathcal{N}}_{s_2}}, \tag{2.140}$$

where $\tilde{\mathcal{S}}_{s_2} = \sum_{k=1}^{N} \left(\tilde{\tilde{\rho}}^{(0)}_{2,r_k,s_1,2}\tilde{\tilde{\rho}}^{(0)}_{2,r_k,2}\right)^2 \tilde{\beta}^2_{r_k,s_2} P_{r_k} P_{s_2} |h_{s_1,r_k}|^2 |h_{s_2,r_k}|^2$ is the signal variance and $\tilde{\mathcal{I}}_{s_2}$ is the ISI variance as given by

$$\tilde{\mathcal{I}}_{s_2} = \sum_{k=1}^{N} P_{r_k} |h_{s_1,r_k}|^2 \times \left(\sum_{i=1}^{2} \tilde{\beta}^2_{r_k,s_i} \sum_{\varsigma=i-2}^{i-1} \left(\tilde{\tilde{\rho}}^{(\varsigma)}_{2,r_k,s_1,i}\right)^2 \left(\sum_{j=1}^{2} P_{s_j} |h_{s_j,r_k}|^2 \sum_{\varepsilon=j-2}^{j-1} \left(\tilde{\tilde{\rho}}^{(\varepsilon)}_{i,r_k,j}\right)^2 \right) - \left(\tilde{\tilde{\rho}}^{(0)}_{2,r_k,s_1,2}\tilde{\tilde{\rho}}^{(0)}_{2,r_k,2}\right)^2 \tilde{\beta}^2_{r_k,s_2} P_{r_k} P_{s_2} |h_{s_1,r_k}|^2 |h_{s_2,r_k}|^2 \right). \tag{2.141}$$

Also, $\tilde{\mathcal{N}}_{s_2}$ is the total noise variance of the correlated noise, as given by

$$\tilde{\mathcal{N}}_{s_2} = \left(\sum_{k=1}^{N} P_{r_k} |h_{s_1,r_k}|^2 \left(\mathcal{B}_{s_2,r_k} + \sum_{i=1}^{2} \tilde{\beta}^2_{r_k,s_i} \tilde{\varrho}^{(0)}_{r_k,s_{i,i}} \sum_{\varsigma=i-2}^{i-1} \left(\tilde{\tilde{\rho}}^{(\varsigma)}_{2,r_k,s_1,i}\right)^2 \right) + \varrho \right) N_0, \tag{2.142}$$

where

$$\mathcal{B}_{s_2,r_k} = \tilde{\beta}_{r_k,s_1}\tilde{\beta}_{r_k,s_2} \left(\left(\tilde{\varrho}^{(0)}_{r_k,s_{1,2}} + \tilde{\varrho}^{(0)}_{r_k,s_{2,1}}\right) \left(\tilde{\tilde{\rho}}^{(0)}_{2,r_k,s_1,1}\tilde{\tilde{\rho}}^{(0)}_{2,r_k,s_1,2}\right)^2 + \left(\tilde{\varrho}^{(1)}_{r_k,s_{1,2}} + \tilde{\varrho}^{(-1)}_{r_k,s_{2,1}}\right) \sum_{\varsigma=-1}^{0} \left(\tilde{\tilde{\rho}}^{(\varsigma)}_{2,r_k,s_1,1}\tilde{\tilde{\rho}}^{(1+\varsigma)}_{2,r_k,s_1,2}\right)^2 \right). \tag{2.143}$$

It can be verified that under perfect timing synchronization, the SINR term in (2.140) reduces that of (2.28). Clearly, the MA-BD-AF scheme is severely affected by the timing synchronization errors that propagated from the broadcasting phase and also by the simultaneous transmissions of the N relay nodes.

2.6.3 Signal Model for RS-BD-AF

Following a similar analysis to that of the TD-BD-AF scheme, the SINR corresponding to symbol x_2 received at source node S_1 due to the transmission of the selected relay node is written as

$$\tilde{\gamma}_{r_{rs},s_2} = \frac{\tilde{\mathcal{S}}_{s_1,r_{rs},s_2}}{\tilde{\mathcal{I}}_{s_1,r_{rs},s_2} + \tilde{\mathcal{N}}_{s_1,r_{rs},s_2}}, \tag{2.144}$$

where $\tilde{\mathcal{S}}_{s_1,r_{rs},s_2}$, $\tilde{\mathcal{I}}_{s_1,r_{rs},s_2}$, and $\tilde{\mathcal{N}}_{s_1,r_{rs},s_2}$ are the signal, ISI and noise variances as given by (2.125), (2.126), and (2.127), respectively. As before, $r_{rs} = r_{ors}$ under the ORS-BD-AF scheme and $r_{rs} = r_{srs}$ under the SRS-BD-AF scheme.

2.7 Simulation Results

In this section, the approximate probability of relay selection and the QPSK SER performance and achievable rate of source node S_2 are evaluated. Equal power allocation (EPA) is

assumed between the source and relay nodes such that $P_{s_1} = P_{s_2} = P/4$ while the total relay power is given by $P_R = P/2$, which is also split equally between the N relay nodes under the TD-BD-AF and MA-BD-AF schemes. The simulations assume a path-loss exponent of $\nu = 3$, a correlation coefficient of $\rho = 0.25$ and the topology shown in Fig. 2.4. In the simulation results, relay nodes R_1 to R_N are employed for each simulated value of N.

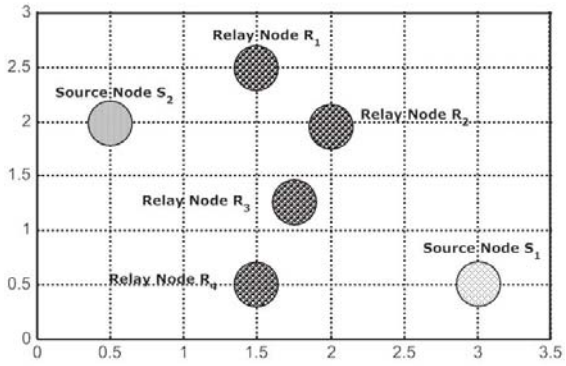

Figure 2.4: Bi-Directional Relaying - Simulation Scenario

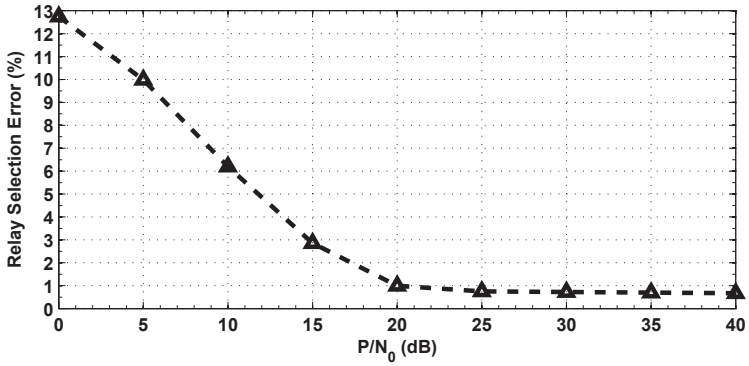

Figure 2.5: Relay Selection Error between the ORS-BD-AF and SRS-BD-AF Schemes

The relay selection error of the proposed SRS-BD-AF scheme in comparison with the ORS-BD-AF scheme is shown in Fig. 2.5. It is clear that the error decreases with the increase in the SNR (less than 1% at high SNR), as the proposed selection metric becomes more accurate in comparison with the ORS-BD-AF scheme.

2.7.1 Approximate Probability of Relay Selection

The approximate probability of selecting each relay under the SRS-BD-AF scheme for $N = 2$, $N = 3$, and $N = 4$ is illustrated in Figs. 2.6, 2.7, and 2.8, respectively. As can be seen, the theoretical approximation of relay selection probability agrees with that of the simulated selection probability. The slight discrepancy in the selection probability values is due to the approximation of the harmonic mean distribution as an exponential distribution.

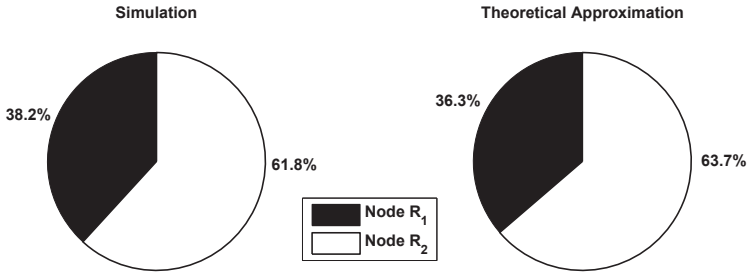

Figure 2.6: Probability of Relay Selection with $N = 2$ - Perfect Timing Synchronization

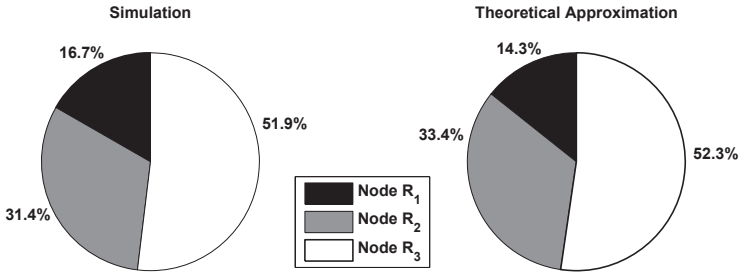

Figure 2.7: Probability of Relay Selection with $N = 3$ - Perfect Timing Synchronization

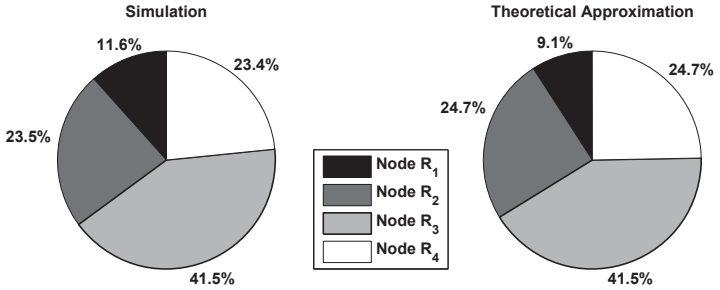

Figure 2.8: Probability of Relay Selection with $N = 4$ - Perfect Timing Synchronization

2.7.2 SER Performance Comparison

In Fig. 2.9, the SER performance of the TD-BD-AF scheme is evaluated. It is clear that the derived approximate SER expressions match the simulated SER performance for the different numbers of relay nodes, except for a slight discrepancy at low SNR. In addition, the upper-bound SER performance curves are asymptotically tight at high SNR. It is also clear that with the increase in the number of relay nodes, the SER performance improves due to the increase in the diversity order. Moreover, the optimal power allocation is shown to yield a gain of about 1.5 dB for the different values of N.

The SER performance of the MA-BD-AF scheme is depicted in Fig. 2.10. Clearly, only minor improvement in the performance is achieved with the increase in N, which is due to the noise amplification and accumulation of the multiple-access transmission. In addition, the slopes of the curves for each value of N have been numerically verified to be the same and that of diversity order 1. Also, the SER performance of the MA-BD-AF scheme with suboptimal power allocation (S-OPA) yields a significant performance improvement and

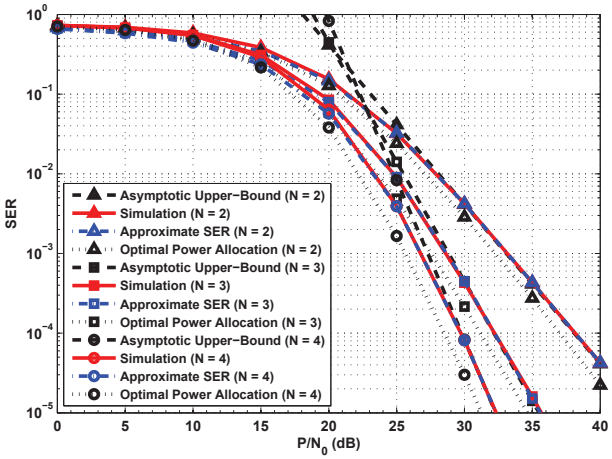

Figure 2.9: QPSK SER Performance of the TD-BD-AF Scheme - Perfect Timing Synchronization and EPA

coincides with that of the SRS-BD-AF scheme. Evidently, the performance of the SRS-BD-AF and ORS-BD-AF schemes is comparable with that of the ORS-BD-AF scheme being marginally better.

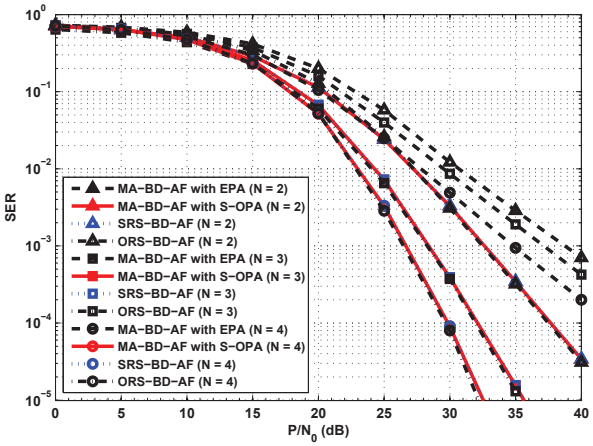

Figure 2.10: QPSK SER Performance of the MA-BD-AF and RS-BD-AF Schemes - Perfect Timing Synchronization

The SER performance of the ORS-BD-AF and SRS-BD-AF schemes is illustrated in Fig. 2.11. Clearly, the derived approximate upper- and lower-bound SER expressions coincide with the simulated SER performance of both schemes for the different numbers of relay nodes. In addition, the slopes of the derived bounds match the SER performance curves of the ORS-BD-AF and SRS-BD-AF schemes at high SNR. Moreover, with the increase in the number of relay nodes, the SER performance improves due to the increase in the diversity order. Comparing the different bi-directional relaying schemes, it is evident that the TD-BD-AF, ORS-BD-AF and SRS-BD-AF schemes have comparable SER performance as they all achieve full diversity order and thus are superior to the MA-BD-AF scheme.

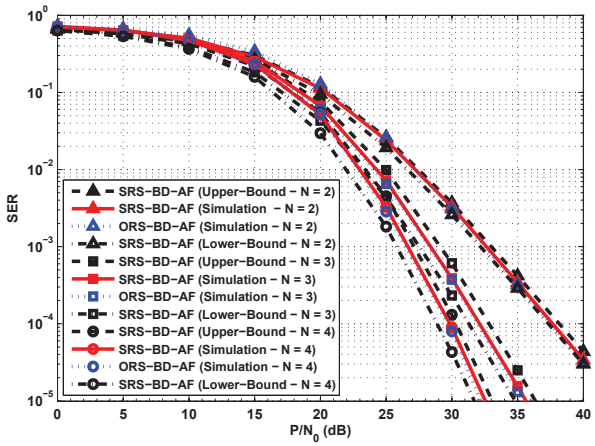

Figure 2.11: QPSK SER Performance of the RS-BD-AF Schemes - Perfect Timing Synchronization and EPA

In Fig. 2.12, the SER performance of the TD-BD-AF and MA-BD-AF schemes with imperfect timing synchronization is shown. As expected, the performance of source node S_2 under both schemes degrades with the increase in the average timing offset value $\Delta T_s/2$ between the source nodes and the intermediate relays. Moreover, it is evident that the TD-BD-AF scheme is less sensitive to timing mismatches than the MA-BD-AF scheme which suffers from high irreducible error floors with the increase in N. This is because under the TD-BD-AF scheme, the timing synchronization errors are averaged out across the N relay nodes. On the other hand, Fig. 2.13 illustrates the SER performance of the SRS-BD-AF scheme where it is clear that the proposed scheme suffers more from the timing offsets, when compared with the TD-BD-AF scheme (see Fig. 2.12). This is attributed to the fact that although relay selection is based on the channel coefficients and allocated total relay power, it does not take into account timing offsets. In other words, the selected relay node under perfect timing synchronization is not necessarily the suboptimal one with timing offsets[4]. In general, the MA-BD-AF scheme has the worst SER with timing offsets when compared with the TD-BD-AF and SRS-BD-AF schemes.

2.7.3 Achievable Rate Comparison

From Fig. 2.14, it can be seen that the ORS-BD-AF and the proposed SRS-BD-AF schemes result in almost the same achievable rate with the ORS-BD-AF scheme being marginally better. In addition, both relay selection schemes are superior to the TD-BD-AF and MA-BD-AF schemes. Furthermore, with the increase in the number of relay nodes N, the achievable rate under the ORS-BD-AF, SRS-BD-AF and MA-BD-AF schemes increases, while under the TD-BD-AF scheme, the achievable rate decreases as a result of

[4]Based on (2.144), finding a closed-form solution for the sum-of-rates maximizing relay selection metric with timing offsets is extremely difficult. Also, the performance of the ORS-BD-AF scheme is not shown as it is similar to the SRS-BD-AF scheme.

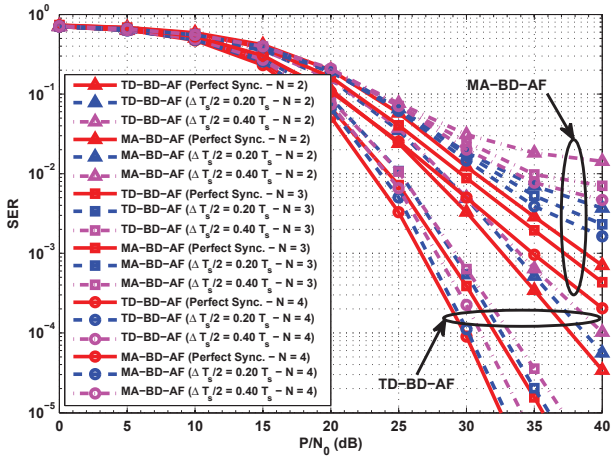

Figure 2.12: QPSK SER Performance of the TD-BD-AF and MA-BD-AF Schemes - Imperfect Timing Synchronization and EPA

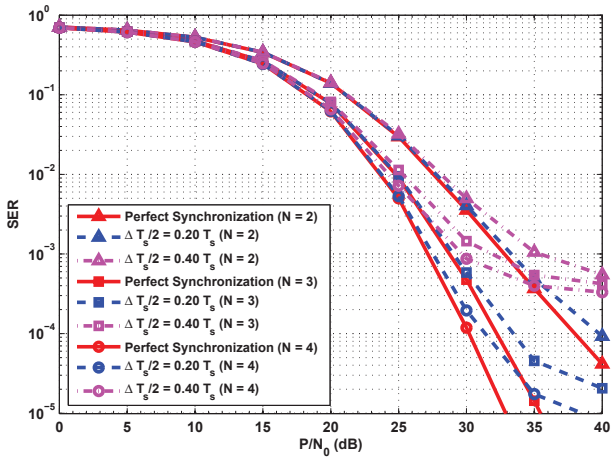

Figure 2.13: QPSK SER Performance of the SRS-BD-AF Scheme - Imperfect Timing Synchronization

the TDMA time-slotted cooperative transmission of each relay node. Fig. 2.14 also shows the achievable rate under the TD-BD-AF scheme with optimal power allocation. As can be seen, there is an improvement—although not very significant—in the rate of source node S_2. Moreover, it is evident that there is a significant improvement in the achievable rate of the MA-BD-AF scheme with S-OPT such that it coincides with that of the SRS-BD-AF scheme. It is also noticed that under the MA-BD-AF and SRS-BD-AF schemes, the improvement in the rate becomes marginal with the increase in the number of relay nodes.

Fig. 2.15 illustrates the achievable rate of source node S_2 with timing offsets under the different bi-directional relaying schemes. As expected, the achievable rate degrades with the increase in the average timing offset $\Delta T_s/2$ value. Evidently, the proposed SRS-BD-AF scheme is superior to the other two schemes and the MA-BD-AF scheme achieves a higher rate than the TD-BD-AF scheme for all values of N.

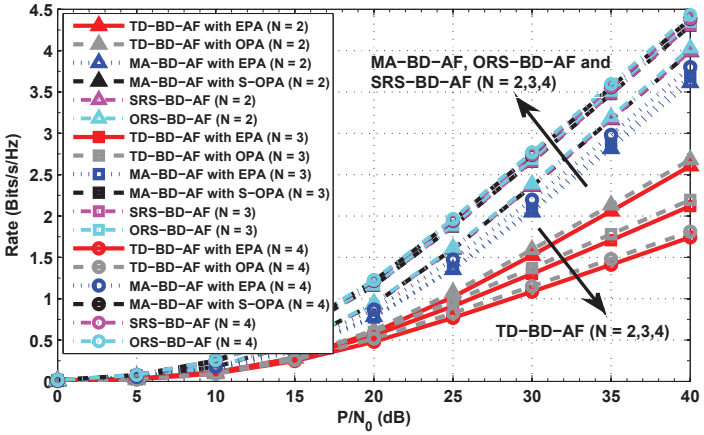

Figure 2.14: Achievable Rates of the TD-BD-AF, MA-BD-AF, ORS-BD-AF and SRS-BD-AF Schemes - Perfect Timing Synchronization

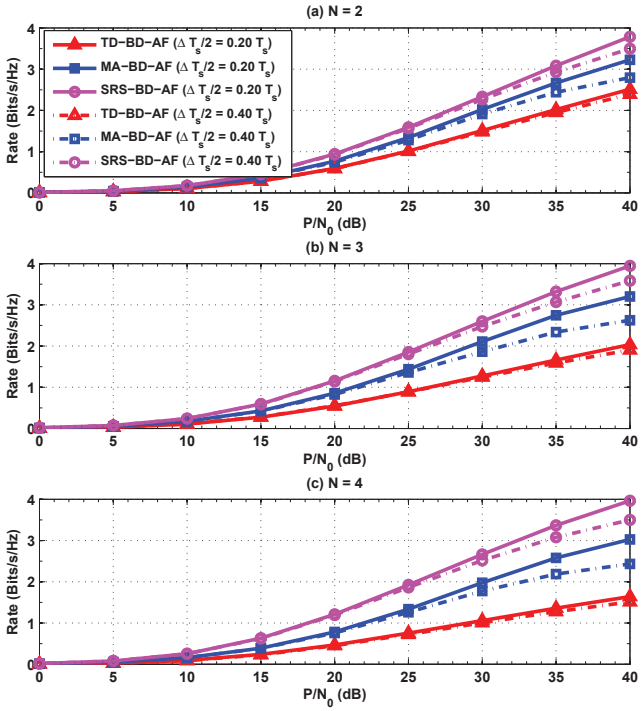

Figure 2.15: Achievable Rates of the TD-BD-AF, MA-BD-AF and SRS-BD-AF Schemes - Imperfect Timing Synchronization and EPA

Finally, Fig. 2.16 shows the sum-of-rates performance of the different bi-directional relaying schemes with an average timing offset of $\Delta T_s/2 = 0.40T_s$. Clearly, the proposed scheme is still superior to the other two schemes in terms of the sum-of-rates performance.

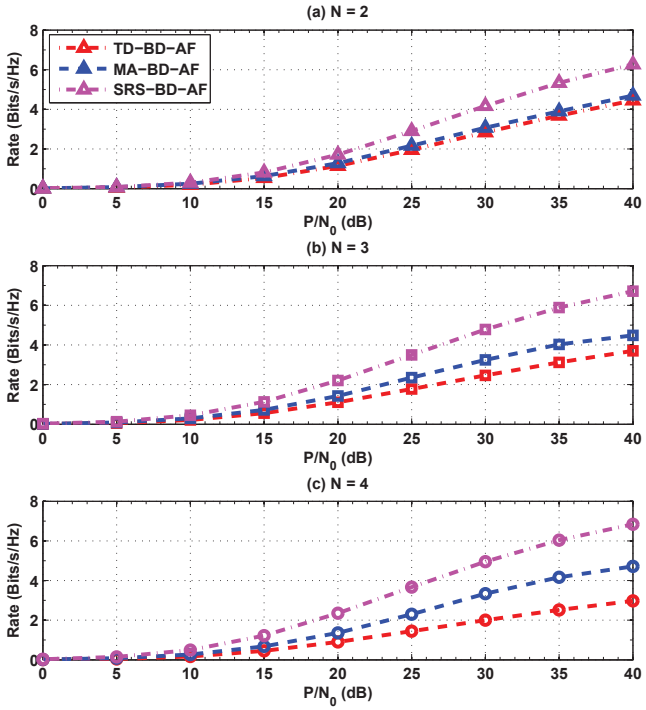

Figure 2.16: Sum-of-Rates of the TD-BD-AF, MA-BD-AF and SRS-BD-AF - Timing Offset of $\Delta T_s/2 = 0.40T_s$ and EPA

2.8 Conclusions and Final Remarks

In this chapter, different bi-directional amplify-and-forward relaying schemes are studied, namely the TD-BD-AF, MA-BD-AF and SRS-BD-AF. A SER performance analysis has been presented for the different schemes along with simulation results to validate the theoretical derivations. It has been shown that both the TD-BD-AF and SRS-BD-AF schemes achieve full diversity order and also result in a comparable SER performance while the MA-BD-AF has the worst SER performance. In addition, optimal and suboptimal sum-of-rates maximizing power allocation is proposed for both the TD-BD-AF and MA-BD-AF schemes, respectively. It has been shown that under suboptimal power allocation, the MA-BD-AF scheme reduces to the SRS-BD-AF scheme. Moreover, it has been shown that the MA-BD-AF scheme is the most affected scheme in terms of the SER performance by timing synchronization errors, while the TD-BD-AF scheme is the least affected one. In terms of the achievable rate, the proposed SRS-BD-AF scheme has been established to be superior to the TD-BD-AF and MA-BD-AF schemes, even with timing offsets. Finally, although this chapter has provided an analysis on the effect of timing synchronization errors, practical and advanced successive and iterative multiuser detectors with ISI cancelation techniques exist in the literature [96] [97] [100]. For the studied bi-directional relaying schemes to lend themselves for practical implementation, timing synchronization errors must be mitigated with minimal computational complexity.

Chapter 3

Space-Time Network Coding

3.1 Introduction

In the previous chapter, the communication between two source nodes through a set of distributed relay nodes was studied. However, the more general case is when more than two nodes desire to communicate with each other and potentially relay each other's data. Although many cooperative communication protocols that can fully exploit diversity gains have been proposed in the literature, such protocols suffer from low-bandwidth efficiency when applied to multinode relay communications. This is attributed to the TDMA single node transmission at any given time which introduces large transmission delays [20]. For instance, in conventional amplify-and-forward (AF) relay networks with N nodes, $N-2$ nodes act as relays between the source and destination nodes with the available channel resources split into $N-1$ orthogonal channels through TDMA [56]. In this case, $N-1$ diversity order is achieved (assuming a direct link between the source and destination nodes) [56]. For each node to communicate with all the other nodes and still achieve a diversity order of $N-1$, a total of N^2 time-slots is required. Hence, the increase in the number of potential nodes results in inefficient network bandwidth utilization and gives rise to the necessity of reducing the number of transmissions.

Network coding has recently emerged as an important design paradigm for wireless networks that allows multinode communications and also improves data distribution and network throughput [29]. As most conventional multinode cooperative communication schemes are not directly applicable to information exchange across many geographically distributed nodes, wireless network coding has become increasingly attractive. A few recent works have proposed the use of wireless network coding for multinode cooperative communications in wireless networks. For instance, in [37], the concept of wireless network cocast (WNC) that employs wireless network coding is proposed to achieve aggregate transmission power and delay reduction while achieving incremental diversity in location-aware networks. In [101], complex field network coding (CFNC) was employed to achieve full diversity gain and

throughput as high as 1/2 symbol per user per channel use. However, the communication is limited to N_S source nodes and a common destination through a single relay or N_R dedicated relay nodes but not between the source nodes themselves.

Research thus far had not fully exploited the joint potential of wireless network coding and cooperative diversity until the introduction of the novel concept of *space-time network coding* (STNC) [102] [103]. In [102], the multipoint-to-point (M2P) and point-to-multipoint (P2M) space-time network codes were proposed to allow multiple source transmissions within a TDMA framework to a common node and the reverse common node transmission to multiple destinations, respectively. It was also shown that for a network of N nodes deploying M2P-STNC or P2M-STNC, only $2N$ time-slots are required while achieving a diversity order of N per transmitted symbol. In [103], the many-to-many space-time network coding (M2M-STNC) for a network of N decode-and-forward (DF) nodes is proposed to achieve a diversity order of $N-1$ per node over a total of $2N$ time-slots while maintaining a stable network throughput of 1/2 symbol per time-slot per node. The operation of the M2M-STNC scheme is based on the assumption of $N-1$ perfectly synchronized simultaneous transmissions in every time-slot of the cooperation phase; however, the work in [103] did not analyze the impact of timing synchronization errors on the network performance. In practice, simultaneous transmissions from multiple nodes are extremely challenging due to the imperfect timing synchronization and the potential mobility of the network nodes. Most research in cooperative communications—when focusing on simultaneous transmissions from distributed nodes—assume perfect timing synchronization [8, 101, 104]. Overlooking the impact of timing synchronization errors could lead to detrimental effects on the network performance [105]. Also, channel state information errors at the receiving nodes are inevitable in practice. Such errors could drastically diminish diversity gains and thus must be carefully characterized.

Based on the foregoing discussion, this work aims at better exploiting the potentials of the M2M-STNC communication scheme for amplify-and-forward (AF) cooperative networks by: (1) characterizing the symbol error rate (SER) performance for M-ary phase shift keying (M-PSK) modulation, (2) solving the sum-of-rates maximizing optimal power allocation problem, and (3) analyzing the impact of timing synchronization and channel estimation errors on the SER performance and achievable rate. To reduce the number of simultaneous transmissions while allowing N distributed AF nodes to exchange their data symbols, achieve a diversity order of $N-1$ per node and maintain a stable network throughput of 1/2 symbol per time-slot per node, the M2M-STNC scheme is augmented with optimal node selection (i.e. M2M-STNC-ONS). This work also analyzes the SER performance and achievable rate of the proposed M2M-STNC-ONS scheme and studies the impact of timing synchronization errors and imperfect channel state information. Although selection in cooperative networks is not a new concept, the novelty and contribution of this work are manifested by augmenting it with a many-to-many cooperative communications scheme so as to achieve full diversity and mitigate the adverse effects of timing offsets and channel estimation errors.

In the remainder of this chapter, the system model of the M2M-STNC scheme is presented in Section 3.2, while the proposed M2M-STNC-ONS scheme is discussed in Section 3.3. The

theoretical symbol error rate of both the M2M-STNC and M2M-STNC-ONS schemes is analyzed in Section 3.4. The theoretical approximate probability of node selection is studied in Section 3.5 while the sum-of-rates maximizing optimal power allocation under the M2M-STNC scheme is analyzed in Section 3.6. The impact of timing offsets and channel estimation errors on the performance of the M2M-STNC and M2M-STNC-ONS schemes is characterized in Sections 3.7 and 3.8, respectively. In Section 3.9, the simulation results are contrasted with the analytical results. Finally, chapter conclusions are drawn in Section 3.10.

3.2 System Model

The M2M-STNC system model is based on a wireless network with N single antenna amplify-and-forward nodes denoted S_1, S_2, ..., S_N for $N \geq 4$. Each node S_j for $j \in \{1, 2, \ldots, N\}$ is assumed to have its own data symbol x_j to exchange with all the other $N-1$ nodes in the network. In this work, the channel between any two nodes is modeled as flat Rayleigh fading with additive white Gaussian noise (AWGN). Let $h_{j,i}$ denote a generic channel coefficient representing the channel between any two nodes S_j and S_i for $j \neq i$ and $h_{j,i}$ is modeled as a zero-mean complex Gaussian random variable with variance $\sigma_{j,i}^2$ (i.e. $h_{j,i} \sim \mathcal{CN}(0, \sigma_{j,i}^2)$), where the channel variance $\sigma_{j,i}^2 = d_{j,i}^{-\nu}$ with $d_{j,i}$ and ν being the distance between the two nodes and the path-loss exponent, respectively. The channel gain $|h_{j,i}|$ is then a Rayleigh random variable while the channel gain squared $|h_{j,i}|^2$ is a exponential random variable with mean $\sigma_{j,i}^2$. Also, the channel $h_{j,i}$ between nodes S_j and S_i is assumed to be reciprocal (i.e. $h_{i,j} = h_{j,i}$), with perfect channel estimation at each node. Moreover, the channel coefficients are assumed to be quasi-static throughout the network operation. Finally, perfect timing synchronization between all the N nodes in the network is assumed.

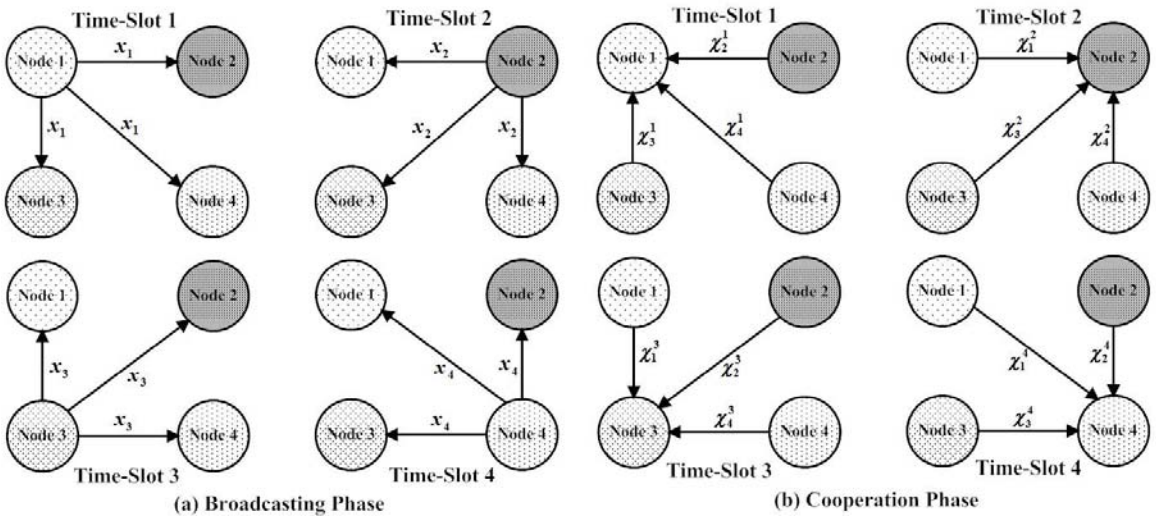

Figure 3.1: M2M-STNC Scheme with $N = 4$ Nodes

The cooperative communication between all the nodes (depicted in Fig. 3.2 for $N = 4$) is performed over a total of $2N$ time-slots and is split into two phases (N time-slots each):

(a) the broadcasting phase (BP) and (b) the cooperation phase (CP). The communication under the two phases can be expressed in matrix form as

$$\begin{array}{c} \\ T_1 \\ \vdots \\ T_j \\ \vdots \\ T_N \end{array} \overbrace{\begin{array}{c} \begin{array}{ccccc} S_1 & \cdots & S_j & \cdots & S_N \end{array} \\ \left[\begin{array}{ccccc} x_1 & \cdots & 0 & \cdots & 0 \\ \vdots & \ddots & \vdots & \cdots & \vdots \\ 0 & \cdots & x_j & \cdots & 0 \\ \vdots & \cdots & \vdots & \ddots & \vdots \\ 0 & \cdots & 0 & \cdots & x_N \end{array}\right] \end{array}}^{\text{Broadcasting Phase}} \quad \begin{array}{c} \\ T_{N+1} \\ \vdots \\ T_{N+i} \\ \vdots \\ T_{2N} \end{array} \overbrace{\begin{array}{c} \begin{array}{ccccc} S_1 & \cdots & S_i & \cdots & S_N \end{array} \\ \left[\begin{array}{ccccc} 0 & \cdots & \mathcal{X}_i^1 & \cdots & \mathcal{X}_N^1 \\ \vdots & \ddots & \vdots & \cdots & \vdots \\ \mathcal{X}_1^i & \cdots & 0 & \cdots & \mathcal{X}_N^i \\ \vdots & \cdots & \vdots & \ddots & \vdots \\ \mathcal{X}_1^N & \cdots & \mathcal{X}_i^N & \cdots & 0 \end{array}\right] \end{array}}^{\text{Cooperation Phase}}. \tag{3.1}$$

3.2.1 Broadcasting Phase

In the broadcasting phase, source node S_j is assigned a time-slot T_j in which it broadcasts its own data symbol x_j to the $N-1$ other nodes S_i in the network for $i \in \{1, 2, \ldots, N\}$ for $i \neq j$. For source separation at each receiving node, each transmitted symbol x_j is spread using a signature waveform $c_j(t)$ where it is assumed that each node knows the signature waveforms of all the other nodes. The cross-correlation of $c_i(t)$ and $c_j(t)$ is $\rho_{i,j} = \langle c_i(t), c_j(t) \rangle \triangleq (1/T_s) \int_0^{T_s} c_i(t) c_j^*(t) dt$ for $i \neq j$ with $\rho_{j,j} = 1$ and T_s being the symbol duration. Thus, the signal received at node S_i for $i \neq j$ in time-slot T_j is expressed as

$$y_{j,i}(t) = \sqrt{P_j^B} h_{j,i} x_j c_j(t) + n_{j,i}(t), \tag{3.2}$$

where P_j^B is the transmit power in the broadcasting phase at node S_j and $h_{j,i}$ is the Rayleigh flat fading channel coefficient between nodes S_j and S_i. Also, $n_{j,i}(t)$ is the AWGN sample at node S_i due to the signal transmitted by node S_j, modeled as a zero-mean complex Gaussian random variable with variance N_0. To extract data symbol x_j at node S_i, the received signal $y_{j,i}(t)$ (given in (3.2)) is cross-correlated with the signature waveform $c_j(t)$ to obtain

$$y_{j,i} = \langle y_{j,i}(t), c_j(t) \rangle = \sqrt{P_j^B} h_{j,i} x_j + n_{j,i}, \tag{3.3}$$

where $n_{j,i} \sim \mathcal{CN}(0, N_0)$. Upon the completion of the broadcasting phase, each node S_j will have exchanged its data symbol x_j with the other nodes and received a set of $N-1$ signals $\{y_{j,i}\}_{j=1,j\neq i}^N$ comprising symbols $x_1, \ldots, x_{i-1}, x_{i+1}, \ldots, x_N$ for $j \neq i$ from all the other nodes in the network. Node S_i then performs a matched filtering operation on each of the received signals $y_{j,i}$ and the SNR at the output of the matched-filter is expressed as [56]

$$\gamma_{j,i}^{BP} = \frac{P_j^B |h_{j,i}|^2}{N_0}. \tag{3.4}$$

The received signals at all the nodes in the network at the end of the broadcasting phase can be expressed in a matrix form as

$$\mathbf{Y} = \begin{bmatrix} - & y_{2,1} & \cdots & y_{N-1,1} & y_{N,1} \\ y_{1,2} & - & \cdots & y_{N-1,2} & y_{N,2} \\ \vdots & \vdots & \ddots & \vdots & \vdots \\ y_{1,N-1} & y_{2,N-1} & \cdots & - & y_{N,N-1} \\ y_{1,N} & y_{2,N} & \cdots & y_{N-1,N} & - \end{bmatrix}, \tag{3.5}$$

where the i^{th} row represents the signals received at S_i while the j^{th} column represents the signals received in time-slot T_j from S_j.

3.2.2 Cooperation Phase

The cooperation phase involves two operations: (1) signal transmission, and (2) multinode signal detection, which are discussed in the following subsections, respectively. In what follows, perfect timing synchronization is assumed.

Signal Transmission

In the cooperation phase, each node S_i acts as the destination node in time-slot T_{N+i} for $i \in \{1, 2, \ldots, N\}$ and receives simultaneous transmissions from the other $N-1$ nodes. In particular, each node S_k with $k \neq i$ forms a linearly coded signal $\mathcal{X}_k^i(t)$ which is composed from the received $N-2$ signals of the k^{th} row of matrix $\boldsymbol{Y}$ in (3.5), excluding the received signal from node S_i. Node S_k then transmits $\mathcal{X}_k^i(t)$ which is given by

$$\mathcal{X}_k^i(t) = \sum_{\substack{m=1 \\ m\neq i, m\neq k}}^{N} \beta_{m,k,i} y_{m,k} c_m(t) \tag{3.6}$$

where $c_m(t)$ is the signature waveform associated with symbol x_m and $\beta_{m,k,i}$ is [56]

$$\beta_{m,k,i} = \sqrt{\frac{P_{m,k,i}^C}{P_m^B |h_{m,k}|^2 + N_0}}. \tag{3.7}$$

From (3.6), it should be noted that node S_k relays the received signals from the other $N-2$ nodes. Moreover, the received signal at node S_i during time-slot T_{N+i} is given by

$$\mathcal{Y}_i(t) = \sum_{k=1, k\neq i}^{N} h_{k,i} \mathcal{X}_k^i(t) + w_i(t) = \sum_{m=1, m\neq i}^{N} \alpha_{m,i} x_m c_m(t) + \bar{w}_i(t), \tag{3.8}$$

where $\alpha_{m,i}$ is defined as

$$\alpha_{m,i} = \sqrt{P_m^B} \sum_{\substack{k=1 \\ k\neq i, k\neq m}}^{N} \beta_{m,k,i} h_{m,k} h_{k,i}, \tag{3.9}$$

In (3.8), $w_i(t)$ is the zero-mean N_0-variance AWGN sample at node S_i and $\bar{w}_i(t)$ is the equivalent noise term which can be expressed as

$$\bar{w}_i(t) = w_i(t) + \sum_{m=1,m\neq i}^{N} \sum_{\substack{k=1 \\ k\neq i,k\neq m}}^{N} \beta_{m,k,i} h_{k,i} n_{m,k}(t) c_m(t). \tag{3.10}$$

The total transmit power at node S_m for exchanging symbol x_m with the other nodes in the network is given by $P_m = P_m^B + P_m^C$, where $P_m^B = \delta_m^B P_m$ is the broadcast power and $P_m^C = \sum_{i=1,i\neq m}^{N} P_{m,i}^C = \delta_m^C P_m$ is the total cooperative power with $0 < \delta_m^B \leq 1$ and $\delta_m^C = 1 - \delta_m^B$ being the power allocation fractions to the broadcasting and cooperation phases, respectively. Also, $P_{m,i}^C$ is the total cooperative power associated with relaying symbol x_m to destination node S_i for $i \neq m$ such that $P_{m,i}^C = \delta_{m,i}^C P_m^C$ with $0 \leq \delta_{m,i}^C \leq 1$ and $\sum_{i=1,i\neq m}^{N} \delta_{m,i}^C = 1$. Thus, $P_{m,i}^C$ is given by $P_{m,i}^C = \sum_{\substack{k=1 \\ k\neq i,k\neq m}}^{N} P_{m,k,i}^C$ with each relaying node S_k for $k \neq m$ and $k \neq i$ being allocated cooperative power $P_{m,k,i}^C = \delta_{m,k,i}^C P_{m,i}^C$ with $0 \leq \delta_{m,k,i}^C \leq 1$ and $\sum_{\substack{k=1 \\ k\neq i,k\neq m}}^{N} \delta_{m,k,i}^C = 1$. Additionally, the transmit power associated with transmitting symbol x_m is assumed to be the same for all the N nodes (i.e. $P_m = P, \forall m \in \{1, 2, \ldots, N\}$).

Multinode Signal Detection

Upon receiving signal $\mathcal{Y}_i(t)$, a multinode signal detection operation is performed by node S_i to extract each of the $N-1$ symbols x_j, for $j \in \{1, 2, \ldots, N\}_{j\neq i}$. This is achieved by passing the received signal $\mathcal{Y}_i(t)$ through a matched filter bank (MFB) of $N-1$ branches, matched to the corresponding nodes' signature waveforms $c_j(t)$, yielding

$$\mathcal{Y}_{j,i} = \langle \mathcal{Y}_i(t), c_j(t) \rangle = \sum_{m=1,m\neq i}^{N} \alpha_{m,i} x_m \rho_{m,j} + \bar{w}_{j,i}, \tag{3.11}$$

where $\rho_{m,j}$ is the correlation coefficient between $c_m(t)$ and $c_j(t)$. The output of the MFB can be put in a vector form of all the $N-1$ $\mathcal{Y}_{i,j}$'s signals as follows

$$\boldsymbol{\mathcal{Y}}_i = \boldsymbol{R}_i \boldsymbol{A}_i \boldsymbol{x}_i + \bar{\boldsymbol{w}}_i, \tag{3.12}$$

where

$$\boldsymbol{\mathcal{Y}}_i = [\mathcal{Y}_{1,i}, \ldots, \mathcal{Y}_{i-1,i}, \mathcal{Y}_{i+1,i}, \ldots, \mathcal{Y}_{N,i}]^T, \tag{3.13}$$

$$\boldsymbol{x}_i = [x_1, \ldots, x_{i-1}, x_{i+1}, \ldots, x_N]^T, \tag{3.14}$$

$\bar{\boldsymbol{w}}_i = [\bar{w}_{1,i}, \ldots, \bar{w}_{i-1,i}, \bar{w}_{i+1,i}, \ldots, \bar{w}_{N,i}]^T \sim \mathcal{CN}(\boldsymbol{0}, N_0(\mathbf{I} + \boldsymbol{G}_i)\boldsymbol{R}_i)$ and $\boldsymbol{R}_i$, $\boldsymbol{A}_i$ and $\mathbf{I}$, $\boldsymbol{G}_i$ are $(N-1) \times (N-1)$ matrices with $\mathbf{I}$ being the identity matrix while $\boldsymbol{R}_i$ being defined as

$$\boldsymbol{R}_i = \begin{bmatrix} 1 & \cdots & \rho_{1,(i-1)} & \rho_{1,(i+1)} & \cdots & \rho_{1,N} \\ \vdots & \ddots & \vdots & \vdots & \cdots & \vdots \\ \rho_{(i-1),1} & \cdots & 1 & \rho_{(i-1),(i+1)} & \cdots & \rho_{(i-1),N} \\ \rho_{(i+1),1} & \cdots & \rho_{(i+1),(i-1)} & 1 & \cdots & \rho_{(i+1),N} \\ \vdots & \cdots & \vdots & \vdots & \ddots & \vdots \\ \rho_{N,1} & \cdots & \rho_{N,(i-1)} & \rho_{N,(i+1)} & \cdots & 1 \end{bmatrix}, \tag{3.15}$$

and the diagonal matrices $\boldsymbol{A}_i$ and $\boldsymbol{G}_i$ are respectively written as

$$\boldsymbol{A}_i = \text{diag}\left[\alpha_{1,i}, \ldots, \alpha_{(i-1),i}, \alpha_{(i+1),i}, \ldots, \alpha_{N,i}\right], \tag{3.16}$$

and

$$\boldsymbol{G}_i = \text{diag}\left[g_{1,i}^2, \ldots, g_{i-1,i}^2, g_{i+1,i}^2, \ldots, g_{N,i}^2\right], \tag{3.17}$$

with $g_{j,i}^2$ being defined as $g_{j,i}^2 = \sum_{\substack{k=1 \\ k\neq i, k\neq j}}^{N} \beta_{j,k,i}^2 |h_{k,i}|^2$ for $j \neq i$. The received signal vector $\boldsymbol{\mathcal{Y}}_i$ can then be decorrelated (assuming matrix $\boldsymbol{R}_i$ is invertible) as $\bar{\boldsymbol{\mathcal{Y}}}_i = \boldsymbol{R}_i^{-1}\boldsymbol{\mathcal{Y}}_i = \boldsymbol{A}_i\boldsymbol{x}_i + \bar{\bar{\boldsymbol{w}}}_i$, where $\bar{\bar{\boldsymbol{w}}}_i = \boldsymbol{R}_i^{-1}\bar{\boldsymbol{w}}_i$ and $\bar{\bar{\boldsymbol{w}}}_i \sim \mathcal{CN}(\boldsymbol{0}, N_0\boldsymbol{R}_i^{-1}(\boldsymbol{\mathrm{I}} + \boldsymbol{G}_i))$. Thus, at node S_i, the decorrelated received signal $\bar{\mathcal{Y}}_{j,i}$ corresponding to symbol x_j is obtained as

$$\bar{\mathcal{Y}}_{j,i} = \sqrt{P_j^B}\left(\sum_{\substack{k=1 \\ k\neq i, k\neq j}}^{N} \beta_{j,k,i} h_{j,k} h_{k,i}\right) x_j + \bar{\bar{w}}_{j,i}, \tag{3.18}$$

where $\bar{\bar{w}}_{j,i} \sim \mathcal{CN}(0, N_0\varrho_{j,i}(1 + g_{j,i}^2))$ and $\varrho_{j,i}$ is the j^{th} diagonal element of matrix $\boldsymbol{R}_i^{-1}$. Without loss of generality, it is assumed that $\rho_{i,j} = \rho, \forall i \neq j$ and thus [103]

$$\varrho_{j,i} = \frac{1 + (N-3)\rho}{1 + (N-3)\rho - (N-2)\rho^2} \triangleq \varrho_{N-1}. \tag{3.19}$$

It should be noted that upon the completion of the broadcasting and cooperation phases, each node S_i for $i = 1, 2, \ldots, N$ has received $N-1$ signals containing symbol x_j for $j = 1, 2, \ldots, N$ and $j \neq i$; a direct signal from the source node S_j in the broadcasting phase and $N-2$ signals from nodes S_m for $m \neq i$ and $m \neq j$, in the cooperation phase.

The total signal power of the decorrelated signal $\bar{\mathcal{Y}}_{j,i}$ received in the cooperation phase is determined as

$$P_{S_{j,i}}^C = P_j^B\left(\sum_{\substack{k=1 \\ k\neq i, k\neq j}}^{N} |\beta_{j,k,i}|^2 |h_{j,k}|^2 |h_{k,i}|^2\right) = P_j^B\left(\sum_{\substack{k=1 \\ k\neq i, k\neq j}}^{N} \frac{P_{j,k,i}^C |h_{j,k}|^2 |h_{k,i}|^2}{P_j^B |h_{j,k}|^2 + N_0}\right), \tag{3.20}$$

while the total noise power is obtained as

$$P_{N_{j,i}}^C = N_0\varrho_{N-1}\left(1 + \sum_{\substack{k=1 \\ k\neq i, k\neq j}}^{N} \beta_{j,k,i}^2 |h_{k,i}|^2\right) = N_0\varrho_{N-1}\left(1 + \sum_{\substack{k=1 \\ k\neq i, k\neq j}}^{N} \frac{P_{j,k,i}^C |h_{k,i}|^2}{P_j^B |h_{j,k}|^2 + N_0}\right). \tag{3.21}$$

Thus, the instantaneous SNR at the output of the matched-filter at node S_i corresponding to symbol x_j is given by

$$\gamma_{j,i} = \gamma_{j,i}^{BP} + \gamma_{j,i}^{CP}, \tag{3.22}$$

where $\gamma_{j,i}^{BP}$ is an exponential random variable as in (3.4) with mean $\lambda_{j,i}^{BP} = \frac{N_0}{P_j^B \sigma_{j,i}^2}$, and $\gamma_{j,i}^{CP}$ is given by

$$\gamma_{j,i}^{CP} = \frac{P_j^B}{N_0 \varrho_{N-1} \left(1 + \sum_{\substack{k=1 \\ k\neq i, k\neq j}}^{N} \frac{P_{j,k,i}^C |h_{k,i}|^2}{P_j^B |h_{j,k}|^2 + N_0}\right)} \left(\sum_{\substack{k=1 \\ k\neq i, k\neq j}}^{N} \frac{P_{j,k,i}^C |h_{j,k}|^2 |h_{k,i}|^2}{P_j^B |h_{j,k}|^2 + N_0} \right). \tag{3.23}$$

It is clear from (3.23) that $\gamma_{j,i}^{CP}$ is adversely affected by the noise amplification due to the simultaneous transmissions of the $N-2$ nodes. The achievable rate between source node S_j and destination node S_i is given by

$$\mathcal{R}_{j,i}^{\text{M2M-STNC}}(\gamma_{j,i}) = \frac{1}{2N} \log_2 \left(1 + \frac{P_j^B |h_{j,i}|^2}{N_0} + \frac{P_j^B \left(\sum_{\substack{k=1 \\ k\neq i, k\neq j}}^{N} \frac{P_{j,k,i}^C |h_{j,k}|^2 |h_{k,i}|^2}{P_j^B |h_{j,k}|^2 + N_0} \right)}{N_0 \varrho_{N-1} \left(1 + \sum_{\substack{k=1 \\ k\neq i, k\neq j}}^{N} \frac{P_{j,k,i}^C |h_{k,i}|^2}{P_j^B |h_{j,k}|^2 + N_0}\right)} \right), \tag{3.24}$$

and the total achievable rate of node S_j is expressed as $\mathcal{R}_j^{\text{M2M-STNC}} = \sum_{i=1, i\neq j}^{N} \mathcal{R}_{j,i}^{\text{M2M-STNC}}(\gamma_{j,i})$.

It should be noted that the M2M-STNC scheme requires stringent timing synchronization between the relaying nodes, and synchronizing all the distributed N nodes—as will be discussed later in this chapter—is practically prohibitive. In turn, selecting the optimal node to relay each symbol to each destination is highly desirable, as presented in the following section.

3.3 Space-Time Network Coding with Optimal Node Selection

When node S_i acts as a destination node in its assigned time-slot T_{N+i}, the intermediate node the transmitted signal of which results in the highest cumulative SNR value for symbol x_m of source node S_m for $m \neq i$ is selected. Specifically, for each source node, optimal relaying nodes are selected and then all the nodes selected for at least one source node transmit simultaneously. The node selection metric used by the destination node S_i to determine the optimal node S_k to "relay" symbol x_m received from source node S_m for $k \neq i$ and $k \neq m$ is based on the *scaled* harmonic mean of the instantaneous source, intermediate and destination nodes' scaled channel gains, as follows[1] [20] [27] [77]

$$\gamma_{m,k,i} \triangleq \mu_H(X_{m,k}^B; X_{m,k,i}^C) = \frac{X_{m,k}^B X_{m,k,i}^C}{X_{m,k}^B + X_{m,k,i}^C}, \tag{3.25}$$

where $X_{m,k}^B = P_m^B |h_{m,k}|^2$ and $X_{m,k,i}^C = P_{m,k,i}^C |h_{k,i}|^2$ are exponential random variables corresponding to the broadcast transmission of symbol x_m from source node S_m to intermediate node S_k with transmit power P_m^B and the cooperative transmission of symbol x_m from intermediate node S_k to the destination node S_i with cooperative transmit power $P_{m,k,i}^C = P_{m,i}^C$.

[1]Node selection is achieved via control messages exchange prior to the cooperation phase [106] and is only updated when the respective channels' coherence time elapses.

Thus, the scaled harmonic mean values corresponding to symbol x_m, for $m \neq i$ at node S_k for $k \neq i$ and $k \neq m$ when node S_i is the destination node is summarized in matrix form as

$$\mathbf{\Gamma}_i = \begin{array}{c} \begin{array}{cccccc} x_1 & \cdots & x_{i-1} & x_{i+1} & \cdots & x_N \end{array} \\ \left[\begin{array}{cccccc} - & \cdots & \gamma_{i-1,1,i} & \gamma_{i+1,1,i} & \cdots & \gamma_{N,1,i} \\ \vdots & \cdots & \vdots & \vdots & \cdots & \vdots \\ \gamma_{1,i-1,i} & \cdots & - & \gamma_{i+1,i-1,i} & \cdots & \gamma_{N,i-1,i} \\ \gamma_{1,i+1,i} & \cdots & \gamma_{i-1,i+1,i} & - & \cdots & \gamma_{N,i+1,i} \\ \vdots & \cdots & \vdots & \vdots & \cdots & \vdots \\ \gamma_{1,N,i} & \cdots & \gamma_{i-1,N,i} & \gamma_{i+1,N,i} & \cdots & - \end{array}\right] \begin{array}{c} S_1 \\ \vdots \\ S_{i-1} \\ S_{i+1} \\ \vdots \\ S_N \end{array} \end{array}. \tag{3.26}$$

For node S_i to receive symbol x_m for $m \neq i$, the optimally selected node to forward symbol x_m among the $N-2$ nodes that received independent copies of symbol x_m during the broadcasting phase is defined by $k_{m,i}^{opt} = \arg\max_{k=1,2,\ldots,N}\{\gamma_{m,k,i}\}_{k\neq i,k\neq m}$. Hence, in time-slot T_{N+i} for each symbol x_m for $m \neq i$, the system reduces to a source node S_m, a destination node S_i and an optimally selected node for the relaying of x_m. Thus, each symbol x_m is associated with a set of indicator functions in the form of $\mathcal{I}_{m,i} = \{\mathcal{I}_{m,k,i}\}_{k=1,k\neq i,k\neq m}^{N}$, where $\mathcal{I}_{m,k,i}$ for $k \neq i, k \neq m$ acts as a binary indicator function when node S_i is the receiving node; while S_k is the optimally selected node transmitting signal $y_{m,k}$ corresponding to symbol x_m. Hence, $\mathcal{I}_{m,k,i}$ is defined by $\mathcal{I}_{m,k,i} = 1$ if $k = k_{m,i}^{opt}$; otherwise $\mathcal{I}_{m,k,i} = 0$.

As before, each node S_k then possibly forms a linearly-coded signal $\mathcal{Z}_k^i(t)$ from its received signals in the broadcasting phase and transmits it to node S_i during time-slot T_{N+i}. Specifically, $\mathcal{Z}_k^i(t)$ is composed from the received signals of the k^{th} row of matrix $\boldsymbol{Y}$ in (3.5) in the form of

$$\mathcal{Z}_k^i(t) = \sum_{\substack{m=1 \\ m\neq i, m\neq k}}^{N} \beta_{m,k,i} y_{m,k} \mathcal{I}_{m,k,i} c_m(t) \tag{3.27}$$

It should be noted that if node S_k is not an optimal node to forward any of the x_m for $m \neq i, m \neq k$ data signals to node S_i, then $\mathcal{Z}_k^i(t) = 0$; otherwise, node S_k is an optimal node to forward at least one symbol x_m and $\mathcal{Z}_k^i(t) \neq 0$. Following the steps of the previous section, the received signal at node S_i during time-slot T_{N+i} is given by

$$\hat{\mathcal{Y}}_i(t) = \sum_{k=1,k\neq i}^{N} h_{k,i} \mathcal{Z}_k^i(t) + w_i(t) = \sum_{m=1,m\neq i}^{N} \hat{\alpha}_{m,i} x_m c_m(t) + \hat{w}_i(t), \tag{3.28}$$

where $\hat{\alpha}_{m,i}$ is defined as

$$\hat{\alpha}_{m,i} = \beta_{m,opt,i} \bar{h}_{m,opt,i} \sqrt{P_m^B} \hat{h}_{m,opt,i}, \tag{3.29}$$

with $\bar{h}_{m,opt,i}$ being the channel coefficient between the source node S_m and the optimally selected node to forward symbol x_m to node S_i for $m \neq i$, as implied by $k = k_{m,i}^{opt}$, and $\beta_{m,opt,i}$ is the scaling factor defined in (3.7). Also, $\hat{h}_{m,opt,i}$ is the channel coefficient between the

optimally selected node and node S_i for the transmission of symbol x_m for $m \neq i$. In (3.28), $\hat{w}_i(t)$ is the equivalent noise term which can be expressed as

$$\hat{w}_i(t) = w_i(t) + \sum_{m=1, m\neq i}^{N} \beta_{m,opt,i} \hat{h}_{m,opt,i} n_{m,opt,i}(t) c_m(t), \tag{3.30}$$

where $n_{m,opt,i}$ is the noise sample at the optimally selected node by node S_i for the transmission of symbol x_m, for $m \neq i$. It should be noted that under the M2M-STNC-ONS scheme, the total cooperative transmit power associated with relaying symbol x_m to node S_i is set to $P^C_{m,opt,i} = P^C_{m,i} = \delta^C_{m,i} P^C_m$, where $P^C_{m,opt,i}$ is the cooperative transmit power allocated to the optimally selected node. Thus, the total power associated with transmitting symbol x_m is given by $P = P^B_m + \sum_{i=1, i\neq m}^{N} P^C_{m,opt,i}$.

To extract symbol x_j, the received signal $\hat{\mathcal{Y}}_i(t)$ is passed through a MFB and the output of the j^{th} branch is expressed as $\hat{\mathcal{Y}}_{j,i} = \sum_{m=1, m\neq i}^{N} \hat{\alpha}_{m,i} x_m \rho_{m,j} + \hat{w}_{j,i}$ which in vector form is expressed as $\hat{\boldsymbol{\mathcal{Y}}}_i = \boldsymbol{R}_i \hat{\boldsymbol{A}}_i \boldsymbol{x}_i + \hat{\boldsymbol{w}}_i$. In particular, $\hat{\boldsymbol{w}}_i = [\hat{w}_{1,i}, \ldots, \hat{w}_{i-1,i}, \hat{w}_{i+1,i}, \ldots, \hat{w}_{N,i}]^T \sim \mathcal{CN}(\boldsymbol{0}, N_0(\mathbf{I} + \hat{\boldsymbol{G}}_i)\boldsymbol{R}_i)$, with $\boldsymbol{R}_i$ being defined in (3.15) while $\hat{\boldsymbol{A}}_i$ and $\hat{\boldsymbol{G}}_i$ are defined as

$$\hat{\boldsymbol{A}}_i = \text{diag}\left[\hat{\alpha}_{1,i}, \ldots, \hat{\alpha}_{(i-1),i}, \hat{\alpha}_{(i+1),i}, \ldots, \hat{\alpha}_{N,i}\right], \tag{3.31}$$

and

$$\hat{\boldsymbol{G}}_i = \text{diag}\left[\hat{g}^2_{1,i}, \ldots, \hat{g}^2_{i-1,i}, \hat{g}^2_{i+1,i}, \ldots, \hat{g}^2_{N,i}\right], \tag{3.32}$$

with $\hat{g}^2_{j,i}$ being defined as $\hat{g}^2_{j,i} = \beta^2_{j,opt,i} |\hat{h}_{j,opt,i}|^2$ for $j \neq i$. The decorrelated received signal $\hat{\mathcal{Y}}_{j,i}$ is obtained as

$$\hat{\mathcal{Y}}_{j,i} = \beta_{j,opt,i} \bar{h}_{j,opt,i} \sqrt{P^B_j} \hat{h}_{j,opt,i} x_j + \hat{\hat{w}}_{j,i}, \tag{3.33}$$

where $\hat{\hat{w}}_{j,i} \sim \mathcal{CN}(0, N_0 \varrho_{N-1}(1 + \beta^2_{j,opt,i} |\hat{h}_{j,opt,i}|^2))$. At the end of the broadcasting and cooperation phases, two signals comprising symbol x_j are received at node S_i; the first comes from the direct transmission in the broadcasting phase while the other is from the optimally selected node in the cooperation phase. Therefore, at the output of the matched-filter, the instantaneous SNR is given by

$$\hat{\gamma}_{j,i} = \gamma^{BP}_{j,i} + \hat{\gamma}^{CP}_{j,i}, \tag{3.34}$$

where $\hat{\gamma}^{CP}_{j,i}$ is given by

$$\hat{\gamma}^{CP}_{j,i} = \frac{P^C_{j,i} P^B_j |\bar{h}_{j,opt,i}|^2 |\hat{h}_{j,opt,i}|^2}{N_0 \varrho_{N-1} (P^B_j |\bar{h}_{j,opt,i}|^2 + P^C_{j,i} |\hat{h}_{j,opt,i}|^2 + N_0)}, \tag{3.35}$$

which at high SNR can be tightly approximated as [56]

$$\bar{\hat{\gamma}}^{CP}_{j,i} \simeq \frac{P^C_{j,i} P^B_j |\bar{h}_{j,opt,i}|^2 |\hat{h}_{j,opt,i}|^2}{N_0 \varrho_{N-1} (P^B_j |\bar{h}_{j,opt,i}|^2 + P^C_{j,i} |\hat{h}_{j,opt,i}|^2)} = \mu_H \left(X^B_{j,opt,i}; X^C_{j,opt,i}\right), \tag{3.36}$$

where it is straightforward to verify that $\bar{\hat{\gamma}}_{j,i}^{CP}$ is the harmonic mean corresponding to the two exponential random variables

$$X_{j,opt,i}^{B} = \frac{P_j^B |\bar{h}_{j,opt,i}|^2}{N_0 \varrho_{N-1}} \text{ and } X_{j,opt,i}^{C} = \frac{P_{j,i}^C |\hat{h}_{j,opt,i}|^2}{N_0 \varrho_{N-1}}, \tag{3.37}$$

with means $\lambda_{j,opt,i}^{B} = \frac{N_0 \varrho_{N-1}}{P_j^B \bar{\sigma}_{j,opt,i}^2}$ and $\lambda_{j,opt,i}^{C} = \frac{N_0 \varrho_{N-1}}{P_{j,i}^C \hat{\sigma}_{j,opt,i}^2}$, respectively. Note that $\bar{\hat{\gamma}}_{j,i}^{CP}$ corresponds to the optimally selected node with the maximum harmonic mean. The means of $\gamma_{j,i}^{BP}$, $X_{j,opt,i}^{B}$ and $X_{j,opt,i}^{C}$ can be redefined respectively as $\lambda_{j,i}^{BP} = \frac{N_0}{\delta_j^B P \sigma_{j,i}^2}$, $\lambda_{j,opt,i}^{B} = \frac{N_0 \varrho_{N-1}}{\delta_j^B P \bar{\sigma}_{j,opt,i}^2}$ and $\lambda_{j,opt,i}^{C} = \frac{N_0 \varrho_{N-1}}{\delta_{j,i}^C (1-\delta_j^B) P \hat{\sigma}_{j,opt,i}^2}$ for $j \neq i, \forall i, j \in \{1, 2, \ldots, N\}$. Thus, $\hat{\gamma}_{j,i}$ is redefined as $\bar{\hat{\gamma}}_{j,i} = \gamma_{j,i}^{BC} + \bar{\hat{\gamma}}_{j,i}^{CP}$.

The achievable rate between source node S_j and destination node S_i under the M2M-STNC-ONS scheme is given by

$$\mathcal{R}_{j,i}^{\text{M2M-STNC-ONS}}(\hat{\gamma}_{j,i}) = \frac{1}{2N} \log_2 \left(1 + \frac{P_j^B |h_{j,i}|^2}{N_0} + \frac{P_{j,i}^C P_j^B |\bar{h}_{j,opt,i}|^2 |\hat{h}_{j,opt,i}|^2}{N_0 \varrho_{N-1} (P_j^B |\bar{h}_{j,opt,i}|^2 + P_{j,i}^C |\hat{h}_{j,opt,i}|^2 + N_0)} \right), \tag{3.38}$$

where $\hat{\gamma}_{j,i}$ is defined in (3.34) and thus $\mathcal{R}_j^{\text{M2M-STNC-ONS}} = \sum_{i=1, i\neq j}^{N} \mathcal{R}_{j,i}^{\text{M2M-STNC-ONS}}(\hat{\gamma}_{j,i})$ is the total achievable rate of node S_j. When $N = 3$, the instantaneous SNR due to the cooperative transmission $\gamma_{j,i}^{CP}$ under the M2M-STNC scheme reduces to that of the M2M-STNC-ONS scheme (i.e. $\gamma_{j,i}^{CP} = \hat{\gamma}_{j,i}^{CP}$). In this case, the SER performance and achievable rate of the M2M-STNC and M2M-STNC-ONS schemes are equivalent.

3.4 Symbol Error Rate (SER) Performance Analysis

In general, the SER for M-PSK modulation conditional on the channel state information (CSI) for SNR γ is given by [83]

$$\Psi_{|\{h\}}(\gamma) = \frac{1}{\pi} \int_0^{(M-1)\pi/M} \exp\left(-\frac{b_{psk}\gamma}{\sin^2 \theta} \right) d\theta, \tag{3.39}$$

where $b_{psk} = \sin^2(\pi/M)$.

3.4.1 M2M-STNC

The derived instantaneous SNR due to the cooperative transmission $\gamma_{j,i}^{CP}$ in (3.23) is extremely difficult to manipulate and thus only the conditional SER of symbol x_j detected at node S_i for $i \neq j$ is provided, which can be evaluated numerically as

$$P_{SER}^{\text{M2M-STNC}} = \Psi_{|\{h_{j,i}\}_{j,i=1,j\neq i}^{N}} \left(\gamma_{j,i}^{BP} + \gamma_{j,i}^{CP} \right), \tag{3.40}$$

where $\gamma_{j,i}^{BP} + \gamma_{j,i}^{CP} = \gamma_{j,i}$, as defined in (3.22).

3.4.2 M2M-STNC-ONS

Denoting the moment generating function (MGF) of a random variable γ with probability density function (PDF) $p_\gamma(\gamma)$ as

$$\mathcal{M}_\gamma(s) = \int_{-\infty}^{\infty} e^{-s\gamma} p_\gamma(\gamma) d\gamma, \tag{3.41}$$

and averaging the conditional SER over the Rayleigh fading channel statistics, the approximate SER expression is given by [56]

$$\tilde{P}_{SER}^{\text{M2M-STNC-ONS}} = \Psi\left(\gamma_{j,i}^{BP} + \bar{\hat{\gamma}}_{j,i}^{CP}\right) = \frac{1}{\pi}\int_0^{(M-1)\pi/M} \mathcal{M}_{\gamma_{j,i}^{BP}}\left(\frac{b_{psk}}{\sin^2\theta}\right) \mathcal{M}_{\bar{\hat{\gamma}}_{j,i}^{CP}}\left(\frac{b_{psk}}{\sin^2\theta}\right) d\theta, \tag{3.42}$$

where $\mathcal{M}_{\gamma_{j,i}^{BP}}(s)$ is defined as [56]

$$\mathcal{M}_{\gamma_{j,i}^{BP}}(s) = \frac{1}{1 + s\delta_j^B P\sigma_{j,i}^2/N_0}. \tag{3.43}$$

To determine the MGF of $\bar{\hat{\gamma}}_{j,i}^{CP}$, the cumulative distribution function (CDF) of $\bar{\hat{\gamma}}_{j,i}^{CP}$ can be derived as [56] [77]

$$P_{\bar{\hat{\gamma}}_{j,i}^{CP}}(\gamma) = \Pr\left[\max_{\substack{k=1,2,\ldots,N \\ k\neq i, k\neq j}} \hat{\gamma}_{j,k,i} \leq \gamma\right] = \prod_{\substack{k=1 \\ k\neq i, k\neq j}}^{N} P_{\hat{\gamma}_{j,k,i}}(\gamma), \tag{3.44}$$

where $P_{\hat{\gamma}_{j,k,i}}(\gamma) = 1 - 2\gamma\sqrt{\hat{\lambda}_{j,k}^B \hat{\lambda}_{j,k,i}^C} e^{-\gamma(\hat{\lambda}_{j,k}^B + \hat{\lambda}_{j,k,i}^C)} K_1\left(2\gamma\sqrt{\hat{\lambda}_{j,k}^B \hat{\lambda}_{j,k,i}^C}\right)$ with $\hat{\lambda}_{j,k}^B$ and $\hat{\lambda}_{j,k,i}^C$ being defined as $\hat{\lambda}_{j,k}^B = \frac{N_0\varrho_{N-1}}{\delta_j^B P\sigma_{j,k}^2}$ and $\hat{\lambda}_{j,k,i}^C = \frac{N_0\varrho_{N-1}}{\delta_{j,i}^C(1-\delta_j^B)P\sigma_{k,i}^2}$, respectively. Also, $K_1(\cdot)$ is the first-order modified Bessel function of the second kind [80]. At high SNR, $K_1(\cdot)$ can be approximated for small x as $K_1(x) \approx 1/x$ [80], and thus the CDF of $\hat{\gamma}_{j,k,i}$ simplifies to $P_{\hat{\gamma}_{j,k,i}}(\gamma) \approx 1 - e^{-\gamma(\hat{\lambda}_{j,k}^B + \hat{\lambda}_{j,k,i}^C)}$. For convenience, define $\hat{\lambda}_{j,k,i}^{BC} \triangleq \hat{\lambda}_{j,k}^B + \hat{\lambda}_{j,k,i}^C = \frac{N_0\varrho_{N-1}}{P}\Phi_{j,k,i}$, where

$$\Phi_{j,k,i} = \frac{\delta_j^B\sigma_{j,k}^2 + \delta_{j,i}^C(1-\delta_j^B)\sigma_{k,i}^2}{\delta_{j,i}^C(1-\delta_j^B)\delta_j^B\sigma_{j,k}^2\sigma_{k,i}^2}. \tag{3.45}$$

Therefore, the PDF of $\bar{\hat{\gamma}}_{j,i}^{CP}$ can be obtained as

$$p_{\bar{\hat{\gamma}}_{j,i}^{CP}}(\gamma) = \sum_{\substack{m=1 \\ m\neq i, m\neq j}}^{N} p_{\hat{\gamma}_{j,m,i}}(\gamma) \prod_{\substack{k=1, k\neq m \\ k\neq i, k\neq j}}^{N} \left(1 - e^{-\gamma\hat{\lambda}_{j,k,i}^{BC}}\right), \tag{3.46}$$

where $p_{\hat{\gamma}_{j,m,i}}(\gamma) = \hat{\lambda}_{j,m,i}^{BC} e^{-\gamma\hat{\lambda}_{j,m,i}^{BC}}$ is the PDF of $\hat{\gamma}_{j,m,i}$. Using (3.46) to determine the MGF of $\bar{\hat{\gamma}}_{j,i}^{CP}$ is quite difficult [20]; however, by using the relationship between the CDF of a random variable X and its MGF, as given by $\mathcal{M}_X(s) = s\mathcal{L}\{P_X(x)\}$ with $\mathcal{L}\{\cdot\}$ being the Laplace Transform of the parameter [80], the MGF of $\bar{\hat{\gamma}}_{j,i}^{CP}$ can be shown to be

$$\mathcal{M}_{\bar{\gamma}_{j,i}^{CP}}(s) = 1 - \sum_{\substack{k=1 \\ k\neq i,k\neq j}}^{N} \frac{s}{s+\hat{\lambda}_{j,k,i}^{BC}} + \sum_{\substack{k=1 \\ k\neq i,k\neq j}}^{N} \sum_{\substack{m=1,m\neq k \\ m\neq i,m\neq j}}^{N} \frac{s}{s+\hat{\lambda}_{j,k,i}^{BC}+\hat{\lambda}_{j,m,i}^{BC}} - \cdots + \frac{(-1)^N s}{s+\sum_{\substack{k=1 \\ k\neq i,k\neq j}}^{N} \hat{\lambda}_{j,k,i}^{BC}}. \tag{3.47}$$

Thus, by substituting (3.43) and (3.47) into (3.42), the approximate SER performance for symbol x_j detected at node S_i for $i \neq j$ can be determined using

$$\tilde{P}_{SER}^{\text{M2M-STNC-ONS}} \approx$$
$$\frac{1}{\pi}\int_0^{(M-1)\pi/M} \frac{1}{\left(1+\frac{b_{psk}\delta_j^B P\sigma_{j,i}^2}{\sin^2(\theta)N_0}\right)} \left(1 - \sum_{\substack{k=1 \\ k\neq i,k\neq j}}^{N} \frac{\frac{Pb_{PSK}}{\sin^2(\theta)N_0\varrho_{N-1}}}{\frac{Pb_{PSK}}{\sin^2(\theta)N_0\varrho_{N-1}}+\Phi_{j,k,i}} + \cdots + \frac{(-1)^N \frac{Pb_{PSK}}{\sin^2(\theta)N_0\varrho_{N-1}}}{\frac{Pb_{PSK}}{\sin^2(\theta)N_0\varrho_{N-1}}+\sum_{\substack{k=1 \\ k\neq i,k\neq j}}^{N}\Phi_{j,k,i}}\right) d\theta. \tag{3.48}$$

Upper Bound

An upper bound on the SER performance is derived by first noticing that at high SNR, the MGF of $\gamma_{j,i}^{BP}$ given in (3.43) can be upper-bounded (by ignoring the 1 term) as [56]

$$\mathcal{M}_{\gamma_{j,i}^{BP}}(s) \lesssim \frac{N_0}{s\delta_j^B P\sigma_{j,i}^2}. \tag{3.49}$$

Second, an upper-bound for $\mathcal{M}_{\bar{\gamma}_{j,i}^{CP}}(s)$ at high SNR can be determined by approximating $e^x \simeq (1+x)$ when $x \to 0$ in the PDF of $\bar{\hat{\gamma}}_{j,i}^{CP}$ defined in (3.46) which is now given by

$$p_{\bar{\gamma}_{j,i}^{CP}}(\gamma) \approx \sum_{\substack{m=1 \\ m\neq i,m\neq j}}^{N} \hat{\lambda}_{j,m,i}^{BC}(1-\gamma\hat{\lambda}_{j,m,i}^{BC})\gamma^{N-3} \prod_{\substack{k=1,k\neq m \\ k\neq i,k\neq j}}^{N} \hat{\lambda}_{j,k,i}^{BC}. \tag{3.50}$$

Since $\hat{\lambda}_{j,k,i}^{BC} = \frac{N_0\varrho_{N-1}}{P}\Phi_{j,k,i}$, so by substituting (3.50) into (3.41) and after a series of manipulations, it can be shown that

$$\mathcal{M}_{\bar{\gamma}_{j,i}^{CP}}(s) \lesssim (N-2)! \left(\frac{N_0\varrho_{N-1}}{sP}\right)^{N-2} \prod_{\substack{k=1 \\ k\neq i,k\neq j}}^{N} \Phi_{j,k,i}. \tag{3.51}$$

Hence, by substituting (3.49) and (3.51) into (3.42), the upper-bound SER expression is obtained as

$$\bar{P}_{UB-SER}^{\text{M2M-STNC-ONS}} \lesssim \left(\frac{N_0}{P}\right)^{N-1} \frac{(N-2)!\Theta(N-1)(\varrho_{N-1})^{N-2}}{\delta_j^B\sigma_{j,i}^2 b_{PSK}^{N-1}} \prod_{\substack{k=1 \\ k\neq i,k\neq j}}^{N} \Phi_{j,k,i}, \tag{3.52}$$

with $\Theta(N-1)$ being defined as $\Theta(N-1) = \frac{1}{\pi}\int_0^{(M-1)\pi/M} \left(\sin^2(\theta)\right)^{N-1} d\theta$.

Diversity Order Analysis

The diversity order is determined by $\Gamma = -\lim_{SNR\to\infty} \log\left(\bar{P}_{UB-SER}^{\text{M2M-STNC-ONS}}\right) / \log(SNR)$, where $SNR = P/N_0$ [56]. Thus, it is easily verified that the M2M-STNC-ONS achieves a full diversity order of $\Gamma = N - 1$ per node.

3.5 Approximate Probability of Node Selection

It should be noted that the selected node can be probabilistically determined as follows. First, notice that a harmonic mean random variable $\gamma_{j,k,i}$ (as defined in (3.25)) can be approximated as an exponential random variable with CDF and PDF given by $P_{\gamma_{j,k,i}} \approx 1 - e^{-\gamma(\lambda_{j,k}^B + \lambda_{j,k,i}^C)}$ and $p_{\gamma_{j,k,i}}(\gamma) = (\lambda_{j,k}^B + \lambda_{j,k,i}^C)e^{-\gamma(\lambda_{j,k}^B + \lambda_{j,k,i}^C)}$, respectively, with $\lambda_{j,k}^B = \frac{1}{P_j^B \sigma_{j,k}^2}$ and $\lambda_{j,k,i}^C = \frac{1}{P_{j,k,i}^C \sigma_{k,i}^2}$. Also, let $\lambda_{j,k,i}^{BC} \triangleq \lambda_{j,k}^B + \lambda_{j,k,i}^C = \frac{P_j^B \sigma_{j,k}^2 + P_{j,k,i}^C \sigma_{k,i}^2}{P_j^B P_{j,k,i}^C \sigma_{j,k}^2 \sigma_{k,i}^2}$.

The approximate probability that node S_k is selected as the optimal node for relaying symbol x_j to destination node S_i for $N = 4$ is given by

$$\Pr\left[\gamma_{j,k,i} = \max_{\substack{q=1,2,\ldots,4 \\ q\neq i, q\neq j}} \gamma_{j,q,i}\right] = \Pr\left[\gamma_{j,k,i} > \gamma_{j,q,i}\right] = \frac{\lambda_{j,q,i}^{BC}}{\lambda_{j,k,i}^{BC} + \lambda_{j,q,i}^{BC}}, \tag{3.53}$$

for $k \neq q$. For $N = 5$, the approximate probability of optimal node selection can be determined as

$$\Pr\left[\gamma_{j,k,i} > \{\gamma_{j,q,i}\}_{\substack{q=1,2,\ldots,5 \\ q\neq i, q\neq j, q\neq k}}\right] = \Pr\left[\gamma_{j,k,i} > \gamma_{j,q,i} > \gamma_{j,l,i}\right] + \Pr\left[\gamma_{j,k,i} > \gamma_{j,l,i} > \gamma_{j,q,i}\right], \tag{3.54}$$

for $k \neq q \neq l$. Furthermore, it can be verified that

$$\begin{aligned}\Pr\left[\gamma_{j,k,i} > \gamma_{j,q,i} > \gamma_{j,l,i}\right] &= \Pr\left[\gamma_{j,k,i} > \gamma_{j,q,i} | \gamma_{j,l,i} = \min\{\gamma_{j,l,i}, \gamma_{j,q,i}, \gamma_{j,k,i}\}\right] \Pr\left[\gamma_{j,l,i} = \min\{\gamma_{j,l,i}, \gamma_{j,q,i}, \gamma_{j,k,i}\}\right] \\ &= \left(\frac{\lambda_{j,q,i}^{BC}}{\lambda_{j,k,i}^{BC} + \lambda_{j,q,i}^{BC}}\right)\left(\frac{\lambda_{j,l,i}^{BC}}{\lambda_{j,k,i}^{BC} + \lambda_{j,q,i}^{BC} + \lambda_{j,l,i}^{BC}}\right),\end{aligned} \tag{3.55}$$

and similarly

$$\begin{aligned}\Pr\left[\gamma_{j,k,i} > \gamma_{j,l,i} > \gamma_{j,q,i}\right] &= \Pr\left[\gamma_{j,k,i} > \gamma_{j,l,i} | \gamma_{j,q,i} = \min\{\gamma_{j,l,i}, \gamma_{j,q,i}, \gamma_{j,k,i}\}\right] \Pr\left[\gamma_{j,q,i} = \min\{\gamma_{j,l,i}, \gamma_{j,q,i}, \gamma_{j,k,i}\}\right] \\ &= \left(\frac{\lambda_{j,l,i}^{BC}}{\lambda_{j,k,i}^{BC} + \lambda_{j,l,i}^{BC}}\right)\left(\frac{\lambda_{j,q,i}^{BC}}{\lambda_{j,k,i}^{BC} + \lambda_{j,q,i}^{BC} + \lambda_{j,l,i}^{BC}}\right).\end{aligned} \tag{3.56}$$

In general, to find the probability that node S_k is the optimal node to relay symbol x_j to node S_i for $N > 5$ is recursively determined using

$$\Pr\left[\gamma_{j,k,i} > \{\gamma_{j,q,i}\}_{\substack{q=1,2,\ldots,N \\ q\neq i, q\neq j, q\neq k}}\right] \tag{3.57}$$

for the different inequality permutations of $\gamma_{j,q,i}, \forall q \in \{1, 2, \ldots, N\}$ and $q \neq i \neq j \neq k$.

3.6 Optimal Power Allocation

The performance of the M2M-STNC scheme can be further improved by optimally allocating cooperative transmit power $P_j^C = \sum_{i=1,i\neq j}^{N} P_{j,i}^C$ with $P_{j,i}^C = \sum_{\substack{k=1\\k\neq i,k\neq j}}^{N} P_{j,k,i}^C$ among the relaying nodes so as to improve the total achievable rate of node S_j, $\forall j \in \{1,2,\ldots,N\}$ and $j \neq i$. From (3.23), define $\xi_{j,k,i}$ as

$$\xi_{j,k,i} = \frac{|h_{k,i}|^2}{P_j^B |h_{j,k}|^2 + N_0}, \tag{3.58}$$

and hence the instantaneous SNR due to the cooperative transmission $\gamma_{j,i}^{CP}$ is re-defined as

$$\gamma_{j,i}^{CP} = \frac{P_j^B \left(\sum_{\substack{k=1\\k\neq i,k\neq j}}^{N} P_{j,k,i}^C |h_{j,k}|^2 \xi_{j,k,i} \right)}{N_0 \varrho_{N-1} \left(1 + \sum_{\substack{k=1\\k\neq i,k\neq j}}^{N} P_{j,k,i}^C \xi_{j,k,i} \right)}. \tag{3.59}$$

Thus, the achievable rate between source node S_j and destination node S_i is expressed as

$$\mathcal{R}_{j,i}^{\text{M2M-STNC}}(\gamma_{j,i}) = \frac{1}{2N} \log_2 \left(1 + \frac{P_j^B |h_{j,i}|^2}{N_0} + \frac{P_j^B \left(\sum_{\substack{k=1\\k\neq i,k\neq j}}^{N} P_{j,k,i}^C |h_{j,k}|^2 \xi_{j,k,i} \right)}{N_0 \varrho_{N-1} \left(1 + \sum_{\substack{k=1\\k\neq i,k\neq j}}^{N} P_{j,k,i}^C \xi_{j,k,i} \right)} \right), \tag{3.60}$$

which can be verified to be strictly increasing and concave in $P_{j,k,i}^C, \forall k \in \{1,2,\ldots,N\}$ with $k \neq j$ and $k \neq i$ for fixed P_j^B. Therefore, the total rate $\mathcal{R}_j^{\text{M2M-STNC}}$ maximizing cooperative power allocation problem for source node S_j for $j \in \{1,2,\ldots,N\}$ can be formulated as

$$\begin{aligned} \max_{P_{j,k,i}^C \geq 0} \quad & \sum_{i=1,i\neq j}^{N} \mathcal{R}_{j,i}^{\text{M2M-STNC}}(\gamma_{j,i}) \\ \text{s.t.} \quad & \sum_{\substack{k=1\\k\neq i,k\neq j}}^{N} P_{j,k,i}^C \leq P_{j,i}^C, \qquad \forall i \in \{1,2,\ldots,N\} \text{ and } i \neq j, \\ & \sum_{i=1,i\neq j}^{N} P_{j,i}^C \leq P_j^C. \end{aligned} \tag{3.61}$$

Note that if the power fraction $\delta_{j,i}^C = P_{j,i}^C / P_j^C$ of node S_j to transmit its symbol x_j to node $S_i, \forall i \in \{1,2,\ldots,N\}$ and $j \neq i$ is known, then the above problem is separated as follows

$$\begin{aligned} \max_{P_{j,k,i}^C \geq 0} \quad & \mathcal{R}_{j,i}^{\text{M2M-STNC}}(\gamma_{j,i}) \\ \text{s.t.} \quad & \sum_{\substack{k=1\\k\neq i,k\neq j}}^{N} P_{j,k,i}^C \leq P_{j,i}^C, \quad \text{and } j \neq i, \end{aligned} \tag{3.62}$$

leading to the following theorem.

Theorem 3.1: Under the sum-of-rates maximizing optimal power allocation, the M2M-STNC scheme reduces to the M2M-STNC-ONS scheme[2].

Proof: The aim is to show that although the selection rule has not been imposed explicitly, the solution to the optimization problem is that power is optimally allocated to only one relaying node and that node is the one that has the maximum resulting cooperative SNR, when allocated all the available cooperative power $P_{j,i}^{C}$. Define the Lagrangian problem as

$$\mathcal{L}\left(\lambda,\{\upsilon_{j,k,i}\}_{l=1,k\neq j,i}^{N}\right)=-\mathcal{R}_{j,i}^{\text{M2M-STNC}}+\lambda\left(\sum_{\substack{k=1\\k\neq i,k\neq j}}^{N}P_{j,k,i}^{C}-P_{j,i}^{C}\right)-\sum_{\substack{k=1\\k\neq i,k\neq j}}^{N}\upsilon_{j,k,i}P_{j,k,i}^{C}. \tag{3.63}$$

Let $\eta_j^B = P_j^B/(2NN_0\varrho_{N-1}\ln 2)$, then the Karush-Kuhn-Tucker (KKT) conditions for node S_l for $l\in\{1,2,\ldots,N\}$ and $l\neq j,i$ are obtained as

$$\frac{-\eta_j^B}{\left(1+\sum_{\substack{k=1\\k\neq i,k\neq j}}^{N}P_{j,k,i}^{C}\xi_{j,k,i}\right)}\left(\frac{|h_{j,l}|^2\xi_{j,l,i}+\sum_{\substack{k=1\\k\neq i,k\neq j}}^{N}P_{j,k,i}^{C}(|h_{j,l}|^2\xi_{j,l,i}\xi_{j,k,i}-|h_{j,k}|^2\xi_{j,k,i}\xi_{j,l,i})}{\left(1+\sum_{\substack{k=1\\k\neq i,k\neq j}}^{N}P_{j,k,i}^{C}\xi_{j,k,i}\right)(1+P_j^B|h_{j,i}|^2/N_0)+\frac{P_j^B\left(\sum_{\substack{k=1\\k\neq i,k\neq j}}^{N}P_{j,k,i}^{C}|h_{j,k}|^2\xi_{j,k,i}\right)}{N_0\varrho_{N-1}}}\right)+\lambda=\upsilon_{j,l,i}, \tag{3.64}$$

$$\lambda\left(\sum_{\substack{k=1\\k\neq i,k\neq j}}^{N}P_{j,k,i}^{C}-P_{j,i}^{C}\right)=0,$$

$$\upsilon_{j,l,i}P_{j,l,i}^{C}=0,\quad \forall l\in\{1,2,\ldots,N\}\text{ and }l\neq j,i,$$

with $\lambda\geq 0$ and $\upsilon_{j,l,i}\geq 0,\forall l\in\{1,2,\ldots,N\}$ and $l\neq j,i$ being the Lagrange multipliers associated with the total power constraint and power positivity, respectively. Now, consider the case where $P_{j,l,i}^{C}>0$, $\forall l\in\{1,2,\ldots,N\}$ and $l\neq j,i$, which by complimentary slackness implies that $\upsilon_{j,l,i}=0$. This in turn leads to

$$\frac{\eta_j^B}{\left(1+\sum_{\substack{k=1\\k\neq i,k\neq j}}^{N}P_{j,k,i}^{C}\xi_{j,k,i}\right)}\left(\frac{|h_{j,l}|^2\xi_{j,l,i}+\sum_{\substack{k=1\\k\neq i,k\neq j}}^{N}P_{j,k,i}^{C}(|h_{j,l}|^2\xi_{j,l,i}\xi_{j,k,i}-|h_{j,k}|^2\xi_{j,k,i}\xi_{j,l,i})}{\left(1+\sum_{\substack{k=1\\k\neq i,k\neq j}}^{N}P_{j,k,i}^{C}\xi_{j,k,i}\right)(1+P_j^B|h_{j,i}|^2/N_0)+\frac{P_j^B\left(\sum_{\substack{k=1\\k\neq i,k\neq j}}^{N}P_{j,k,i}^{C}|h_{j,k}|^2\xi_{j,k,i}\right)}{N_0\varrho_{N-1}}}\right)=\lambda. \tag{3.65}$$

Consequently,

$$|h_{j,l}|^2\xi_{j,l,i}+\sum_{\substack{k=1\\k\neq i,k\neq j}}^{N}P_{j,k,i}^{C}(|h_{j,l}|^2\xi_{j,l,i}\xi_{j,k,i}-|h_{j,k}|^2\xi_{j,k,i}\xi_{j,l,i})=|h_{j,q}|^2\xi_{j,q,i}+\sum_{\substack{k=1\\k\neq i,k\neq j}}^{N}P_{j,k,i}^{C}(|h_{j,q}|^2\xi_{j,q,i}\xi_{j,k,i}-|h_{j,k}|^2\xi_{j,k,i}\xi_{j,q,i}) \tag{3.66}$$

for $\forall q\in\{1,2,\ldots,N\}$ and $q\neq j,i,l$. Rearranging (3.66) yields

$$|h_{j,l}|^2\xi_{j,l,i}-|h_{j,q}|^2\xi_{j,q,i}+\sum_{\substack{k=1\\k\neq i,k\neq j}}^{N}P_{j,k,i}^{C}\left((|h_{j,l}|^2\xi_{j,l,i}-|h_{j,q}|^2\xi_{j,q,i})\xi_{j,k,i}-|h_{j,k}|^2\xi_{j,k,i}(\xi_{j,l,i}-\xi_{j,q,i})\right)=0, \tag{3.67}$$

[2]A similar result has recently appeared in [107].

which cannot simultaneously be true for any two nodes S_l and S_q for $l \neq q$. Since the rate function can be verified to be strictly increasing in the cooperative power, then the optimal solution always happens on the boundary of the feasible set (i.e. $P^C_{j,opt,i} = P^C_{j,i}$). Hence, when power is optimally allocated, only one node is allocated all the available cooperative power $P^C_{j,i}$ and that node's cooperative transmission maximizes the achievable rate. □

3.7 Timing Synchronization Analysis

It is well-known that due to the diagonal structure of the broadcasting phase, as shown in (3.1), the problem of perfect timing synchronization is alleviated since within the TDMA framework, only one source node is allowed to transmit at any one time-slot [9]. Moreover, the analysis so far assumed perfect "in-phase" synchronization among the transmitting nodes in the cooperation phase. However, simultaneous transmissions of the distributed nodes during the cooperation phase impose a major practical challenge, especially for a large number of transmitting nodes, scattered over a large area in the network. The mismatches in clocks of the geographically distributed nodes result in different transmission times. Also, the lack of tracking at the receiving node for all the other cooperating nodes and the lack of compensation for propagation delays can have detrimental effects on the network performance. Therefore, this section aims at analyzing the timing synchronization errors in the cooperation phase and their impact on the SER performance and achievable rate of the M2M-STNC and M2M-STNC-ONS schemes.

3.7.1 Signal Model Under M2M-STNC Scheme

In the cooperation phase, consider the scenario where node S_i is the receiving node while the remaining distributed nodes S_m for $m \in \{1, 2, \ldots, N\}_{m \neq i}$ are assumed to transmit asynchronously. Let $\tau_{i,m}$ be the time-offset for each transmitting node S_m during the i^{th} time-slot. Moreover, assume that each distributed node initiates and terminates it transmissions within T_s time units of each other within each TDMA time-slot. Due to the fractional-symbol delay between the different nodes, the channels can become extremely dispersive even for flat-fading channels. Moreover, the effect of the different propagation delays is manifested in the form of superposition of pulses from each node S_m for $m \in \{1, 2, \ldots, N\}_{m \neq i}$ that are shifted by $\tau_{i,m}$. This in turn implies that neighboring symbols will introduce intersymbol interference (ISI) to the desired symbol. In this work, only the ISI contribution from the neighboring symbols to the desired symbol is considered while the higher-order terms are neglected due to their smaller effect [108]. Thus, from (3.8), the received signal at node S_i during the i^{th} time-slot is expressed as[3] [109] [110]

[3]It is assumed that the channel coefficients are time-invariant during each time-slot but are randomly time-varying from one time-slot to another.

$$\mathcal{Y}_i(t) = \sum_{m=1,m\neq i}^{N} \alpha_{m,i} \sum_{l=-1}^{1} x_m(l) c_m\left(t - lT_s - \tau_{i,m}\right) + \bar{w}_i(t), \tag{3.68}$$

where $\alpha_{m,i}$ is defined in (3.9) and $\bar{w}_i(t)$ is written as

$$\bar{w}_i(t) = w_i(t) + \sum_{m=1,m\neq i}^{N} \sum_{\substack{k=1 \\ k\neq i,k\neq m}}^{N} \beta_{m,k,i} h_{k,i} \sum_{l=-1}^{1} n_{m,k}\left(t - lT_s\right) c_m\left(t - lT_s - \tau_{i,m}\right). \tag{3.69}$$

Without loss of generality, the random time-shifts between the $N-1$ nodes and the receiving node S_i are ordered such that $0 \leq \tau_{i,1} \leq \ldots \leq \tau_{i,i-1} \leq \tau_{i,i+1} \leq \ldots \leq \tau_{i,N} < T_s$. As before, the received signal is then fed into a bank of $N-1$ filters, matched to the nodes' signature waveforms, and sampled at $t = lT_s + \Delta_i$, where Δ_i is the timing-shift chosen by the receiving node S_i to compensate for the average delay of the transmitting nodes. Thus, the received signal at node S_i is given by [111]

$$\mathcal{Y}_{j,i}(l) = \langle \mathcal{Y}_i(t), c_j(t) \rangle = \int_{lT_s+\Delta_i}^{lT_s+T_s+\Delta_i} \mathcal{Y}_i(t) c_j^*(t - lT_s - \Delta_i)\, dt, \tag{3.70}$$

with $c_j(t)$ being zero outside the duration of T_s time units. Now, define the $(N-1)\times(N-1)$ cross-correlation matrix $\boldsymbol{R}_i(l)$ whose entries are in general modeled for $l = 1$, $l = 0$ and $l = -1$ as [99]

$$\tilde{\rho}_{m,j}^{(1)} = \begin{cases} \frac{1}{T_s}\int_{\Delta_i}^{\tau_{i,m}} c_m(t-\tau_{i,m}) c_j^*(t-\Delta_i)\, dt = \rho_{m,j}\left(\frac{\tau_{i,m}-\Delta_i}{T_s}\right), & \tau_{i,m} > \Delta_i \\ 0, & \text{otherwise} \end{cases}, \tag{3.71}$$

$$\bar{\rho}_{m,j}^{(0)} = \frac{1}{T_s}\int_{\max(\tau_{i,m},\Delta_i)}^{\min(\tau_{i,m},\Delta_i)+T_s} c_m(t-\tau_{i,m}) c_j^*(t-\Delta_i)\, dt = \begin{cases} \rho_{m,j}\left(1 - \frac{\Delta_i-\tau_{i,m}}{T_s}\right), & \Delta_i \geq \tau_{i,m} \\ \rho_{m,j}\left(1 - \frac{\tau_{i,m}-\Delta_i}{T_s}\right), & \Delta_i < \tau_{i,m} \end{cases}, \tag{3.72}$$

and

$$\tilde{\rho}_{m,j}^{(-1)} = \begin{cases} \frac{1}{T_s}\int_{\tau_{i,m}}^{\Delta_i} c_m(t-\tau_{i,m}) c_j^*(t-\Delta_i)\, dt = \rho_{m,j}\left(\frac{\Delta_i-\tau_{i,m}}{T_s}\right), & \tau_{i,m} < \Delta_i \\ 0, & \text{otherwise} \end{cases}, \tag{3.73}$$

respectively, where $\boldsymbol{R}_i(l) = 0, \forall |l| > 1$, $\boldsymbol{R}_i(l) = \boldsymbol{R}_i^T(-l)$, and as before, it is assumed that $\rho_{m,j} = \rho, \forall m \neq i$. Furthermore, the time-shifts are assumed to be uniformly distributed as $\tau_{i,m} - \Delta_i \sim U\left[-\Delta T_s/2, \Delta T_s/2\right]$ around the reference clock Δ_i, $\forall m \in \{1,2,\ldots,N\}_{m\neq i}$, where $\Delta T_s \in [0, T_s)$ is the maximum time-shift value. Intuitively, the smaller are the time-shifts, the less severe are the timing synchronization errors.

For convenience, let $\boldsymbol{R}_i(0) = \bar{\boldsymbol{R}}_i$ be defined as

$$\bar{\boldsymbol{R}}_i = \begin{bmatrix} 1 & \cdots & \bar{\rho}^{(0)}_{1,(i-1)} & \bar{\rho}^{(0)}_{1,(i+1)} & \cdots & \bar{\rho}^{(0)}_{1,N} \\ \vdots & \ddots & \vdots & \vdots & \cdots & \vdots \\ \bar{\rho}^{(0)}_{(i-1),1} & \cdots & 1 & \bar{\rho}^{(0)}_{(i-1),(i+1)} & \cdots & \bar{\rho}^{(0)}_{(i-1),N} \\ \bar{\rho}^{(0)}_{(i+1),1} & \cdots & \bar{\rho}^{(0)}_{(i+1),(i-1)} & 1 & \cdots & \bar{\rho}^{(0)}_{(i+1),N} \\ \vdots & \cdots & \vdots & \vdots & \ddots & \vdots \\ \bar{\rho}^{(0)}_{N,1} & \cdots & \bar{\rho}^{(0)}_{N,(i-1)} & \bar{\rho}^{(0)}_{N,(i+1)} & \cdots & 1 \end{bmatrix}, \tag{3.74}$$

and $\boldsymbol{R}_i(1) = \boldsymbol{R}_i^T(-1) = \tilde{\boldsymbol{R}}_i$, where $\tilde{\boldsymbol{R}}_i$ is defined as follows [112]

$$\tilde{\boldsymbol{R}}_i = \begin{bmatrix} 0 & \cdots & \tilde{\rho}^{(1)}_{1,(i-1)} & \tilde{\rho}^{(1)}_{1,(i+1)} & \cdots & \tilde{\rho}^{(1)}_{1,N} \\ \vdots & \ddots & \vdots & \vdots & \cdots & \vdots \\ 0 & \cdots & 0 & \tilde{\rho}^{(1)}_{(i-1),(i+1)} & \cdots & \tilde{\rho}^{(1)}_{(i-1),N} \\ 0 & \cdots & 0 & 0 & \cdots & \tilde{\rho}^{(1)}_{(i+1),N} \\ \vdots & \cdots & \vdots & \vdots & \ddots & \vdots \\ 0 & \cdots & 0 & 0 & \cdots & 0 \end{bmatrix}. \tag{3.75}$$

Thus, the output of the matched filter bank can be expressed as [111] [112]

$$\boldsymbol{\mathcal{Y}}_i(l) = \tilde{\boldsymbol{R}}_i^T \boldsymbol{A}_i \boldsymbol{x}_i(l+1) + \bar{\boldsymbol{R}}_i \boldsymbol{A}_i \boldsymbol{x}_i(l) + \tilde{\boldsymbol{R}}_i \boldsymbol{A}_i \boldsymbol{x}_i(l-1) + \bar{\boldsymbol{w}}_i(l), \tag{3.76}$$

where matrix $\boldsymbol{A}_i$ is defined in (3.16) whereas $\boldsymbol{x}_i(l+\varsigma)$ is defined in general as

$$\boldsymbol{x}_i(l+\varsigma) = [x_1(l+\varsigma), \ldots, x_{i-1}(l+\varsigma), x_{i+1}(l+\varsigma), \ldots, x_N(l+\varsigma)]^T \tag{3.77}$$

for $\varsigma \in \{-1, 0, 1\}$. Also, $\bar{\boldsymbol{w}}_i(l)$ is the noise vector with variance given by

$$E\left[\bar{\boldsymbol{w}}_i(l)\bar{\boldsymbol{w}}_i^H(l+\varsigma)\right] = \begin{cases} N_0\left((\mathbf{I}+\boldsymbol{G}_i)\bar{\boldsymbol{R}}_i^T + \boldsymbol{G}_i\tilde{\boldsymbol{R}}_i\right), & \text{if } \varsigma = 1 \\ N_0\left((\mathbf{I}+\boldsymbol{G}_i)\bar{\boldsymbol{R}}_i + \boldsymbol{G}_i\tilde{\boldsymbol{R}}_i^T + \boldsymbol{G}_i\tilde{\boldsymbol{R}}_i\right), & \text{if } \varsigma = 0 \\ N_0\left((\mathbf{I}+\boldsymbol{G}_i)\bar{\boldsymbol{R}}_i + \boldsymbol{G}_i\tilde{\boldsymbol{R}}_i^T\right), & \text{if } \varsigma = -1 \\ 0, & \text{otherwise} \end{cases}, \tag{3.78}$$

where $E[\cdot]$ is the expectation operator and matrix $\boldsymbol{G}_i$ is defined in (3.17). As before, the vector $\boldsymbol{\mathcal{Y}}_i(n)$ can be decorrelated as

$$\bar{\boldsymbol{\mathcal{Y}}}_i(l) = \boldsymbol{R}_i^{-1}\boldsymbol{\mathcal{Y}}_i(l) = \acute{\boldsymbol{R}}_i \boldsymbol{A}_i \boldsymbol{x}_i(l+1) + \bar{\bar{\boldsymbol{R}}}_i \boldsymbol{A}_i \boldsymbol{x}_i(l) + \grave{\boldsymbol{R}}_i \boldsymbol{A}_i \boldsymbol{x}_i(l-1) + \bar{\bar{\boldsymbol{w}}}_i(l), \tag{3.79}$$

where $\boldsymbol{R}_i$ is as defined in (3.15) with off-diagonal elements equal to ρ, $\bar{\bar{\boldsymbol{R}}}_i = \boldsymbol{R}_i^{-1}\bar{\boldsymbol{R}}_i$, $\acute{\boldsymbol{R}}_i = \boldsymbol{R}_i^{-1}\tilde{\boldsymbol{R}}_i^T$, $\grave{\boldsymbol{R}}_i = \boldsymbol{R}_i^{-1}\tilde{\boldsymbol{R}}_i$ and $\bar{\bar{\boldsymbol{w}}}_i(l) = \boldsymbol{R}_i^{-1}\bar{\boldsymbol{w}}_i(l)$ with

$$E\left[\bar{\bar{\boldsymbol{w}}}_i(l)\bar{\bar{\boldsymbol{w}}}_i^H(l+\varsigma)\right] = \begin{cases} N_0\boldsymbol{R}_i^{-1}\left((\mathbf{I}+\boldsymbol{G}_i)\bar{\boldsymbol{R}}_i^T + \boldsymbol{G}_i\tilde{\boldsymbol{R}}_i\right)\boldsymbol{R}_i^{-T}, & \text{if } \varsigma = 1 \\ N_0\boldsymbol{R}_i^{-1}\left((\mathbf{I}+\boldsymbol{G}_i)\bar{\boldsymbol{R}}_i + \boldsymbol{G}_i\tilde{\boldsymbol{R}}_i^T + \boldsymbol{G}_i\tilde{\boldsymbol{R}}_i\right)\boldsymbol{R}_i^{-T}, & \text{if } \varsigma = 0 \\ N_0\boldsymbol{R}_i^{-1}\left((\mathbf{I}+\boldsymbol{G}_i)\bar{\boldsymbol{R}}_i + \boldsymbol{G}_i\tilde{\boldsymbol{R}}_i^T\right)\boldsymbol{R}_i^{-T}, & \text{if } \varsigma = -1 \\ 0, & \text{otherwise} \end{cases}. \tag{3.80}$$

The decorrelated received signal $\bar{\mathcal{Y}}_{j,i}(l)$ at the output of the j^{th} MFB branch is given by

$$\bar{\mathcal{Y}}_{j,i}(l) = \underbrace{\alpha_{j,i}\bar{\bar{\rho}}_{j,j}x_j(l)}_{\text{Desired Symbol}} + \underbrace{\sum_{m=1,m\neq i}^{N}\alpha_{m,i}\left(\acute{\rho}_{j,m}x_m(l+1)+\grave{\rho}_{j,m}x_m(l-1)\right)+\sum_{m=1,m\neq i,j}^{N}\alpha_{m,i}\bar{\bar{\rho}}_{j,m}x_m(l)}_{\text{ISI Symbols}}+\bar{\bar{w}}_{j,i}(l), \tag{3.81}$$

where $\bar{\bar{\rho}}_{j,j}$, is the j^{th} diagonal element of matrix $\bar{\bar{\boldsymbol{R}}}_i$, while $\acute{\rho}_{j,m}$ and $\grave{\rho}_{j,m}$ are the $(j,m)^{th}$ element of matrices $\acute{\boldsymbol{R}}_i$ and $\grave{\boldsymbol{R}}_i$, respectively. Additionally, $\bar{\bar{w}}_{j,i}(l) \sim \mathcal{CN}(0, \bar{\bar{\varrho}}_{j,i}N_0)$ where $\bar{\bar{\varrho}}_{j,i}$ is the j^{th} diagonal element of matrix $\boldsymbol{R}_i^{-1}\left((\mathbf{I}+\boldsymbol{G}_i)\bar{\boldsymbol{R}}_i+\boldsymbol{G}_i\tilde{\boldsymbol{R}}_i^T+\boldsymbol{G}_i\tilde{\boldsymbol{R}}_i\right)\boldsymbol{R}_i^{-T}$. Based on the above analysis, the instantaneous conditional signal-to-interference-plus-noise ratio (SINR) at the output of the MRC of node S_i of symbol x_j for $j \neq i$ is obtained as

$$\gamma_{j,i} = \frac{P_j^B|h_{j,i}|^2}{N_0} + \frac{P_j^B\left(\sum_{\substack{k=1\\k\neq i,k\neq j}}^{N}\frac{P_{j,k,i}^C|h_{j,k}|^2|h_{k,i}|^2}{P_j^B|h_{j,k}|^2+N_0}\right)\bar{\bar{\rho}}_{j,j}^2}{\mathcal{I}_{j,i}+\bar{\bar{\varrho}}_{j,i}N_0}, \tag{3.82}$$

where $\mathcal{I}_{j,i}$ is the ISI variance as defined by

$$\mathcal{I}_{j,i} = \sum_{m=1,m\neq i}^{N}P_m^B\left(\sum_{\substack{k=1\\k\neq i,k\neq m}}^{N}\frac{P_{m,k,i}^C|h_{m,k}|^2|h_{k,i}|^2}{P_m^B|h_{m,k}|^2+N_0}\right)(\acute{\rho}_{j,m}^2+\grave{\rho}_{j,m}^2)+\sum_{m=1,m\neq i,j}^{N}P_m^B\left(\sum_{\substack{k=1\\k\neq i,k\neq m}}^{N}\frac{P_{m,k,i}^C|h_{m,k}|^2|h_{k,i}|^2}{P_m^B|h_{m,k}|^2+N_0}\right)\bar{\bar{\rho}}_{j,m}^2, \tag{3.83}$$

and it is assumed that data symbols are statistically independent. That is,

$$E\left[x_m(l)x_j(l+\varsigma)\right] = \begin{cases}1, & \text{if } \varsigma = 0 \text{ and } m = j\\ 0, & \text{otherwise}\end{cases}. \tag{3.84}$$

Based on (3.82), finding a closed-form solution for the SER for M-PSK modulation is extremely difficult. Thus, conditional SER given the channel knowledge can be obtained by substituting (3.82) into (3.39) and then numerically evaluating it. Moreover, it can be verified that if $\tau_{i,m} - \Delta_i = 0, \forall i, m \in \{1, 2, \ldots, N\}$ and $i \neq m$, then $\bar{\rho}_{m,j}^{(0)} = \rho_{m,j}$ and also $\tilde{\rho}_{m,j}^{(-1)} = \tilde{\rho}_{m,j}^{(1)} = 0$. Hence, the SINR term in (3.82) reduces to the SNR term of (3.22).

3.7.2 Signal Model Under M2M-STNC-ONS Scheme

From (3.28), the received signal at node S_i is given by

$$\hat{\mathcal{Y}}_i(t) = \sum_{m=1,m\neq i}^{N}\hat{\alpha}_{m,i}\sum_{l=-1}^{1}x_m(l)c_m\left(t-lT_s-\tau_{i,m}\right)+\bar{w}_i(t), \tag{3.85}$$

where $\hat{\alpha}_{m,i}$ is defined in (3.29) and $\hat{w}_i(t)$ is written as

$$\hat{w}_i(t) = w_i(t) + \sum_{m=1,m\neq i}^{N}\beta_{m,opt,i}\hat{h}_{m,opt,i}\sum_{l=-1}^{1}n_{m,opt,i}\left(t-lT_s\right)c_m\left(t-lT_s-\tau_{i,m}\right). \tag{3.86}$$

Following the analysis of the M2M-STNC scheme and replacing matrices $\boldsymbol{A}_i$ and $\boldsymbol{G}_i$ with $\hat{\boldsymbol{A}}_i$ and $\hat{\boldsymbol{G}}_i$, respectively (see (3.31) and (3.32)), the instantaneous conditional SINR of symbol x_j at node S_i can be shown to be

$$\hat{\gamma}_{j,i} = \frac{P_j^B |h_{j,i}|^2}{N_0} + \frac{P_j^B \left(\frac{P_{j,i}^C |\bar{h}_{j,opt,i}|^2 |\hat{h}_{j,opt,i}|^2}{P_j^B |\bar{h}_{j,opt,i}|^2 + N_0} \right) \bar{\bar{\rho}}_{j,j}^2}{\hat{\mathcal{I}}_{j,i} + \hat{\hat{\varrho}}_{j,i} N_0}, \tag{3.87}$$

where $\hat{\hat{\varrho}}_{j,i}$ is the j^{th} diagonal element of matrix $\boldsymbol{R}_i^{-1} \left((\mathbf{I} + \hat{\boldsymbol{G}}_i) \bar{\boldsymbol{R}}_i + \hat{\boldsymbol{G}}_i \tilde{\boldsymbol{R}}_i^T + \hat{\boldsymbol{G}}_i \tilde{\boldsymbol{R}}_i \right) \boldsymbol{R}_i^{-T}$, and

$$\hat{\mathcal{I}}_{j,i} = \sum_{m=1, m \neq i}^{N} P_m^B \left(\frac{P_{m,i}^C |\bar{h}_{m,opt,i}|^2 |\hat{h}_{m,opt,i}|^2}{P_m^B |\bar{h}_{m,opt,i}|^2 + N_0} \right) (\acute{\rho}_{j,m}^2 + \grave{\rho}_{j,m}^2) + \sum_{m=1, m \neq i,j}^{N} P_m^B \left(\frac{P_{m,i}^C |\bar{h}_{m,opt,i}|^2 |\hat{h}_{m,opt,i}|^2}{P_m^B |\bar{h}_{m,opt,i}|^2 + N_0} \right) \bar{\bar{\rho}}_{j,m}^2. \tag{3.88}$$

3.8 Imperfect Channel State Information

So far, perfect channel state information (CSI) has been assumed and in practice, such assumption is not valid. Channel estimation errors are possibly caused by inaccurate channel estimation/equalization, noise or Doppler shift. Conventionally, channel estimation is based on transmitting a known pilot "training" sequence with a particular power, prior to data transmission. Inaccurate channel estimation results in a channel estimation error with variance, denoted as ε. At the end of the training phase, the receiving node has imperfect CSI for channel equalization and data detection. In the following subsections, the impact of channel estimation errors on the performance of the M2M-STNC and M2M-STNC-ONS schemes—assuming perfect timing synchronization—is studied and characterized.

3.8.1 M2M-STNC

In the broadcasting phase, the received signal at node S_i from node S_j with channel estimation error is expressed as

$$y_{j,i}^{\varepsilon}(t) = \sqrt{P_j^B} (h_{j,i} + h_{j,i}^{\varepsilon}) x_j c_j(t) + n_{j,i}(t), \tag{3.89}$$

where $h_{j,i}^{\varepsilon}$ denotes the channel estimation error. Consequently, $\sqrt{P_j^B} h_{j,i}^{\varepsilon} x_j$ is the added noise term that scales with the broadcasting power. Furthermore, the channel estimation error $h_{j,i}^{\varepsilon}$ is modeled as a zero-mean complex Gaussian random variable with variance $\varepsilon_{j,i}$. Thus, the additional self-noise term $\sqrt{P_j^B} h_{j,i}^{\varepsilon} x_j$ is a zero-mean complex Gaussian random variable with variance $\varepsilon_{j,i} P_j^B$. Equation (3.89) is re-written as

$$y_{j,i}^{\varepsilon}(t) = \sqrt{P_j^B} h_{j,i} x_j c_j(t) + n_{j,i}^{\varepsilon}(t) \tag{3.90}$$

where $n_{j,i}^{\varepsilon}(t) = \sqrt{P_j^B} h_{j,i}^{\varepsilon} x_j c_j(t) + n_{j,i}(t)$ is a zero-mean Gaussian random variable with variance $\varepsilon_{j,i} P_j^B + N_0$. Thus, the SNR after matched-filtering is given by

$$\gamma_{j,i}^{BP} = \frac{P_j^B |h_{j,i}|^2}{\varepsilon_{j,i} P_j^B + N_0}. \tag{3.91}$$

In the cooperation phase, the received signal at node S_i is given by

$$\mathcal{Y}_i^{\varepsilon}(t) = \sum_{m=1, m\neq i}^{N} \alpha_{m,i}^{\varepsilon} x_m c_m(t) + \bar{w}_i^{\varepsilon}(t), \tag{3.92}$$

where $\alpha_{m,i}^{\varepsilon}$ is defined as

$$\alpha_{m,i}^{\varepsilon} = \sqrt{P_m^B} \sum_{\substack{k=1 \\ k\neq i, k\neq m}}^{N} \beta_{m,k,i}^{\varepsilon} h_{m,k} h_{k,i}, \tag{3.93}$$

and

$$\beta_{m,k,i}^{\varepsilon} = \sqrt{\frac{P_{m,k,i}^C}{P_m^B (|h_{m,k}|^2 + \varepsilon_{m,k}) + N_0}}. \tag{3.94}$$

As before, $w_i(t)$ is the zero-mean N_0-variance AWGN sample at node S_i and $\bar{w}_i^{\varepsilon}(t)$ is the equivalent noise term, expressed as

$$\bar{w}_i^{\varepsilon}(t) = w_i(t) + \sum_{m=1, m\neq i}^{N} \sum_{\substack{k=1 \\ k\neq i, k\neq m}}^{N} \beta_{m,k,i}^{\varepsilon} \left((h_{k,i} + h_{k,i}^{\varepsilon}) n_{m,k} + (h_{k,i} h_{m,k}^{\varepsilon} + h_{m,k} h_{k,i}^{\varepsilon} + h_{m,k}^{\varepsilon} h_{k,i}^{\varepsilon}) x_m \right) c_m(t). \tag{3.95}$$

After multinode signal detection, the received signal corresponding to symbol x_j is given by

$$\bar{\mathcal{Y}}_{j,i}^{\varepsilon} = \sqrt{P_j^B} \left(\sum_{\substack{k=1 \\ k\neq i, k\neq j}}^{N} \beta_{j,k,i}^{\varepsilon} h_{j,k} h_{k,i} \right) x_j + \bar{\bar{w}}_{j,i}^{\varepsilon}, \tag{3.96}$$

where $\bar{\bar{w}}_{j,i}^{\varepsilon} \sim \mathcal{CN}\left(0, \varrho_{N-1} \bar{g}_{j,i}^{\varepsilon}\right)$ and

$$\bar{g}_{j,i}^{\varepsilon} = N_0 \left(1 + \sum_{\substack{k=1 \\ k\neq i, k\neq j}}^{N} (\beta_{j,k,i}^{\varepsilon})^2 (|h_{k,i}|^2 + \varepsilon_{k,i}) \right) + \sum_{\substack{k=1 \\ k\neq i, k\neq j}}^{N} (\beta_{j,k,i}^{\varepsilon})^2 \left(|h_{k,i}|^2 \varepsilon_{j,k} + |h_{j,k}|^2 \varepsilon_{k,i} + \varepsilon_{j,k} \varepsilon_{k,i} \right). \tag{3.97}$$

In turn, the SNR at the output of the matched filter of node S_i is expressed as

$$\gamma_{j,i}^{CP} = \frac{P_j^B \left(\sum_{\substack{k=1 \\ k\neq i, k\neq j}}^{N} \frac{P_{j,k,i}^C |h_{j,k}|^2 |h_{k,i}|^2}{P_j^B (|h_{j,k}|^2 + \varepsilon_{j,k}) + N_0} \right)}{\varrho_{N-1} \left(N_0 \left(1 + \sum_{\substack{k=1 \\ k\neq i, k\neq j}}^{N} \frac{P_{j,k,i}^C (|h_{k,i}|^2 + \varepsilon_{k,i})}{P_j^B (|h_{j,k}|^2 + \varepsilon_{j,k}) + N_0} \right) + \sum_{\substack{k=1 \\ k\neq i, k\neq j}}^{N} \frac{P_{j,k,i}^C (|h_{k,i}|^2 \varepsilon_{j,k} + |h_{j,k}|^2 \varepsilon_{k,i} + \varepsilon_{j,k} \varepsilon_{k,i})}{P_j^B (|h_{j,k}|^2 + \varepsilon_{j,k}) + N_0} \right)}. \tag{3.98}$$

In the case of perfect CSI (i.e. $\varepsilon_{j,i} = 0$, $\forall j, i \in \{1, 2, \ldots, N\}$ and $j \neq i$), then the SNR expressions in (3.91) and (3.98) reduce to (3.4) and (3.22), respectively.

3.8.2 M2M-STNC-ONS

Under the M2M-STNC-ONS scheme[4], the received signal (see (3.28)) in the cooperation phase at node S_i is given by

$$\hat{\mathcal{Y}}_i(t) = \sum_{m=1,m\neq i}^{N} \hat{\alpha}^{\varepsilon}_{m,i} x_m c_m(t) + \hat{w}^{\varepsilon}_i(t), \tag{3.99}$$

where $\hat{\alpha}^{\varepsilon}_{m,i}$ is defined as

$$\hat{\alpha}^{\varepsilon}_{m,i} = \beta^{\varepsilon}_{m,opt,i} \bar{h}_{m,opt,i} \sqrt{P^B_m} \hat{h}_{m,opt,i}. \tag{3.100}$$

Moreover, $\hat{w}^{\varepsilon}_i(t)$ is equivalent interference plus noise term, defined as

$$\hat{w}^{\varepsilon}_i(t) = w_i(t) + \sum_{m=1,m\neq i}^{N} \beta^{\varepsilon}_{m,opt,i} \left((\hat{h}_{m,opt,i} + \hat{h}^{\varepsilon}_{m,opt,i}) n_{m,opt,i} + (\hat{h}_{m,opt,i} \bar{h}^{\varepsilon}_{m,opt,i} + \bar{h}_{m,opt,} \hat{h}^{\varepsilon}_{m,opt,i} + \hat{h}^{\varepsilon}_{m,opt,i} \bar{h}^{\varepsilon}_{m,opt,i}) x_m \right) c_m(t). \tag{3.101}$$

Following (3.33), the decorrelated signal can be obtained as

$$\hat{\mathcal{Y}}^{\varepsilon}_{j,i} = \beta^{\varepsilon}_{j,opt,i} \bar{h}_{j,opt,i} \sqrt{P^B_j} \hat{h}_{j,opt,i} x_j + \hat{\hat{w}}^{\varepsilon}_{j,i}, \tag{3.102}$$

where $\hat{\hat{w}}^{\varepsilon}_{j,i} \sim \mathcal{CN}(0, \varrho_{N-1} \hat{g}^{\varepsilon}_{j,i})$, where

$$\hat{g}^{\varepsilon}_{j,i} = N_0 \left(1 + (\beta^{\varepsilon}_{j,opt,i})^2 (|\hat{h}_{j,opt,i}|^2 + \hat{\varepsilon}_{j,opt,i}) \right) + (\beta^{\varepsilon}_{j,opt,i})^2 \left(|\hat{h}_{j,opt,i}|^2 \bar{\varepsilon}_{j,opt,i} + |\bar{h}_{j,opt,i}|^2 \hat{\varepsilon}_{j,opt,i} + \hat{\varepsilon}_{j,opt,i} \bar{\varepsilon}_{j,opt,i} \right). \tag{3.103}$$

Therefore, the SNR at the output of the matched filter is expressed as

$$\hat{\gamma}^{CP}_{j,i} = \frac{P^B_j P^C_{j,i} |\bar{h}_{j,opt,i}|^2 |\hat{h}_{j,opt,i}|^2}{\varrho_{N-1} \left(N_0 \left(P^B_j (|\bar{h}_{j,opt,i}|^2 + \bar{\varepsilon}_{j,opt,i}) + P^C_{j,i} (|\hat{h}_{j,opt,i}|^2 + \hat{\varepsilon}_{j,opt,i}) + N_0 \right) + P^C_{j,i} (|\hat{h}_{j,opt,i}|^2 \bar{\varepsilon}_{j,opt,i} + |\bar{h}_{j,opt,i}|^2 \hat{\varepsilon}_{j,opt,i} + \hat{\varepsilon}_{j,opt,i} \bar{\varepsilon}_{j,opt,i}) \right)}. \tag{3.104}$$

As before, in the perfect CSI case, the SNR expression in (3.104) reduces to that of (3.35).

3.9 Performance Evaluation

In this section, the analytical derivations of the performance of the M2M-STNC and M2M-STNC-ONS schemes for $N = 4$ and $N = 5$ are evaluated and compared for symbol x_1 received at node S_4. For simplicity, equal power allocation between the two transmission phases is assumed, such that $P^B_1 = P^C_1 = P/2$, $P^C_{1,i} = P^C_1/(N-1) = P/(2(N-1)), \forall i \in \{2, \ldots, N\}$ and $P^C_{1,k,i} = P^C_{1,i}/(N-2) = P/(2(N-1)(N-2)), \forall k \in \{2, \ldots, N\}$ and $k \neq i$. The network

[4]The node selection criterion is now based on the channel coefficients with estimation errors, which implies that the selected node with imperfect CSI is not necessarily the selected node under perfect CSI.

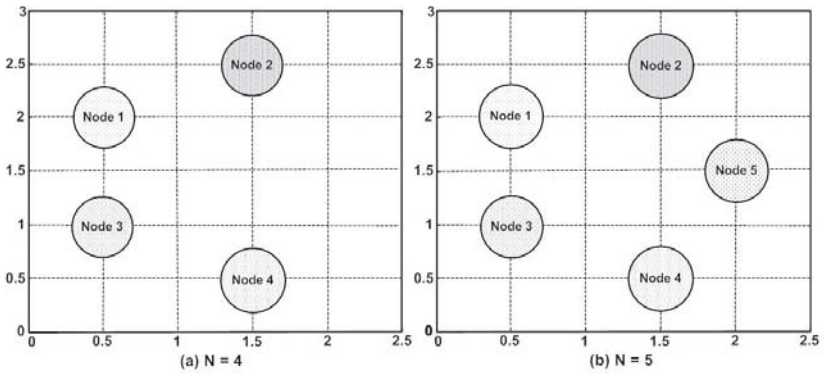

Figure 3.2: Network Configuration with (a) $N = 4$ and (b) $N = 5$ Nodes

nodes are located as shown in Fig. 3.2 with the channel variance between nodes S_j and S_i being defined as $h_{j,i} \sim \mathcal{CN}(0, d_{j,i}^{-\nu}), \forall j, i \in \{1, 2, \ldots, N\}$ for $j \neq i$ and $\nu = 3$. Non-orthogonal signature waveforms with a cross-correlation of $\rho_{j,i} = \rho = 0.5$ for $j \neq i$ are also assumed. The channel estimation error variance is assumed to be the same between any two nodes (i.e. $\varepsilon_{j,i} = \varepsilon, \forall j, i \in \{1, 2, \ldots, N\}$ for $j \neq i$).

3.9.1 Approximate Probability of Node Selection

The approximate probability of node selection for $N = 4$ nodes is illustrated in Fig. 3.3(a) with perfect timing synchronization and CSI. As can be seen, the simulated node selection coincides with the derived probabilistic approximation. In addition, it is noticed that node S_3 is selected—on average—83% of the time and this is due to its location being closer to both source node S_1 and its destination node S_4. A similar observation can be seen in Fig. 3.3(b) for $N = 5$ nodes, with the theoretical approximation agreeing with the simulated optimal node selection. As before, node S_3 is selected most of the time to relay symbol x_1 to destination node S_4.

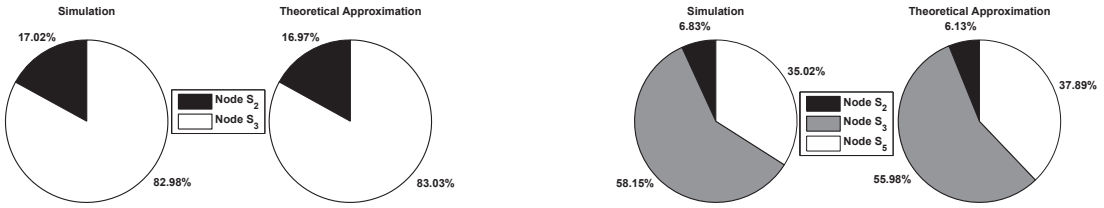

(a) $N = 4$ (b) $N = 5$

Figure 3.3: Approximate Probability of Node Selection for (a) $N = 4$ with Intermediate Nodes S_2 and S_3, and (b) $N = 5$ with Intermediate Nodes S_2, S_3, and S_5 - Perfect Timing Synchronization and CSI

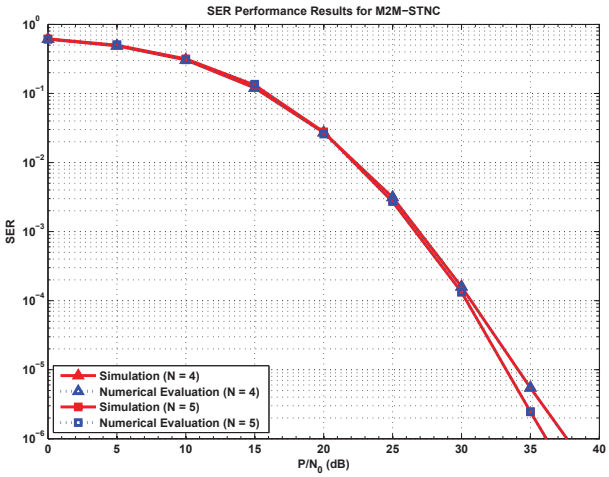

Figure 3.4: QPSK SER Performance of the M2M-STNC Scheme - Perfect Timing Synchronization and CSI

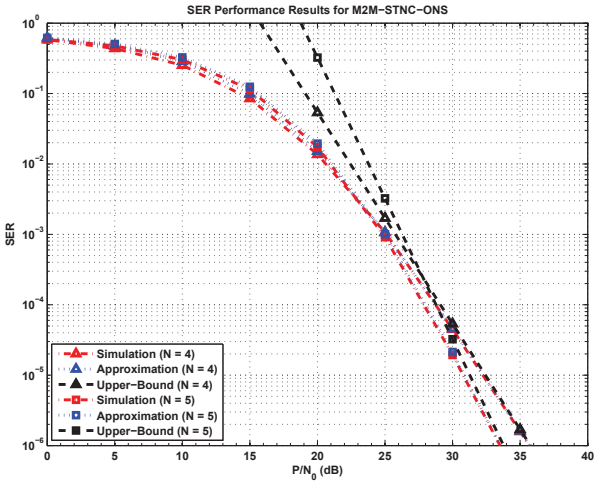

Figure 3.5: QPSK SER Performance of the M2M-STNC-ONS Scheme - Perfect Timing Synchronization and CSI

3.9.2 Symbol Error Rate Performance

From Fig. 3.4 and assuming perfect synchronization and CSI, it is clear that as the number of cooperating nodes in the network N increases, the SER performance of the M2M-STNC scheme improves; however, insignificantly. Moreover, the numerically evaluated SER performance of the M2M-STNC scheme perfectly agrees with its simulated performance. Fig. 3.5 illustrates the SER performance of the proposed M2M-STNC-ONS scheme. Clearly, the derived approximate SER theoretical expression coincides with the simulated performance except for a slight deviation at low SNR which is attributed to the approximation used in the theoretical analysis which assumed high enough SNR. Also, the derived upper-bound happens to be asymptotic at high SNR and thus confirms the achievable diversity order per

node. Based on Figs. 3.4 and 3.5, the proposed M2M-STNC-ONS scheme outperforms its counterpart scheme and achieves full diversity order.

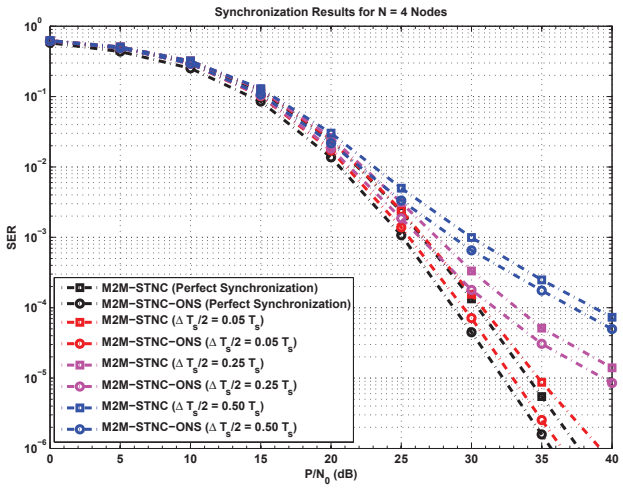

Figure 3.6: QPSK SER Performance with Timing Synchronization Errors for $N = 4$ Nodes - Perfect CSI

In Fig. 3.6, the SER performance of the M2M-STNC and M2M-STNC-ONS schemes is compared with timing synchronization errors and perfect CSI for $N = 4$ nodes. Clearly, the M2M-STNC-ONS scheme is more resistant to timing offsets than its counterpart scheme. This is because the number of simultaneous transmissions in each time-slot is reduced and only the node achieving the highest cooperative SNR at the receiving node relays its received signal. A similar observation is seen in the case of $N = 5$ nodes (see Fig. 3.7). However, it is noticed that the impact of timing offsets on the SER performance is less severe despite the increase in the number of transmitting nodes, which is due to the increased diversity order.

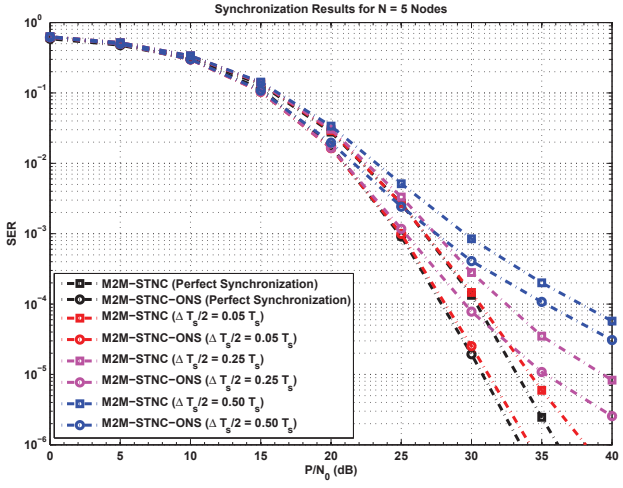

Figure 3.7: QPSK SER Performance with Timing Synchronization Errors for $N = 5$ Nodes - Perfect CSI

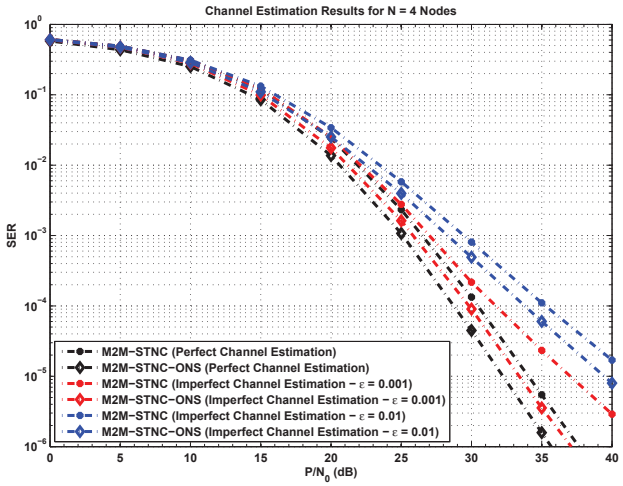

Figure 3.8: QPSK SER Performance with Imperfect CSI for $N = 4$ Nodes - Perfect Timing Synchronization

The performance of the M2M-STNC and M2M-STNC-ONS schemes with channel estimation errors and perfect timing synchronization for $N = 4$ nodes is demonstrated in Fig. 3.8. It is clear that with the increase in channel estimation error variance ε, the SER performance of both schemes degrades with the M2M-STNC-ONS scheme still significantly outperforming its counterpart scheme. The case of $N = 5$ nodes is shown in Fig. 3.9 with the SER performance of both schemes being less affected by channel estimation errors due to the increased diversity gains, as aforementioned.

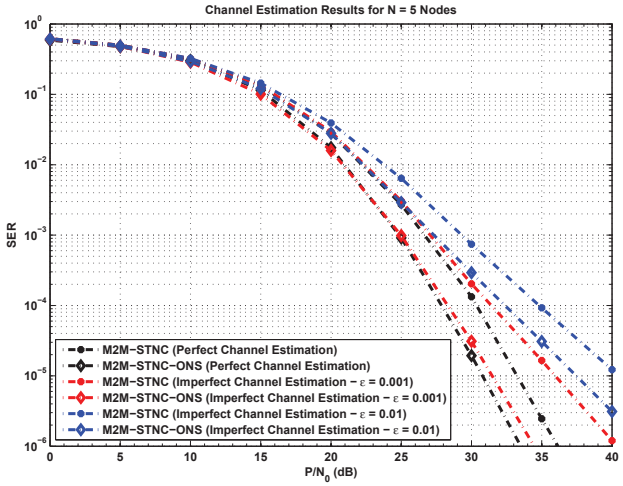

Figure 3.9: QPSK SER Performance with Imperfect CSI for $N = 5$ Nodes - Perfect Timing Synchronization

3.9.3 Achievable Rate Performance

In Fig. 3.10, the achievable rate of node S_1 at node S_4 for $N = 4$ and $N = 5$ nodes is illustrated. It is evident that the proposed M2M-STNC-ONS scheme with perfect synchronization and CSI achieves a better transmission rate than the M2M-STNC scheme. The achievable rate when $N = 5$ is less than that when $N = 4$, which is due to the increased number of time-slots required for communication between all the nodes. The same observation holds for the different cases of perfect and imperfect timing synchronization and CSI.

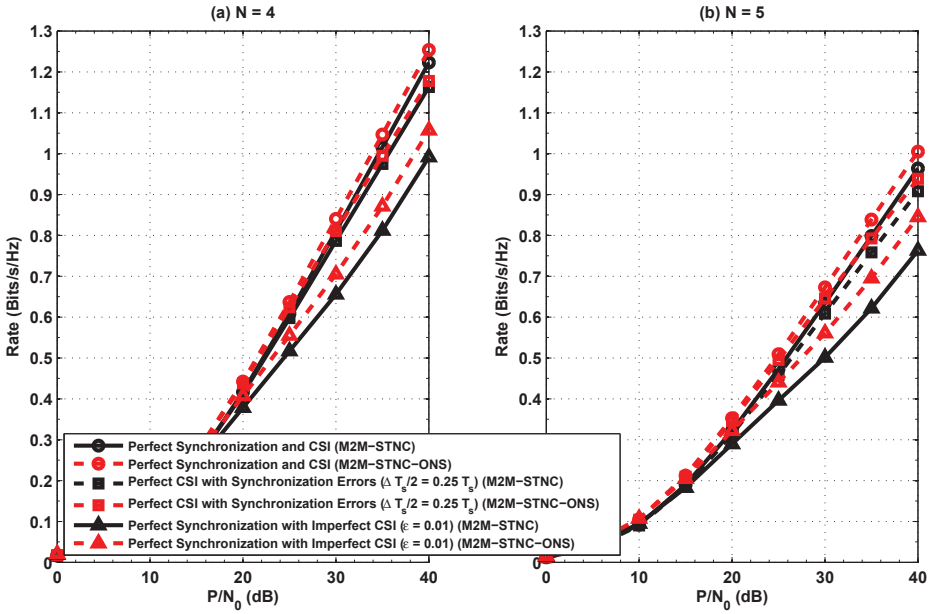

Figure 3.10: Achievable Rate of Node S_1 at Node S_4 for (a) $N = 4$, and (b) $N = 5$ Nodes

Fig. 3.11 illustrates the total achievable rate of source node S_1 for $N = 4$ and $N = 5$ nodes networks. It is clear that the proposed M2M-STNC-ONS scheme is superior to the M2M-STNC scheme and the total achievable rate for a network with $N = 5$ nodes is higher than that of a network with $N = 4$, despite the decrease in the rate between node S_1 and all the other nodes in the networks. Finally, the gain in rate of the M2M-STNC-ONS scheme compared with its counterpart M2M-STNC scheme is higher for the network with $N = 5$ nodes. This again can be seen for the different cases of perfect and imperfect synchronization and CSI.

3.10 Conclusions

In this chapter, both the M2M-STNC and the M2M-STNC-ONS multinode cooperative communication schemes are presented and analyzed. It has been shown that both schemes allow N amplify-and-forward nodes to exchange their data symbols over a total of $2N$ time-

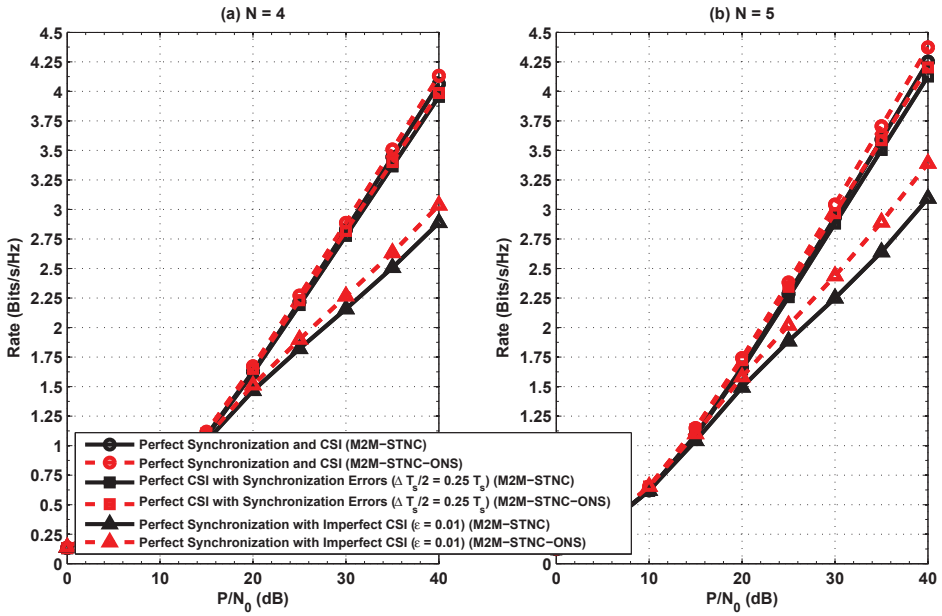

Figure 3.11: Total Achievable Rate of Source Node S_1 for a Network of $N = 4$ and $N = 5$ Nodes

slots and thus maintain a network throughput of 1/2 symbol per time-slot. Moreover, an analytical expression for the conditional SER of the M2M-STNC scheme has been provided while approximate and asymptotic upper-bound SER expressions for the M2M-STNC-ONS scheme have been derived and shown to coincide with the simulated results.

The superiority of the M2M-STNC-ONS scheme with N nodes manifests itself in the fact that only two time-slots are effectively required per node to achieve a diversity order of $N-1$ per transmitted symbol while allowing all the N nodes to exchange their data symbols simultaneously over a total of $2N$ time-slots as opposed to the conventional multinode relay networks that require N^2 time-slots to achieve the same diversity order of $N-1$ per node even with optimal relay selection [24]. In addition, the M2M-STNC-ONS reduces the total number of transmissions in each time-slot in the cooperation phase in comparison with the M2M-STNC scheme, which in turn reduces the effect of noise amplification and more importantly reduces the effect of timing synchronization errors. Also, the effect of imperfect channel state information is mitigated.

Due to the envisioned merits of the M2M-STNC-ONS scheme, its potential applications include but are not limited to cluster-based communications for cooperative spectrum sensing and decision fusion in cognitive radio networks [113], and also for reliable and energy-efficient inter- and intra-cluster data gathering in wireless sensor networks [114]. Moreover, the M2M-STNC-ONS scheme can be used for improved network connectivity in clustered mobile ad-hoc networks [115]. Hence, it is expected that the M2M-STNC-ONS scheme will serve as a potential candidate for many-to-many cooperative communications in amplify-and-forward cooperative networks.

Chapter 4

Auction-Based Power Allocation for Single-Relay Cooperative Networks

4.1 Introduction

In the previous two chapters, sum-of-rates maximizing power allocation has been formulated and proposed for bi-directional and multinode cooperative communications. Such power allocation is assumed to be performed by a centralized controller. In addition, the selected nodes were assumed to voluntarily share their transmission resources (i.e. bandwidth and power). However, in decentralized and fully distributed ad-hoc wireless networks without a single authority and with network users acting as independent entities, rational users may selfishly aim at maximizing their utility and use of resources. Moreover, selfish users might not have any incentive to share their resources if they cannot gain some reward in return. In other cases, several users could compete in order to consume transmission resources from a particular user who might be willing to assist in relaying their data transmissions towards a destination for a price. Further, rational, selfish users may overstate or otherwise not truthfully report their resource demands if doing so can improve their utility. In other scenarios, revealing such proprietary information may have an adverse strategic long-term impact. Hence, a key problem in ad-hoc wireless networks is how to allocate transmission resources efficiently among competing selfish users. Overall, the modeling of repeated interaction of network users is rooted in game and auction theories.

An important thrust of recent research deals with user selfishness and cooperation in wireless networks from a game-theoretic perspective. For instance, in [116], a Stackelberg game is proposed for multinode relay selection and power control when a single source node communicates with a single destination. In another line of work, Huang *et al.* propose two distributed auction mechanisms that achieve a unique Nash Equilibrium for relay selection and power allocation, namely, the SNR auction and the power auction [117]. It is shown that the SNR auction offers a flexible tradeoff between fairness and efficiency, while the power

auction achieves efficient power allocation by maximizing the total rate increase. In [118], a second-price auction is proposed for fair allocation of a wireless fading channel for different channel state distributions. In [119], the authors propose a quasi-share auction approach for cooperative video transmission relay networks to minimize end-to-end expected distortion and achieve near-optimal bandwidth/power allocation.

In this chapter, the power allocation problem in single-relay cooperative ad-hoc wireless networks is formulated as an auction game and two distributed auction algorithms are proposed, namely the conventional ascending-clock auction (C-ACA) and the alternative ascending-clock auction (A-ACA) [47][49]. In particular, the proposed auction algorithms are proven to converge in a finite number of time-steps. Additionally, it is shown that the A-ACA algorithm enforces truth-telling while the C-ACA algorithm does not. Finally, it is demonstrated that both the C-ACA and A-ACA algorithms maximize the social welfare (i.e. the sum of utilities of the source nodes and the relay). It is envisioned that the presented work will pave the way for a practical distributed and efficient power allocation mechanism in single-relay cooperative communications in ad-hoc wireless networks.

In the remainder of this chapter, the network model is presented in Section 4.2. The game-theoretic framework for the source nodes and the relay is presented in Section 4.3 while the ascending clock auction-based relay power allocation algorithms are discussed in Section 4.4. The properties of the proposed algorithms are numerically evaluated in Section 4.5. Some practical performance issues are discussed in Section 4.6, while the conclusions are finally drawn in Section 4.7.

4.2 Network Model

Consider an ad-hoc wireless network consisting of N source nodes ($N \geq 2$), denoted S_1, S_2, ..., S_N. The N nodes are assumed to have their own data symbols $x_1, x_2, \ldots, x_N$, respectively, and each node aims at communicating its data symbol to a common destination node D. In addition, assume that there is a relay node R that is willing to share its transmission power P_R to forward the source nodes' data symbols to the destination. In this network (shown in Fig. 4.1 for $N = 2$), each node is equipped with a single antenna and the relay node's cooperative transmission follows the amplify-and-forward (AF) protocol [56]. The channels between any two nodes are modeled as narrow-band Rayleigh fading channels with additive white Gaussian noise (AWGN). Let $h_{j,i}$ denote a generic channel coefficient representing the channel between any two nodes j and i, then $h_{j,i} \sim \mathcal{CN}(0, \sigma_{j,i}^2)$, where $\sigma_{j,i}^2 = d_{j,i}^{-\nu}$ is the channel gain with $d_{j,i}$ and ν being the distance between the two nodes and the path-loss exponent, respectively.

The communication between the source nodes and the destination node is performed over a total of $N + 1$ time-slots and is split into two phases, namely the broadcasting phase (of N time-slots) and the cooperation phase (of a single time-slot).

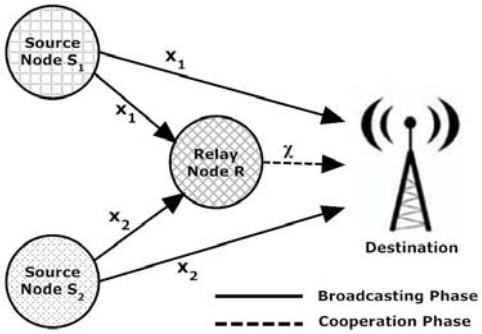

Figure 4.1: Single-Relay Cooperative Network with $N = 2$ Source Nodes

4.2.1 Broadcasting Phase

In the broadcasting phase, each source node S_j for $j \in \{1, 2, \ldots, N\}$ is assigned a time-slot T_j in which it broadcasts its own data symbol x_j to the rest of the network. The received signal $y_{j,r}(t)$ at the relay node R in time-slot T_j is expressed as

$$y_{j,r} = \sqrt{P_{B_j}} h_{j,r} x_j + n_{j,r}, \tag{4.1}$$

while the received signal at the destination node D is expressed as

$$y_{j,d} = \sqrt{P_{B_j}} h_{j,d} x_j + n_{j,d}, \tag{4.2}$$

where P_{B_j} is the broadcasting transmit power at node S_j and $n_{j,r}$ and $n_{j,d}$ are the zero-mean complex additive white Gaussian noise (AWGN) processes with variance N_0, at the relay and destination nodes R and D, respectively. Upon completion of the broadcasting phase, relay and destination nodes R and D will each have received a set of N signals $\{y_{j,r}\}_{j=1}^{N}$ and $\{y_{j,d}\}_{j=1}^{N}$, respectively, comprising symbols $\{x_j\}_{j=1}^{N}$ of the N source nodes.

4.2.2 Cooperation Phase

The cooperation phase involves two operations: (1) signal transmission via the relay node, and (2) multinode signal detection, which are discussed in the following subsections.

Signal Transmission

In the cooperation phase, relay node R in its assigned time-slot T_{N+1} forms a linear network code based on its received symbols $\{y_{m,r}\}_{m=1}^{N}$, during the broadcasting phase and transmits it to the destination. For source separation of each transmitted symbol of the different source nodes at the destination, each received signal $y_{m,r}$ is spread using a signature waveform, $c_m(t)$. It is assumed that the relay and destination nodes know the signature waveforms of all the source nodes. The cross-correlation of $c_m(t)$ and $c_j(t)$ is $\rho_{m,j} = \langle c_m(t), c_j(t) \rangle \triangleq (1/T_s) \int_0^{T_s} c_m(t) c_j^*(t) dt$ for $m \neq j$ with $\rho_{j,j} = 1$, T_s being the symbol

duration and $(\cdot)^*$ denoting complex conjugation. The resulting signal transmitted by the relay, $\mathcal{X}(t)$ is written as

$$\mathcal{X}(t) = \sum_{m=1}^{N} \beta_{m,r} y_{m,r} c_m(t), \tag{4.3}$$

where $c_m(t)$ is the signature waveform associated with source node S_m and $\beta_{m,r}$ is a scaling factor defined as [56]

$$\beta_{m,r} = \sqrt{\frac{P_{C_m}}{P_{B_m}|h_{m,r}|^2 + N_0}}. \tag{4.4}$$

where P_{C_m} is the cooperative transmit power of symbol x_m at the relay node R. The received signal at the destination during time-slot T_{N+1} is given by

$$\mathcal{Y}_{r,d}(t) = h_{r,d}\mathcal{X}(t) + n_d(t), \tag{4.5}$$

where $n_d(t)$ is the AWGN sample at the destination. Upon substitution of (4.1), (4.3) and (4.4) into (4.5), the received signal can be expressed as

$$\mathcal{Y}_{r,d}(t) = \sum_{m=1}^{N} \alpha_{m,r,d} x_m c_m(t) + \bar{n}_d(t), \tag{4.6}$$

where $\alpha_{m,r,d} = \beta_{m,r}\sqrt{P_{B_m}} h_{m,r} h_{r,d}$ and $\bar{n}_d(t)$ is the equivalent noise term, defined as

$$\bar{n}_d(t) = n_d(t) + h_{r,d} \sum_{m=1}^{N} \beta_{m,r} n_{m,r} c_m(t). \tag{4.7}$$

Multinode Signal Detection

Upon receiving signal $\mathcal{Y}_{r,d}(t)$ from the relay, a multinode signal detection is performed by the destination to extract each symbol x_j, for $j \in \{1, 2, \ldots, N\}$. This is achieved by passing the received signal $\mathcal{Y}_{r,d}(t)$ through a matched filter bank (MFB) of N branches, matched to the corresponding nodes' signature waveforms $c_j(t)$, yielding

$$\mathcal{Y}_{j,r,d} = \langle \mathcal{Y}_{r,d}(t), c_j(t) \rangle = \sum_{m=1}^{N} \alpha_{m,r,d} x_m \rho_{m,j} + \bar{n}_{j,d}. \tag{4.8}$$

Recall that $\rho_{m,j}$ is the correlation coefficient between $c_m(t)$ and $c_j(t)$. Without loss of generality, let $\rho_{m,j} = \rho$, $\forall m \neq j$. Thus, the decorrelated received signal $\tilde{\mathcal{Y}}_{j,r,d}$ corresponding to symbol x_j is obtained as [120]

$$\tilde{\mathcal{Y}}_{j,r,d} = \beta_{j,r}\sqrt{P_{B_j}} h_{j,r} h_{r,d} x_j + \tilde{n}_{j,d}, \tag{4.9}$$

where $\tilde{n}_{j,d} \sim \mathcal{CN}(0, N_0 \varrho_N (\beta_{j,r}^2 |h_{r,d}|^2 + 1))$ and ϱ_N is given by [103]

$$\varrho_N = \frac{1+(N-2)\rho}{1+(N-2)\rho-(N-1)\rho^2}. \tag{4.10}$$

Upon the completion of the broadcasting and cooperation phases, the destination will have received two signals of each symbol x_j for $j \in \{1, 2, \ldots, N\}$; a direct signal from the source node S_j in the broadcasting phase and a relayed signal in the cooperation phase. The detection of symbol x_j, denoted as $\tilde{x}_j$, is achieved through maximal-ratio-combining (MRC) of the signals received in the broadcasting and cooperation phases as [56]

$$\tilde{x}_j = \frac{\sqrt{P_{B_j}}h^*_{j,d}}{N_0} y_{j,d} + \frac{\beta_{j,r}\sqrt{P_{B_j}}h^*_{j,r}h^*_{r,d}}{N_0\varrho_N(\beta^2_{j,r}|h_{r,d}|^2+1)}\tilde{\mathcal{Y}}_{j,r,d}, \tag{4.11}$$

where $y_{j,d}$ and $\tilde{\mathcal{Y}}_{j,r,d}$ follow (4.2) and (4.9), respectively. Thus, the instantaneous SNR at the output of the MRC of symbol x_j is given by $\gamma_j = \gamma^B_{j,d} + \gamma^C_{j,d}$, where $\gamma^B_{j,d}$ is the SNR due to the broadcast "direct" transmission from the source to the destination and is defined as $\gamma^B_{j,d} = P_{B_j}|h_{j,d}|^2/N_0$, while $\gamma^C_{j,d}$ is the SNR due to the cooperative transmission via relay node R and is defined as

$$\gamma^C_{j,d} = \frac{P_{B_j}P_{C_j}|h_{j,r}|^2|h_{r,d}|^2}{N_0\varrho_N(P_{B_j}|h_{j,r}|^2 + P_{C_j}|h_{r,d}|^2 + N_0)}. \tag{4.12}$$

Since a single data symbol is exchanged between every source node S_j, for $j \in \{1, 2, \ldots, N\}$, and the destination once every $N+1$ time-slots, the achievable rate for each source node can be determined using

$$R_{j,d}(P_{C_j}) = \frac{1}{N+1}\log_2\left(1 + \frac{P_{B_j}|h_{j,d}|^2}{N_0} + \frac{P_{B_j}P_{C_j}|h_{j,r}|^2|h_{r,d}|^2}{N_0\varrho_N(P_{B_j}|h_{j,r}|^2 + P_{C_j}|h_{r,d}|^2 + N_0)}\right). \tag{4.13}$$

4.3 Game-Theoretic Framework

This section presents a game-theoretic framework for the cooperative relay power allocation among the N source nodes.

4.3.1 Source Node Utility Function

The utility function of each source node is based on the improvement in the transmission rate achieved by relay node's cooperative transmission. Accordingly, the utility function of source node S_j for cooperative data transmission to the destination via the relay node is

$$U^S_j(P_{C_j}) = \Delta R_{j,d}(P_{C_j}) - \xi P_{C_j}, \tag{4.14}$$

where ξ is the price per unit of power charged by the relay node to forward data symbols to the destination, and $\Delta R_{j,d}(P_{C_j})$ is the improvement in the transmission rate due to the cooperative relaying which is given by

$$\Delta R_{j,d}(P_{C_j}) = \frac{1}{N+1}\log_2\left(1+\frac{P_{C_j}\Omega_{j,r,d}}{P_{C_j}+\Upsilon_{j,r,d}}\right), \tag{4.15}$$

where

$$\Omega_{j,r,d} = \frac{P_{B_j}|h_{j,r}|^2}{\varrho_N(P_{B_j}|h_{j,d}|^2+N_0)}, \tag{4.16}$$

and

$$\Upsilon_{j,r,d} = \frac{P_{B_j}|h_{j,r}|^2+N_0}{|h_{r,d}|^2}. \tag{4.17}$$

Thus, $\Delta R_{j,d}(P_{C_j})$ defines the cooperation gain to node S_j in terms of an improvement in the transmission rate to the destination, when the relay node cooperates. Clearly, $\Delta R_{j,d}(P_{C_j})$ is a monotonically increasing function of P_{C_j}.

Each source node aims at maximizing its utility subject to the total transmit power P_R available at the relay. Thus, each source node's cooperative power demand problem can be modeled as

$$\begin{aligned} \max_{P_{C_j}\geq 0} \quad & U_j^S(P_{C_j}) = \Delta R_{j,d}(P_{C_j}) - \xi P_{C_j}, \\ \text{s.t.} \quad & 0 \leq P_{C_j} \leq P_R, \quad \forall j \in \{1,2,\ldots,N\}. \end{aligned} \tag{4.18}$$

Clearly, the utility function $U_j^S(P_{C_j})$ is concave in P_{C_j}, and taking the derivative of $U_j^S(P_{C_j})$ with respect to P_{C_j}, yields

$$\frac{\partial U_j^S(P_{C_j})}{\partial P_{C_j}} = \frac{\partial \Delta R_{j,d}(P_{C_j})}{\partial P_{C_j}} - \xi = 0. \tag{4.19}$$

By using the identity $\log_2(x) = \ln(x)/\ln 2$, defining $\eta = \frac{1}{(N+1)\ln 2}$ and substituting $\Delta R_{j,d}(P_{C_j})$ in (4.15) into (4.19), the utility function $U_{j,d}(P_{C_j})$ is maximized at $P_{C_j}(\xi)$ which is expressed $\forall j \in \{1,2,\ldots,N\}$ as

$$P_{C_j}(\xi) = \max\left[0, \min\left(\frac{1}{2(\Omega_{j,r,d}+1)}\left(\sqrt{\Omega_{j,r,d}^2\Upsilon_{j,r,d}^2 + \frac{4\eta\Omega_{j,r,d}\Upsilon_{j,r,d}(\Omega_{j,r,d}+1)}{\xi}} - (\Omega_{j,r,d}+2)\Upsilon_{j,r,d}\right), P_R\right)\right]. \tag{4.20}$$

4.3.2 Relay Node Utility Function

The relay node's utility function is based on selling its cooperative transmit power P_R to the source nodes to forward their data symbols to the destination and cover its cooperation cost ζ per unit power (i.e. for processing, transmission and receiving). Thus, the relay's utility function is given by

$$U_r(P_R) = \vartheta_r(P_R) - \zeta P_R, \tag{4.21}$$

with $\vartheta_r(P_R) = \sum_{j=1}^{N} \vartheta_j(P^{\star}_{C_j})$ being the total payment the relay receives from the N source nodes for transmitting their data symbols, and $\vartheta_j(P^{\star}_{C_j})$ is the payment source node S_j makes when it is assigned cooperative transmit power $P^{\star}_{C_j}$ such that $\sum_{j=1}^{N} P^{\star}_{C_j} \leq P_R$ (as will be formally established in the following section). It should be noted that $\zeta P^{\star}_{C_j}$ is the cooperation cost due to the transmission of source node S_j's data symbol.

4.4 Proposed Power Allocation Auction Algorithms

The idea of pricing as a distributed control mechanism aims at encouraging autonomous and independent network users to make rational decisions that result in a social benefit for the entire network. Towards this end, two distributed auction algorithms for efficient power allocation are proposed, namely the conventional ascending-clock auction (C-ACA) [47] and the alternative ascending-clock auction (A-ACA) [49]. In particular, the relay "auctioneer" announces a price, the N source nodes "bidders" report back their cooperative power demanded at that price and power is allocated to source nodes at the current price whenever they are "clinched". The relay then raises the announced price and the process repeats until the total power demand meets the available power supply (in which case all the relay's transmit power P_R is allocated).

4.4.1 Conventional Ascending-Clock Auction

In the C-ACA based power allocation algorithm at each time $\tau = 0, 1, \ldots$, the relay announces a price ξ^{τ} to the N source nodes. For the relay to cover the cooperation cost per unit power ζ, it initially sets a reserve price of $\xi^0 = \zeta$ and announces it to the source nodes. Based on the announced price ξ^{τ}, each source node S_j responds with a bid in the form of an optimal power demand $P_{C_j}(\xi^{\tau})$ to the relay. After receiving all the demands at each time-step, the relay compares the total demanded power $P^{C}_{Total}(\xi^{\tau}) = \sum_{j=1}^{N} P_{C_j}(\xi^{\tau})$ with the total available power P_R. If the total demand exceeds the supply (i.e. $P^{C}_{Total}(\xi^{\tau}) > P_R$), the auction proceeds to time $\tau + 1$ and the associated price is increased to $\xi^{\tau+1} = \xi^{\tau} + \mu = \zeta + (\tau + 1)\mu$, where μ is an appropriate step-size. The increased price is then announced to the source nodes and each source node S_j reports its optimal power demand $P_{C_j}(\xi^{\tau+1})$ to the relay. On the other hand, if the supply meets the total demand (i.e. $P^{C}_{Total}(\xi^{\tau}) \leq P_R$), the current time is denoted as T and the auction concludes. It is possible, for a certain increase in price, that the supply is not fully covered at the final price ξ^{T} (i.e. $P^{C}_{Total}(\xi^{T}) < P_R$). In turn, a proportional rationing rule is applied and power allocation is achieved according to [49][121]

$$P^{\star}_{C_j} = P_{C_j}(\xi^{T}) + \frac{P_{C_j}(\xi^{T-1}) - P_{C_j}(\xi^{T})}{\sum_{j=1}^{N} P_{C_j}(\xi^{T-1}) - \sum_{j=1}^{N} P_{C_j}(\xi^{T})} \left(P_R - \sum_{i=1}^{N} P_{C_i}(\xi^{T}) \right), \tag{4.22}$$

with $\sum_{j=1}^{N} P^{\star}_{C_j} = P_R$. Hence, each source node S_j is assigned its demanded cooperative transmit power of $P^{\star}_{C_j}$ which in turn makes a payment of $\vartheta^{C}_{j}(P^{\star}_{C_j}) = \xi^{T} P^{\star}_{C_j}$. In this case,

the surplus the relay obtains from node S_j is $\mathcal{B}_A(P^{\star}_{C_j}) = (\xi^T - \zeta)P^{\star}_{C_j}$ and the relay's utility is obtained as $U_R(P_R) = (\xi^T - \zeta)P_R$. The distributed C-ACA power allocation algorithm is summarized in 4.1.

Table 4.1: Conventional Ascending-Clock Auction Algorithm for Single-Relay Power Allocation

1 Relay initializes time-index at $\tau = 0$ and step-size to $\mu > 0$ and then announces initial price of $\xi^0 = \zeta$.
2 Each source node S_j computes and submits its optimal power demand $P_{C_j}(\xi^0)$.
3 Relay sums up all demands $P^C_{Total}(\xi^0) = \sum_{j=1}^{N} P_{C_j}(\xi^0)$.
4 WHILE $(P^C_{Total}(\xi^\tau) > P_R)$
5 Set $\xi^{\tau+1} = \xi^\tau + \mu$ and $\tau = \tau + 1$.
6 Price ξ^τ is announced to source nodes.
7 Each source node S_j computes and submits its optimal demand $P_{C_j}(\xi^\tau)$.
8 Relay sums up all demands $P^C_{Total}(\xi^\tau)$=$\sum_{j=1}^{N} P_{C_j}(\xi^\tau)$.
9 END.
10 Let $\tau = T$ be the time at which the auction concluded and assign $P^{\star}_{C_j}$ to source node S_j, which makes a payment of $\vartheta^C_j(P^{\star}_{C_j}) = \xi^T P^{\star}_{C_j}$ to the relay node.

4.4.2 Alternative Ascending-Clock Auction

The proposed algorithm of the A-ACA is similar to that of the C-ACA; however, at every time-step τ, the relay calculates the cumulative vector of quantities $C_j(\xi^\tau)$, clinched by source node S_j at prices up to ξ^τ as given by

$$C_j(\xi^\tau) = \max\left(0, P_R - \sum_{i=1, i\neq j}^{N} P_{C_i}(\xi^\tau)\right), \quad \forall j \in \{1, 2, \ldots, N\}. \tag{4.23}$$

The process repeats as in the C-ACA until supply meets demand (i.e. $P^C_{Total}(\xi^\tau) \leq P_R$) and the final clinched cooperative power is given by

$$C_j(\xi^T) = P_{C_j}(\xi^T) + \frac{P_{C_j}(\xi^{T-1}) - P_{C_j}(\xi^T)}{\sum_{j=1}^{N} P_{C_j}(\xi^{T-1}) - \sum_{j=1}^{N} P_{C_j}(\xi^T)} \left(P_R - \sum_{i=1}^{N} P_{C_i}(\xi^T)\right), \tag{4.24}$$

with $\sum_{j=1}^{N} C_j(\xi^T) = P_R$. Thus, each source node S_j is allocated a cooperative transmit power of $P^{\star}_{C_j} = C_j(\xi^T)$. Also, the payment from source node S_j to the relay is written as

$$\vartheta^A_j(P^{\star}_{C_j}) = C_j(\xi^0)\xi^0 + \sum_{\tau=1}^{T} \xi^\tau (C_j(\xi^\tau) - C_j(\xi^{\tau-1})), \tag{4.25}$$

where the total payment the relay node receives for allocating its power P_R is $\vartheta_r(P_R) = \sum_{j=1}^{N} \vartheta^A_j(P^{\star}_{C_j})$. It is easily verified that

$$P^{\star}_{C_j} = C_j(\xi^0) + \sum_{\tau=1}^{T} (C_j(\xi^\tau) - C_j(\xi^{\tau-1})). \tag{4.26}$$

Also, by substituting $\xi^\tau = \zeta + \mu\tau$ into (4.25), the payment of source node S_j is rewritten as

$$\vartheta_j^A(P_{C_j}^\star) = \zeta P_{C_j}^\star + \mathcal{B}(P_{C_j}^\star), \tag{4.27}$$

where

$$\mathcal{B}_A(P_{C_j}^\star) = \sum_{\tau=1}^{T} \mu\tau(C_j(\xi^\tau) - C_j(\xi^{\tau-1})) \tag{4.28}$$

is the surplus the relay obtains from node S_j upon allocating power $P_{C_j}^\star$. The distributed power allocation algorithm based on the proposed A-ACA is summarized in Table 4.2.

Table 4.2: Alternative Ascending-Clock Auction Algorithm for Single-Relay Power Allocation

1 Relay initializes time-index at $\tau = 0$ and step-size to $\mu > 0$ and then announces initial price of $\xi^0 = \zeta$.
2 Each source node S_j computes and submits its optimal power demand $P_{C_j}(\xi^0)$.
3 Relay sums up all demands $P_{Total}^C(\xi^0) = \sum_{j=1}^N P_{C_j}(\xi^0)$.
4 WHILE $(P_{Total}^C(\xi^\tau) > P_R)$
5 Compute $C_j(\xi^\tau) = \max\left(0, P_R - \sum_{i=1, i\neq j}^N P_{C_i}(\xi^\tau)\right)$.
6 Set $\xi^{\tau+1} = \xi^\tau + \mu$ and $\tau = \tau + 1$.
7 Price ξ^τ is announced to source nodes.
8 Each source node S_j computes and submits its optimal demand $P_{C_j}(\xi^\tau)$.
9 Relay sums up all demands $P_{Total}^C(\xi^\tau) = \sum_{j=1}^N P_{C_j}(\xi^\tau)$.
10 END.
11 Let $\tau = T$ be the time at which the auction concluded, compute $C_j(\xi^T)$ and assign $P_{C_j}^\star = C_j(\xi^T)$ to source node S_j, which makes a payment of $\vartheta_j^A(P_{C_j}^\star)$ to the relay node.

Based on the above analysis, the payment each source node S_j makes under the A-ACA algorithm is upper-bounded by that of the C-ACA algorithm. This is verified by observing that for a sufficiently small step-size μ, $C_j(\xi^T) \approx P_{C_j}(\xi^T) = P_{C_j}^\star$, the following holds

$$\vartheta_j^A(P_{C_j}^\star) = C_j(\xi^0)\xi^0 + \sum_{\tau=1}^{T} \xi^\tau(C_j(\xi^\tau) - C_j(\xi^{\tau-1})) \lesssim \xi^T C_j(\xi^T) = \xi^T P_{C_j}^\star = \vartheta_j^C(P_{C_j}^\star). \tag{4.29}$$

Lemma 4.1: In the C-ACA and A-ACA algorithms, the optimal power demand $P_{C_j}(\xi)$ at the relay is non-increasing in its price.

Proof: Taking the first derivative of the optimal power allocation of node S_j with respect to price ξ, gives

$$\frac{\partial P_{C_j}(\xi)}{\partial \xi} =$$

$$\begin{cases} 0, & \text{if } \frac{1}{2(\Omega_{j,r,d}+1)}\sqrt{\Omega_{j,r,d}^2\Upsilon_{j,r,d}^2 + \frac{4\eta\Omega_{j,r,d}\Upsilon_{j,r,d}(\Omega_{j,r,d}+1)}{\xi}} - (\Omega_{j,r,d}+2)\Upsilon_{j,r,d} \geq P_R \\ \frac{-\eta\Omega_{j,r,d}\Upsilon_{j,r,d}}{\xi^2\sqrt{\Omega_{j,r,d}^2\Upsilon_{j,r,d}^2 + \frac{4\eta\Omega_{j,r,d}\Upsilon_{j,r,d}(\Omega_{j,r,d}+1)}{\xi}}} < 0, & \text{if } 0 < \frac{1}{2(\Omega_{j,r,d}+1)}\sqrt{\Omega_{j,r,d}^2\Upsilon_{j,r,d}^2 + \frac{4\eta\Omega_{j,r,d}\Upsilon_{j,r,d}(\Omega_{j,r,d}+1)}{\xi}} - (\Omega_{j,r,d}+2)\Upsilon_{j,r,d} < P_R \\ 0, & \text{if } \frac{1}{2(\Omega_{j,r,d}+1)}\sqrt{\Omega_{j,r,d}^2\Upsilon_{j,r,d}^2 + \frac{4\eta\Omega_{j,r,d}\Upsilon_{j,r,d}(\Omega_{j,r,d}+1)}{\xi}} - (\Omega_{j,r,d}+2)\Upsilon_{j,r,d} \leq 0 \end{cases}. \tag{4.30}$$

Clearly, $P_{C_j}(\xi)$ is a non-increasing function of ξ. □

4.4.3 Properties of Proposed Algorithms

Convergence

Theorem 4.1 (Convergence): The proposed C-ACA and A-ACA distributed algorithms conclude in a finite number of time-steps.

Proof: From Lemma 4.1, $P_{C_j}(\xi^\tau)$ is non-increasing in ξ^τ and hence $P_{C_j}(\xi^\tau) \geq P_{C_j}(\xi^{\tau+1})$ with equality occurring when $P_{C_j}(\xi^{\tau+1}) = P_{C_j}(\xi^\tau) = 0$ or $P_{C_j}(\xi^{\tau+1}) = P_{C_j}(\xi^\tau) = P_R$, $\forall \tau$. Since for a sufficiently large τ, $P_{C_j}(\xi^{\tau+1}) < P_{C_j}(\xi^\tau) < P_R$, then there exists a finite number T such that $\sum_{j=1}^{N} P_{C_j}(\xi^T) \leq P_R$ and thus the auction concludes at time-step T. □

Truth-Telling

Theorem 4.2: The C-ACA algorithm does not enforce truthful power demand and all sources nodes have the incentive to falsely report their power demands.

Proof: Assuming that all the other nodes truthfully report their power demands at every time-step, let ξ^T and $P_{C_j}^T$ be the price and allocated power to node S_j at the end of the auction, respectively when it truthfully reports its power demand at every time-step τ for $0 \leq \tau \leq T$. Also, let $\tilde{\xi}^{\tilde{T}}$ and $\tilde{P}_{C_j}\left(\tilde{\xi}^{\tilde{T}}\right)$ be the price and allocated power when the node S_j falsely reports its power demand at least once. Accordingly, the utility of node S_j under both cases are given by

$$U_j^S\left(P_{C_j}(\xi^T)\right) = \Delta R_{j,d}\left(P_{C_j}(\xi^T)\right) - \xi^T P_{C_j}(\xi^T), \tag{4.31}$$

and

$$U_j^S\left(\tilde{P}_{C_j}\left(\tilde{\xi}^{\tilde{T}}\right)\right) = \Delta R_{j,d}\left(\tilde{P}_{C_j}\left(\tilde{\xi}^{\tilde{T}}\right)\right) - \tilde{\xi}^{\tilde{T}}\tilde{P}_{C_j}\left(\tilde{\xi}^{\tilde{T}}\right), \tag{4.32}$$

respectively. Thus,

$$U_j^S\left(P_{C_j}(\xi^T)\right) - U_j^S\left(\tilde{P}_{C_j}\left(\tilde{\xi}^{\tilde{T}}\right)\right) = \Delta R_{j,d}\left(P_{C_j}(\xi^T)\right) - \Delta R_{j,d}\left(\tilde{P}_{C_j}\left(\tilde{\xi}^{\tilde{T}}\right)\right) - \xi^T P_{C_j}(\xi^T) + \xi^{\tilde{T}}\tilde{P}_{C_j}\left(\tilde{\xi}^{\tilde{T}}\right). \tag{4.33}$$

If $\Delta R_{j,d}\left(\tilde{P}_{C_j}\left(\tilde{\xi}^{\tilde{T}}\right)\right) - \Delta R_{j,d}\left(P_{C_j}(\xi^T)\right) + \xi^T P_{C_j}(\xi^T) > \xi^{\tilde{T}}\tilde{P}_{C_j}\left(\tilde{\xi}^{\tilde{T}}\right)$, then $U_j^S\left(P_{C_j}(\xi^T)\right) < U_j^S\left(\tilde{P}_{C_j}\left(\tilde{\xi}^{\tilde{T}}\right)\right)$. Hence, the C-ACA algorithm does not enforce truth-telling and all the source nodes have an incentive to falsely report their power demands to obtain a higher utility. □

Theorem 4.3: Reporting optimal cooperative power demand truthfully at every time-step in the A-ACA algorithm is a mutual best response for all source nodes.

Proof: Assuming that all the other source nodes truthfully report their power demands, let

$$\Sigma_j(T) = \left\{P_{C_j}(\xi^0), \ldots, P_{C_j}(\xi^T); C_j(\xi^0), \ldots, C_j(\xi^T); T\right\} \tag{4.34}$$

be the auction profile when source node S_j when it reports its power demand truthfully on every time-step τ. Also, let

$$\Sigma_j(\tilde{T}) = \left\{ P_{C_j}(\xi^0), \ldots, \tilde{P}_{C_j}(\xi^{\tilde{\tau}}), \ldots, \tilde{P}_{C_j}\left(\tilde{\xi}^{\tilde{T}}\right); C_j(\xi^0), \ldots, \tilde{C}_j(\xi^{\tilde{\tau}}), \ldots, \tilde{C}_j\left(\tilde{\xi}^{\tilde{T}}\right); \tilde{T} \right\} \tag{4.35}$$

be the auction profile of source node S_j when it falsely demands power on time-step $\tau = \tilde{\tau}$ for $0 \leq \tilde{\tau} \leq \tilde{T}$ while nodes $S_i, \forall i \in \{1, 2, \ldots, N\}$ and $i \neq j$ truthfully report their power demands. Moreover, let $\tilde{P}_{C_j}\left(\xi^{\tilde{\tau}}\right)$ be the power allocated to node S_j at the end of the auction when it falsely demands power. Now, consider the following two cases:

- If $\tilde{P}_{C_j}(\xi^{\tilde{\tau}}) \leq P_{C_j}(\xi^{\tau})$, then $\tilde{P}_{C_j}\left(\tilde{\xi}^{\tilde{T}}\right) \leq P_{C_j}(\xi^T)$, which implies that $\tilde{T} \leq T$. From (4.14) and (4.25), it is easily shown that

$$\begin{aligned} U_j^S\left(\Sigma_j(T)\right) - U_j^S\left(\Sigma_j(\tilde{T})\right) = \Delta R_{j,d}(P_{C_j}(\xi^T)) - \Delta R_{j,d}\left(\tilde{P}_{C_j}\left(\tilde{\xi}^{\tilde{T}}\right)\right) \\ - \vartheta_j^A(P_{C_j}(\xi^T)) + \vartheta_j^A\left(\tilde{P}_{C_j}\left(\tilde{\xi}^{\tilde{T}}\right)\right). \end{aligned} \tag{4.36}$$

  Since $\xi^{\tilde{T}+1}\tilde{C}_j(\xi^{\tilde{T}}) \leq \xi^T\tilde{C}_j(\xi^{\tilde{T}})$, then it is straightforward to verify that $\vartheta_j^A(P_{C_j}(\xi^T)) - \vartheta_j^A(\tilde{P}_{C_j}(\xi^{\tilde{T}})) \leq \xi^T C_j(\xi^T) - \xi^T\tilde{C}_j\left(\tilde{\xi}^{\tilde{T}}\right) = \xi^T P_{C_j}(\xi^T) - \xi^T\tilde{P}_{C_j}\left(\tilde{\xi}^{\tilde{T}}\right)$. Hence,

$$U_j^S\left(\Sigma_j(T)\right) - U_j^S\left(\Sigma_j(\tilde{T})\right) \geq \Delta R_{j,d}(P_{C_j}(\xi^T)) - \Delta R_{j,d}\left(\tilde{P}_{C_j}(\xi^{\tilde{T}})\right) - \xi^T P_{C_j}(\xi^T) + \xi^T\tilde{P}_{C_j}\left(\tilde{\xi}^{\tilde{T}}\right) \geq 0, \tag{4.37}$$

  where the last inequality holds from $P_{C_j}(\xi^T) = \arg\max U_j^S(P_{C_j}(\xi^T))$ in (4.18).

- If $\tilde{P}_{C_j}(\tilde{\xi}^{\tilde{\tau}}) \geq P_{C_j}(\xi^{\tau})$, then $\tilde{P}_{C_j}\left(\tilde{\xi}^{\tilde{T}}\right) \geq P_{C_j}(\xi^T)$, and thus $\tilde{T} \geq T$. Thus, it can be similarly verified that $\vartheta_j^A(\tilde{P}_{C_j}(\xi^{\tilde{T}})) - \vartheta_j^A(P_{C_j}(\xi^T)) \geq \xi^T\tilde{C}_j\left(\tilde{\xi}^{\tilde{T}}\right) - \xi^T C_j(\xi^T) = \xi^T\tilde{P}_{C_j}\left(\tilde{\xi}^{\tilde{T}}\right) - \xi^T P_{C_j}(\xi^T)$ and hence

$$U_j^S\left(\Sigma_j(T)\right) - U_j^S\left(\Sigma_j(\tilde{T})\right) \geq \Delta R_{j,d}(P_{C_j}(\xi^T)) - \Delta R_{j,d}\left(\tilde{P}_{C_j}(\xi^{\tilde{T}})\right) - \xi^T P_{C_j}(\xi^T) + \xi^T\tilde{P}_{C_j}\left(\tilde{\xi}^{\tilde{T}}\right) \geq 0, \tag{4.38}$$

  where the last inequality also holds from $P_{C_j}(\xi^T) = \arg\max U_j^S(P_{C_j}(\xi^T))$ in (4.18).

From (4.37) and (4.38), falsely demanding power at least once (at time-step $\tau = \tilde{\tau}$) yields a lower utility than demanding power truthfully at every time-step. Thus, the best strategy is to truthfully demand power at each time-step τ for $0 \leq \tau \leq T$. □

In the proposed distributed C-ACA algorithm, every source node has an incentive to falsely report its power demand to increase its utility. On the other hand, each participant has full incentive to truthfully reveal its true power demand in the A-ACA algorithm because the price each source node pays depends solely on opposing nodes' bids and need not report their private information (i.e. the mechanism also preserves privacy). Thus, the proposed A-ACA based power allocation enforces truth-telling and the best strategy of each source node is to submit its true/optimal power demand at every time-step.

Social Welfare Maximization

Theorem 4.4 (Maximization of Social Welfare): The proposed C-ACA and A-ACA power allocation $(P^{\star}_{C_1}, P^{\star}_{C_2}, \ldots, P^{\star}_{C_N})$ maximizes the social welfare.

Proof: The proof is based on showing that the outcome of both the C-ACA and the A-ACA algorithms is $(P^{\star}_{C_1}, P^{\star}_{C_2}, \ldots, P^{\star}_{C_N})$, which is equivalent to solving the following optimization problem:

$$\begin{aligned} \max_{P_{C_j} \geq 0} \quad & \sum_{j=1}^{N} \Delta R_{j,d}(P_{C_j}) \\ \text{s.t.} \quad & \sum_{j=1}^{N} P_{C_j} \leq P_R, \\ & 0 \leq P_{C_j} \leq P_R, \quad \forall j \in \{1, 2, \ldots, N\}. \end{aligned} \tag{4.39}$$

It can be verified that the optimization problem in (4.39) is convex, since ΔR_j is concave in P_{C_j} and the constraint set is linear and thus convex. Hence, it can be formulated as a Lagrangian problem as [94]

$$\mathcal{L}(P_{C_j}, \lambda, \omega_j, \upsilon_j) = -\sum_{j=1}^{N} \Delta R_{j,d}(P_{C_j}) + \lambda \left(\sum_{j=1}^{N} P_{C_j} - P_R \right) + \sum_{j=1}^{N} \omega_j (P_{C_j} - P_R) - \sum_{j=1}^{N} \upsilon_j P_{C_j}, \tag{4.40}$$

and, the Karush-Kuhn-Tucker (KKT) conditions are given by:

$$\begin{aligned} -\frac{\eta \Omega_{j,r,d} \Upsilon_{j,r,d}}{((\Omega_{j,r,d}+1)P_{C_j} + \Upsilon_{j,r,d})(P_{C_j} + \Upsilon_{j,r,d})} + \lambda + \omega_j - \upsilon_j = 0 \\ \lambda \left(\sum_{j=1}^{N} P_{C_j} - P_R \right) = 0, \\ \omega_j (P_{C_j} - P_R) = 0, \forall j \in \{1, 2, \ldots, N\}, \\ \upsilon_j P_{C_j} = 0, \forall j \in \{1, 2, \ldots, N\}, \\ 0 \leq P_{C_j} \leq P_R, \forall j \in \{1, 2, \ldots, N\}, \\ \sum_{j=1}^{N} P_{C_j} \leq P_R, \end{aligned} \tag{4.41}$$

where $\eta = \frac{1}{(N+1)\ln 2}$ while $\lambda \geq 0, \omega_j \geq 0, \upsilon_j \geq 0, \forall j \in \{1, 2, \ldots, N\}$ are the dual variables associated with the power constraint and transmit power positivity. The solution to the optimization problem is known as water-filling [122], in the form of $P_{C_j}(\lambda)$ in (4.20), $\forall j \in \{1, 2, \ldots, N\}$, where λ satisfies $\sum_{j=1}^{N} P_{C_j}(\lambda) = P_R$. Thus, for a sufficiently small step-size μ, the outcome of the C-ACA and A-ACA algorithms, $(P^{\star}_{C_1}, P^{\star}_{C_2}, \ldots, P^{\star}_{C_N})$ is the solution to the optimization problem in (4.39) that maximizes the sum of the source nodes and the relay node utilities when the relay node fully sells out its cooperative transmit power P_R. □

Simplicity and Applicability

The key characteristic of the proposed C-ACA and A-ACA algorithms is the relative simplicity of the auction process during the iterative clock phase and the final power demand allocation. In other words, the computational complexity on both the N source nodes and the relay is low in the sense that each source node needs to calculate its optimal power demand $P_{C_j}(\xi^\tau)$ based on the announced price ξ^τ while ascertaining that it is within available power P_R and then submit a bid. Further, the assessment of excess demand and calculation of the cumulative clinch at the relay in the A-ACA algorithm, are relatively trivial. Another important characteristic is the fact that the relay's aim is to drive the excess demand out of the system by raising the price without ending up with excess power supply. This in turn implies the auction process achieves all gains from trade and is allocatively efficient [123].

The discussed properties of the proposed C-ACA and A-ACA algorithms are summarized in Table 4.3, where it is shown that A-ACA is superior to the C-ACA as it enforces truth-telling. It is noteworthy that the C-ACA algorithm results in a higher utility for the relay than in the A-ACA algorithm and this is due to the higher payment the relay receives from each source node under the C-ACA algorithm. Correspondingly, the utility of each source is lower under the C-ACA algorithm. This suggests a trade-off between the higher utility (or revenue) the relay achieves under the C-ACA algorithm against the critical truth-telling property achieved under the A-ACA algorithm. It is concluded that the proposed A-ACA is superior to the C-ACA algorithm and lends itself to practical ad-hoc network implementation.

Table 4.3: Summary of Properties of Proposed Auction Algorithms

Algorithm	Property		
	Convergence	Truth-Telling	Social Welfare Maximization
C-ACA	✓	✗	✓
A-ACA	✓	✓	✓

4.5 Evaluation of Proposed Distributed Algorithms

To validate the proposed C-ACA and A-ACA relay power allocation algorithms, a network with three source nodes S_1, S_2 and S_3 and a relay R (see Fig. 4.2) is simulated. The network topology illustrates a scenario where the distance between any source node S_j for $j \in \{1, 2, 3\}$ and the destination is equal (i.e. $d_{1,d} = d_{2,d} = d_{3,d}$). Also, the relay is closest to node S_2 and closer to S_1 than S_3. The simulations assume a path-loss exponent of $\nu = 3$, non-orthogonal signature waveforms with a cross-correlation of $\rho = 0.5$, step-size of $\mu = 10^{-3}$, reserve price of $\xi^0 = 10^{-2}$, source broadcasting transmit power $P_{B_j} = 10$ mW, $\forall j \in \{1, 2, 3\}$, and noise variance $N_0 = 10^{-5}$ W.

It is evident from Fig. 4.3 that—under both algorithms—with the increase in the available relay power P_R, the utility of each source node increases, with node S_2 having the highest utility while node S_3 having the lowest. This is attributed to the location of node S_2 with the

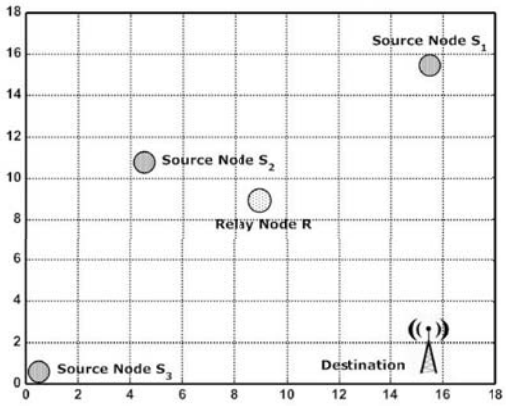

Figure 4.2: Single-Relay Cooperative Network - Simulation Scenario

relay being closer to it than to the destination and hence the effect of path-loss and channel noise is less severe. Thus, using the relay is significantly beneficial to node S_2 which is translated into a higher cooperative power allocation and rate improvement (as evident from Fig. 4.4). The lowest utility corresponding to node S_3 is justified by a converse argument to that of node S_2.

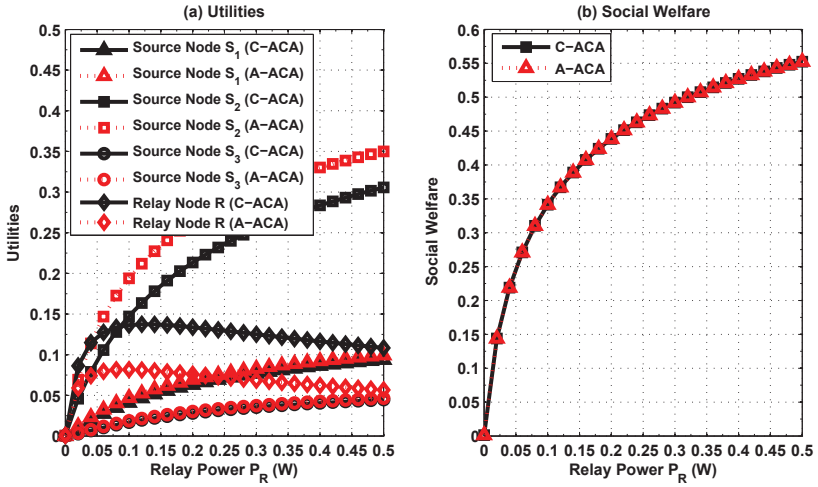

Figure 4.3: Utilities and Social Welfare

Interesting to observe in Fig. 4.3 is the utility of the relay which peaks at $P_R \simeq 0.11$ W under both algorithms and then starts to degrade. This is explained by noticing that when P_R is high enough (i.e. $P_R \gtrsim 0.11$ W), there is abundant cooperative power for each of the source nodes (i.e. the total power demanded by the source nodes is less than the supply relay power P_R). Hence, the relay does not get to raise the price so much in the auction to extract higher revenue (i.e. higher payments) but instead sells most of the power early in the auction at a relatively lower price, which can be seen in the form of lower payments in Fig. 4.5. On the other hand, It is also observed in Fig. 4.3 that the source nodes have a lower

utility under the C-ACA algorithm than under the A-ACA algorithm. This is attributed to the higher payment each source node must make to the relay under the C-ACA, as noted in (4.29). By a similar argument, the utility of the relay node under the C-ACA algorithm is higher than that achieved under the A-ACA algorithm.

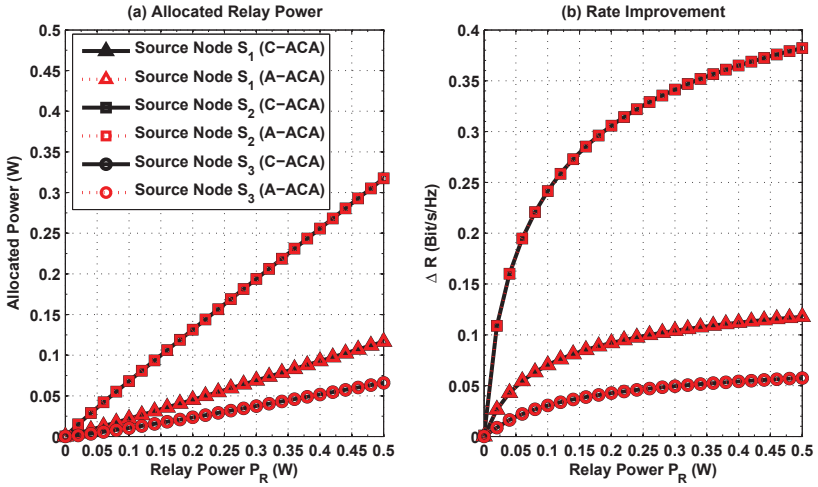

Figure 4.4: (a) Power Allocation, and (b) Rate Improvement of Each Source Node

In general, it is noticed that the power allocated to each source node under both algorithms (and thus the rate improvement) is identical (see Fig. 4.4). In Fig. 4.6, the optimal price at which the auction concludes is illustrated for both algorithms. It is evident that the C-ACA and A-ACA algorithms achieve the same optimal price which yields the optimal power allocation to each source node and thus maximizes the social welfare, as seen in Fig. 4.3.

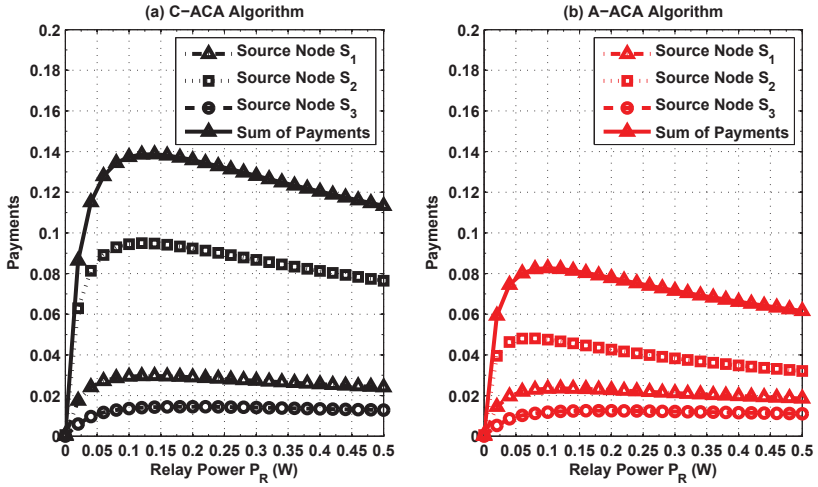

Figure 4.5: Payment of Each Source Node Under: (a) C-ACA, and (b) A-ACA Algorithms

In Fig. 4.7, the utility of the source node S_1 is evaluated under both algorithms at $P_R = 0.3$ W when it falsely reports a demand of $\tilde{P}_{C_1}(\xi^\tau) = \max\left[0, \min\left(\delta P_{C_1}(\xi^\tau), P_R\right)\right]$, $\forall \tau = 0, 1, \ldots, T$ with $\delta \geq 0$ being the demand factor. Nodes S_2 and S_3 report their truthful

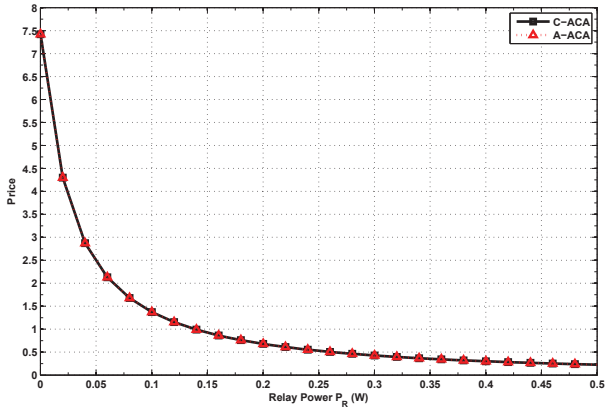

Figure 4.6: Optimal Price of Each Algorithm

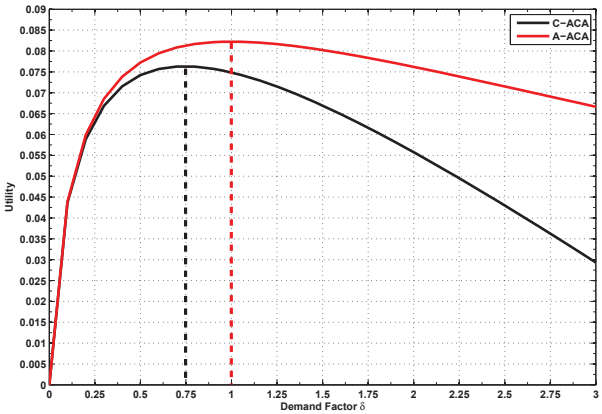

Figure 4.7: Truthful Demand Verification of Source Node S_1's Utility - $P_R = 0.3$ W

power demands $P_{C_2}(\xi^\tau)$ and $P_{C_3}(\xi^\tau)$, respectively, $\forall \tau = 0, 1, \ldots, T$. Under both algorithms, it is clear that as δ increases, the utility of S_1 improves until it reaches its maximum value at $\delta \approx 0.75$ under the C-ACA algorithm, and $\delta = 1$ under the A-ACA algorithm, and beyond which δ value the utility degrades. Thus, the proposed A-ACA enforces truth-telling and each source node must submit its true power demand to maximize their utility.

4.6 Practical Performance Issues

4.6.1 Mitigating Rate Unfairness

As illustrated in Section 4.4.3, the proposed auction-based algorithms inherently maximize the sum-of-rates. As shown in Section 4.5 and specifically in Fig. 4.4, the resulting power allocation and rate improvement are grossly unfair and significantly favor source node S_2, which is due to its location being relatively closer to the relay. To mitigate this problem, a modified power allocation problem is proposed that imposes a rate improvement constraint ΔR^{max} on each source node (or possibly a global constraint), and improves fairness.

Modified Problem Formulation

The modified power demand of source node S_j, for $j \in \{1, 2, \ldots, N\}$ is expressed as[1]

$$\begin{aligned} \max_{P_{C_j} \geq 0} \quad & U_j^S(P_{C_j}) = \Delta R_{j,d}(P_{C_j}) - \xi P_{C_j}, \\ \text{s.t.} \quad & 0 \leq P_{C_j} \leq P_R, \quad \forall j \in \{1, 2, \ldots, N\}, \\ & 0 \leq \Delta R_{j,d}(P_{C_j}) \leq \Delta R_j^{max} \quad \forall j \in \{1, 2, \ldots, N\}. \end{aligned} \tag{4.42}$$

Notice that P_{C_j} the second constraint can be rearranged as

$$0 \leq P_{C_j} \leq \max\left[0, \frac{\Upsilon_{j,r,d}(1 - e^{\Delta R_j^{max}/\eta})}{e^{\Delta R_j^{max}/\eta} - (1 + \Omega_{j,r,d})}\right]. \tag{4.43}$$

Following the same procedure in Section 4.3, the optimal power demand can be shown to be

$$P_{C_j}(\xi) = \begin{cases} \max\left[0, \min\left(P_{D_j}(\xi), P_R\right)\right], & \text{if } \frac{\Upsilon_{j,r,d}(1-e^{\Delta R_j^{max}/\eta})}{e^{\Delta R_j^{max}/\eta}-(1+\Omega_{j,r,d})} \leq 0, \\ \max\left[0, \min\left(P_{D_j}(\xi), \frac{\Upsilon_{j,r,d}(1-e^{\Delta R_j^{max}/\eta})}{e^{\Delta R_j^{max}/\eta}-(1+\Omega_{j,r,d})}, P_R\right)\right], & \text{if } \frac{\Upsilon_{j,r,d}(1-e^{\Delta R_j^{max}/\eta})}{e^{\Delta R_j^{max}/\eta}-(1+\Omega_{j,r,d})} > 0, \end{cases} \tag{4.44}$$

where $\eta = \frac{1}{(N+1)\ln 2}$ and

$$P_{D_j}(\xi) = \frac{1}{2(\Omega_{j,r,d}+1)}\left(\sqrt{\Omega_{j,r,d}^2\Upsilon_{j,r,d}^2 + \frac{4\eta\Omega_{j,r,d}\Upsilon_{j,r,d}(\Omega_{j,r,d}+1)}{\xi}} - (\Omega_{j,r,d}+2)\Upsilon_{j,r,d}\right). \tag{4.45}$$

It is noteworthy that in order to enforce the rate improvement constraints, the discussed C-ACA and A-ACA algorithms are modified such that no proportional rationing rule is applied. This is because any additional power allocation due to that rule could result in a violation of the rate improvement constraint at the last time-step of the algorithm. This in turn implies that not all the available relay power is necessarily utilized.

4.6.2 Alternative Utility-Based Power Allocation

Although it is highly desirable to achieve high data rates (and possibly meet target QoS), nodes may not be willing to achieve it at arbitrarily high transmission power levels. Practically speaking, increasing transmission power (which increases the achievable rate) should not indefinitely increase a source node's utility. Therefore, the rate (or QoS) requirement must be viewed as a utility function that represents a source node's level of satisfaction while taking power cost into account. In this section, a Sigmoid-like utility function is utilized.

Problem Reformulation

Let the utility of source node S_j in (4.18) be re-defined as $U_j^S(P_{C_j}) = \mathcal{S}_j(\Delta R_{j,d}(P_{C_j})) - \xi P_{C_j}$, where $\mathcal{S}_j(\Delta R_{j,d}(P_{C_j}))$ is a Sigmoid function defined as[2] [124]

[1]Note: the rate constraint is performed on the demand side and thus requires a mechanism to enforce it.

[2]Notice that in Section 4.3.1, $\mathcal{S}_j(\Delta R_{j,d}(P_{C_j}))$ was inherently defined as $\mathcal{S}_j(\Delta R_{j,d}(P_{C_j})) = \Delta R_{j,d}(P_{C_j})$.

$$\mathcal{S}_j(\Delta R_{j,d}(P_{C_j})) = \frac{1}{1+e^{-a_j(\Delta R_{j,d}(P_{C_j})-b_j)}}, \tag{4.46}$$

where $a_j, b_j \geq 0, \forall j \in \{1,2,\ldots,N\}$. When a_j increases, $\mathcal{S}_j(\Delta R_{j,d}(P_{C_j}))$ becomes steep, and as $a_j \to \infty$, the Sigmoid function becomes a step function at $\Delta R_{j,d}(P_{C_j}) = b_j$. When fixing a_j and varying b_j, the Sigmoid function will be centered at b_j. For simplicity, it is assumed that $a_j = a$ and $b_j = b, \forall j \in \{1,2,\ldots,N\}$. The Sigmoid function is particularly attractive for our analysis and modeling due to the above stated properties, except that $\mathcal{S}_j(0) = 1/(1+\exp(a_j b_j)) \neq 0$. This can be fixed by using the following linear transformation

$$\bar{\mathcal{S}}_j(\Delta R_{j,d}(P_{C_j})) = \frac{\frac{1}{1+e^{-a(\Delta R_{j,d}(P_{C_j})-b)}} - \frac{1}{1+e^{ab}}}{1-\frac{1}{1+e^{ab}}}. \tag{4.47}$$

In the meantime, the Sigmoid function defined in (4.46) is utilized. Following the procedure in Section 4.3.1, gives

$$\frac{\partial U_j^S(P_{C_j})}{\partial P_{C_j}} = a\mathcal{S}_j(\Delta R_{j,d}(P_{C_j}))\left(1-\mathcal{S}_j(\Delta R_{j,d}(P_{C_j}))\right)\frac{\eta\Omega_{j,r,d}\Upsilon_{j,r,d}}{((\Omega_{j,r,d}+1)P_{C_j}+\Upsilon_{j,r,d})(P_{C_j}+\Upsilon_{j,r,d})} - \xi = 0, \tag{4.48}$$

where no explicit solution for $P_{C_j}(\xi)$ can be found and thus is evaluated numerically. As with the rate constraint modified problem, the rationing rule is not applied.

It is well-known that the sigmoidal function in (4.46) is characterized with a convex part at low rate and a concave part at high rate, and a single inflexion point separating the two parts. In turn, the resulting optimal power demand by each source or generally, the social welfare maximization problem becomes a non-convex optimization problem and is significantly harder to analyze, even by centralized computational algorithms. This is because a local optimal solution might not necessarily be the global one and the duality gap might be strictly positive [125]. Thus, the proposed auction algorithms might lead to infeasible/suboptimal power allocation or simply diverge. Hence, the proposed A-ACA and C-ACA algorithms have been carefully designed to ensure convergence.

4.6.3 Numerical Results

Rate Improvement Constraint

The following results are based on the same simulation parameters used in Section 4.5 while setting the rate improvement constraint as $\Delta R^{max} = 0.1$ bits/s/Hz, $\forall j \in \{1,2,3\}$.

In 4.8a, the power allocation to each source node is illustrated while the rate improvement is shown in Fig. 4.8b. First, notice that in Fig. 4.4b, node S_2 achieved a rate improvement of $\Delta R_{2,d} \approx 0.385$ bits/s/Hz while node S_1 achieved $\Delta R_{1,d} \approx 0.13$ bits/s/Hz, both at $P_R = 0.5$ W. On the other hand, node S_3 achieved only $\Delta R_{3,d} \approx 0.06$ bits/s/Hz. Now, setting the rate improvement constraint to $\Delta R^{max} = 0.1$ bits/s/Hz has changed the power allocation

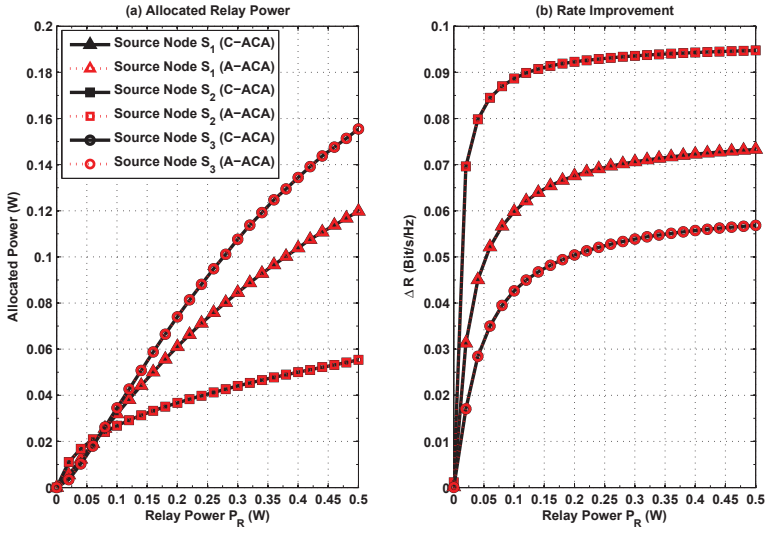

Figure 4.8: (a) Power Allocation, and (b) Rate Improvement of Each Source Node with $\Delta R^{max} = 0.1$ Bits/s/Hz

in comparison with the case where there is no rate improvement constraints (see Fig. 4.4a). Specifically, node S_2 is no longer allocated most of the relay power; on the contrary, it is allocated the least amount of relay power and this because its rate improvement has now been constrained to a lesser value and thus it requires less relay power to achieve the rate constraint of 0.1 bits/s/Hz. The same observation also applies to node S_1. However, node S_3 is allocated most of the relay power, as it is still below the rate constraint. The important thing to notice is that by setting a rate constraint, the power allocation and the rate improvement have become less biased and thus fairer.

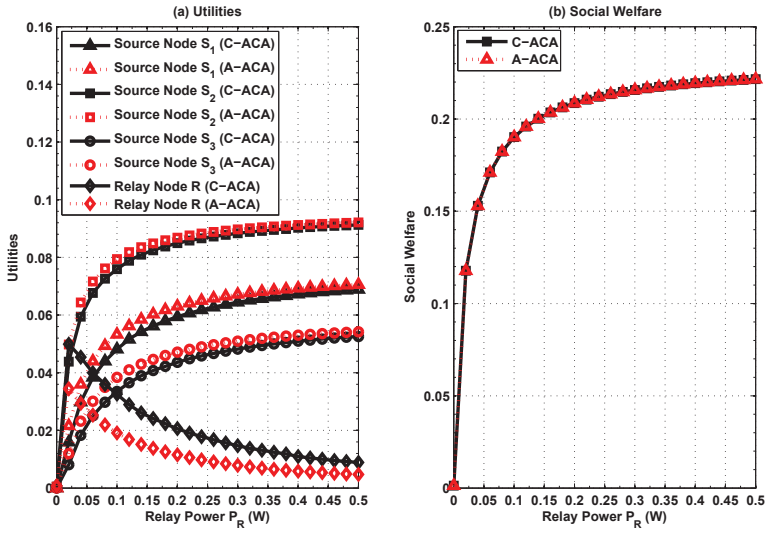

Figure 4.9: Utilities and Social Welfare with $\Delta R^{max} = 0.1$ Bits/s/Hz

The utilities of the source nodes and the relay are demonstrated in Fig. 4.9a. As before, the utility of the source nodes under the A-ACA algorithm are higher than under the C-ACA algorithm, and vice versa for the relay node. Also, the values of the utilities are smaller than the case with no constraint, as can be seen from Fig. 4.3a. A similar observation can be seen in the social welfare values, in Fig. 4.9b. With respect to the payments made by each source node, it can be seen from 4.10 that the values are lower than in the case with no constraints (see Fig. 4.5), due to the smaller amount of power allocated to each source node.

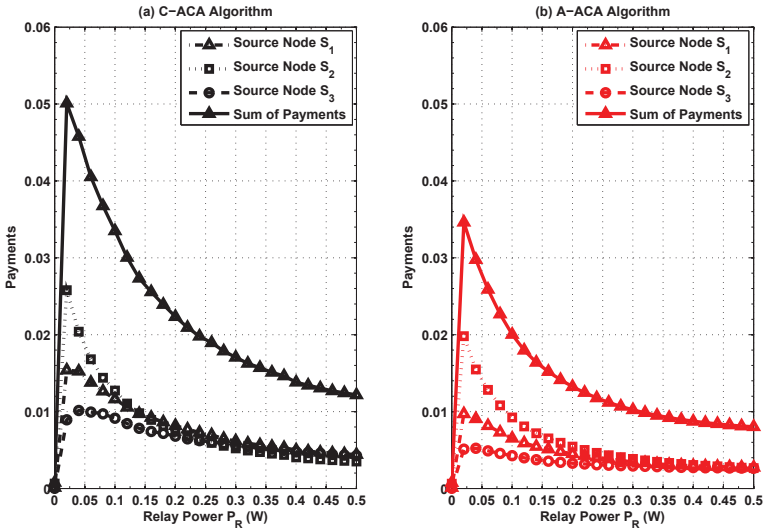

Figure 4.10: Payment of Each Source Node Under: (a) C-ACA, and (b) A-ACA Algorithms with $\Delta R^{max} = 0.1$ Bits/s/Hz

In comparison with the price at which power is allocated to source nodes under the rate constraint, it can be seen from Fig. 4.11 that prices diminish quickly for $P_R \gtrsim 0.1$ W when compared with 4.6. This is because there is less competition on the available power due to the rate improvement constraint.

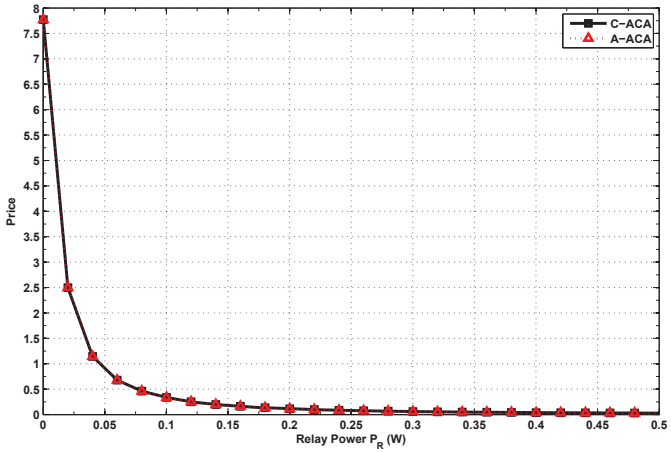

Figure 4.11: Optimal Price of Each Algorithm with $\Delta R^{max} = 0.1$ Bits/s/Hz

Modified Utility

In this section, the proposed algorithms are evaluated using the re-defined utility function discussed in Section 4.6.2 with $a = 10$ and $b = 0.1$. In comparison with the results of Section 4.5, a similar observation to the power allocation and rate improvement, utility values of the source and relay nodes, and payments is noticed in Figs. 4.12, 4.13, and 4.14, respectively.

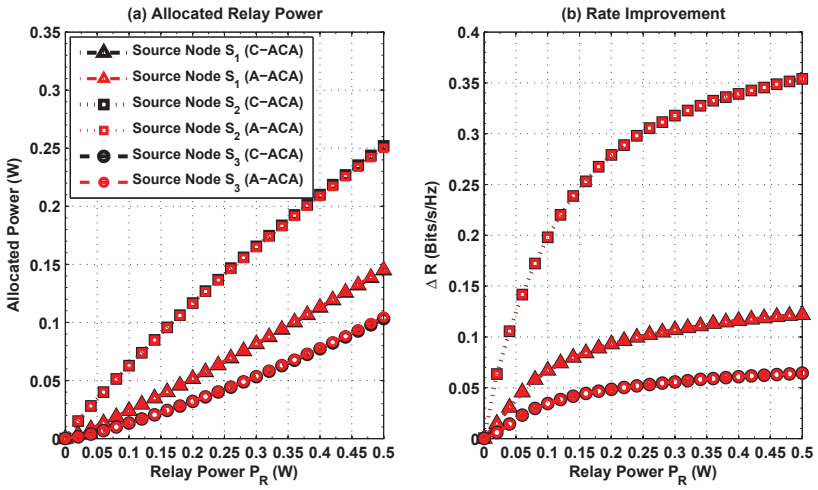

Figure 4.12: (a) Power Allocation, and (b) Rate Improvement of Each Source Node - Using Sigmoid Function

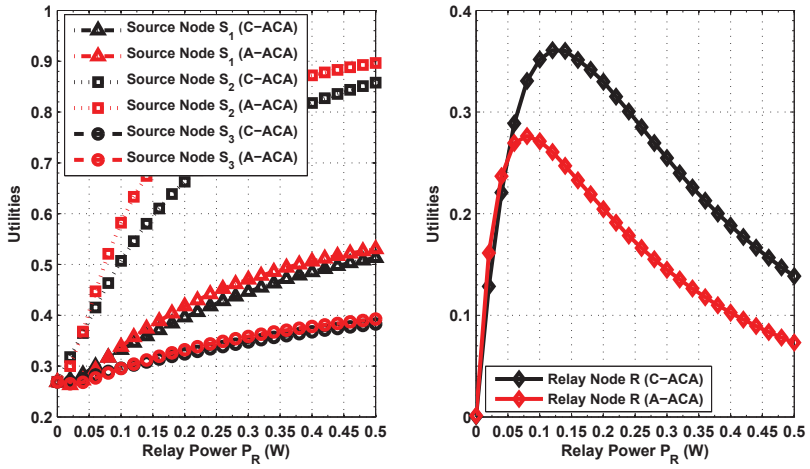

Figure 4.13: Utilities - Using Sigmoid Function

In Fig. 4.15, the Sigmoid function and its normalized function are illustrated. As can be seen, both functions flat-out at high values of relay power, which suggests that increasing the relay power indefinitely does not increase the Sigmoid function value indefinitely. This is because the relationship between rate improvement and utility is no longer linear. In addition, the Sigmoid function can be made to reach its limiting value at lower relay power

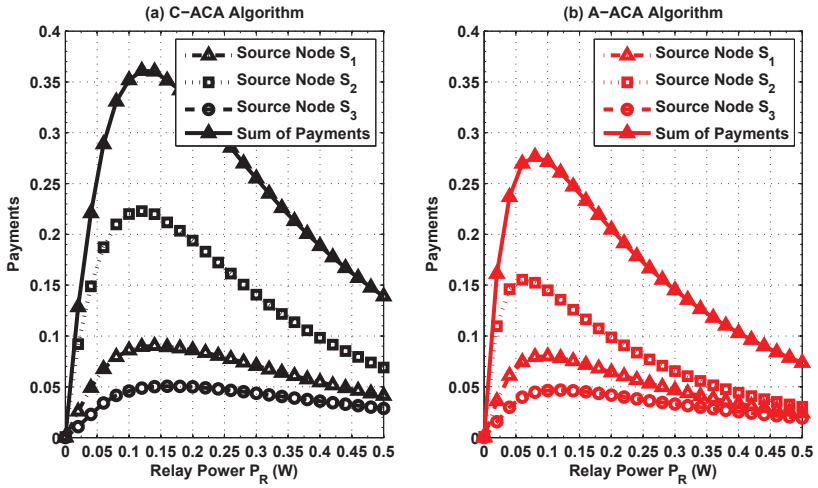

Figure 4.14: Payment of Each Source Node Under: (a) C-ACA, and (b) A-ACA Algorithms - Using Sigmoid Function

values by increasing the value of parameter a. In comparison with Fig. 4.6, the prices under the modified utility function are much higher, as evident from Fig. 4.16. This is because the Sigmoid function suppresses large increases in each source node's utility function and thus there is higher competition for relay power which results in higher prices and payments.

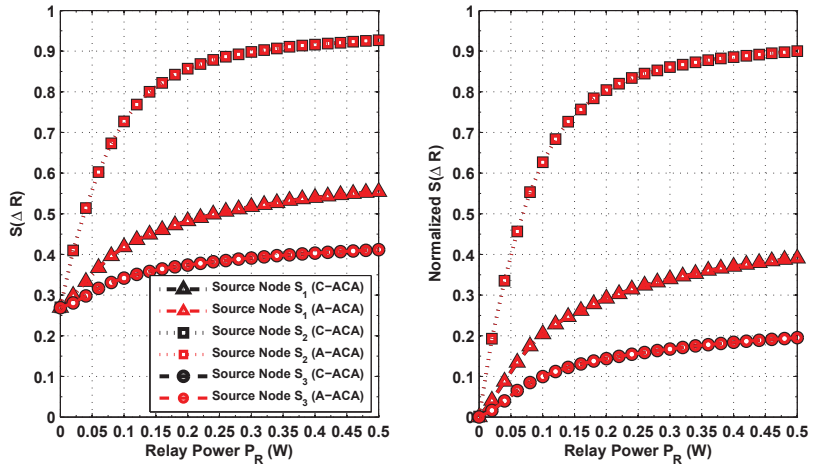

Figure 4.15: Sigmoid and Normalized Sigmoid Functions

4.7 Conclusions

In this chapter, the problem of single-relay distributed power allocation in ad-hoc wireless networks is investigation. In particular, two ascending-clock auction algorithms are proposed, namely the conventional ascending-clock auction (C-ACA) and the alternative ascending-clock auction (A-ACA). It has been shown that both the C-ACA and A-ACA algorithms

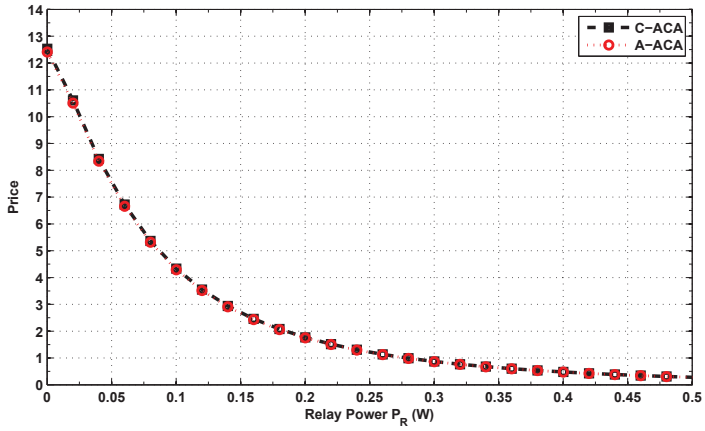

Figure 4.16: Optimal Price of Each Algorithm - Using Sigmoid Function

converge in a finite number of time-steps to an optimal power allocation that maximizes the social welfare. Moreover, the A-ACA algorithm enforces truthful power demands whereas the C-ACA algorithm does not. In conclusion, the proposed alternative ascending-clock auction-based power allocation algorithm lends itself to practical implementation in ad-hoc wireless networks.

Chapter 5

Auction-Based Power Allocation for Multi-Relay Cooperative Networks

5.1 Introduction

In the previous chapter, the single-relay distributed power allocation scenario was studied. The general scenario is when several nodes act as relays and share their transmission power to forward other source nodes' data. However, such multi-relay power allocation not only requires complete channel state information but also entails formidable centralized computations. Therefore, the design of distributed power allocation algorithms that can enforce truthful power demands and yield performance that is comparable with that of a centralized algorithm is highly desirable.

Recently, several works have considered game- and auction-theoretic resource allocation and sharing in cooperative wireless networks. For instance, in [116], a Stackelberg game for a single source-destination pair is proposed for distributed relay selection and power allocation. However, the previous work did not consider the scenario where multiple source nodes are allocated power from the different relays in the network, and also assumed that each relay knows the demand function of the source node, which violates privacy. In [126], the multiuser power control problem in multi-cell multi-hop cellular systems is addressed using game-theory. In particular, a Gaussian interference relay game which possesses a unique Nash Equilibrium (NE) is studied, a sufficient condition under which the NE achieves Pareto-optimality is characterized and a distributed algorithm that converges to the unique NE is proposed. A Nash bargaining solution to a achieve a win-win strategy for cooperative relaying in a cooperative relay network of two users is studied in [127]. In [117], two auction mechanisms are proposed for non-convex power allocation in single- and multi-relay networks, namely the SNR auction and the power auction. It was shown that the former auction achieves efficiency while the latter yields a flexible tradeoff between fairness and efficiency. In addition, the authors show that both auction mechanisms globally converge to the unique NE

in an asynchronous manner but have not considered the issue of truthful power demands. In [128], single-object and multiple-object second-price auction-based decentralized mechanisms are studied for cooperative partner selection in cooperative wireless networks such that a desired quality-of-service is maintained and an improved outage probability performance is achieved. To the best of the author's knowledge, no prior research work has considered distributed multi-source multi-relay auction-based power allocation.

In this chapter, a distributed ascending-clock auction-based algorithm is proposed for multi-source power allocation via a set of cooperative relay nodes. Specifically, each source node reports its optimal power demand to each relay node in response to the prices announced by the relay nodes. The distributed cooperative relay power is such that the sum of the source nodes' rates is maximized. It is proven that the proposed distributed algorithm enforces truthful power demands and converges in a finite number of time-steps to the unique Walrasian Equilibrium (WE) which maximizes the social welfare. In addition, the proposed algorithm is shown to maximize the source nodes' sum of rates which coincides with centralized power control based on convex optimization. Further, the distributed algorithm results in a good tradeoff between speed of convergence and social welfare.

The rest of the chapter is organized as follows. The network model is presented in Section 5.2. The utility functions of the source and relay nodes are discussed in Section 5.3. The proposed ascending-clock auction-based power allocation algorithm is presented in Section 5.4 while its properties are discussed in Section 5.5. A summary of the network operation is presented in Section 5.6 while the numerical results are presented in Section 5.7. Section 5.8 discusses some practical issues while implementation issues based on the IEEE802.11g standard are discussed in Section 5.9. Finally, conclusions are drawn in Section 5.10.

5.2 Network Model

Consider an ad-hoc wireless network consisting of N source nodes ($N \geq 2$), denoted S_1, S_2, ..., S_N. The N nodes are assumed to have data symbols $x_1, x_2, \ldots, x_N$, respectively, and aim at communicating their data symbols to a common destination node D via a set of K relay nodes ($K \geq 2$). The relay nodes are denoted R_1, R_2, ..., R_K, each with transmission power P_{R_k} for $k \in \{1, 2, \ldots, K\}$. In this network (shown in Fig. 5.1), each node is equipped with a single antenna and the relays' cooperative transmissions follow the amplify-and-forward (AF) protocol [56]. The channel between any two nodes is modeled as a narrowband Rayleigh fading channel with additive white Gaussian noise (AWGN). Let $h_{j,k}$ denote the channel coefficient representing the channel between any two nodes j and k, then $h_{j,k} \sim \mathcal{CN}(0, \sigma_{j,k}^2)$, where $\sigma_{j,k}^2$ is the channel gain. Also, perfect channel estimation is assumed at each source/relay node.

The communication between the source nodes and the destination node is performed over a total of $N + K$ time-slots and is split into two phases, namely the broadcasting phase (of N time-slots) and the cooperation phase (of K time-slots).

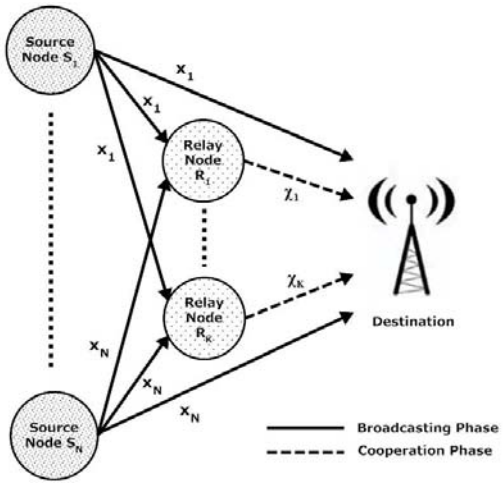

Figure 5.1: Multi-Relay Cooperative Network with N Source and K Relay Nodes

5.2.1 Broadcasting Phase

In this phase, each source node S_j for $j \in \{1, 2, \ldots, N\}$ is assigned a time-slot T_j in which it broadcasts its data symbol x_j to the rest of the network. The received signal $y_{j,k}$ at relay node R_k for $k \in \{1, 2, \ldots, K\}$ in time-slot T_j is expressed as

$$y_{j,k} = \sqrt{P_{B_j}} h_{j,k} x_j + n_{j,k}, \tag{5.1}$$

while the signal received at the destination is given by

$$y_{j,d} = \sqrt{P_{B_j}} h_{j,d} x_j + n_{j,d}, \tag{5.2}$$

where P_{B_j} is the broadcast transmit power of source node S_j and $n_{j,k}$ and $n_{j,d}$ are zero-mean complex additive white Gaussian noise (AWGN) samples with variance N_0, at relay node R_k and the destination, respectively. Upon completion of the broadcasting phase, each relay node R_k and the destination will have received a set of N signals $\{y_{j,k}\}_{j=1}^{N}$ and $\{y_{j,d}\}_{j=1}^{N}$, respectively, which comprise symbols $\{x_j\}_{j=1}^{N}$ of the N source nodes.

5.2.2 Cooperation Phase

In the cooperation phase, relay node R_k in its assigned time-slot T_{N+k} for $k \in \{1, 2, \ldots, K\}$ forms a linear network code based on its received symbols $\{y_{m,k}\}_{m=1}^{N}$, during the broadcasting phase and transmits it to destination. For multi-source separation at the destination node, each received signal $y_{m,k}$ is spread using a signature waveform, $c_m(t)$, where it is assumed that the destination node knows the signature waveforms of all the source nodes. The cross-correlation of $c_m(t)$ and $c_j(t)$ is $\rho_{m,j} = \langle c_m(t), c_j(t) \rangle \triangleq (1/T_s) \int_0^{T_s} c_m(t) c_j^*(t) dt$ for $m \neq j$ with $\rho_{j,j} = 1$, T_s being the symbol duration and $(\cdot)^*$ denoting complex conjugation. The resulting signal $\mathcal{X}_k(t)$ transmitted by relay node R_k is written as

$$\mathcal{X}_k(t) = \sum_{m=1}^{N} \beta_{m,k} y_{m,k} c_m(t), \tag{5.3}$$

where $\beta_{m,k}$ is a scaling factor defined as [56]

$$\beta_{m,k} = \sqrt{\frac{P_{C_{m,k}}}{P_{B_m}|h_{m,k}|^2 + N_0}}. \tag{5.4}$$

where $P_{C_{m,k}}$ is the cooperative power of symbol x_m at the relay node R_k. The received signal at the destination node is given by

$$\mathcal{Y}_{k,d}(t) = h_{k,d}\mathcal{X}_k(t) + n_{k,d}(t), \tag{5.5}$$

where $n_{k,d}(t)$ is the AWGN process at the destination during node R_k's transmission. Substituting (5.1) and (5.3) into (5.5), yields

$$\mathcal{Y}_{k,d}(t) = \sum_{m=1}^{N} \alpha_{m,k,d} x_m c_m(t) + \bar{n}_{k,d}(t), \tag{5.6}$$

where $\alpha_{m,k,d} = \beta_{m,k}\sqrt{P_{B_m}} h_{m,k} h_{k,d}$ and $\bar{n}_{k,d}(t)$ is the equivalent noise term, defined as

$$\bar{n}_{k,d}(t) = n_{k,d}(t) + h_{k,d} \sum_{m=1}^{N} \beta_{m,k} n_{m,k} c_m(t). \tag{5.7}$$

Upon receiving signal $\mathcal{Y}_{k,d}(t)$ from relay node R_k, multiuser detection is performed by the destination to extract each symbol x_j for $j \in \{1, 2, \ldots, N\}$. Namely, $\mathcal{Y}_{k,d}(t)$ is passed through a matched filter bank (MFB) of N branches, yielding

$$\mathcal{Y}_{j,k,d} = \langle \mathcal{Y}_{k,d}(t), c_j(t) \rangle = \sum_{m=1}^{N} \alpha_{m,k,d} x_m \rho_{m,j} + \bar{n}_{j,k,d}. \tag{5.8}$$

Without loss of generality, it is assumed that $\rho_{m,j} = \rho, \forall m \neq j$. Thus, the decorrelated received signal $\tilde{\mathcal{Y}}_{j,k,d}$ is obtained as [120]

$$\tilde{\mathcal{Y}}_{j,k,d} = \beta_{j,k}\sqrt{P_{B_j}} h_{j,k} h_{k,d} x_j + \tilde{n}_{j,k,d}, \tag{5.9}$$

where $\tilde{n}_{j,k,d} \sim \mathcal{CN}(0, N_0 \varrho_N (\beta_{j,k}^2 |h_{k,d}|^2 + 1))$ and ϱ_N is given by

$$\varrho_N = \frac{1 + (N-2)\rho}{1 + (N-2)\rho - (N-1)\rho^2}. \tag{5.10}$$

Upon the completion of the broadcasting and cooperation phases, the destination will have received $K + 1$ signals of symbol x_j for $j \in \{1, 2, \ldots, N\}$. Using maximal-ratio-combining (MRC), the detected symbol is obtained as [56]

$$\tilde{x}_j = \frac{\sqrt{P_{B_j}} h_{j,d}^*}{N_0} y_{j,d} + \sum_{k=1}^{K} \frac{\beta_{j,k}\sqrt{P_{B_j}} h_{j,k}^* h_{k,d}^*}{N_0 \varrho_N (\beta_{j,k}^2 |h_{k,d}|^2 + 1)} \tilde{\mathcal{Y}}_{j,k,d}, \tag{5.11}$$

where $y_{j,d}$ and $\tilde{\mathcal{Y}}_{j,k,d}$ follow (5.2) and (5.9), respectively. Thus, the instantaneous cumulative SNR at the output of the MRC of symbol x_j is given by $\gamma_j = \gamma_{j,d}^B + \sum_{k=1}^K \gamma_{j,k,d}^C$, where $\gamma_{j,d}^B = P_{B_j}|h_{j,d}|^2/N_0$ while $\gamma_{j,k,d}^C$ is defined as

$$\gamma_{j,k,d}^C = \frac{P_{B_j} P_{C_{j,k}} |h_{j,k}|^2 |h_{k,d}|^2}{N_0 \varrho_N (P_{B_j}|h_{j,k}|^2 + P_{C_{j,k}}|h_{k,d}|^2 + N_0)}. \tag{5.12}$$

Let $\mathcal{P}_{C_j} = \left(P_{C_{j,1}}, P_{C_{j,2}}, \ldots, P_{C_{j,K}}\right)$ be the vector of cooperative powers allocated to source node S_j. Then, the achievable rate for $j \in \{1, 2, \ldots, N\}$ can be determined using

$$R_{j,d}(\mathcal{P}_{C_j}) = \frac{1}{N+K} \log_2 \left(1 + \frac{P_{B_j}|h_{j,d}|^2}{N_0} + \sum_{k=1}^K \frac{P_{B_j} P_{C_{j,k}} |h_{j,k}|^2 |h_{k,d}|^2}{N_0 \varrho_N (P_{B_j}|h_{j,k}|^2 + P_{C_{j,k}}|h_{k,d}|^2 + N_0)}\right). \tag{5.13}$$

5.3 Utility Functions

5.3.1 Source Node Utility Function

The utility function of source node S_j, for $j \in \{1, 2, \ldots, N\}$ is based on the transmission rate achievable via the K relay nodes' cooperative transmissions as[1]

$$U_j^S(\mathcal{P}_{C_j}, \boldsymbol{\xi}) = R_{j,d}(\mathcal{P}_{C_j}) - \sum_{k=1}^K \xi_k P_{C_{j,k}}, \tag{5.14}$$

where ξ_k is the price per unit of power charged by relay node R_k to forward a source node's data symbols to the destination and $\boldsymbol{\xi} = (\xi_1, \xi_2, \ldots, \xi_K)$ is the vector of prices set by the K relay nodes. Each source node S_j maximizes its utility subject to the total transmit power P_{R_k} available at node R_k for $k \in \{1, 2, \ldots, K\}$ by solving the cooperative power demand problem as modeled by

$$\begin{aligned} \max_{P_{C_{j,k}} \geq 0} \quad & U_j^S(\mathcal{P}_{C_j}, \boldsymbol{\xi}) = R_{j,d}(\mathcal{P}_{C_j}) - \sum_{k=1}^K \xi_k P_{C_{j,k}}, \\ \text{s.t.} \quad & 0 \leq P_{C_{j,k}} \leq P_{R_k}, \quad \forall k \in \{1, 2, \ldots, K\}. \end{aligned} \tag{5.15}$$

Now, define $\tilde{\gamma}_{j,d}^B = 1 + \gamma_{j,d}^B$ and by using the identity $\log_2(x) = \ln(x)/\ln 2$, rearrange the achievable rate term in (5.13) as

$$R_{j,d}(\mathcal{P}_{C_j}) = \eta \ln \tilde{\gamma}_{j,d}^B + \eta \ln \left(1 + \sum_{k=1}^K \tilde{\gamma}_{j,k,d}^C\right), \tag{5.16}$$

where $\eta = \frac{1}{(N+K)\ln 2}$ and

[1]Node S_j's utility is quasi-linear upon the allocation of $\mathcal{P}_{C_j}$ at a price vector $\boldsymbol{\xi}$.

$$\tilde{\gamma}^{C}_{j,k,d} = \frac{P_{C_{j,k}}\Omega_{j,k,d}}{P_{C_{j,k}} + \Upsilon_{j,k,d}}, \tag{5.17}$$

with $\Omega_{j,k,d}$ and $\Upsilon_{j,k,d}$ being defined as

$$\Omega_{j,k,d} = \frac{P_{B_j}|h_{j,k}|^2}{\varrho_N(P_{B_j}|h_{j,d}|^2 + N_0)}, \tag{5.18}$$

and

$$\Upsilon_{j,k,d} = \frac{P_{B_j}|h_{j,k}|^2 + N_0}{|h_{k,d}|^2}, \tag{5.19}$$

respectively. The optimal cooperative power demand $P_{C_{j,k}}$ from relay R_k is determined as

$$\frac{\partial U_j^S(\mathcal{P}_{C_j}, \boldsymbol{\xi})}{\partial P_{C_{j,k}}} = \frac{\partial R_{j,d}(\mathcal{P}_{C_j})}{\partial P_{C_{j,k}}} - \xi_k = 0. \tag{5.20}$$

Substituting $R_{j,d}(\mathcal{P}_{C_j})$ in (5.13) into (5.20), yields

$$\frac{\eta}{\left(1 + \sum_{k=1}^{K} \frac{P_{C_{j,k}}\Omega_{j,k,d}}{P_{C_{j,k}} + \Upsilon_{j,k,d}}\right)} = \frac{\xi_k}{\Omega_{j,k,d}\Upsilon_{j,k,d}} \left(P_{C_{j,k}} + \Upsilon_{j,k,d}\right)^2, \tag{5.21}$$

Since the left-hand-side (LHS) of (5.21) is the same for any relay node, then equating the right-hand-side (RHS) of (5.21) for relay nodes R_k and R_l for $k \neq l$ gives

$$P_{C_{j,l}} = \sqrt{\frac{\xi_k \Omega_{j,l,d}\Upsilon_{j,l,d}}{\xi_l \Omega_{j,k,d}\Upsilon_{j,k,d}}} \left(P_{C_{j,k}} + \Upsilon_{j,k,d}\right) - \Upsilon_{j,k,d}. \tag{5.22}$$

Substituting (5.22) into (5.17) and rearranging yields

$$\frac{P_{C_{j,k}}\Omega_{j,k,d}}{P_{C_{j,k}} + \Upsilon_{j,k,d}} = \Omega_{j,l,d} - \sqrt{\frac{\xi_l \Omega_{j,k,d}\Upsilon_{j,k,d}}{\xi_k \Omega_{j,l,d}\Upsilon_{j,l,d}}} \frac{\Omega_{j,l,d}\Upsilon_{j,l,d}}{\left(P_{C_{j,k}} + \Upsilon_{j,k,d}\right)}. \tag{5.23}$$

Then, the denominator of the LHS of (5.21) can be rewritten as

$$1 + \sum_{l=1}^{K} \frac{P_{C_{j,l}}\Omega_{j,l,d}}{P_{C_{j,l}} + \Upsilon_{j,l,d}} = \Lambda_j - \sqrt{\frac{\Omega_{j,k,d}\Upsilon_{j,k,d}}{\xi_k \left(P_{C_{j,k}} + \Upsilon_{j,k,d}\right)^2}} \Gamma_j(\boldsymbol{\xi}), \tag{5.24}$$

where $\Lambda_j = 1 + \sum_{l=1}^{K} \Omega_{j,l,d}$ and $\Gamma_j(\boldsymbol{\xi}) = \sum_{l=1}^{K} \sqrt{\xi_l \Omega_{j,l,d}\Upsilon_{j,l,d}}$. Then by substituting (5.24) into (5.21) and after a series of manipulations, the utility function $U_j^S(\mathcal{P}_{C_j}, \boldsymbol{\xi})$ is maximized at $P_{C_{j,k}}(\boldsymbol{\xi})$, which is defined $\forall j \in \{1, 2, \ldots, N\}$ as

$$P_{C_{j,k}}(\boldsymbol{\xi}) = \max\left[0, \min\left(\sqrt{\frac{\Omega_{j,k,d}\Upsilon_{j,k,d}}{\xi_k}} \frac{\Gamma_j(\boldsymbol{\xi}) + \sqrt{\Gamma_j^2(\boldsymbol{\xi}) + 4\eta\Lambda_j}}{2\Lambda_j} - \Upsilon_{j,k,d}, P_{R_k}\right)\right]. \tag{5.25}$$

Clearly, the cooperative power demand $P_{C_{j,k}}(\boldsymbol{\xi})$ of source node S_j from relay node R_k is not only affected by the price ξ_k set by R_k, but also by the prices of the remaining $K-1$ relay nodes (as seen from the definition of $\Gamma_j(\boldsymbol{\xi})$). The following properties are also identified.

Property 5.1: The optimal power demand of source node S_j at relay node R_k, $P_{C_{j,k}}(\boldsymbol{\xi})$ is a non-increasing function of its price ξ_k when the prices of the other relay nodes are fixed.

Proof: Taking the first derivative of the optimal power allocation of node S_j with respect to price ξ_k while all the other prices are fixed, yields

$$\frac{\partial P_{C_{j,k}}(\boldsymbol{\xi})}{\partial \xi_k} = \begin{cases} 0, & \text{if } \sqrt{\frac{\Omega_{j,k,d}\Upsilon_{j,k,d}}{\xi_k}}\ \frac{\Gamma_j(\boldsymbol{\xi})+\sqrt{\Gamma_j^2(\boldsymbol{\xi})+4\eta\Lambda_j}}{2\Lambda_j} - \Upsilon_{j,k,d} \geq P_{R_j} \\ \sqrt{\frac{\Omega_{j,k,d}\Upsilon_{j,k,d}}{\xi_k}}\frac{\Gamma_j(\boldsymbol{\xi})+\sqrt{\Gamma_j^2(\boldsymbol{\xi})+4\eta\Lambda_j}}{2\Lambda_j}\left[-\frac{1}{2\xi_k}\left(1-\frac{\sqrt{\xi_k\Omega_{j,k,d}\Upsilon_{j,k,d}}}{\sqrt{\Gamma_j^2(\boldsymbol{\xi})+4\eta\Lambda_j}}\right)\right] < 0, & \text{if } 0 < \sqrt{\frac{\Omega_{j,k,d}\Upsilon_{j,k,d}}{\xi_k}}\frac{\Gamma_j(\boldsymbol{\xi})+\sqrt{\Gamma_j^2(\boldsymbol{\xi})+4\eta\Lambda_j}}{2\Lambda_j} - \Upsilon_{j,k,d} < 0 \\ 0, & \text{if } \sqrt{\frac{\Omega_{j,k,d}\Upsilon_{j,k,d}}{\xi_k}}\ \frac{\Gamma_j(\boldsymbol{\xi})+\sqrt{\Gamma_j^2(\boldsymbol{\xi})+4\eta\Lambda_j}}{2\Lambda_j} - \Upsilon_{j,k,d} \leq 0 \end{cases}. \tag{5.26}$$

Thus, $P_{C_{j,k}}(\boldsymbol{\xi})$ is non-increasing in ξ_k when all the other prices are fixed. □

Property 5.2 (Strict Concavity): The utility function $U_j^S(\mathcal{P}_{C_j}, \boldsymbol{\xi})$ of each source node S_j is jointly strictly concave for $0 < P_{C_{j,k}} < P_{R_k}$, in $\mathcal{P}_{C_j} = \left(P_{C_{j,1}}, P_{C_{j,2}}, \ldots, P_{C_{j,K}}\right) \forall j \in \{1, 2, \ldots, N\}$, when ξ_k is fixed $\forall k \in \{1, 2, \ldots, K\}$.

Proof: Note that $U_j^S(\mathcal{P}_{C_j}, \boldsymbol{\xi})$ is a function on the convex set $\{P_{C_{j,k}} | 0 \leq P_{C_{j,k}} \leq P_{R_k}, k \in \{1, 2, \ldots, K\}\}$ with continuous partial derivatives of first and second orders. Partial derivatives of the second order can easily be shown to be strictly negative:

$$\begin{aligned} \frac{\partial^2 U_j^S(\mathcal{P}_{C_j}, \boldsymbol{\xi})}{\partial^2 P_{C_{j,k}}} = &- \frac{\eta}{\left(1 + \sum_{k=1}^{K} \frac{P_{C_{j,k}}\Omega_{j,k,d}}{P_{C_{j,k}}+\Upsilon_{j,k,d}}\right)} \left(\frac{\Omega_{j,k,d}\Upsilon_{j,k,d}}{\left(P_{C_{j,k}} + \Upsilon_{j,k,d}\right)^2}\right)^2 \\ &- \frac{2\eta}{\left(1 + \sum_{k=1}^{K} \frac{P_{C_{j,k}}\Omega_{j,k,d}}{P_{C_{j,k}}+\Upsilon_{j,k,d}}\right)} \frac{\Omega_{j,k,d}\Upsilon_{j,k,d}}{\left(P_{C_{j,k}} + \Upsilon_{j,k,d}\right)^3} < 0, \end{aligned} \tag{5.27}$$

and

$$\frac{\partial^2 U_j^S(\mathcal{P}_{C_j}, \boldsymbol{\xi})}{\partial P_{C_{j,k}} \partial P_{C_{j,l}}} = - \frac{\eta}{\left(1 + \sum_{k=1}^{K} \frac{P_{C_{j,k}}\Omega_{j,k,d}}{P_{C_{j,k}}+\Upsilon_{j,k,d}}\right)} \times \frac{\Omega_{j,k,d}\Upsilon_{j,k,d}}{\left(P_{C_{j,k}} + \Upsilon_{j,k,d}\right)^2} \frac{\Omega_{j,l,d}\Upsilon_{j,l,d}}{\left(P_{C_{j,l}} + \Upsilon_{j,l,d}\right)^2} < 0, \tag{5.28}$$

for $k \neq l$. Recall that $\eta = \frac{1}{(N+K)\ln 2} > 0$ and $\Omega_{j,k,d} > 0$ and $\Upsilon_{j,k,d} > 0$. It can also be verified that $\frac{\partial^2 U_j^S(\mathcal{P}_{C_j}, \boldsymbol{\xi})}{\partial^2 P_{C_{j,k}}} \frac{\partial^2 U_j^S(\mathcal{P}_{C_j}, \boldsymbol{\xi})}{\partial^2 P_{C_{j,l}}} - \left(\frac{\partial^2 U_j^S(\mathcal{P}_{C_j}, \boldsymbol{\xi})}{\partial P_{C_{j,k}} \partial P_{C_{j,l}}}\right)^2 > 0, \forall k \neq l$. Hence, $U_j^S(\mathcal{P}_{C_j}, \boldsymbol{\xi})$ is strictly concave in $P_{C_{j,k}}, \forall k \in \{1, 2, \ldots, K\}$. □

Consequently, the optimal cooperative power in (5.25) is the global optimal that maximizes source node S_j's utility $U_j^S(\mathcal{P}_{C_j}, \boldsymbol{\xi})$.

Property 5.3 (Weak Gross Substitutability): If the prices of some relay nodes are increased while the prices of all the other relay nodes are fixed, then a source node's cooperative power demand from the relay nodes whose prices were fixed is non-decreasing.

Proof: Taking the first derivative of $P_{C_{j,k}}(\boldsymbol{\xi})$ with respect to ξ_l for $l \neq k$ while fixing all the other prices gives

$$\frac{\partial P_{C_{j,k}}(\boldsymbol{\xi})}{\partial \xi_l} =$$

$$\begin{cases} 0, & \text{if } \sqrt{\frac{\Omega_{j,k,d}\Upsilon_{j,k,d}}{\xi_k}}\ \frac{\Gamma_j(\boldsymbol{\xi})+\sqrt{\Gamma_j^2(\boldsymbol{\xi})+4\eta\Lambda_j}}{2\Lambda_j} - \Upsilon_{j,k,d} \geq P_{R_k} \\ \sqrt{\frac{\Omega_{j,k,d}\Upsilon_{j,k,d}}{\xi_k}}\ \frac{\Gamma_j(\boldsymbol{\xi})+\sqrt{\Gamma_j^2(\boldsymbol{\xi})+4\eta\Lambda_j}}{2\Lambda_j} \times \left(\frac{1}{2\xi_l}\ \frac{\sqrt{\xi_l\Omega_{j,l,d}\Upsilon_{j,l,d}}}{\sqrt{\Gamma_j^2(\boldsymbol{\xi})+4\eta\Lambda_j}}\right) > 0, & \text{if } 0 < \sqrt{\frac{\Omega_{j,k,d}\Upsilon_{j,k,d}}{\xi_k}}\ \frac{\Gamma_j(\boldsymbol{\xi})+\sqrt{\Gamma_j^2(\boldsymbol{\xi})+4\eta\Lambda_j}}{2\Lambda_j} - \Upsilon_{j,k,d} < P_{R_k} \\ 0, & \text{if } \sqrt{\frac{\Omega_{j,k,d}\Upsilon_{j,k,d}}{\xi_k}}\ \frac{\Gamma_j(\boldsymbol{\xi})+\sqrt{\Gamma_j^2(\boldsymbol{\xi})+4\eta\Lambda_j}}{2\Lambda_j} - \Upsilon_{j,k,d} \leq 0 \end{cases} . \tag{5.29}$$

Thus, $P_{C_{j,k}}(\boldsymbol{\xi})$ is a non-decreasing function of ξ_l when all the other prices are fixed. □

5.3.2 Relay Node Utility Function

The utility function of relay node R_k for $k \in \{1, 2, \ldots, K\}$ is based on selling its cooperative transmit power P_{R_k} to the source nodes to forward their symbols to the destination. Thus, relay node R_k's utility is defined as the total payment it receives by selling its transmit power to the source nodes minus its own cost of cooperation $\zeta_k \geq 0$ per unit power, which is given by

$$U_k^R(P_{R_k}, \boldsymbol{\xi}) = \vartheta_k(P_{R_k}, \boldsymbol{\xi}) - \zeta_k P_{R_k}, \tag{5.30}$$

with $\vartheta_k(P_{R_k}, \boldsymbol{\xi}) = \sum_{j=1}^{N} \vartheta_{j,k}(P_{C_{j,k}}(\boldsymbol{\xi}))$ being the total payment relay node R_k receives from the N source nodes for transmitting their data symbols, and $\vartheta_{j,k}(P_{C_{j,k}}(\boldsymbol{\xi}))$ is the payment source node S_j makes to node R_k based on the announced price vector $\boldsymbol{\xi}$ when it is assigned cooperative transmit power $P_{C_{j,k}}(\boldsymbol{\xi})$ such that $\sum_{j=1}^{N} P_{C_{j,k}}(\boldsymbol{\xi}) \leq P_{R_k}, \forall k \in \{1, 2, \ldots, K\}$. Note that $\zeta_k P_{C_{j,k}}(\boldsymbol{\xi})$ is the cooperation cost due to source node S_j's symbol transmission.

5.4 Proposed Ascending-Clock Auction Algorithm

In this work, the K relay nodes wish to allocate their transmission powers P_{R_k} for $k \in \{1, 2, \ldots, K\}$ among the N source nodes through a distributed dynamic ascending-clock auction. The relay nodes act as sellers who simultaneously and iteratively announce prices to the source nodes and aim to earn payments that cover cooperation cost and maximize revenue. The source nodes are buyers who aim to improve their transmission rates by making payments to the relay nodes in return for their cooperative relaying. Each source node responds to the relay nodes' announced prices with power demands at the announced prices and relay power is "credited" to the source nodes at the current prices when power is "clinched". This process repeats until the total power demand by the source nodes meets all relay power supply, at which time the auction concludes and the source nodes are allocated their cooperative transmit powers and make corresponding payments [129].

Two main issues must be considered when designing a distributed algorithm implementing a dynamic ascending-clock auction [129]. First, since the power demand of a source node S_j

from a relay node R_k is a function of the announced price ξ_k as well as the prices announced by the other relay nodes, then a source node might increase its power demand from a particular relay node when the prices of other relay nodes increase. Thus, power that was earlier clinched by a source node may now be debited and "unclinched" and then re-credited to another demanding source node. Second, since K auctions are running simultaneously, it is not clear how the clinching of cooperative power in one auction affects the progress of another auction. This entails a formal interaction between the source and the relay nodes in the form of simultaneous bidding, price adjustment, and power crediting and debiting.

Let the available relay transmission powers vector be defined as $\mathcal{P}_R = (P_{R_1}, P_{R_2}, \ldots, P_{R_K})$. At each time $\tau = 0, 1, \ldots$, the relay nodes announce their current prices in the form of a price vector $\boldsymbol{\xi}^\tau = (\xi_1^\tau, \xi_2^\tau, \ldots, \xi_K^\tau)$ to the N source nodes. Based on the announced price vector $\boldsymbol{\xi}^\tau$, each source node S_j for $j \in \{1, 2, \ldots, N\}$ reports its power demands to all relay nodes in the form of a power demand vector $\mathcal{P}_{C_j}(\boldsymbol{\xi}^\tau) = \Big(P_{C_{j,1}}(\boldsymbol{\xi}^\tau), P_{C_{j,2}}(\boldsymbol{\xi}^\tau), \ldots, P^\tau_{C_{j,K}}(\boldsymbol{\xi}^\tau)\Big)$. Let

$$\mathcal{D}_{R_k}(\boldsymbol{\xi}^\tau) = \sum_{j=1}^{N} P_{C_{j,k}}(\boldsymbol{\xi}^\tau), \quad \forall k \in \{1, 2, \ldots, K\}, \tag{5.31}$$

and

$$E_{R_k}(\boldsymbol{\xi}^\tau) = \mathcal{D}_{R_k}(\boldsymbol{\xi}^\tau) - P_{R_k}, \quad \forall k \in \{1, 2, \ldots, K\}. \tag{5.32}$$

denote the total and excess power demand at relay node R_k at price vector $\boldsymbol{\xi}^\tau$, respectively. Also, define $E_R(\boldsymbol{\xi}^\tau) = (E_{R_1}(\boldsymbol{\xi}^\tau), E_{R_2}(\boldsymbol{\xi}^\tau), \ldots, E_{R_K}(\boldsymbol{\xi}^\tau)) = \mathcal{D}_R(\boldsymbol{\xi}^\tau) - \mathcal{P}_R$, where $\mathcal{D}_R(\boldsymbol{\xi}^\tau) = (\mathcal{D}_{R_1}(\boldsymbol{\xi}^\tau), \mathcal{D}_{R_2}(\boldsymbol{\xi}^\tau), \ldots, \mathcal{D}_{R_K}(\boldsymbol{\xi}^\tau))$. Moreover, let [130]

$$\mathcal{V} = \{E_R(\boldsymbol{\xi}) \geq 0\} \tag{5.33}$$

denote the set of price vectors where the relays' power supply are in excess demand. In order for the relay nodes to cover the cooperation cost per unit power ζ_k for $k \in \{1, 2, \ldots, K\}$, each relay node initially sets a reserve price of $\xi_k^0 = \zeta_k$ and the price vector $\boldsymbol{\xi}^0 = (\zeta_1, \zeta_2, \ldots, \zeta_K)$ (where it is assumed that $\boldsymbol{\xi}^0 \in \mathcal{V}$) is announced to the source nodes. The assumption that $\boldsymbol{\xi}^0 \in \mathcal{V}$ is satisfied when the ascending-clock auction starts at zero price or at a "reasonably low" price [130].

After receiving all the power demands at each time-step τ, each relay node R_k computes the total demanded power of the N source nodes $\mathcal{D}_{R_k}(\boldsymbol{\xi}^\tau)$ and compares it with the total available power P_{R_k}. If the total demand exceeds the supply (i.e. $E_{R_k}(\boldsymbol{\xi}^\tau) > 0$), the associated price is increased to $\xi_k^{\tau+1} = \xi_k^\tau + \mu$, where μ is an appropriate step-size. Relay R_k then calculates the cumulative clinch and credits $\bar{P}_{j,k}(\boldsymbol{\xi}^\tau)$ to source S_j at the price of ξ_k^τ, where

$$\bar{P}_{j,k}(\boldsymbol{\xi}^\tau) = \max\left(0, P_{R_k} - \sum_{i=1, i\neq j}^{N} P_{C_{i,k}}(\boldsymbol{\xi}^\tau)\right), \quad \forall j \in \{1, 2, \ldots, N\}. \tag{5.34}$$

On the other hand, if the supply meets the total demand for relay node R_k for $k \in \{1, \ldots, K\}$ (i.e. $\mathcal{D}_{R_k}(\boldsymbol{\xi}^\tau) \leq P_{R_k}$), then the price of relay node R_k is fixed (i.e. $\xi_k^{\tau+1} = \xi_k^\tau$). Since it is possible that the supply P_{R_k} is not fully covered at price ξ_k^τ (i.e. $\mathcal{D}_{R_k}(\boldsymbol{\xi}^\tau) < P_{R_k}$), a

proportional rationing rule is applied and the cumulative clinch credited to source node S_j is [121][129]

$$\bar{P}_{j,k}(\boldsymbol{\xi}^{\tau}) = P_{C_{j,k}}(\boldsymbol{\xi}^{\tau}) + \frac{P_{C_{j,k}}(\boldsymbol{\xi}^{\tau-1}) - P_{C_{j,k}}(\boldsymbol{\xi}^{\tau})}{\sum_{j=1}^{N} P_{C_{j,k}}(\boldsymbol{\xi}^{\tau-1}) - \sum_{j=1}^{N} P_{C_{j,k}}(\boldsymbol{\xi}^{\tau})} \left(P_{R_k} - \sum_{i=1}^{N} P_{C_{i,k}}(\boldsymbol{\xi}^{\tau}) \right), \tag{5.35}$$

such that $\sum_{j=1}^{N} \bar{P}_{j,k}(\boldsymbol{\xi}^{\tau}) = P_{R_k}$. Note that it is possible that $P_{C_{j,k}}(\boldsymbol{\xi}^{\tau}) > P_{C_{j,k}}(\boldsymbol{\xi}^{\tau-1})$ for some values of τ. This represents cases in which a power amount of $\Delta\bar{P}_{j,k}(\boldsymbol{\xi}^{\tau}) = \bar{P}_{j,k}(\boldsymbol{\xi}^{\tau}) - \bar{P}_{j,k}(\boldsymbol{\xi}^{\tau-1})$ is debited (or "unclinched") from the other source nodes at a price of ξ_k^{τ}. In particular, this can occur when another source node's demand for power from relay node R_k increases from one time-step to the next. Provided that at least one relay node has unmet demand and has increased its price, the auction continues to time $\tau + 1$ with announcing the updated price vector $\boldsymbol{\xi}^{\tau+1}$ [129].

If the supply meets demand for all K relay nodes, the auction concludes at time-step denoted as $\tau = T$ with an equilibrium price vector of $\boldsymbol{\xi}^{\star} = \boldsymbol{\xi}^{T}$. Each source node S_j is assigned its demanded cooperative transmit power from relay node R_k as $P_{C_{j,k}}(\boldsymbol{\xi}^{\star}) = \bar{P}_{j,k}(\boldsymbol{\xi}^{\star})$ as given in (5.35). Moreover, it is easily verified that

$$P_{C_{j,k}}(\boldsymbol{\xi}^{\star}) = \bar{P}_{j,k}(\boldsymbol{\xi}^{0}) + \sum_{\tau=1}^{T} (\bar{P}_{j,k}(\boldsymbol{\xi}^{\tau}) - \bar{P}_{j,k}(\boldsymbol{\xi}^{\tau-1})), \tag{5.36}$$

while the payment relay node R_k receives from source node S_j is expressed as

$$\vartheta_{j,k}(P_{C_{j,k}}(\boldsymbol{\xi}^{\star})) = \bar{P}_{j,k}(\boldsymbol{\xi}^{0})\xi_k^{0} + \sum_{\tau=1}^{T} \xi_k^{\tau} (\bar{P}_{j,k}(\boldsymbol{\xi}^{\tau}) - \bar{P}_{j,k}(\boldsymbol{\xi}^{\tau-1})), \tag{5.37}$$

which handles power debiting appropriately. In turn, the total payment source node S_j makes when allocated optimal cooperative power by the K relay nodes is given by $\sum_{k=1}^{K} \vartheta_{j,k}(P_{C_{j,k}}(\boldsymbol{\xi}^{\star}))$. Moreover, the total payment relay node R_k receives for allocating its power P_{R_k} is $\vartheta_k(P_{R_k}, \boldsymbol{\xi}^{\star}) = \sum_{j=1}^{N} \vartheta_{j,k}(P_{C_{j,k}}(\boldsymbol{\xi}^{\star}))$.

The proposed distributed ascending-clock based power allocation algorithm is summarized in Table 5.1. Such a distributed algorithm has the advantage of low overhead in the sense that the only signaling required to exchange between the relay nodes and each source node are the announced prices $\boldsymbol{\xi}^{\tau} = (\xi_1, \ldots, \xi_K)$ and the demanded power $P_{C_{j,k}}(\boldsymbol{\xi})$, $\forall j \in \{1, 2, \ldots, N\}, \forall k \in \{1, 2, \ldots, K\}$.

5.5 Properties of Proposed Auction Algorithm

Definition 5.1: An allocation $(\boldsymbol{\xi}, \mathcal{P}_C(\boldsymbol{\xi}))$ is a price vector $\boldsymbol{\xi} = (\xi_1, \xi_2, \ldots, \xi_K)$ and a set of power allocations $\mathcal{P}_C(\boldsymbol{\xi}) = (\mathcal{P}_{C_1}(\boldsymbol{\xi}), \mathcal{P}_{C_2}(\boldsymbol{\xi}), \ldots, \mathcal{P}_{C_N}(\boldsymbol{\xi}))$.

Definition 5.2: A Walrasian Equilibrium (WE) allocation is a price vector $\boldsymbol{\xi}^{\star}$ and a power allocation vector $\mathcal{P}_C(\boldsymbol{\xi}^{\star})$ such that for any allocation $(\boldsymbol{\xi}, \mathcal{P}_C(\boldsymbol{\xi}))$ with $\boldsymbol{\xi} \neq \boldsymbol{\xi}^{\star}$, the following hold [129] [131]:

Table 5.1: Ascending-Clock Auction Algorithm for Multi-Relay Power Allocation

All relay nodes initialize their time-index at $\tau = 0$ and step-size to $\mu > 0$ and then each relay node R_k announces its initial price of $\xi_k^0 = \zeta_k$.
Each source node S_j submits its power demand $P_{C_{j,k}}(\boldsymbol{\xi}^0)$ to each relay node R_k based on announced price vector $\boldsymbol{\xi}^0 = (\xi_1^0, \ldots, \xi_K^0)$.
Each relay R_k computes $\mathcal{D}_{R_k}(\boldsymbol{\xi}^0)$ and compares it with P_{R_k}.
WHILE $(E_R(\boldsymbol{\xi}^\tau) \geq 0)$
  IF $(\mathcal{D}_{R_k}(\boldsymbol{\xi}^\tau) > P_{R_k})$
    Relay node R_k computes and credits $\bar{P}_{j,k}(\boldsymbol{\xi}^\tau) = \max\left(0, P_{R_k} - \sum_{i=1, i\neq j}^{N} P_{C_{i,k}}(\boldsymbol{\xi}^\tau)\right)$ to source node S_j and then price is increased to $\xi_k^{\tau+1} = \xi_k^\tau + \mu$.
  ELSE
    Calculate cumulative clinch credited to source node S_j according to $\bar{P}_{j,k}(\boldsymbol{\xi}^\tau) = P_{C_{j,k}}(\boldsymbol{\xi}^\tau) + \frac{P_{C_{j,k}}(\boldsymbol{\xi}^{\tau-1}) - P_{C_{j,k}}(\boldsymbol{\xi}^\tau)}{\sum_{j=1}^{N} P_{C_{j,k}}(\boldsymbol{\xi}^{\tau-1}) - \sum_{j=1}^{N} P_{C_{j,k}}(\boldsymbol{\xi}^\tau)} \left(P_{R_k} - \sum_{i=1}^{N} P_{C_{i,k}}(\boldsymbol{\xi}^\tau)\right)$, and then price is fixed (i.e. $\xi_k^{\tau+1} = \xi_k^\tau$).
  END.
  Set $\tau = \tau + 1$ and prices $\boldsymbol{\xi}^\tau = (\xi_1^\tau, \ldots, \xi_K^\tau)$ announced to the source nodes.
  Each source node S_j submits its demand $P_{C_{j,k}}(\boldsymbol{\xi}^\tau)$ to each relay node R_k.
  Each relay R_k, $\forall k \in \{1, \ldots, K\}$ computes $\mathcal{D}_{R_k}(\boldsymbol{\xi}^\tau)$ and compares it with P_{R_k}.
END.
Let $\tau = T$ be the time at which the auction concluded, compute $\bar{P}_{j,k}(\boldsymbol{\xi}^\star) = \bar{P}_{j,k}(\boldsymbol{\xi}^T)$ and assign $P_{C_{j,k}}(\boldsymbol{\xi}^\star) = \bar{P}_{j,k}(\boldsymbol{\xi}^\star)$ to source node S_j which makes a payment of $\vartheta_{j,k}(P_{C_{j,k}}(\boldsymbol{\xi}^\star))$ to R_k.

1. $R_{j,d}(\mathcal{P}_C(\boldsymbol{\xi}^\star)) - \sum_{k=1}^{K} \vartheta_{j,k}(P_{C_{j,k}}(\boldsymbol{\xi}^\star)) \geq R_{j,d}(\mathcal{P}_{C_j}(\boldsymbol{\xi})) - \sum_{k=1}^{K} \vartheta_{j,k}(P_{C_{j,k}}(\boldsymbol{\xi})),\ \forall j \in \{1, 2, \ldots, N\}$.

2. $P_{R_k} = \sum_{j=1}^{N} P_{C_{j,k}}(\boldsymbol{\xi}^\star), \forall k \in \{1, 2, \ldots, K\}$.

The first condition states the utility of each source node S_j under the WE allocation is at least as good as any other allocation. On the other hand, the second condition states each relay node fully sells out its available power under the WE allocation.

5.5.1 Existence

Since weak gross substitutability holds at all announced prices $\boldsymbol{\xi}^\tau \in \mathcal{V}, \forall \tau$, then the concavity of the source nodes' utility functions suffices for the existence of a Walrasian equilibrium allocation [130] [132].

5.5.2 Convergence

The dynamic auction process based on the price vector evolution of relay node R_k inherently takes the form of the Walrasian tâtonnement price adjustment process[2] $\mathcal{W}_k(\cdot)$ which

[2]Tâtonnement processes comprise a broad class of price-update rules that adjust prices based on excess demands [133].

has been used to study the stability of Walrasian general price equilibrium. In this work, the core principle of the standard Walrasian model is considered, in which the price vector changes are directly driven by the excess demand of relay power. Mathematically, this process is modeled (assuming conditions sufficient to generate a differentiable excess demand function) as a simple differential equation in the prices of the form $\dot{\xi}_k^\tau = \mathcal{W}_k\left(E_R(\boldsymbol{\xi}^\tau)\right)$. In particular, $\mathcal{W}_k(\cdot)$ is a function that adjusts prices as [134] [135]

$$\xi_k^{\tau+1} = \xi_k^\tau + \dot{\xi}_k^\tau. \tag{5.38}$$

According to the ascending-clock process, if there is excess demand at some relay node R_k (i.e. $E_{R_k}(\boldsymbol{\xi}^\tau) > 0$), then price ξ_k^τ increases by $\dot{\xi}_k^\tau = \mathcal{W}_k(E_R(\boldsymbol{\xi}^\tau)) = \mu$. However, if supply meets demand at node R_k, then price is fixed and thus $\dot{\xi}_k^\tau = \mathcal{W}_k(E_R(\boldsymbol{\xi}^\tau)) = 0$. Hence, the price evolution is determined by (5.38) such that $E_{R_k}(\boldsymbol{\xi}^\tau) \to \mathbf{0}, \forall k \in \{1, 2, \ldots, K\}$ as $\boldsymbol{\xi}^\tau \to \boldsymbol{\xi}^\star$, provided weak gross substitutability holds [130] [135] [136].

To prove the stability and thus convergence of a dynamical system, an appropriate Lyapunov function is identified and shown to have a negative drift. More specifically, to prove the convergence of the proposed ascending-clock auction algorithm, a Lyapunov differentiable function is specified in terms of the excess demand and a process (in this case the Walrasian tâtonnement process) for coordinating the price evolution [137]. In this work, the following differentiable Lyapunov function is utilized [129]

$$\mathcal{L}(\boldsymbol{\xi}^\tau) = \boldsymbol{\xi}^\tau \cdot \mathcal{P}_R + \sum_{j=1}^{N} U_j^S(\mathcal{P}_{C_j}(\boldsymbol{\xi}^\tau), \boldsymbol{\xi}^\tau), \tag{5.39}$$

where $\dot{\mathcal{L}}(\boldsymbol{\xi}^\star) = 0$ and $\dot{\mathcal{L}}(\boldsymbol{\xi}^\tau) < 0$, $\forall \boldsymbol{\xi}^\tau \neq \boldsymbol{\xi}^\star$. The Lyapunov function in (5.39) is particularly attractive as its subgradient at $\boldsymbol{\xi}^\tau$ is $\mathcal{D}_R(\boldsymbol{\xi}^\tau) - \mathcal{P}_R$ [129]. Therefore, the proposed auction algorithm continues as long as $\boldsymbol{\xi}^{\tau+1} \neq \boldsymbol{\xi}^\tau$ and at equilibrium, excess power demands must identically be zero (i.e. $\sum_{k=1}^{K} E_{R_k}(\boldsymbol{\xi}^\star) = 0$ or equivalently $\sum_{k=1}^{K} \mathcal{P}_{R_k} - \mathcal{D}_{R_k}(\boldsymbol{\xi}^\star) = 0$). In other words, the source and the relay nodes alternate between their optimal power demands and updating prices respectively, until the difference between power demands and available relay power supply approaches zero.

Theorem 5.1 (Convergence): Starting from any initial price vector $\boldsymbol{\xi}^0 \in \mathcal{V}$ and for a sufficiently small price increase μ, the proposed distributed algorithm converges in a finite number of time-steps, assuming weak gross substitutability between relay power at different relay nodes.

Proof: Given the strictly concave utility functions along with the compact and convex supporting set $\{P_{C_{j,k}} | 0 \leq P_{C_{j,k}} \leq P_{R_k}, \forall j \in \{1, 2, \ldots, N\}, \forall k \in \{1, 2, \ldots, K\}\}$, and using the definition of the Lyapunov function in (5.39), it is straightforward to show that

$$\dot{\mathcal{L}}(\boldsymbol{\xi}^\tau) = (\mathcal{P}_R - \mathcal{D}_R(\boldsymbol{\xi}^\tau)) \cdot \dot{\boldsymbol{\xi}}^\tau \leq 0. \tag{5.40}$$

Note that in the price adjustment process in (5.38), the term $\dot{\xi}_k^\tau = \mathcal{W}_k\left(E_R(\boldsymbol{\xi}^\tau)\right)$ has the opposite sign of $P_{R_k} - \mathcal{D}_{R_k}(\boldsymbol{\xi}^\tau)$. Also, it can be verified that $\mathcal{L}(\boldsymbol{\xi}^\tau)$ is convex and thus, any local

minimum is also a global minimum. Moreover, since $\boldsymbol{\xi}^{\tau}$ in the proposed algorithm increases with a sufficiently small fixed step-size $\mu > 0$, then $\dot{\mathcal{L}}(\boldsymbol{\xi}^{\tau}) \to 0$ as $\boldsymbol{\xi}^{\tau} \to \boldsymbol{\xi}^{\star}$ for a sufficiently large τ. □

5.5.3 Truth-Telling

Theorem 5.2 (Truth-Telling): In the proposed distributed algorithm, truthfully reporting optimal power demand at every time-step is the mutual best response for every source node.

Proof: Given that all other source nodes truthfully report their power demands, the proof is based on showing that if a source node S_j falsely reports its optimal power demand to at least one relay node R_k for $k \in \{1, 2, \ldots, K\}$ at least once, then its utility will be less than or equal to that when it reports truthfully. Let the auction conclude at time-step T when node S_j truthfully reports its optimal power demand at every time-step τ, resulting in a utility of $U_j^S\left(\mathcal{P}_{C_j}(\boldsymbol{\xi}^T), \boldsymbol{\xi}^T\right) = R_{j,d}\left(\mathcal{P}_{C_j}(\boldsymbol{\xi}^T)\right) - \sum_{k=1}^{K} \vartheta_{j,k}\left(P_{C_{j,k}}(\boldsymbol{\xi}^T)\right) \geq 0$, where $\vartheta_{j,k}\left(P_{C_{j,k}}(\boldsymbol{\xi}^T)\right)$ is defined in (5.37). Also, let $\tilde{T}$ be the time-step at which the auction concludes when node S_j falsely reports its power demand on time-step $\tau = \tilde{\tau}$, for $0 \leq \tilde{\tau} \leq \tilde{T}$. Also, let $\tilde{\boldsymbol{\xi}}^{\tilde{T}}$ be the final price vector at time-step $\tilde{T}$ and $\tilde{\mathcal{P}}_{C_j}\left(\tilde{\boldsymbol{\xi}}^{\tilde{T}}\right)$ be the power allocation vector to node S_j at the end of the auction process. In this case, source node S_j's utility is—by definition—obtained as $U_j^S\left(\tilde{\mathcal{P}}_{C_j}\left(\tilde{\boldsymbol{\xi}}^{\tilde{T}}\right), \tilde{\boldsymbol{\xi}}^{\tilde{T}}\right) = R_{j,d}\left(\tilde{\mathcal{P}}_{C_j}\left(\tilde{\boldsymbol{\xi}}^{\tilde{T}}\right)\right) - \sum_{k=1}^{K} \vartheta_{j,k}\left(\tilde{P}_{C_{j,k}}\left(\tilde{\boldsymbol{\xi}}^{\tilde{T}}\right)\right) \geq 0$.

Two cases could occur:

- If $\tilde{P}_{C_{j,k}}\left(\tilde{\boldsymbol{\xi}}^{\tilde{\tau}}\right) \leq P_{C_{j,k}}(\boldsymbol{\xi}^{\tau})$, then $\tilde{P}_{C_{j,k}}\left(\tilde{\boldsymbol{\xi}}^{\tilde{T}}\right) \leq P_{C_{j,k}}(\boldsymbol{\xi}^{T})$, $\tilde{T} \leq T$ and $\tilde{\boldsymbol{\xi}}^{\tilde{T}} \leq \boldsymbol{\xi}^{T}$. Then,

$$\begin{aligned} U_j^S\left(\mathcal{P}_{C_j}(\boldsymbol{\xi}^T), \boldsymbol{\xi}^T\right) - U_j^S\left(\tilde{\mathcal{P}}_{C_j}\left(\tilde{\boldsymbol{\xi}}^{\tilde{T}}\right), \tilde{\boldsymbol{\xi}}^{\tilde{T}}\right) &= R_{j,d}\left(\mathcal{P}_{C_j}\left(\boldsymbol{\xi}^T\right)\right) - R_{j,d}\left(\tilde{\mathcal{P}}_{C_j}\left(\tilde{\boldsymbol{\xi}}^{\tilde{T}}\right)\right) \\ &\quad - \sum_{k=1}^{K} \vartheta_{j,k}\left(P_{C_{j,k}}(\boldsymbol{\xi}^T)\right) + \sum_{k=1}^{K} \vartheta_{j,k}\left(\tilde{P}_{C_{j,k}}\left(\tilde{\boldsymbol{\xi}}^{\tilde{T}}\right)\right), \end{aligned} \tag{5.41}$$

  where it can be verified that

$$\sum_{k=1}^{K} \vartheta_{j,k}\left(P_{C_{j,k}}(\boldsymbol{\xi}^T)\right) - \sum_{k=1}^{K} \vartheta_{j,k}\left(\tilde{P}_{C_{j,k}}\left(\tilde{\boldsymbol{\xi}}^{\tilde{T}}\right)\right) \leq \sum_{k=1}^{K} \xi_k^T\left(\bar{P}_{j,k}(\boldsymbol{\xi}^T) - \tilde{\bar{P}}_{j,k}\left(\tilde{\boldsymbol{\xi}}^{\tilde{T}}\right)\right) \tag{5.42}$$

  Therefore,

$$\begin{aligned} &U_j^S\left(\mathcal{P}_{C_j}(\boldsymbol{\xi}^T), \boldsymbol{\xi}^T\right) - U_j^S\left(\tilde{\mathcal{P}}_{C_j}\left(\tilde{\boldsymbol{\xi}}^{\tilde{T}}\right), \tilde{\boldsymbol{\xi}}^{\tilde{T}}\right) \\ &\quad = R_{j,d}\left(\mathcal{P}_{C_j}(\boldsymbol{\xi}^T)\right) - \sum_{k=1}^{K} \xi_k^T \bar{P}_{j,k}(\boldsymbol{\xi}^T) - R_{j,d}\left(\tilde{\mathcal{P}}_{C_j}\left(\tilde{\boldsymbol{\xi}}^{\tilde{T}}\right)\right) + \sum_{k=1}^{K} \xi_k^T \tilde{\bar{P}}_{j,k}\left(\tilde{\boldsymbol{\xi}}^{\tilde{T}}\right) \geq 0, \end{aligned} \tag{5.43}$$

where the last inequality follows from the fact that $\mathcal{P}_{C_j}\left(\boldsymbol{\xi}^T\right) = \arg\ \max\ U_j^S(\mathcal{P}_{C_j}(\boldsymbol{\xi}^T), \boldsymbol{\xi}^T)$, as defined in (5.15).

- If $\tilde{P}_{C_{j,k}}\left(\tilde{\boldsymbol{\xi}}^{\tilde{\tau}}\right) \geq P_{C_{j,k}}(\boldsymbol{\xi}^{\tau})$, then $\tilde{P}_{C_{j,k}}\left(\tilde{\boldsymbol{\xi}}^{\tilde{T}}\right) \geq P_{C_{j,k}}(\xi^T)$, $\tilde{T} \geq T$ and $\tilde{\boldsymbol{\xi}}^{\tilde{T}} \geq \boldsymbol{\xi}^T$. Similarly, it can be verified that

$$\sum_{k=1}^{K} \vartheta_{j,k}\left(\tilde{P}_{C_{j,k}}\left(\tilde{\boldsymbol{\xi}}^{\tilde{T}}\right)\right) - \sum_{k=1}^{K} \vartheta_{j,k}(P_{C_{j,k}}(\boldsymbol{\xi}^T)) \geq \sum_{k=1}^{K} \xi_k^T\left(\tilde{P}_{C_{j,k}}\left(\tilde{\boldsymbol{\xi}}^{\tilde{T}}\right) - P_{C_{j,k}}(\xi^T)\right). \quad (5.44)$$

Hence,

$$\begin{aligned} &U_j^S\left(\mathcal{P}_{C_j}(\boldsymbol{\xi}^T), \boldsymbol{\xi}^T\right) - U_j^S\left(\tilde{\mathcal{P}}_{C_j}\left(\tilde{\boldsymbol{\xi}}^{\tilde{T}}\right), \tilde{\boldsymbol{\xi}}^{\tilde{T}}\right) \\ &= R_{j,d}\left(\mathcal{P}_{C_j}(\boldsymbol{\xi}^T)\right) - \sum_{k=1}^{K} \xi_k^T \bar{P}_{j,k}(\boldsymbol{\xi}^T) - R_{j,d}\left(\tilde{\mathcal{P}}_{C_j}\left(\tilde{\boldsymbol{\xi}}^{\tilde{T}}\right)\right) + \sum_{k=1}^{K} \xi_k^T \tilde{\bar{P}}_{j,k}\left(\tilde{\boldsymbol{\xi}}^{\tilde{T}}\right) \geq 0, \end{aligned} \quad (5.45)$$

where the last inequality also follows from $\mathcal{P}_{C_j}\left(\boldsymbol{\xi}^T\right) = \arg\max U_j^S\left(\mathcal{P}_{C_j}(\boldsymbol{\xi}^T), \boldsymbol{\xi}^T\right)$, as defined in (5.15).

Based on (5.43) and (5.45), it has been shown that in either case $U_j^S\left(\mathcal{P}_{C_j}(\boldsymbol{\xi}^T), \boldsymbol{\xi}^T\right) \geq U_j^S\left(\tilde{\mathcal{P}}_{C_j}\left(\tilde{\boldsymbol{\xi}}^{\tilde{T}}\right), \tilde{\boldsymbol{\xi}}^{\tilde{T}}\right)$. Hence, given that all other source nodes truthfully report their power demands at every time-step, the best strategy for source node S_j is to truthfully report its power demand at every time-step. Therefore, truthfully reporting power demand at every time-step is the mutual best response for every source node. □

5.5.4 Social Welfare Maximization

Theorem 5.3 (Social Welfare Maximization): The proposed distributed algorithm achieves the Walrasian Equilibrium allocation $(\boldsymbol{\xi}^\star, \mathcal{P}_C(\boldsymbol{\xi}^\star))$ which maximizes the sum of rates, i.e. $\mathcal{P}_C(\boldsymbol{\xi}^\star)$ is the solution to the following convex optimization problem

$$\begin{aligned} \max_{\mathcal{P}_C} \quad & \sum_{j=1}^{N} R_{j,d}(\mathcal{P}_{C_j}) \\ \text{s.t.} \quad & \sum_{j=1}^{N} P_{C_{j,k}} \leq P_{R_k}, \quad \forall k \in \{1, 2, \ldots, K\}, \\ & 0 \leq P_{C_{j,k}} \leq P_{R_k}, \quad \forall j \in \{1, 2, \ldots, N\},\ \forall k \in \{1, 2, \ldots, K\}. \end{aligned} \quad (5.46)$$

Proof: According to Theorems 5.1 and 5.2, the proposed distributed algorithm concludes in a finite number of time-steps and if all source nodes truthfully report their optimal power demands then the auction process converges to an allocation $(\boldsymbol{\xi}^\star, \mathcal{P}_C(\boldsymbol{\xi}^\star))$. The optimization problem in (5.46) is convex since the objective function is convex in $\mathcal{P}_{C_j}, \forall j \in \{1, 2, \ldots, N\}$

and the constraints are linear and thus convex. In turn, a dual decomposition approach is utilized to decompose the original "separable" optimization problem into independent subproblems [94]. Define the Lagrangian function as

$$\mathcal{L}(\mathcal{P}_C, \boldsymbol{\lambda}) = \sum_{j=1}^{N} R_{j,d}(\mathcal{P}_{C_j}) - \sum_{k=1}^{K} \lambda_k \left(\sum_{j=1}^{N} P_{C_{j,k}} - P_{R_k} \right), \tag{5.47}$$

where $\boldsymbol{\lambda} = [\lambda_1, \ldots, \lambda_K]^T$ and $\lambda_k \geq 0, \forall k \in \{1, 2, \ldots, K\}$ are the Lagrangian multipliers for the K total relay power constraints. The Lagrangian function in (5.47) is rearranged as

$$\mathcal{L}(\mathcal{P}_C, \boldsymbol{\lambda}) = \sum_{j=1}^{N} \left(R_{j,d}(\mathcal{P}_{C_j}) - \sum_{k=1}^{K} \lambda_k P_{C_{j,k}} \right) + \sum_{k=1}^{K} \lambda_k P_{R_k}. \tag{5.48}$$

Since the original problem is convex, then strong duality holds[3] and correspondingly, the dual problem can be expressed in terms of a "master" problem [94]

$$\begin{aligned} \min_{\boldsymbol{\lambda}} \quad & \mathcal{D}(\boldsymbol{\lambda}) \\ \text{s.t.} \quad & \boldsymbol{\lambda} \geq 0, \end{aligned} \tag{5.49}$$

and a "slave" problem defined by the dual function $\mathcal{D}(\boldsymbol{\lambda})$ as given by

$$\begin{aligned} \mathcal{D}(\boldsymbol{\lambda}) = \max \quad & \mathcal{L}(\mathcal{P}_C, \boldsymbol{\lambda}) \\ \text{s.t.} \quad & 0 \leq P_{C_{j,k}} \leq P_{R_k}, \quad \forall j \in \{1, 2, \ldots, N\}, \ \forall k \in \{1, 2, \ldots, K\}. \end{aligned} \tag{5.50}$$

The slave problem in (5.50) is decomposed and determined by solving the N following subproblems of each source node S_j as given by

$$\begin{aligned} \max \quad & \mathcal{L}_j(\mathcal{P}_{C_j}, \boldsymbol{\lambda}) = R_{j,d}(\mathcal{P}_{C_j}) - \sum_{k=1}^{K} \lambda_k P_{C_{j,k}} \\ \text{s.t.} \quad & 0 \leq P_{C_{j,k}} \leq P_{R_k}, \quad \forall k \in \{1, 2, \ldots, K\}, \end{aligned} \tag{5.51}$$

where $\mathcal{L}_j(\mathcal{P}_{C_j}, \boldsymbol{\lambda})$ is the j^{th} term in the first summation in (5.48). Now, let $\mathcal{L}_j^{\star}(\boldsymbol{\lambda}) = R_{j,d}(\mathcal{P}_{C_j}(\boldsymbol{\lambda})) - \sum_{k=1}^{K} \lambda_k P_{C_{j,k}}(\boldsymbol{\lambda})$ denote the optimal value of $\mathcal{L}_j(\mathcal{P}_{C_j}, \boldsymbol{\lambda})$ by solving (5.51). It is interesting to notice the similarity between (5.51) and (5.15), where in this case λ_k is interpreted as the price per unit power $P_{C_{j,k}}$ (i.e. the shadow price). Thus, maximizing $\mathcal{L}_j(\mathcal{P}_{C_j}, \boldsymbol{\lambda})$, $\forall j \in \{1, 2, \ldots, N\}$ is equivalent to maximizing the source nodes utilities with $P_{C_{j,k}}(\boldsymbol{\lambda})$ as defined in (5.25).

The dual master problem in (5.49) can be re-expressed as

$$\begin{aligned} \min \quad & \mathcal{D}(\boldsymbol{\lambda}) = \sum_{j=1}^{N} \mathcal{L}_j^{\star}(\boldsymbol{\lambda}) + \sum_{k=1}^{K} \lambda_k P_{R_k} \\ \text{s.t.} \quad & \lambda_k \geq 0, \quad k \in \{1, 2, \ldots, K\}. \end{aligned} \tag{5.52}$$

[3]Strong quality implies the duality gap is zero and hence the minimized objective of the Lagrange dual problem is equal to the maximized sum-rate in the primal problem.

Thus, by iteratively solving problems (5.51) and then (5.52), the optimal power allocation is solved. It is noteworthy that problem (5.52) aims at finding the optimal shadow prices such that the dual problem is minimized which by complementary slackness at optimality can be achieved when $\sum_{k=1}^{K} \lambda_k^\star P_{R_k} = \sum_{j=1}^{N} \sum_{k=1}^{K} \lambda_k^\star P_{C_{j,k}}(\boldsymbol{\lambda}^\star)$ which in turn implies that $P_{R_k} = \sum_{j=1}^{N} P_{C_{j,k}}(\boldsymbol{\lambda}^\star)$, for $\lambda_k^\star \geq 0, \forall k \in \{1, 2, \ldots, K\}$. Thus, the solution the optimization problem in (5.46) is given by

$$P_{C_{j,k}}(\boldsymbol{\lambda}^\star) = \max \left[0, \min \left(\sqrt{\frac{\Omega_{j,k,d} \Upsilon_{j,k,d}}{\lambda_k^\star}} \, \frac{\Gamma_j(\boldsymbol{\lambda}^\star) + \sqrt{\Gamma_j^2(\boldsymbol{\lambda}^\star) + 4\eta\Lambda_j}}{2\Lambda_j} - \Upsilon_{j,k,d}, P_{R_k} \right) \right], \quad (5.53)$$

$\forall j \in \{1, 2, \ldots, N\}$ and hence $(\boldsymbol{\lambda}^\star, \mathcal{P}_C(\boldsymbol{\lambda}^\star))$ is the Walrasian Equilibrium allocation that maximizes the social welfare. □

The power allocation produced by the proposed distributed algorithm is equivalent to that of a centralized optimal power allocation scheme that maximizes the sum of rates. However, significant overheads and signaling would be required by a central controller to obtain complete channel state information (i.e. $\{h_{k,d}\}_{k=1}^{K}$, $\{h_{j,k}\}_{k=1}^{K}$, $\{h_{j,d}\}, \forall j \in \{1, 2, \ldots, N\}$) in order to compute an optimal power allocation that fully distributes $\mathcal{P}_R$.

5.5.5 Uniqueness

Due to the strict monotonicity and concavity of source node S_j's rate function $R_{j,d}(\mathcal{P}_{C_j})$, $\forall j \in \{1, 2, \ldots, N\}$, the Walrasian Equilibrium allocation $(\boldsymbol{\xi}^\star, \mathcal{P}_C(\boldsymbol{\xi}^\star))$ is unique [129].

In summary, starting from any initial price vector $\boldsymbol{\xi}^0 \in \mathcal{V}$ with a small enough price increment μ, strictly concave source nodes' utility functions, and truthful optimal power demands at every time-step, the price vector converges to the unique Walrasian equilibrium price and power allocation $(\boldsymbol{\xi}^\star, \mathcal{P}_C(\boldsymbol{\xi}^\star))$ which maximizes the social welfare. Finally, according to the first welfare theorem of economics, the Walrasian equilibrium allocation is also Pareto-efficient [138] [139].

5.6 Summary of Network Operation

Initially, a coordination phase takes places in which several source nodes send transmission requests for cooperation to form a cluster. Other nodes—who are willing to act as relays and share their transmission resources—send reply messages declaring their intent. A node is elected as a cluster-head (possibly the destination node), which conveys control information, signature waveform assignment, and transmission schedule to the rest of the cluster via appropriate control channels [115]. For distributed clock synchronization, the cluster-head is responsible for exchanging timing information (i.e. the SYNC signal) through periodic beacon transmissions. A host synchronizes its clock according to the timestamp in the beacon. For a more detailed discussion on practical solutions for distributed timing synchronization in ad-hoc wireless networks, the reader is referred to [140][141]. The auction mechanism

takes place after the coordination phase and involves exchanging small packets—via appropriate control channels—between the source and relay nodes for power demands and price announcements, until convergence to an allocation $(\boldsymbol{\xi}, \mathcal{P}_C(\boldsymbol{\xi}))$. After that, the broadcasting and cooperation phases occur alternately. Finally, the coordination and auction mechanism phases repeat in case of topology changes or nodes joining/leaving the cluster.

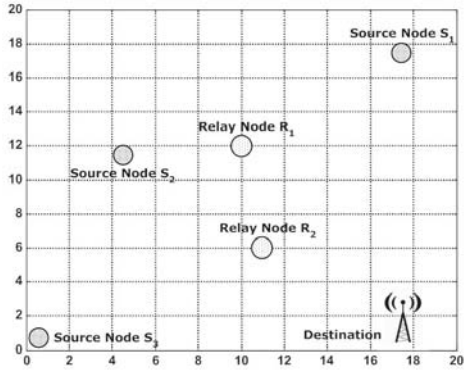

Figure 5.2: Multi-Relay Cooperative Network - Simulation Scenario

5.7 Simulation Results

In this section, the properties of the proposed distributed auction algorithm are numerically verified. Consider a wireless network with three source nodes S_1, S_2 and S_3 being equidistant from the destination, and two relay nodes R_1 and R_2, as illustrated in Fig. 5.2. The channel gain between any two nodes is given by $\sigma_{j,k}^2 = d_{j,k}^{-\nu}$, where $d_{j,k}$ and ν are the distance between the two nodes and the path-loss exponent, respectively. The simulations assume signature waveforms with $\rho = 0.5$, path-loss exponent of $\nu = 3$, step-size of $\mu = 10^{-4}$, reserve price of $\xi_k^0 = \zeta_k = 10^{-2}$, $\forall k \in \{1, 2\}$, source broadcasting transmit power $P_{B_j} = 50$ mW, $\forall j \in \{1, 2, 3\}$, noise variance of $N_0 = 10^{-5}$, and that $P_{R_1} = P_{R_2}$.

In Fig. 5.3, it is seen that the prices set by relay nodes R_1 and R_2 coincide with those of optimum centralized algorithm. Also, it is noticed that node R_2 sets a higher price than R_1 when $P_{R_1} = P_{R_2} \lesssim 0.12$ W. This is translated to a higher utility, as evident from Fig. 5.4. Beyond 0.12 W, the price of R_1 is higher and thus achieves a higher utility. In order for relay node R_1 (R_2) to maximize its utility, it should not sell more than 0.28 W (0.06 W) of its transmit power, as abundant power results in excessively low prices. Also shown in Fig 5.3 are the achievable rates which agree with the centralized algorithm[4]. Fig. 5.4 illustrates that node S_2 achieves the highest utility while node S_3 achieves the lowest. This is due to the location of S_2 being relatively closer to both relay nodes than source nodes S_1 and S_3; therefore its received signal at the relay nodes suffers the least from noise and path-loss. Since the proposed algorithm inherently maximizes the sum of rates, then it is expected that most of the relays' power will be allocated to source S_2, as evident from Fig. 5.5. Also, due

[4]The solution of the centralized scheme is obtained using `fmincon` from the MATLAB optimization toolbox [142].

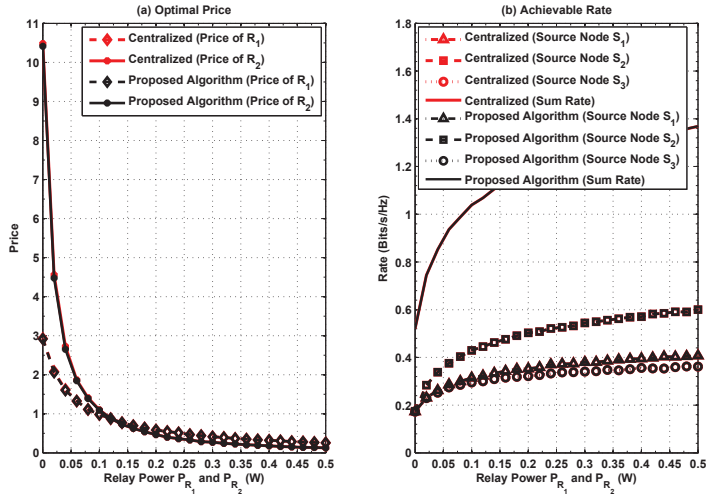

Figure 5.3: Centralized vs. Proposed Algorithm - Optimal Prices and Achievable Rate

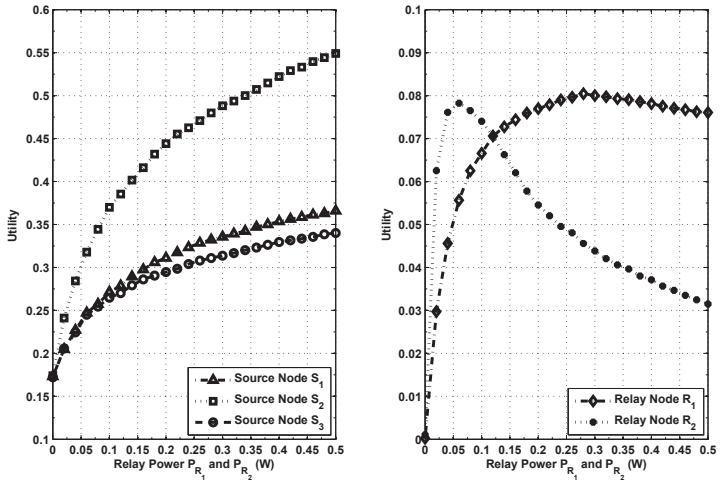

Figure 5.4: Source and Relay Nodes Utilities

to node S_1 relatively closer location to relay R_1 than that of node S_3, it is allocated more power than node S_3. An opposite argument can be made for relay R_2's transmit power. This is also reflected in the payments each source node makes to the relay nodes, as demonstrated in Fig. 5.6. For instance, source node S_2 makes the highest payment to R_1, which is followed by node S_1's payment and finally S_3 makes the lowest payment. Contrarily, nodes S_2 and S_1 make the highest and lowest payments to node R_2, respectively.

In Fig. 5.7, the utility of the source and relay nodes are plotted at $P_{R_1} = P_{R_2} = 0.3$ W when source nodes S_1 and S_3 truthfully report their demands while node S_2 falsely reports its demand to be $\tilde{P}_{C_{2,k}}(\boldsymbol{\xi}^\tau) = \max\left[0, \min(\delta P_{C_{2,k}}(\boldsymbol{\xi}^\tau), P_{R_k})\right]$, $\forall k \in \{1, 2\}$ and $\forall \tau = 0, 1, \ldots, T$ with $\delta \geq 0$ being the demand factor. Clearly, S_2's utility and the sum of utilities peak at $\delta = 1$ (i.e. truthful demand).

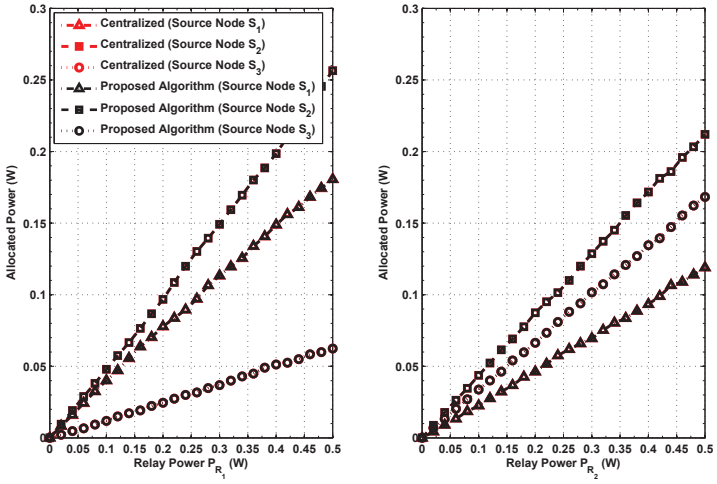

Figure 5.5: Centralized vs. Proposed Algorithm - Relay Power Allocation

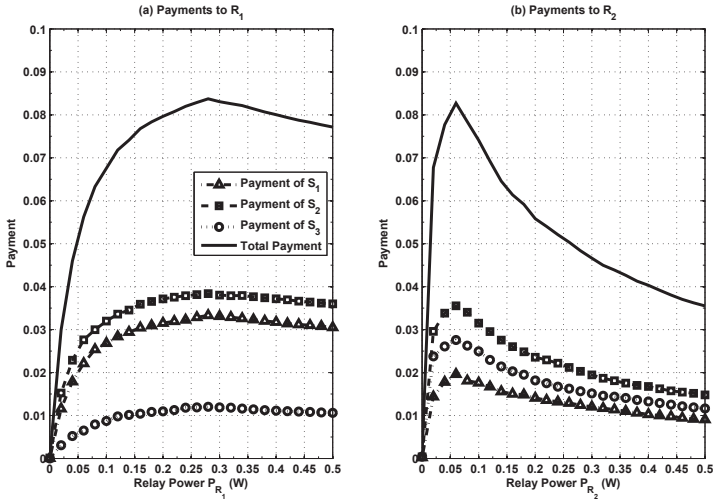

Figure 5.6: Payments to Relay Nodes R_1 and R_2

It is noteworthy that the accuracy of the proposed auction-based relay allocation is highly dependent on the chosen step-size μ by which prices ascend. If the step-size is made small enough, the auction algorithm takes too long to converge to the Walrasian Equilibrium allocation. Contrarily, if the step-size is made larger, the auction algorithm converges faster to an allocation that is not necessarily the Walrasian one. This is evident from Fig. 5.8, where for $\mu = 10^{-4}$ the auction algorithm converges to the optimal Walrasian prices but takes on average 3115 iterations, as the power allocation is accurate to four decimal places. However, for a step-size of $\mu = 5 \times 10^{-2}$, the auction algorithm converges in only 9 iterations but is far from the Walrasian Equilibrium prices, leading to suboptimal power allocation. Table 5.2 summarizes the results of the size-step μ and the decreasing average number of iterations $\mathcal{I}(\mu)$.

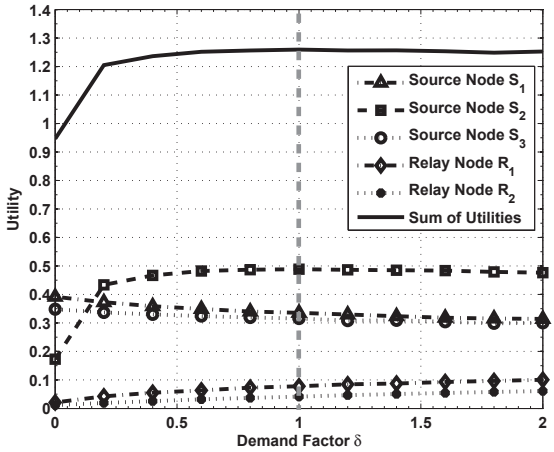

Figure 5.7: Utilities vs. Demand Factor δ - $P_{R_1} = P_{R_2} = 0.3$ W

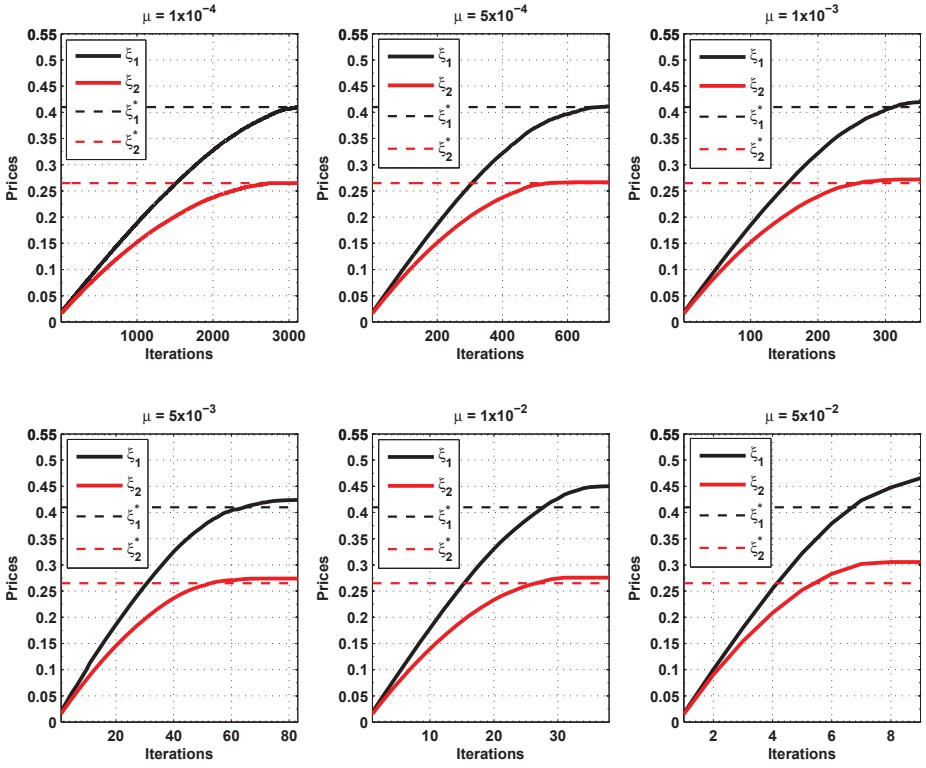

Figure 5.8: Step-Size vs. Average Number of Iterations - $P_{R_1} = P_{R_2} = 0.3$ W

Table 5.2: Summary of Convergence Results - $P_{R_1} = P_{R_2} = 0.3$ W

Step-Size μ	1×10^{-4}	5×10^{-4}	1×10^{-3}	5×10^{-3}	1×10^{-2}	5×10^{-2}	1×10^{-1}
Number of Iterations $\mathcal{I}(\mu)$	3115	727	352	83	38	9	5

Shown in Fig. 5.9 is the decreasing sum of utilities as a function of the increasing step-size. This result verifies that the highest sum of utilities is achieved at the Walrasian Equilibrium allocation (which occurs when $\mu = 10^{-4}$), and increasing the step-size results in a lower sum of utilities but leads to a faster convergence. Most importantly, this decrease of about 0.02 in the sum of utilities value is not severe which suggests a good tradeoff between the speed of convergence and social welfare.

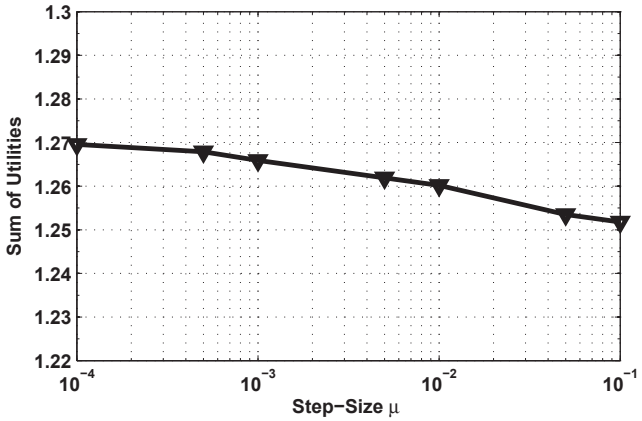

Figure 5.9: Sum of Utilities vs. Step-Size - $P_{R_1} = P_{R_2} = 0.3$ W

In Fig. 5.10, the achievable rate of each source node is shown as a function of the algorithm step-size. As can be seen, the decrease in the rate with the increase in the step-size is insignificant. This is due to the fact that although the algorithm converges faster and the power allocation is not the Walrasian one, most of the cooperative power has been allocated in the first few iterations and the finite accuracy in the power allocation takes place in the remaining iterations. This is evident from the power allocation values as summarized in Table 5.3.

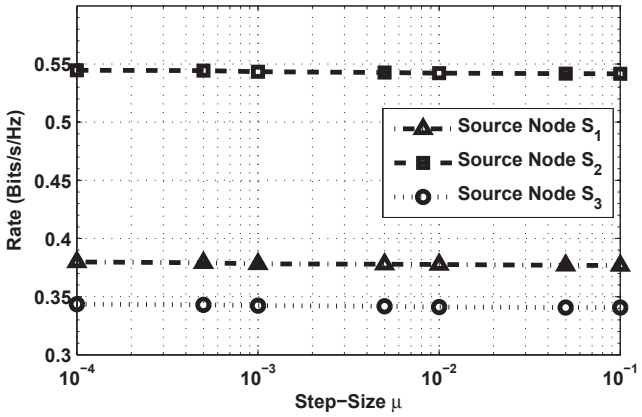

Figure 5.10: Achievable Rate vs. Step-Size - $P_{R_1} = P_{R_2} = 0.3$ W

Table 5.3: Summary of Relay Power Allocation to Each Source Node - $P_{R_1} = P_{R_2} = 0.3$ W

Source Node	Relay Node	Step-Size μ						
		1×10^{-4}	5×10^{-4}	1×10^{-3}	5×10^{-3}	1×10^{-2}	5×10^{-2}	1×10^{-1}
S_1	R_1	0.1135	0.1132	0.1126	0.1113	0.1110	0.1107	0.1076
	R_2	0.0695	0.0703	0.0717	0.0718	0.0715	0.0687	0.0674
S_2	R_1	0.1494	0.1489	0.1485	0.1505	0.1511	0.1519	0.1560
	R_2	0.1289	0.1285	0.1291	0.1295	0.1304	0.1338	0.1371
S_3	R_1	0.0371	0.0379	0.0389	0.0382	0.0379	0.0374	0.0364
	R_2	0.1016	0.1012	0.0992	0.0987	0.0981	0.0975	0.0955

5.8 Discussion

5.8.1 Utility Functions

Although network nodes naturally desire to achieve high data rates (or at least meet target QoS), they may not be willing to do so at arbitrarily high transmission power levels as they may have different satisfaction levels and/or views of power consumption. Thus, different classes of utility functions are required, such as sigmoid functions (first convex and then concave), which can be used to control user power/rate demands [124]. Also, $\alpha-$fair utility functions can be used to control the tradeoff between efficiency and fairness [143]. However, the use of such utility functions makes the social welfare maximization problem non-convex, which makes the problem more difficult to analyze, even by centralized algorithms [125]. In turn, distributed algorithms may lead to infeasible/suboptimal power allocation or simply diverge, and thus must be carefully designed. Reformulating the proposed auction-based power allocation with different classes of utility functions is an interesting topic and will be studied in future work.

5.8.2 Channel State Information

In centralized power allocation, a centralized controller must obtain a large amount of information, including perfect global channel state information (CSI), available transmit power and received SNR at each node, and network topology. After collecting the required information, the centralized controller solves the optimization problem in (5.46). This may be infeasible to implement due to the substantial feedback requirements and the latency in collecting/exchanging such parameters and sending power control commands to the different source/relay nodes. Also, the computational complexity in optimizing power allocation for a network with large number of nodes becomes practically prohibitive. Add to that the infrastructure-less nature of ad-hoc networks in which centralized control is non-existent in the first place. In the proposed auction mechanism, the power demand of each source node S_j to the K relay nodes depends on the channel coefficients $\{h_{j,k}\}_{k=1}^{K}$, $h_{j,d}$ and $\{h_{k,d}\}_{k=1}^{K}$ (i.e. the inter-channels between itself and the destination). In particular, $\{h_{j,k}\}_{k=1}^{K}$, and $h_{j,d}$

can be estimated by source node S_j while $\{h_{k,d}\}_{k=1}^{K}$ is broadcast by each relay R_k to all the source nodes. Clearly, the overhead at each source/relay node is much less than having a centralized controller collect CSI between all the nodes.

5.8.3 Complexity Analysis and Overhead

During each iteration, each source node transmits a vector of power demands $\mathcal{P}_{C_j}$, which is received by each of the K relay nodes. In addition, each relay node announces its price to the source nodes via appropriate control channels. Therefore, the number of messages exchanged in each iteration is $\mathcal{O}(N+K)$. Now, since the number of iterations $\mathcal{I}(\mu)$ is dependent on the step-size μ, then the total number of messages exchanged of the proposed auction algorithm is $\mathcal{O}((N+K)\mathcal{I}(\mu))$. Additional overhead is due to the initial coordination and clock synchronization between the nodes, as in the case of conventional ad-hoc networks [115][140].

5.9 Implementation Issues

So far, the work has assumed a static network and thus the results obtained are less appropriate for mobile networks, which require the proposed algorithm be repeated with substantial overhead when channel coherence time elapses. The cost of distributed power allocation in terms of additional overhead and signaling, unfortunately, is often overlooked. Communication overhead takes the form of extra feedback for exchanging information and multiple packets for power demands and price announcements.

The following discussion, analysis and qualitative evaluation should provide insights for implementing the proposed distributed algorithm and also provide more solid intuition about protocol design choices and the role of overhead. Specifically, the following subsections consider the IEEE802.11g standard for wireless local area networks as a practical application.

5.9.1 Coordination

Initially, assume the network nodes have detected their neighbors and the TDMA transmission of the source and relay nodes has been coordinated. After coordinating the roles of source and relay nodes, an internet registration policy for each source/relay node must be verified and then each source node must register itself and obtain an electronic certificate. The presence of a registration policy eases the operation of the auction mechanism and its implementation in electronic form. At the beginning of the bidding service, each source node sends its own certificate to all the relays, as a pre-requisite for power demand. When a certificate is verified by all the relays, a common broadcast channel is established between the source and relay nodes.

5.9.2 Auction Mechanism

The auction mechanism starts when each relay node takes turn in announcing "broadcasting" its price at every time-step τ in the form of a data packet. After all the prices have been announced, each source node then takes turn in broadcasting its power demand data packet, which is received by the relay nodes. This process of exchanging price and power demand data packets ends when demand meets supply, at which point the auction mechanism concludes with a total duration of $T_{Auction}$.

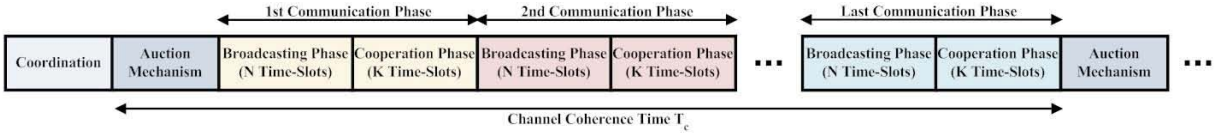

Figure 5.11: Network Operation

5.9.3 Communication Phase

As illustrated in Fig. 5.11, after coordination and auction-based power allocation, data transmission and relaying takes place. Specifically, each communication phase consists of $N + K$ time-slots. The number of communication phases is calculated as

$$\mathcal{C} = \left\lfloor \frac{T_c}{T_{TX}} \right\rfloor, \quad \text{for} \;\; T_{TX} \leq T_c, \tag{5.54}$$

where T_{TX} is the total transmission time which consists of duration of the auction mechanism $T_{Auction}$ in addition to the total time T_{Data} spent transmitting or relaying data in each communication phase (i.e. $(N + K) \cdot T_{Data}$). Furthermore, T_c is the channel coherence time, as will be defined in the following subsections. In this work, a continuous source model is assumed whereby all the source nodes always have data to transmit in every time-slot.

5.9.4 IEEE802.11g Model and Operation

This subsection develops a simple model to calculate the total time duration of the auction mechanism $T_{Auction}$, and also the total data transmission time T_{Data} from each source/relay node to the destination node (e.g. an access point), assuming a TCP protocol. Specifically, a single TCP data packet is followed by a TCP acknowledgement (TCP ACK) packet. As such, the IEEE802.11g MAC requires positive acknowledgement after every transmission, which is sent by the receiving node a short time interval after receiving the packet. If an ACK is not received, the packet is considered lost and a retransmission is arranged. In turn, two IEEE802.11g packets are transmitted, consisting of [144]:

1. TCP data packet:
    - Distributed inter-frame space (DIFS): this inter-frame space indicates that an exchange has completed, and it is safe to access the medium again.

- Data frame containing the TCP data frame.
- Short inter-frame space (SIFS): a small gap between the data frame and its acknowledgement.
- The 802.11 ACK frame.

2. TCP ACK packet:
   - DIFS.
   - Data frame containing the TCP ACK frame.
   - SIFS.
   - The 802.11 ACK frame.

In addition to the payload data, 36 bytes of data are added in the encapsulation process (consisting of $L_{MAC} = 28$ bytes are 802.11 MAC header and $L_{SNAP} = 8$ bytes for SNAP header). Also, $L_{TCP} = 40$ bytes including TCP/IP headers are also added. As for the TCP ACK packet, in addition to the L_{TCP} bytes of TCP/IP header information, it gets $L_{MAC} + L_{SNAP} = 36$ bytes of MAC and SNAP headers, resulting in a total of $L_{TCP} + L_{MAC} + L_{SNAP} = 76$ bytes. Finally, every transmitted frame has a signal extension at the end of duration $T_{EX} = 6$ μs.

5.9.5 Frame Structure

In this work, the IEEE802.11g extended-rate PHY (ERP) frame structure is studied and illustrated in Fig. 5.12. For a detailed description of each field in the frame, the reader is referred to [144].

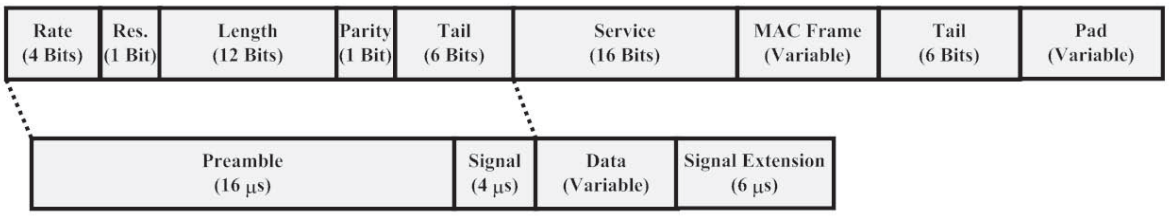

Figure 5.12: ERP-OFDM Frame Structure

Power Demand and Price Announcement Model

Let L_{ξ_k} be the number of bytes representing the price announced by relay node R_k. Also, let $L_{P_{C_{j,k}}}$ be the number of bytes representing source node S_j's power demand to relay node R_k. Without any loss of generality, let $L_{\xi_k} = L_{Price}, \forall k \in \{1, 2, \ldots, K\}$. Also, let $L_{P_{C_{j,k}}} = L_{Power}, \forall j \in \{1, 2, \ldots, N\}$ and $\forall k \in \{1, 2, \ldots, K\}$.

The TCP price announcement frame duration is determined as

$$T_{TCP-Price} = T_{Preamble} + T_{Sig} + T_{SYM} \times \left\lceil \frac{L_{Service} + L_{Tail} + 8(L_{MAC} + L_{TCP} + L_{Price})}{N_{DBPS}} \right\rceil + T_{EX}, \tag{5.55}$$

where N_{DBPS} is the number of data bits per OFDM symbol. On the other hand, the time duration involved in transmitting each source node's power demand is given by

$$T_{TCP-Power} = T_{Preamble} + T_{Sig} + T_{SYM} \times \left\lceil \frac{L_{Service} + L_{Tail} + 8(L_{MAC} + L_{TCP} + L_{Power})}{N_{DBPS}} \right\rceil + T_{EX}. \tag{5.56}$$

The time duration involved in transmitting the TCP ACK frame is given by

$$T_{TCP-ACK} = T_{Preamble} + T_{Sig} + T_{SYM} \times \left\lceil \frac{L_{Service} + L_{Tail} + 8(L_{MAC} + L_{TCP} + L_{SNAP})}{N_{DBPS}} \right\rceil + T_{EX}, \tag{5.57}$$

The duration of the 802.11 ACK frame is obtained as

$$T_{ACK} = T_{Preamble} + T_{Sig} + T_{SYM} \times \left\lceil \frac{8L_{ACK}}{N_{DBPS}} \right\rceil + T_{EX}, \tag{5.58}$$

where L_{ACK} is the number of bytes for packet acknowledgement. Thus, the total time durations involved in announcing a price and submitting a power demand are determined as

$$T_{T-Price} = T_{DIFS} + T_{TCP-Price} + T_{SIFS} + T_{ACK}, \tag{5.59}$$

and

$$T_{T-Power} = T_{DIFS} + T_{TCP-Power} + T_{SIFS} + T_{ACK}, \tag{5.60}$$

respectively. Also, the total duration of transmitting the TCP ACK frame and its 802.11 ACK is determined as

$$T_{T-ACK} = T_{DIFS} + T_{TCP-ACK} + T_{SIFS} + T_{ACK}. \tag{5.61}$$

Hence, the total time durations of each price announcement and power demand and their acknowledgements are given by

$$T_{Price} = T_{T-Price} + T_{T-ACK}, \tag{5.62}$$

and

$$T_{Power} = T_{T-Power} + T_{T-ACK}, \tag{5.63}$$

respectively. In turn, the total time duration of the auction mechanism is given by

$$T_{Auction} = (K \cdot T_{Price} + N \cdot T_{Power}) \cdot \mathcal{I}(\mu), \tag{5.64}$$

where $\mathcal{I}(\mu)$ is the expected number of iterations as function of the algorithm step-size μ.

Data Transmission Model

The TCP data frame duration is calculated as

$$T_{TCP-Data} = T_{Preamble} + T_{Sig} + T_{SYM} \times \left\lceil \frac{L_{Service} + L_{Tail} + 8(L_{MAC} + L_{TCP} + L_{MSDU})}{N_{DBPS}} \right\rceil + T_{EX}, \tag{5.65}$$

where L_{MSDU} refers to the length of the MAC service data unit (i.e. data payload). Thus, the total duration associated with transmitting a data frame and its 802.11 ACK is given by

$$T_{T-Data} = T_{DIFS} + T_{TCP-Data} + T_{SIFS} + T_{ACK}. \tag{5.66}$$

The total time duration of data transmission in each time-slot is given by

$$T_{Data} = T_{T-Data} + T_{T-ACK}. \tag{5.67}$$

Consequently, the total communication duration is given by

$$\begin{aligned} T_{TX} &= T_{Auction} + T_{Data} \\ &= (K \cdot T_{Price} + N \cdot T_{Power}) \cdot \mathcal{I}(\mu) + (N + K) \cdot T_{Data}, \end{aligned} \tag{5.68}$$

such that $T_{TX} \leq T_c$.

5.9.6 Coherence Time

As network nodes move within proximity of each other, communication channels vary with time. A measure of the channel correlation over time is given by the coherence time T_c. A popular rule of thumb for modern digital communications is to define the coherence time as [145]

$$T_c = \sqrt{\frac{9}{16\pi f_m^2}} \approx \frac{0.423}{f_m}, \tag{5.69}$$

with f_m being defined as the maximum Doppler shift as given by $f_m = \frac{v f_c}{c}$, where v is the velocity of the mobile node in m/s, $c = 3 \times 10^8$ m/s is the speed of light in free space, and f_c is the carrier frequency in Hz.

5.9.7 Frame Error Rate Performance

In order to quantify the effective data rate of each source node in the network, the frame error rate performance must be taken into account. For a data frame of length L bytes, the frame error rate of a wireless channel is determined as

$$\mathcal{F}(L) = 1 - (1 - \mathcal{P})^{8L}, \tag{5.70}$$

where $\mathcal{P}$ is the bit error rate. Therefore, the frame error rate for L_{MSDU}-bytes long data frame of source node S_j, taking into account PHY and MAC headers, is derived as [146]

$$\mathcal{F}_{s_j}(L_{MSDU}) = 1 - (1 - \mathcal{F}(L_{PLCP})) \cdot (1 - \mathcal{F}(L_{MAC} + L_{TCP} + L_{MSDU})), \tag{5.71}$$

where $\mathcal{F}(L_{PLCP})$ is the probability of error of the PLCP preamble/header transmitted in the PHY mode, which contains $L_{PLCP} = 24$ bytes. Moreover, $\mathcal{F}(L_{MAC} + L_{TCP} + L_{MSDU})$ is the probability of error of the MSDU, including the MAC overhead.

5.9.8 Throughput

In order to quantify the effect of payload size and channel coherence time, the total amount of data (in bits) transferred *successfully* from each source node S_j to the destination in a specified amount of time. In this work, the throughput (in bits/s) is defined as[5]

$$\mathcal{T}_{s_j} = \frac{\text{Total Successfully Transmitted Data}}{\text{Total Communication Duration}} = \frac{8L_{MSDU} \cdot \mathcal{C} \cdot (1 - \mathcal{F}_{s_j}(L_{MSDU}))}{T_{TX}}. \tag{5.72}$$

It should be noted that overhead due to protocol headers and checksums are not included in the calculation of throughput. In addition, no management frames (i.e. beacon, probe request/response and re-association frames) have been taken into account. Moreover, fragmentation in the MAC layer is not considered, neither is the propagation delay.

5.9.9 Numerical Results

The simulations assume the IEEE802.11g-only network mode with no legacy stations. Also, BPSK 6 Mbps with rate $R_c = 1/2$ convolutional coding using OFDM data transmission mode is simulated [58][59]. At 6 Mbps, each OFDM symbol encodes $N_{DBPS} = 24$ data bits (i.e. 48 coded bits). In addition, the simulations assume $N = 3$ source nodes and $K = 2$ relay nodes, as illustrated in Fig. 5.2 with the same simulation parameters given in Section 5.7 and $P_{R_1} = P_{R_2} = 0.3$ W. The relevant IEEE802.11g parameters are summarized in Table 5.4. To faithfully study the impact of the communication overhead, the following transmission modes are compared:

- Cooperative transmission with sum-of-rate maximizing optimal power allocation (CTX-O). This transmission mode involves the proposed auction mechanism, as discussed throughout this section. In this case, each source node has a total transmit power of $P_{s_j} = P_{B_j} + P_{C_{j,1}} + P_{C_{j,2}}$ where $P_{C_{j,1}}$ and $P_{C_{j,2}}$ are as summarized in Table 5.3.

[5] An ACK frame is transmitted at a rate equals to or lower than the data frame rate, and is only $L_{ACK} = 14$ bytes long, which is usually much shorter than a data frame. Hence, the probability of error of an ACK frame is very low compared to the error probability of the data frame, and thus ignored in the calculation. The same assumption applies the auction mechanism frames.

- Cooperative transmission with equal power allocation (CTX-E). In this case, the auction mechanism phase is eliminated as each relay node equally allocates its cooperative transmit power to the source nodes. Hence, the total transmission time is equivalent to the data transmission time (i.e. $T_{TX} = T_{Data}$). Addition, the total transmit power allocated to each source node is given by $P_{s_j} = P_{B_j} + P_{C_{j,1}} + P_{C_{j,2}} = P_{B_j} + \frac{P_{R_1}+P_{R_2}}{3}, \forall j \in \{1, 2, 3\}$ and $P_{R_1} = P_{R_2} = 0.3$ W.

Table 5.4: IEEE802.11g Simulation Parameters

Parameter	Value
f_c	2.4 GHz
T_{DIFS}	28 μs
T_{SIFS}	10 μs
$T_{Preamble}$	16 μs
T_{Sym}	4 μs
T_{Sig}	4 μs
T_{EX}	6 μs
$L_{Service}$	16 Bits
L_{Tail}	6 Bits
L_{ACK}	14 Bytes
L_{MAC}	28 Bytes
L_{SNAP}	8 Bytes
L_{TCP}	40 Bytes
L_{Power}	4 Bytes
L_{Price}	4 Bytes

Illustrated in Fig. 5.13 is the throughput of source node S_1 as a function of the node velocity and payload size for $\mu = 1 \times 10^{-1}$ (and $\mathcal{I}(\mu) = 5$) for the CTX-O transmission mode (i.e. optimal power allocation) and its counterpart CTX-E (with equal power allocation and no auction mechanism). It is evident that the throughput of node S_1 under the CTX-E mode is higher than that of the CTX-O mode. In addition, it is can be seen that for low vehicular velocities, and small payload size, the throughput is highest under both transmission modes. This is because slowly time-varying channels have longer coherence time and thus channel estimates remain valid for longer periods. Increasing the node's velocity significantly reduces the coherence time which in turn reduces the total transmission time and diminishes the node's data rate. In addition, increasing the payload size severely degrades the throughput due to the increased frame error probability. The same observation is noticed for source node S_3, as shown in Fig. 5.15.

As for source node S_2 (see Fig. 5.14), the throughput under both cooperative transmission modes gradually degrades with the increase in velocity and payload size but not as severe as source nodes S_1 and S_3. In addition, the throughput under the CTX-E transmission mode is higher than that of the CTX-O mode. Looking at Fig. 5.16, it clear that total network throughput under the CTX-E transmission mode is higher than that of the CTX-O mode.

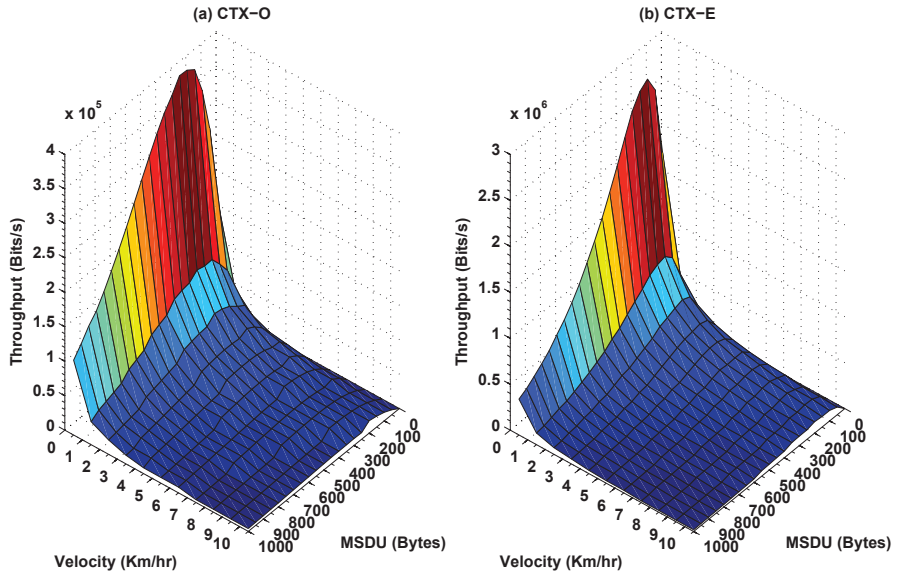

Figure 5.13: Source Node S_1: Throughput vs. MSDU and Velocity - $\mu = 1 \times 10^{-1}$ and $\mathcal{I}(\mu) = 5$ Iterations

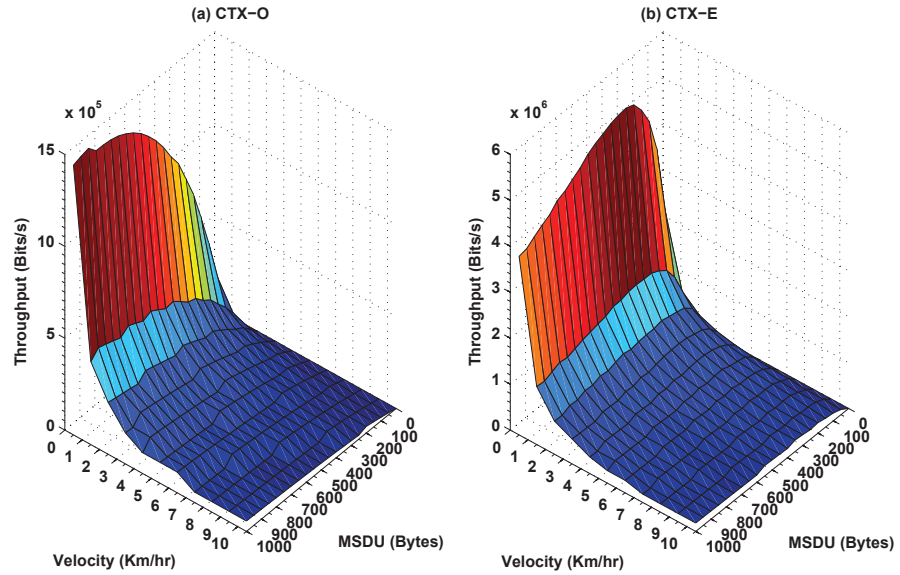

Figure 5.14: Source Node S_2: Throughput vs. MSDU and Velocity - $\mu = 1 \times 10^{-1}$ and $\mathcal{I}(\mu) = 5$ Iterations

Although this result might seem counter-intuitive, however, it should be clear that the total transmission time under the CTX-O mode is shorter than the CTX-E mode and thus each source node has less time to transmit its data, which in turn reduces the total transmitted data. Intuitively, it would be expected that decreasing the auction step-size to $\mu = 5 \times 10^{-2}$ (and $\mathcal{I}(\mu) = 9$) reduces the total transmitted data which in turn further exacerbates the data rate for the CTX-O transmission mode.

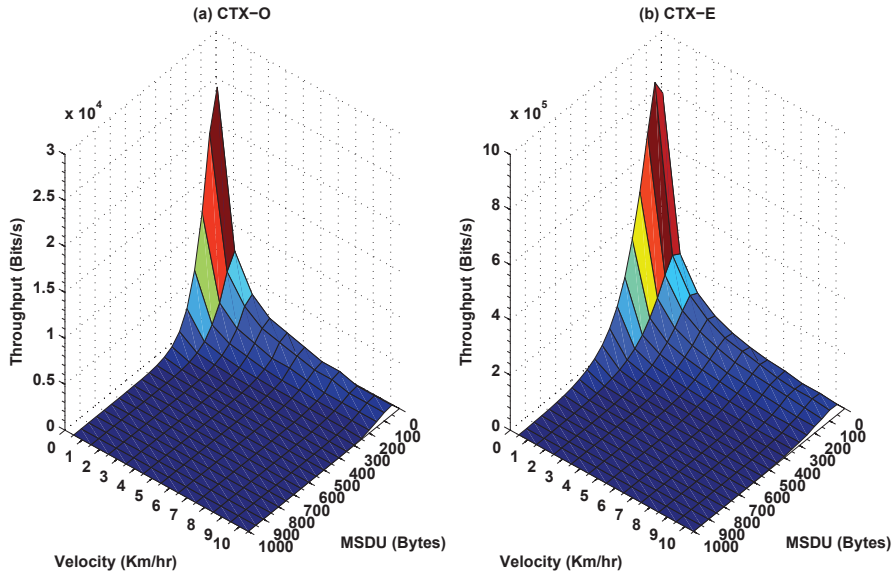

Figure 5.15: Source Node S_3: Throughput vs. MSDU and Velocity - $\mu = 1 \times 10^{-1}$ and $\mathcal{I}(\mu) = 5$ Iterations

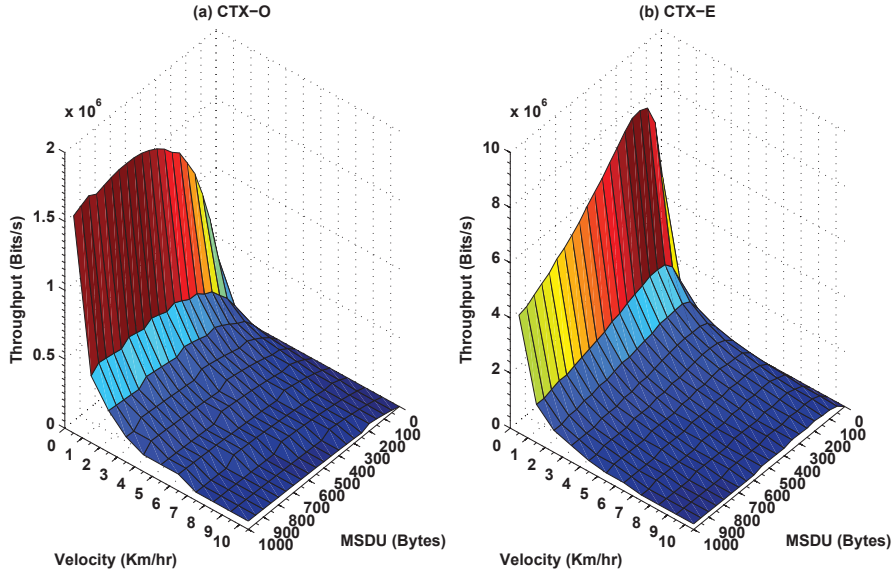

Figure 5.16: Total Throughput vs. MSDU and Velocity - $\mu = 1 \times 10^{-1}$ and $\mathcal{I}(\mu) = 5$ Iterations

It is noteworthy that if the auction-mechanism phase is not considered in the total transmission time, then total throughput under the CTX-O transmission mode becomes higher, although the same observation about the throughput of the different source nodes in comparison with the CTX-E mode would still hold. Moreover, the presented simulation results demonstrate that although decreasing the step-size of the auction mechanism yields a more accurate power allocation (that is closer to the Walrasian one), it significantly reduces the

achievable data rate due to the reduction in the total transmission time as a consequence of the message exchanges of the price announcements and power demands.

5.9.10 Final Remarks

The obtained results in this section are not entirely conclusive. In other words, the proposed auction mechanism might yield a better sum-of-rates performance for a different network topology under which optimal power allocation might result in a BER performance for each source node that is a few orders of magnitude smaller than its counterpart BER performance under equal power allocation. This in turn results in a much smaller frame error rate probability which is reflected in a significant improvement in the throughput. Another possibility would be to consider the case when there is no direct link between each source node and the destination. In such a case, the relays' locations play a significant role in each source node's achievable rate. Finally, for the auction mechanism to be effective in practice, careful design of price and power data packets and their associated headers must take place, and any potential delays must be minimized. This could be achieved by performing the auction mechanism using a higher data rate with higher order modulation (i.e. the shorter is the auction mechanism phase, the higher is the throughput of each source node).

5.10 Conclusions

In this chapter, a distributed ascending-clock auction algorithm is proposed for efficient multi-relay power allocation among a set of source nodes. It is shown that proposed algorithm enforces truth-telling and converges to the Walrasian equilibrium allocation that maximizes social welfare. Also, it was demonstrated that the proposed algorithm presents a tradeoff between the speed of convergence (which is linked to signaling and communication overhead) and maximization of utility and social welfare. Moreover, the proposed algorithm is shown to offer performance that is closely comparable with that of a network with centralized control.

It is acknowledged that this work has only scratched the surface in distributed power allocation through the auction mechanisms in ad-hoc wireless networks. For such mechanisms to be implemented in practice, appropriate modifications to the physical, data link and network layers must be applied. Potential packet loss and retransmission overheads in response to topology changes must also be analyzed to minimize computation/communication costs and not sacrifice network scalability. The multi-layer simulation and experimentation to obtain realistic quantification of the proposed auction mechanism is of great importance and will be pursued in future work. Finally, this work is intended to present an auction-theoretic perspective on algorithmic distributed relay power allocation and raise some practical concerns that are yet to be fully examined and analyzed.

Chapter 6

A Coalitional Game-Theoretic Analysis of Cooperative Networks

6.1 Introduction

As mentioned in the last two chapters, in ad-hoc wireless networks, network nodes are independent, autonomous and selfish by nature and thus may not voluntarily share their transmission resources with other nodes. In other words, there is an element of competition and selfishness since all participating network nodes desire to maximize their utilities by maximizing their share of transmission resources. Moreover, randomly distributed nodes with local information may not know whom to cooperate with even if they are willing to cooperate. Although cooperative communications have been shown to yield significant performance gains [56], cooperation entails several costs, such as bandwidth and power. Ignoring such costs is unwarranted as it may severely affect the nodes' own performance. Particularly, network nodes may not cooperate and instead divert their resources to direct data transmissions. Alternatively, a group of nodes could form a coalition and cooperate to maximize the overall gains of the group and thus promote altruism. Specifically, each node seeks partners to form a cooperative coalition to achieve rate improvement for itself and/or for the whole coalition. In such a case, the greatest immediate benefits may not be achieved by the nodes that bear the greatest costs. Establishing cooperation in ad-hoc wireless networks without a centralized controller is a dynamic process. Hence, designing practical distributed algorithms that can promote cooperation without relying on centralized control is a highly desirable but considerably difficult task.

Coalitional game theory has emerged as an effective mathematical tool for modeling users' cooperation and designing distributed protocols in wireless networks. Several works have considered coalitional formation for user cooperation in wireless networks. For instance, a simple and distributed merge-and-split algorithm is proposed in [147] for the formation of virtual MIMO clusters of selfish single-antenna nodes. In [54], the stability of the grand coalition of transmitter and receiver cooperation in an interference channel is studied for both

flexible transferable and non-transferable apportioning schemes. The curse of the boundary nodes in selfish packet-forwarding wireless networks is resolved using coalitional games in [148]. In [149], fair group coalitions for power-aware routing in wireless networks is studied and distributed algorithms based on max-min fairness are proposed. Distributed coalitional formations with transferable utilities and their stable outcomes in relay networks are studied in [150]. In [151], the authors illustrate that coalition formation could lead to power saving for the individual nodes and thus for the whole coalition.

In this work, a coalitional game-theoretic framework to the study of altruistic coalition formation is considered and the aim is to address the following questions: (1) How can coalitions be formed in a distributed fashion?, (2) What is the impact of different power allocation criteria on coalition formation?, and (3) What is the effect of mobility on the coalition formation process? To form cooperative groups, a coalition formation algorithm based on merge-and-split rules is proposed and proven to converge with arbitrary merge-and-split iterations. In particular, each network node is treated as a player, who seeks partners to form a cooperative group to improve its transmission rate and/or that of the whole group through spatial diversity while incurring some power cost to meet a target SNR for information exchange. This in turn suggests a tradeoff between the gains and costs of cooperation. Moreover, as the size of the cooperative group increases, both the gain and cost also increase to the point where adding an additional node results in a cost that outweighs the diversity gain. Additionally, since network nodes can be either mobile or static, the aim here is to analyze the long-term behavior of network coalition formation when the nodes are mobile within the network area as opposed to their coalition formation when they are static. Centralized power allocation and coalition formation is also studied where it is shown that the proposed algorithm provides a good tradeoff between computational complexity and network sum-rate, and efficiently adapts to nodes' mobility. To the best of the author's knowledge, no existing work has employed coalitional games in the analysis and design of protocols for altruistic coalition formation in network-coded cooperative wireless networks.

In the remainder of this chapter, the system model is presented in Section 6.2. In Section 6.3, the coalitional formation framework is discussed, while the proposed distributed coalition formation algorithm is provided in Section 6.4. The different cooperative power allocation criteria are discussed in Section 6.5, while the centralized power allocation and coalition formation optimization problems are formulated in Section 6.6. The stability, convergence and complexity properties of the proposed distributed algorithm are discussed in Section 6.7, while the studied mobility model is presented in Section 6.8. Numerical results are presented in Section 6.9 while the chapter conclusions are drawn in Section 6.10.

6.2 System Model

Consider an ad-hoc wireless network that initially consists of N single-antenna half-duplex decode-and-forward nodes which are denoted $S_1, S_2, \ldots, S_N$ for $N \geq 3$. Each node wishes to exchange its data symbol x_j for $j \in \{1, 2, \ldots, N\}$ with a common destination node D. The

channel between nodes S_j and S_i is given by $h_{j,i} = e^{\jmath\theta_{j,i}}\sqrt{d_{j,i}^{-\nu}}$, with ν being the path-loss exponent and $\theta_{j,i}$ is the signal's phase uniformly distributed in the interval $[0, 2\pi]$ while $d_{j,i}$ is the distance between the two nodes. Also, the channel $h_{j,i}$ between nodes S_j and S_i is assumed to reciprocal (i.e. $h_{j,i} = h_{i,j}$) with perfect channel estimation at each node.

Further, let $\mathcal{S} = \{S_1, S_2, \ldots, S_N\}$ be the finite, non-empty set of all network nodes that eventually self-organize into K (for $1 \leq K \leq N$) mutually exclusive coalitions of cooperative nodes $\mathcal{C} = \{C_1, C_2, \ldots, C_K\}$ with no cooperation between coalitions. In addition, let $C_k \subseteq \mathcal{S}$ denote a coalition with $|C_k|$ nodes (where $|\cdot|$ defines the cardinality of the parameter set) and $1 \leq |C_k| \leq N$. An individual non-cooperative player is called a singleton coalition while the set $\mathcal{S}$ is called the grand coalition when all the N network nodes cooperate. An example of a network of $N = 5$ nodes with a possible coalition formation is illustrated in Fig. 6.1.

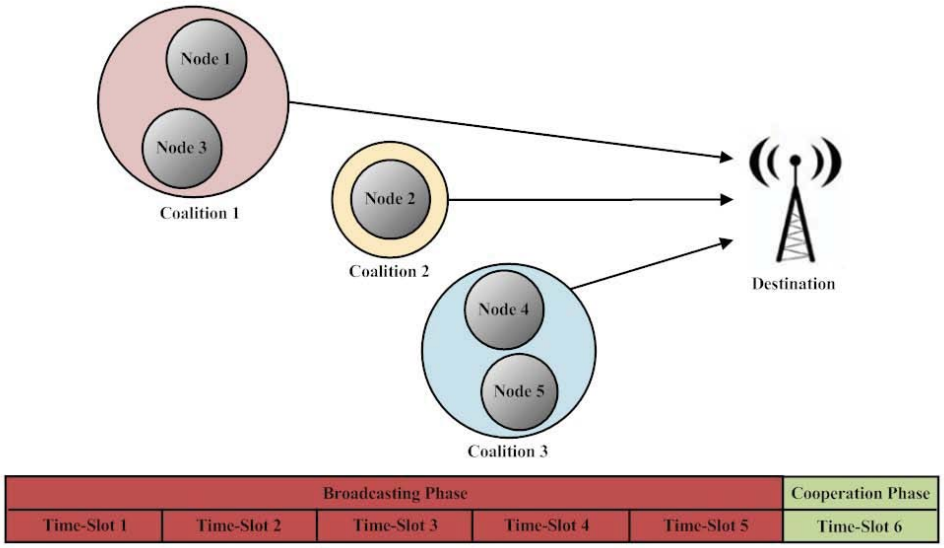

Figure 6.1: Example of Cooperative Coalitions and Their Transmissions

The communication between each node and the destination is performed in a TDMA fashion over $N + 1$ time-slots and is split into two phases, namely the broadcasting phase and the cooperation phase.

6.2.1 Broadcasting Phase

In the broadcasting phase of N time-slots, each node S_j—in its assigned time-slot T_j—broadcasts its data symbol x_j, which is received by the $N - 1$ other nodes S_i in the network for $i \in \{1, 2, \ldots, N\}_{i \neq j}$, as well as the destination. The signal received at node S_i for $i \neq j$ is expressed as

$$y_{j,i} = \sqrt{P_{B_j}} h_{j,i} x_j + n_{j,i}, \tag{6.1}$$

while the received signal at the destination is given by

$$y_{j,d} = \sqrt{P_{B_j}} h_{j,d} x_j + n_{j,d}, \tag{6.2}$$

where P_{B_j} is the transmit power in the broadcasting phase at node S_j, and $n_{j,i}$ and $n_{j,d}$ are zero-mean complex additive white Gaussian noise (AWGN) samples with variance N_0, at node S_i and the destination, respectively. Upon the completion of the broadcasting phase, each node S_i will have received a set of $N-1$ signals $\{y_{j,i}\}_{j=1,j\neq i}^{N}$ comprising symbols $x_1, \ldots, x_{i-1}, x_{i+1}, \ldots, x_N$ from all the other nodes in the network. In addition, the destination will have received N signals $\{y_{j,d}\}_{j=1}^{N}$. Each node S_i then performs a matched filtering operation on each of the received signals $y_{j,i}$ and the signal-to-noise ratio (SNR) at the output of the matched-filter is expressed as [56]

$$\gamma_{j,i}^{BP} = \frac{P_{B_j}|h_{j,i}|^2}{N_0} = \frac{P_{B_j} d_{j,i}^{-\nu}}{N_0}. \tag{6.3}$$

Let f_j denote node S_j's corresponding farthest node in coalition C_k. Thus, each node $S_j \in C_k$ broadcasts its symbol using transmit power P_{B_j} required to maintain a network target SNR of γ between itself and node S_{f_j} as

$$P_{B_j} \geq \gamma N_0 d_{j,f_j}^{\nu}, \tag{6.4}$$

where it is assumed that γ is common to all the nodes in the network. Clearly, there is a tradeoff between the power invested in satisfying the target SNR and power allocated to the other members in coalition C_k. It should be noted that each node has a transmit power constraint of P that is shared between the two transmission phases as given by $P = P_{B_j} + P_{C_j}$, where P_{C_j} is the effective cooperative power at node S_j to relay the symbols of the other nodes in coalition C_k. Specifically, P_{C_j} is given by

$$P_{C_j} = \max\left[0, \min(P - P_{B_j}, P)\right], \tag{6.5}$$

with $P_{C_j} = \sum_{S_i \in C_k, i\neq j} P_{C_{i,j}}$, and $P_{C_{i,j}}$ is the cooperative power node S_j utilizes in relaying node S_i's symbol x_i to the destination, for $i \neq j$.

6.2.2 Cooperation Phase

In the cooperation phase, each node S_i for $S_i \in C_k, \forall C_k \in \mathcal{C}$ and $|C_k| \geq 2$ in time-slot T_{N+1} forms a linearly-coded signal $\mathcal{X}_i(t)$ of the $|C_k|-1$ received signals from the nodes in C_k, during the broadcasting phase[1]. For multiuser detection at the destination, each decoded symbol x_l at node S_i is spread using a signature waveform $c_l(t)$, where it is assumed that each node S_i for $i \neq l$ and the destination know the signature waveforms of all the other nodes in the coalition. The cross-correlation of $c_l(t)$ and $c_i(t)$ is $\rho_{l,i} = \langle c_l(t), c_i(t)\rangle \triangleq (1/T_s)\int_0^{T_s} c_l(t)c_i^*(t)dt$ for $l \neq i$ with $\rho_{i,i} = 1$ and T_s being the symbol duration. Therefore, the transmitted signal by node S_i is expressed as

[1]Coalition formation is discussed in later sections.

$$\mathcal{X}_i(t) = \sum_{S_l \in C_k, l \neq i} \sqrt{P_{C_{l,i}}} x_l c_l(t) \tag{6.6}$$

The received signal at the destination—assuming perfect timing synchronization—is written as

$$\mathcal{Y}_d(t) = \sum_{i=1}^{N} h_{i,d} \mathcal{X}_i(t) + n_d(t), \tag{6.7}$$

where $n_d(t)$ is the AWGN process at the destination. By substituting (6.6) into (6.7), $\mathcal{Y}_d(t)$ is re-written as

$$\mathcal{Y}_d(t) = \sum_{k=1}^{K} \sum_{S_l \in C_k} \left(\sum_{S_i \in C_k, i \neq l} \sqrt{P_{C_{l,i}}} h_{i,d} \right) x_l c_l(t) + n_d(t). \tag{6.8}$$

At the destination, multiuser detection is performed on $\mathcal{Y}_d(t)$ to extract symbol x_j of node $S_j \in C_k, \forall C_k \in \mathcal{C}$. Specifically, $\mathcal{Y}_d(t)$ is passed through a matched filter bank (MFB), yielding

$$\mathcal{Y}_{j,d} = \langle \mathcal{Y}_d(t), c_j(t) \rangle = \sum_{k=1}^{K} \sum_{S_l \in C_k} \alpha_l x_l \rho_{l,j} + \bar{n}_{j,d}, \tag{6.9}$$

where $\bar{n}_{j,d}$ is a zero-mean AWGN noise sample with variance N_0, while α_l is given by

$$\alpha_l = \sum_{S_i \in C_k, i \neq l} \sqrt{P_{C_{l,i}}} h_{i,d}. \tag{6.10}$$

The output of the MFB is expressed in vector form of N signals as $\boldsymbol{Y}_d = \boldsymbol{RAx} + \bar{\boldsymbol{n}}_d$, where $\boldsymbol{Y}_d = [\mathcal{Y}_{1,d}, \ldots, \mathcal{Y}_{N,d}]^T$, $\boldsymbol{x} = [x_1, \ldots, x_N]^T$, and $\bar{\boldsymbol{n}}_d = [\bar{n}_{1,d}, \ldots, \bar{n}_{N,d}]^T \sim \mathcal{CN}(0, N_0 \boldsymbol{R})$. Furthermore, $\boldsymbol{R}$ and $\boldsymbol{A}$ are $N \times N$ matrices, as given by

$$\boldsymbol{R} = \begin{bmatrix} 1 & \rho_{1,2} & \cdots & \rho_{1,N} \\ \rho_{2,1} & 1 & \cdots & \rho_{2,N} \\ \vdots & \vdots & \ddots & \vdots \\ \rho_{N,1} & \rho_{N,2} & \cdots & 1 \end{bmatrix}, \tag{6.11}$$

and

$$\boldsymbol{A} = \begin{bmatrix} \alpha_1 & 0 & \cdots & 0 \\ 0 & \alpha_2 & \cdots & 0 \\ \vdots & \vdots & \ddots & \vdots \\ 0 & 0 & \cdots & \alpha_N \end{bmatrix}, \tag{6.12}$$

respectively. The received signal vector $\boldsymbol{Y}_d$ is then decorrelated (assuming matrix $\boldsymbol{R}$ is nonsingular) as $\tilde{\boldsymbol{Y}}_d = \boldsymbol{R}^{-1}\boldsymbol{Y}_d = \boldsymbol{Ax} + \tilde{\boldsymbol{n}}_d$, where $\tilde{\boldsymbol{n}}_d = \boldsymbol{R}^{-1}\bar{\boldsymbol{n}}_d$ and $\tilde{\boldsymbol{n}}_d \sim \mathcal{CN}(\boldsymbol{0}, N_0 \boldsymbol{R}^{-1})$. It is assumed that $\rho_{l,j} = \rho, \forall l \neq j$. Therefore, the decorrelated received signal is obtained as

$$\tilde{\mathcal{Y}}_{j,d} = \alpha_j x_j + \tilde{n}_{j,d}, \tag{6.13}$$

where $\tilde{n}_{j,d} \sim \mathcal{CN}(0, N_0\varrho_N)$, and ϱ_N is given by

$$\varrho_N = \frac{1 + (N-2)\,\rho}{1 + (N-2)\,\rho - (N-1)\,\rho^2}. \tag{6.14}$$

The received instantaneous SNR of node S_j's symbol (where $S_j \in C_k$) at the destination is given by $\gamma_j = \gamma_j^{BP} + \gamma_j^{CP}$, where γ_j^{BP} is expressed in (6.3), and γ_j^{CP} is obtained by passing $\tilde{\mathcal{Y}}_{j,d}$ through a matched-filter. Therefore, γ_j is obtained as [152]

$$\gamma_j = \frac{P_{B_j}|h_{j,d}|^2}{N_0} + \sum_{S_i \in C_k, i \neq j} \frac{P_{C_{j,i}}|h_{i,d}|^2}{N_0\varrho_N}. \tag{6.15}$$

Upon the completion of the broadcasting and cooperation phases, the destination will have received $|C_k|$ independent copies of symbol x_j of node $S_j \in C_k$ and thus achieving a diversity order of $|C_k|$ [56].

6.3 Coalition Formation Framework

In this section, the coalition formation framework and its properties relevant to the proposed system model are characterized and discussed.

Let $\upsilon_j(C_k)$ denote the payoff of each node S_j in coalition C_k. Based on the discussed system model, a singleton coalition of node S_j occurs when it does not form a cooperative coalition with other nodes. In this case, node S_j utilizes all its available power P and transmits its data once every $N+1$ time-slots. Thus, the payoff of node S_j is obtained as

$$\upsilon_j(\{S_j\}) = R_{j,d}^D = \frac{1}{N+1}\log_2\left(1 + \frac{P|h_{j,d}|^2}{N_0}\right), \tag{6.16}$$

where $R_{j,d}^D$ is the achievable rate with direct transmission. Additionally, $R_{j,d}^D$ represents the non-cooperative payoff of any node S_j for $S_j \in \mathcal{S}$. On the other hand, for coalition C_k with $|C_k| \geq 2$, the achievable rate of node S_j due to the cooperative transmission is given by

$$R_{j,d}^C = \frac{1}{N+1}\log_2\left(1 + \frac{P_{B_j}|h_{j,d}|^2}{N_0} + \sum_{S_i \in C_k, i \neq j} \frac{P_{C_{j,i}}|h_{i,d}|^2}{N_0\varrho_N}\right). \tag{6.17}$$

Therefore, the payoff of each node S_j in coalition C_k is given by $\upsilon_j(C_k) = R_{j,d}^C, \forall S_j \in C_k$. Consequently, the value of a coalition is

$$\upsilon(C_k) = \sum_{S_j \in C_k} \upsilon_j(C_k), \tag{6.18}$$

which is equivalent to the sum-rate of the coalition.

Definition 6.1: A coalition game is said to have a non-transferable utility (NTU) if the coalition value cannot be arbitrarily apportioned among its nodes and each node will have its own value within a coalition.

Based on the proposed system model, the coalition game in hand has a non-transferable utility, as a specific achievable rate value for each node in a coalition is achieved [51]. In addition, the coalition game formulated in this work is in the characteristic function form. That is, utilities achieves by the players in a coalition are unaffected by those outside it.

Definition 6.2: A coalitional game with non-transferable utility is defined by a pair $(\mathcal{S}, \mathcal{V})$, where $\mathcal{S}$ is a finite set of N players, and $\mathcal{V}$ is a set valued function such that for every coalition $C_k \subseteq \mathcal{S}$, $\mathcal{V}(C_k)$ is a closed convex subset of $\mathbb{R}^{|C_k|}$ that contains the payoff vectors the players in C_k can achieve.

In the proposed system model, $\mathcal{V} : C_k \rightarrow \mathbb{R}^{|C_k|}$ such that $\mathcal{V}(\phi) = \phi$, and if $C_k \neq \phi$, then $\mathcal{V}(C_k)$ is non-empty and closed. Moreover, the coalitional set-valued function $\mathcal{V}$ of a coalition $C_k \subseteq \mathcal{S}$ is defined as

$$\mathcal{V}(C_k) = \Big\{ \boldsymbol{v}(C_k) \in \mathbb{R}^{|C_k|} \mid \forall S_j \in C_k, \upsilon_j(C_k) = R^C_{j,d} \geq 0, \text{ if } P_{C_j} > 0, \text{ and } \upsilon_j(C_k) = -R^D_{j,d}, \text{ otherwise.} \Big\}. \tag{6.19}$$

Note that if $P_{C_j} = 0$, then node S_j has no interest in cooperation.

Remark 6.1: The proposed network-coded transmission model is a coalitional game $(\mathcal{S}, \mathcal{V})$ in partition form with non-transferable utility, where $\mathcal{V}(C_k)$ is a singleton set, as defined by (6.19), and is thus a closed and convex subset of $\mathbb{R}^{|C_k|}$.

Remark 6.2: In the proposed NTU coalitional game $(\mathcal{S}, \mathcal{V})$, the grand coalition of all the nodes rarely forms due to the target SNR power costs.

Based on the SNR target defined in (6.4), the power cost for coalition formation depends on the distance between the network nodes which in turn governs coalitions' sizes. As the size of a coalition increases, the cooperative gain and power cost per node also increase (i.e. cooperation gains in a coalition are limited by power costs). However, the power saving due to the diversity gains gradually diminish even with the increase in the number of cooperative nodes in a coalition, at which point, no additional nodes should join the coalition. This prevents cooperative networks from forming a grand coalition and instead form independent disjoint coalitions. In turn, the proposed game is modeled as a coalition formation game, with the aim of finding the network's coalitional structure [51].

It should be noted that solution concepts for coalitional games based on the core are not applicable to the game model in hand due to the power costs of information exchange.

6.4 Design of Distributed Coalition Formation Algorithm

In this section, the aim is to study how coalitions can be formed in a distributed manner. Specifically, a coalition is formed if it is beneficial to at least one node in the coalition and also for the coalition as a whole. Also, the nodes of a coalition can avoid merging with other

coalitions if they are as well off as a result of not merging. Furthermore, when nodes form a coalition, they cannot unilaterally deviate on their own. In turn, coalition structure changes are determined by the members of a coalition interacting with one another as a unit.

Since network nodes are rational and autonomous, the design of an iterative distributed algorithm to form a network coalition structure that improves that network sum-rate is highly desirable. But first, several concepts must be defined.

Definition 6.3: A collection of coalitions, denoted as $\mathcal{C}$, is defined as $\mathcal{C} = \{C_1, C_2, \ldots, C_K\}$ for $2 \leq K \leq N$ mutually disjoint coalitions C_k of $\mathcal{C}$. Equivalently, a collection is any arbitrary group of disjoint coalitions C_k of $\mathcal{C}$ that does not necessarily span all the players of $\mathcal{S}$. If a collection spans all the players in $\mathcal{S}$ (i.e. $\bigcup_{k=1}^{K} C_k = \mathcal{S}$), the collection is a partition of $\mathcal{S}$.

Definition 6.4: A preference operator $\triangleright$ is defined for comparing two collections $\mathcal{Q} = \{Q_1, \ldots, Q_l\}$, and $\mathcal{R} = \{R_1, \ldots, R_p\}$ that are partitions of the same subset $\mathcal{A} \subseteq \mathcal{S}$ (i.e. same players in $\mathcal{Q}$ and $\mathcal{R}$). Thus, $\mathcal{Q} \triangleright \mathcal{R}$ implies that the way $\mathcal{Q}$ partitions $\mathcal{A}$ is preferred to the way $\mathcal{R}$ partitions $\mathcal{A}$.

In the coalitional game theory literature, comparison relations based on orders are split into two categories [153]: individual value orders and coalition value orders. In the former category, comparison is performed on the basis of individual payoffs (e.g. Pareto order). In the latter category, two collections (or partitions) are compared based on the value of the coalitions inside these collections, such as the utilitarian order (e.g. $\mathcal{Q} \triangleright \mathcal{R} \Longrightarrow \sum_{i=1}^{l} \upsilon(Q_i) > \sum_{i=1}^{p} \upsilon(R_i)$). In this work, the utilitarian order comparison relation is assumed as it is more suited to the studied altruistic coalition formation.

There are two successive rules for forming and breaking coalitions, known as merge-and-split rules [153].

Definition 6.5 (Merge Rule): Merge any collection of disjoint coalitions $\{Q_1, \ldots, Q_l\}$, where $\{\bigcup_{k=1}^{l} Q_k\} \triangleright \{Q_1, \ldots, Q_l\}$, thus $\{Q_1, \ldots, Q_l\} \rightarrow \{\bigcup_{k=1}^{l} Q_k\}$.

Definition 6.6 (Split Rule): Split any coalition $\{\bigcup_{k=1}^{l} Q_k\}$, where $\{Q_1, \ldots, Q_l\} \triangleright \{\bigcup_{k=1}^{l} Q_k\}$, thus $\{\bigcup_{k=1}^{l} Q_k\} \rightarrow \{Q_1, \ldots, Q_l\}$.

The merge-and-split rules simply mean that two coalitions will merge if their merger would do more good than harm to the overall coalition value (or equivalently, sum-rate) of the merged coalition. Otherwise, coalitions will split into smaller ones or even singletons.

6.4.1 Algorithm Description

The network operation starts at time-index initialized to $\tau = 0$ with network nodes being partitioned into singleton coalitions (i.e. $C_j = \{S_j\}$ for $1 \leq j \leq N$ such that $\mathcal{C} = \{S_1, S_2, \ldots, S_N\}$) and each node S_j determines its achievable direct transmission rate $R_{j,d}^{D}$. After that, the following three phases take place.

Node Discovery

Each node $S_j \in \mathcal{S}$ discovers the neighboring potential nodes with which it can possibly merge. Specifically, for each node S_j, the potential partners lie within a circle with radius determined by the power $P \geq P_{B_j} \geq \gamma N_0 d_{j,f_j}^{\nu}$ required for symbols' exchange while meeting the target SNR γ, as given by (6.4). Thus, if the received signal at node S_i satisfies γ, it is considered to be decoded correctly. Let $\mathcal{D}_j$ be the set of network nodes that decoded node S_j's symbol correctly, i.e.

$$\mathcal{D}_j = \{\forall S_i \in \mathcal{S} \text{ and } i \neq j : \gamma_{j,i}^{BP} \geq \gamma\}. \tag{6.20}$$

After that, node S_j broadcasts a request-to-send (RTS) message which is received by all the nodes in $\mathcal{D}_j$. Then, each node $S_i \in \mathcal{D}_j$ replies to node S_j with a clear-to-send (CTS) message that contains its CSI with the destination. If the decoding set of node S_j is empty (i.e. $\mathcal{D}_j = \phi$), then it employs direct transmission and does not form a coalition with any other node. Otherwise, node S_j enumerates all the possible distinct coalitions of $S_j \cup \mathcal{D}_j$. In the case of a coalition C_k, the potential nodes lie within the intersection of $|C_k|$ circles, each centered around node $S_j \in C_k$. Clearly, the node discovery phase significantly reduces the coalition formation space.

Adaptive Coalition Formation

In this phase, the time-index is updated to $\tau = \tau + 1$ and each node sequentially proposes to merge with one of its potential partners. If such a merge is desirable by all the nodes according to the utilitarian order, then a coalition with one or more of the potential nodes could form by a merge agreement of all the participating nodes. For all merged coalitions, a random node is elected as a coalition-head [115], which is responsible for periodically exchanging timing information with the rest of the coalition[2]. After that, the power allocation fractions of each node are determined according to one of the power allocation criteria discussed in Section 6.5. After all the nodes have made their merge decisions, the merge process ends, resulting in a partition $\mathcal{M}^{\tau} = \mathbf{Merge}(\mathcal{C}^{\tau-1})$.

If the sum-rate value of a group of nodes achieved by forming a coalition is less than the value achieved before the merger, they split into singletons or coalitions of smaller sizes. At the end of the split process, a partition $\mathcal{C}^{\tau} = \mathbf{Split}(\mathcal{M}^{\tau})$ is obtained. A sequence of merge-and-split processes along with time-index updates take place in a distributed manner via appropriate control channels, depending on the achievable rate improvement of each node and coalition, until there is no need for any merging/splitting in the current partition, in which case the final partition $\mathcal{C}^{*} = \mathcal{C}^{\tau}$ is obtained.

[2]The nodes' transmission within a coalition can be assumed to be perfectly synchronized during the cooperation phase [140][141]. In practice, the distributed timing synchronization between each coalition and the destination may be imperfect; however, this case is beyond the scope of this work.

Data Transmission

In this final phase, data transmission of each node takes place in the form of broadcasting and cooperation, over a total of $N + 1$ time-slots and as described in Section 6.2. Finally, the above three phases repeat in response to topology changes or mobility, as discussed later. The network initialization and proposed distributed merge-and-split coalition formation algorithm are summarized in Table 6.1.

Table 6.1: Network Initialization and Proposed Distributed Merge-and-Split Coalition Formation Algorithm

Initial State:
At the beginning of all time, initialize time-index at $\tau = 0$ with the network being partitioned as $\mathcal{C}^0 = \{S_1, S_2, \ldots, S_N\}$.
Coalition Formation Algorithm:
Phase 1 - Node Discovery:
Each node determines its neighboring nodes and potential coalitions.
Phase 2 - Adaptive Coalition Formation:
Coalition formation using merge-and-split rules occurs.
repeat
(a) Update time-index: $\tau = \tau + 1$.
(b) $\mathcal{M}^\tau = \textbf{Merge}(\mathcal{C}^{\tau-1})$: coalitions in $\mathcal{C}^{\tau-1}$ make merge decisions based on the merge rule.
(c) $\mathcal{C}^\tau = \textbf{Split}(\mathcal{M}^\tau)$: coalitions in $\mathcal{M}^\tau$ make split decisions based on the split rule.
until merge-and-split terminates with final partition denoted $\mathcal{C}^*$.
Phase 3 - Data Transmission:
Each node transmits its data symbol in the broadcasting phase and the nodes within every coalition relay data for each other during the cooperation phase.

It should be noted that the resulting partition from the proposed merge-and-split algorithm is not guaranteed to be optimal (i.e. is not the one that maximizes the network sum-rate). This is because the formed coalitions do not exchange information about their values and thus have no way of knowing whether there are different partitions that could lead to better network sum-rate. Even if all coalition values are known, no known algorithm can determine the optimal partition with time complexity that is polynomial in the number of possible coalitions [154].

6.5 Impact of Different Power Allocation Criteria

It is intuitive to note that network coalition formation is dependent on the cooperative power allocation within each coalition. Therefore, the following power allocation criteria are studied.

6.5.1 Equal Power Allocation (EPA)

Under this criterion, a node $S_i \in C_k$ determines its maximum required broadcasting power as $P_{B_i} = \max\{\gamma N_0/|h_{j,i}|^2\}_{S_j \in C_k, j \neq i}$ and then the cooperative power $P_{C_i} = P - P_{B_i}$ is equally allocated to the other nodes in C_k in the form of

$$\text{(EPA)}: \quad P_{C_{j,i}} = \frac{P - P_{B_i}}{|C_k| - 1}, \quad \forall S_j \in C_k, \text{ and } j \neq i. \tag{6.21}$$

In this case, each node naively allocates its remaining power equally to the other nodes in the coalition.

6.5.2 Sum-of-Rates Maximizing Power Allocation (SRM-PA)

The sum-of-rates maximizing power allocation problem of coalition C_k is solved by the coalition-head and is expressed as

$$\begin{aligned}
\text{(SRM-PA):} \quad \max \quad & \textstyle\sum_{S_i \in C_k} R_{i,d}^C \\
\text{s.t.} \quad & P_{B_i} + \sum_{S_j \in C_k, j \neq i} P_{C_{j,i}} \leq P, && \forall S_i \in C_k, && \text{(6.22a)} \\
& P_{B_i} \geq \gamma N_0/|h_{j,i}|^2, && \forall S_j, S_i \in C_k \text{ and } j \neq i, && \text{(6.22b)} \\
& P_{B_i} \geq 0, && \forall S_i \in C_k, && \text{(6.22c)} \\
& P_{C_{j,i}} \geq 0, && \forall S_j, S_i \in C_k \text{ and } j \neq i. && \text{(6.22d)}
\end{aligned}$$

The first constraint in (6.22) enforces the total power constraint, while the second constraint ensures that the target SNR is met by each node $S_i \in C_k$. The last two constraints impose the non-negativity of the allocated broadcasting and cooperative powers, respectively.

6.5.3 Max-Min Rate Power Allocation (MMR-PA)

The power allocation problem under the max-min rate fairness criterion for coalition C_k solved by the coalition-head is expressed as

$$\begin{aligned}
\max \quad & \min_{S_j \in C_k, i \neq j} \; R_{j,d}^C, \\
\text{s.t.} \quad & P_{B_i} + \sum_{S_j \in C_k, j \neq i} P_{C_{j,i}} \leq P, && \forall S_i \in C_k, && \text{(6.23a)} \\
& P_{B_i} \geq \gamma N_0/|h_{j,i}|^2, && \forall S_j, S_i \in C_k \text{ and } j \neq i, && \text{(6.23b)} \\
& P_{B_i} \geq 0, && \forall S_i \in C_k, && \text{(6.23c)} \\
& P_{C_{j,i}} \geq 0, && \forall S_j, S_i \in C_k \text{ and } j \neq i. && \text{(6.23d)}
\end{aligned}$$

Problem (6.23) is equivalently re-expressed in standard form as

$$\text{(MMR-PA):} \quad \max \quad \eta$$

$$\begin{aligned}
\text{s.t.} \quad & \eta - R_{i,d}^{C} \leq 0, && \forall S_i \in C_k, && \text{(6.24a)}\\
& P_{B_i} + \sum_{S_j \in C_k, j \neq i} P_{C_{j,i}} \leq P, && \forall S_i \in C_k, && \text{(6.24b)}\\
& P_{B_i} \geq \gamma N_0 / |h_{j,i}|^2, && \forall S_j, S_i \in C_k \text{ and } j \neq i, && \text{(6.24c)}\\
& P_{B_i} \geq 0, && \forall S_i \in C_k, && \text{(6.24d)}\\
& P_{C_{j,i}} \geq 0, && \forall S_j, S_i \in C_k \text{ and } j \neq i. && \text{(6.24e)}
\end{aligned}$$

The first constraint imposes max-min rates while the rest of the constraints are as in problem (6.22). Problems SRM-PA and MMR-PA can be verified to be convex [85] and thus can be solved efficiently by any standard convex optimization algorithm [94]. Therefore, solving such problems at a coalition-head should pose no severe computational overhead.

Remark 6.3: Since the achievable rate of each node in a coalition C_k is strictly monotonically increasing in the allocated power, the total power constraint is always met (i.e. $P_{B_i} + \sum_{S_j \in C_k, j \neq i} P_{C_{j,i}} = P, \forall S_i \in C_k$ and $\forall C_k \in \mathcal{C}$).

6.6 Centralized Power Allocation and Coalition Formation

In this section, the centralized power allocation and coalition formation under the sum-of-rates maximizing and max-min rate power allocation criteria are formulated as mixed-integer nonlinear programming (MINLP) problems. First, let $\mathcal{I}_{j,i}$ be a binary variable defined as

$$\mathcal{I}_{j,i} = \begin{cases} 1 & \text{if nodes } S_j \text{ and } S_i \text{ cooperate,} \\ 0 & \text{otherwise} \end{cases}. \qquad \text{(6.25)}$$

6.6.1 Sum-of-Rates Maximizing Power Allocation

The centralized sum-of-rates maximizing power allocation (C-SRM-PA) with coalition formation is formulated as

$$\text{(C-SRM-PA):} \quad \max \quad \frac{1}{|\mathcal{S}|+1} \sum_{S_j \in \mathcal{S}} \log_2 \left(1 + \frac{P_{B_j}|h_{j,d}|^2}{N_0} + \sum_{S_i \in \mathcal{S}, i \neq j} \mathcal{I}_{j,i} \frac{P_{C_{j,i}}|h_{i,d}|^2}{N_0 \varrho_N}\right)$$

$$\begin{aligned}
\text{s.t.} \quad & P_{B_i} + \sum_{S_j \in \mathcal{S}, j \neq i} \mathcal{I}_{j,i} P_{C_{j,i}} \leq P, && \forall S_i \in \mathcal{S}, && \text{(6.26a)}\\
& P_{B_i} \geq \gamma N_0 \mathcal{I}_{j,i} / |h_{j,i}|^2, && \forall S_i, S_j \in \mathcal{S} \text{ and } i \neq j, && \text{(6.26b)}\\
& \mathcal{I}_{j,i} - \mathcal{I}_{j,k}\mathcal{I}_{k,i} \geq 0, && \forall S_i, S_j, S_k \in \mathcal{S} \text{ and } i \neq j \neq k, && \text{(6.26c)}\\
& P_{B_i} \geq 0, && \forall S_i \in \mathcal{S}, && \text{(6.26d)}
\end{aligned}$$

$$P_{C_{j,i}} \geq 0, \qquad \forall S_i, S_j \in \mathcal{S} \text{ and } i \neq j, \tag{6.26e}$$

$$\mathcal{I}_{j,i} \in \{0,1\}, \qquad \forall S_i, S_j \in \mathcal{S} \text{ and } i \neq j. \tag{6.26f}$$

As before, the first and second constraints impose the total power and target SNR γ constraints are satisfied for the nodes forming coalitions, respectively. The third constraint ensures that if a node joins a coalition, then it must cooperate with all its members. The last three constraints define the range of values each decision variable can take.

6.6.2 Max-Min Rate Power Allocation

The centralized max-min rate power allocation (C-MMR-PA) with coalition formation is formulated as

$$\text{(C-MMR-PA):} \quad \max \quad \eta$$

$$\text{s.t.} \quad \eta - \frac{1}{|\mathcal{S}|+1}\log_2\left(1+\frac{P_{B_j}|h_{j,d}|^2}{N_0}+\sum_{S_i\in\mathcal{S},i\neq j}^{N}\mathcal{I}_{j,i}\frac{P_{C_{j,i}}|h_{i,d}|^2}{N_0\varrho_N}\right)\leq 0, \quad \forall S_j \in \mathcal{S}, \tag{6.27a}$$

$$P_{B_i}+\sum_{S_j\in\mathcal{S},j\neq i}\mathcal{I}_{j,i}P_{C_{j,i}} \leq P, \qquad \forall S_i \in \mathcal{S}, \tag{6.27b}$$

$$P_{B_i} \geq \gamma N_0 \mathcal{I}_{j,i}/|h_{j,i}|^2, \qquad \forall S_i, S_j \in \mathcal{S} \text{ and } i \neq j, \tag{6.27c}$$

$$\mathcal{I}_{j,i} - \mathcal{I}_{j,k}\mathcal{I}_{k,i} \geq 0, \qquad \forall S_i, S_j, S_k \in \mathcal{S} \text{ and } i \neq j \neq k, \tag{6.27d}$$

$$P_{B_i} \geq 0, \qquad \forall S_i \in \mathcal{S}, \tag{6.27e}$$

$$P_{C_{j,i}} \geq 0, \qquad \forall S_i, S_j \in \mathcal{S} \text{ and } i \neq j, \tag{6.27f}$$

$$\mathcal{I}_{j,i} \in \{0,1\}, \qquad \forall S_i, S_j \in \mathcal{S} \text{ and } i \neq j. \tag{6.27g}$$

It should be noted that ignoring the coalition formation constraints under the C-SRM-PA and C-MMR-PA optimization problems (see (6.26c) and (6.27d)) results in power allocation without any coalitional structure. In other words, if node S_i cooperates with nodes S_j and S_k, then nodes S_j and S_k do not necessarily have to cooperate. In this case, nodes S_i, S_j and S_k do not form a coalition[3].

The formulated MINLP centralized optimization problems are in general NP-hard [155][156]. This is because finding an optimal partition of a set $\mathcal{S}$ requires iterating over all possible partitions, which grows exponentially with the number of nodes in $\mathcal{S}$, as given by the well-known Bell number [55]. For instance, for a network of $N = 10$ nodes, there are 115975 potential partitions. The number of continuous and binary variables for the C-SRM-PA problem can be verified to be N^2 and $\binom{N}{2}$, respectively. With respect to the C-MMR-PA problem, an additional continuous variable is required for η along with N max-min rate constraints. Moreover, N and $N(N-1)$ constraints are required to enforce the total power and target SNR constraints, respectively. The number of coalition formation constraints F_N

[3]It is noteworthy that in this work, forming a coalition is defined such that the users within the coalition are closed to cooperation from users outside the coalition.

can be determined for $N \geq 4$ as $F_N = N \cdot B_N$, where $B_N = (N-2+B_{N-1})$ and $B_3 = 1$. For instance, for a network of $N = 10$ nodes, the C-SRM-PA problem with coalition formation requires 145 variables and 460 constraints. Thus, the formulated centralized optimization problems can only be solved for very small-sized networks. However, for large-sized networks, the computational complexity becomes prohibitively high and is deemed impractical. The total number of variables and constraints required for the centralized power allocation is summarized in Table 6.2, where it can be seen that C-MMR-PA problem requires more constraints than its counterpart C-SRM-PA problem and is thus more difficult to solve.

Table 6.2: Summary of the Number of Variables and Constraints for Centralized Power Allocation

Power Allocation Criteria		Number of Variables		Number of Constraints			
		Continuous	Binary	Max-Min	Total Power	Target SNR	Coalitions
C-SRM-PA	With Coalition Formation	N^2	$\binom{N}{2}$	—	N	$N(N-1)$	F_N
	Without Coalition Formation	N^2	$\binom{N}{2}$	—	N	$N(N-1)$	—
C-MMR-PA	With Coalition Formation	N^2+1	$\binom{N}{2}$	N	N	$N(N-1)$	F_N
	Without Coalition Formation	N^2+1	$\binom{N}{2}$	N	N	$N(N-1)$	—

6.7 Partition Stability, Convergence and Complexity

In this section, the partition stability, convergence and complexity properties of the proposed algorithm are studied.

6.7.1 Partition Stability

Stable coalition structures in coalition formation games correspond to the equilibrium state in which users do not have incentives to leave the already formed coalitions.

Definition 6.7 ($\mathcal{C}$-Homogeneity): Given a partition $\mathcal{C} = \{C_1, C_2, \ldots, C_K\}$, a partition $\bar{\mathcal{C}} = \{\bar{C}_1, \bar{C}_2, \ldots, \bar{C}_L\}$ is called $\mathcal{C}-$homogenous if for each $j \in \{1, \ldots, L\}$, some $i \in \{1, \ldots, K\}$ exists such that either $\bar{C}_j \subseteq C_i$ or $C_i \subseteq \bar{C}_j$ [157].

Based on Definition 6.7, any $\mathcal{C}-$homogenous partition arises from $\mathcal{C}$ by allowing each coalition either to split into smaller coalitions or to merge with other coalitions.

Definition 6.8 ($\mathcal{C}$-Compatibility): A coalition C of $\mathcal{S}$ is called $\mathcal{C}$-compatible if for some $i \in \{1, \ldots, K\}$, $C \subseteq C_i$, and $\mathcal{C}$-incompatible, otherwise [157].

Definition 6.9 (Defection Function $\mathbb{D}$): A defection function $\mathbb{D}$ associates with each partition $\mathcal{C}$ of $\mathcal{S}$ a set of collections in $\mathcal{S}$ [157].

Based on Definition 6.9, a partition $\mathcal{C}$ is $\mathbb{D}$-stable if no group of players is interested in leaving $\mathcal{C}$ when the players who wish to leave can only form collections allowed by the

defection function $\mathbb{D}(\mathcal{C})$. Specifically, $\mathbb{D}(\mathcal{C})$ consists of all the collections $\mathcal{Q} = \{Q_1, \ldots, Q_l\}$ whose players can leave partition $\mathcal{C}$ by forming a new group of players $\cup_{k=1}^{l} Q_k$ divided according to collection $\mathcal{Q}$.

Definition 6.10 ($\mathbb{D}_{hp}(\mathcal{C})$ Function): For each partition $\mathcal{C}$, $\mathbb{D}_{hp}(\mathcal{C})$, is the family of all $\mathcal{C}-$homogenous partitions in $\mathcal{S}$ [157]. Moreover, $\mathbb{D}_{hp}(\mathcal{C})$ allows the players to leave the partition $\mathcal{C}$ only by means of possibly multiple merges or splittings.

According to Definition 6.10, $\mathbb{D}_{hp}(\mathcal{C})$ associates with each partition $\mathcal{C}$ of $\mathcal{S}$ the group of all partitions of $\mathcal{S}$ that the players can form through merge-and-split processes applied to $\mathcal{C}$.

Theorem 6.1 ($\mathbb{D}_{hp}$-Stability): A partition is $\mathbb{D}_{hp}$-stable if and only if it is the outcome of iterating the merge-and-split rules [157].

Based on Theorem 6.1, to find a $\mathbb{D}_{hp}$-stable partition, it suffices to iterate the merge-and-split rules starting from any initial network partition until partition $\mathcal{C}^*$ is reached.

Proposition 6.1: The resulting final partition $\mathcal{C}^*$ of the proposed coalition formation algorithm is $\mathbb{D}_{hp}$-stable.

Proof: This is an immediate result of the fact that no players have an incentive to leave partition $\mathcal{C}^*$ through merge-and-split to form other partition in $\mathcal{S}$. □

Definition 6.11 ($\mathbb{D}_c(\mathcal{C})$ Function): For each partition $\mathcal{C}$, $\mathbb{D}_c(\mathcal{C})$ is the family of all collections of $\mathcal{S}$. In turn, such a defection function allows any group of players to leave $\mathcal{C}$ and create an arbitrary collection in $\mathcal{S}$ [157].

Theorem 6.2 ($\mathbb{D}_c$-Stability): A partition $\mathcal{C} = \{C_1, \ldots, C_K\}$ of $\mathcal{S}$ is $\mathbb{D}_c$-stable if and only if [157]:

- for each $i \in \{1, \ldots, K\}$ and each pair of disjoint coalitions C_1 and C_2 such that $C_1 \cup C_2 \subseteq C_i$ and $\upsilon(C_1 \cup C_2) \geq \upsilon(C_1) + \upsilon(C_2)$,
- for each $\mathcal{C}$-incompatible coalition $C \subseteq \mathcal{S}$, $\sum_{i=1}^{K} \upsilon(C_i \cap C) \geq \upsilon(C)$.

Proposition 6.2: The proposed coalition formation algorithm converges to the $\mathbb{D}_c$-stable partition, if such a partition exists. Otherwise, the proposed merge-and-split algorithm results in a final $\mathbb{D}_{hp}$-stable network partition.

Proof: This is an immediate consequence of the fact that the first and second conditions of $\mathbb{D}_c$-stability are dependent on the location and power allocation of the network nodes through the utilitarian order. □

Remark 6.4: If no partition of $\mathcal{S}$ can satisfy the $\mathbb{D}_c$-stability conditions, then no $\mathbb{D}_c$-stable partitions of $\mathcal{S}$ exist. Otherwise, the proposed algorithm is guaranteed to converge to the optimal $\mathbb{D}_c$-stable partition that maximizes the social welfare (i.e. maximizes the network sum-rate).

6.7.2 Convergence

Merge-and-split rules are proposed to form cooperative groups and proved to converge to a unique solution with arbitrary merge-and-split iterations.

Proposition 6.3: Each iteration of the merge-and-split rules terminates [157].

Proposition 6.3 is an immediate result of the fact that each iteration of the merge-and-split rules improves the social welfare (or equivalently the network sum-rate). In turn, it guarantees that the proposed algorithm can converge.

Theorem 6.3: The coalition formation process based on the merge-and-split rules converges to a stable partition $\mathcal{C}^*$ [153].

Proof: Theorem 6.3 can be proved by contradiction. Assume that the resulting coalition partition is not the equilibrium one and the final coalition partition is not formed yet. Then, at least two coalitions that could merge to improve their value functions. Therefore, the coalition formation process must iterate through the merge-and-split rules at least one more time. This process repeats until no two coalitions desire to merge, in which case the final partition $\mathcal{C}^*$ is reached. □

6.7.3 Complexity Analysis

Communication Complexity

The communication complexity of the proposed algorithm is related to the number of merge-and-split operations, which is directly related to the total number of coalition formation proposals $\mathcal{P}$ sent by each of the N nodes. Two extreme cases are considered: (1) if all the proposals are rejected, and (2) if all the proposals are accepted. In the first case and as described in Section 6.4.1, each node $S_i \in \mathcal{S}$ submits at most $|\mathcal{D}_i|$ proposals, where $|\mathcal{D}_i| \leq N-1$. Now, if the first node submits $N-1$ proposals and the second submits $N-2$ proposals and so on, then the total number of proposals is $\mathcal{P}_{\text{worst}} = \sum_{i=1}^{N-1} i = \frac{1}{2}N(N-1)$. Thus, in the worst case, the complexity is of the order $\mathcal{O}(N^2)$. In the second case where all the proposals are accepted, the total number of proposals is only $\mathcal{P}_{\text{best}} = N$, and a complexity order of $\mathcal{O}(N)$. In practice, the number of proposals is between these two extreme cases (i.e. $\mathcal{P}_{\text{best}} \leq \mathcal{P} \leq \mathcal{P}_{\text{worst}}$). In fact, the number of proposals is much lower than $\frac{1}{2}N(N-1)$ as the proposed algorithm tends to merge the smaller coalitions first and then the bigger ones but with reduced possibilities. Hence, if $\mathcal{L}$ messages are required per coalition formation proposal, then $\mathcal{L} \times \mathcal{P}$ messages are required until convergence of the algorithm.

Computational Complexity

An equally important factor into the operation of the distributed merge-and-split coalition formation algorithm is the computational complexity involved in the cooperative power allocation. As for the equal power allocation criterion, the calculation of power allocation

at each node is trivial (i.e. with negligible computational complexity) and the main overhead is due to the coalition formation proposals. However, for the sum-of-rates maximizing and max-min rate power allocation criteria, the computational complexity is dependent on the number of nodes in each coalition (which determines the number of variables and constraints). Despite the fact that such problems are convex and can be computed efficiently (i.e. in polynomial-time complexity), doing so repetitively may impose significant overhead and delay to each coalition-head, especially for potentially large coalition sizes. In other words, the computational complexity is likely to increase with the size of the coalition as the complexity of a merge operation can grow significantly with the increase number of candidate nodes in the decoding set of each node. Thus, it takes longer to compute the value/sum-rate of a large coalition compared to a small coalition. However, due to the initial neighbor discovery phase and power costs, most network nodes tend to form coalitions of sizes less than $N/2$ even for dense networks, under the different power allocation criteria (as will be verified in Section 6.9).

6.8 Impact of Mobility on Coalition Formation

It is essential to consider the motion of mobile nodes within a particular deployment area and understand how mobility affects the formed coalitions and the frequency of the coalition formation process. In this work, the mobility of the individual nodes follows the random waypoint (RWP) mobility model [158][159]. When a node moves according the RWP model, the motion involves pausing and staying for a certain period of time in one location. Once this time expires, that node moves to a random destination in the deployment area at a speed uniformly distributed between $[s_{\min}, s_{\max}]$, where $s_{\min}$ and $s_{\max}$ are the minimum and maximum speeds, respectively. This process repeats throughout the network operation time. In turn, each node continuously performs neighbor discovery to determine whether it should merge with other nodes or split from its current coalition and the proposed distributed coalition formation algorithm is executed accordingly.

6.9 Simulation Results

In this section, the simulation results of the proposed distributed coalition formation algorithm with different power allocation criteria are presented and compared with centralized power allocation and coalition formation.

6.9.1 Network Example 1

Consider an ad-hoc network with $N = 10$ nodes in a $40\text{m} \times 40\text{m}$ square area and topology as shown in Fig. 6.2. The path-loss exponent is set to $\nu = 3$, while the correlation coefficient is $\rho = 0.40$. The total power constraint per node is $P = 0.15$ W, while the noise variance is $N_0 = 10^{-5}$ W. The target SNR for information exchange is set to $\gamma = 3$ dB [56].

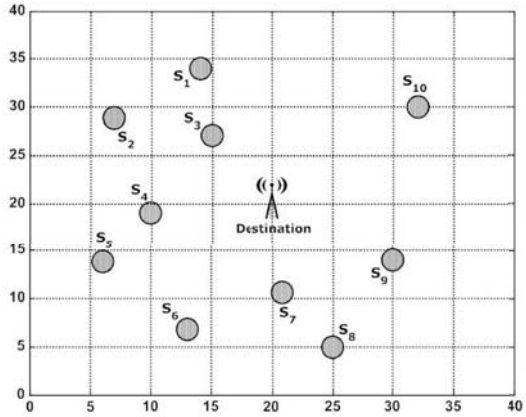

Figure 6.2: Example of Ad-hoc Network with $N = 10$ Nodes

Based on the example network topology shown in Fig. 6.2, each node determines its potential cooperative partners, as summarized in Table 6.3. The proposed distributed coalition formation algorithm under the different power allocation criteria is executed and compared to the centralized power allocation with coalition formation[4] and the results are summarized in Table 6.4. It is evident that the proposed distributed algorithm with SRM-PA criterion results in the highest sum-rate among the other power allocation criteria. The same observation is noted under the centralized power allocation with and without coalition formation.

Table 6.3: Potential Cooperative Partners

Node	S_1	S_2	S_3	S_4	S_5	S_6	S_7	S_8	S_9	S_{10}
S_1	–	✓	✓	✓	✗	✗	✗	✗	✗	✓
S_2	✓	–	✓	✓	✓	✗	✗	✗	✗	✗
S_3	✓	✓	–	✓	✓	✗	✓	✗	✗	✓
S_4	✓	✓	✓	–	✓	✓	✓	✗	✗	✗
S_5	✗	✓	✓	✓	–	✓	✓	✗	✗	✗
S_6	✗	✗	✗	✓	✓	–	✓	✓	✓	✗
S_7	✗	✗	✓	✓	✓	✓	–	✓	✓	✗
S_8	✗	✗	✗	✗	✗	✓	✓	–	✓	✗
S_9	✗	✗	✗	✗	✗	✓	✓	✓	–	✓
S_{10}	✓	✗	✓	✗	✗	✗	✗	✗	✓	–

Fig. 6.3 illustrates the resulting network partition under each power allocation criteria obtained via the proposed distributed algorithm, where it can be seen that SRM-PA criterion results in the smallest number of coalitions and thus the highest number of nodes per coalition. In turn, the SRM-PA criterion promotes altruistic coalition formation with larger coalition sizes than the other two power allocation criteria.

[4]The centralized MINLP power allocation problems are solved using MIDACO [160] with optimization tolerance set to 0.01.

Table 6.4: Sum-Rate Results of Network Example 1

Power Allocation Criteria		Sum-Rate (Bits/s/Hz)
Distributed	EPA	2.8258
	MMR-PA	2.8753
	SRM-PA	2.8884
Centralized	MMR-PA with Coalition Formation	2.8926
	SRM-PA with Coalition Formation	2.9092
	MMR-PA without Coalition Formation	2.9139
	SRM-PA without Coalition Formation	2.9431

The network sum-rates under the centralized MMR-PA and SRM-PA criteria with coalition formation are higher than their distributed counterparts (as seen in Table 6.4). Furthermore, the centralized SRM-PA criteria without coalition formation result in the highest network sum-rates among the other centralized and distributed power allocation criteria. This is because network nodes can cooperate with each other without having to form closed coalitions, as can be seen in Fig. 6.4. In addition, under the SRM-PA criterion, more nodes are cooperating with each other when compared with the MMR-PA criterion, as evident by the number of arcs connecting the nodes.

It should be noted that the obtained results under the centralized algorithms based on MINLP problems (6.26) and (6.27) are suboptimal and may not necessarily be unique. This is due to the fact that such problems are NP-hard and thus determining the optimal sum-rate and network partition is computationally expensive.

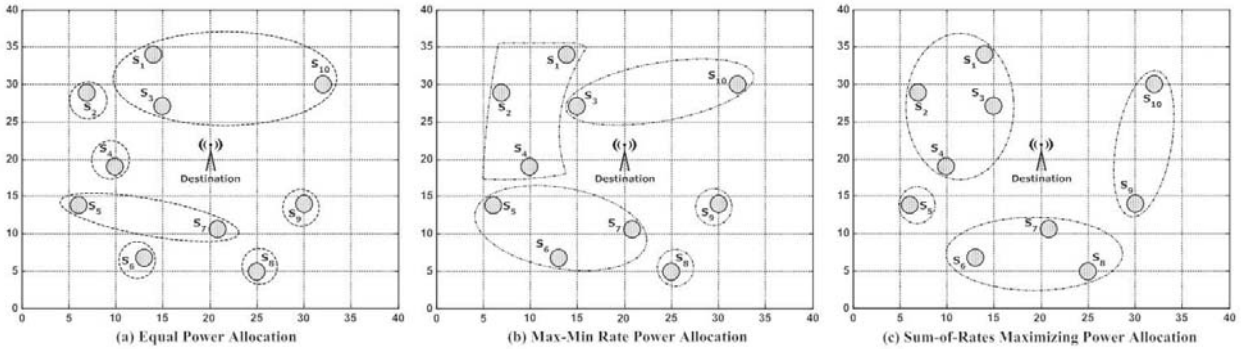

Figure 6.3: Resulting Network Partitions Under Different Power Allocation Obtained via the Proposed Distributed Algorithm

6.9.2 Network Example 2

The following simulations assume a network with $N = 15$ nodes, where the network density varies with the square area of deployment. Also, the simulations assume the same parameters of the previous example and the results are averaged over 10000 independent

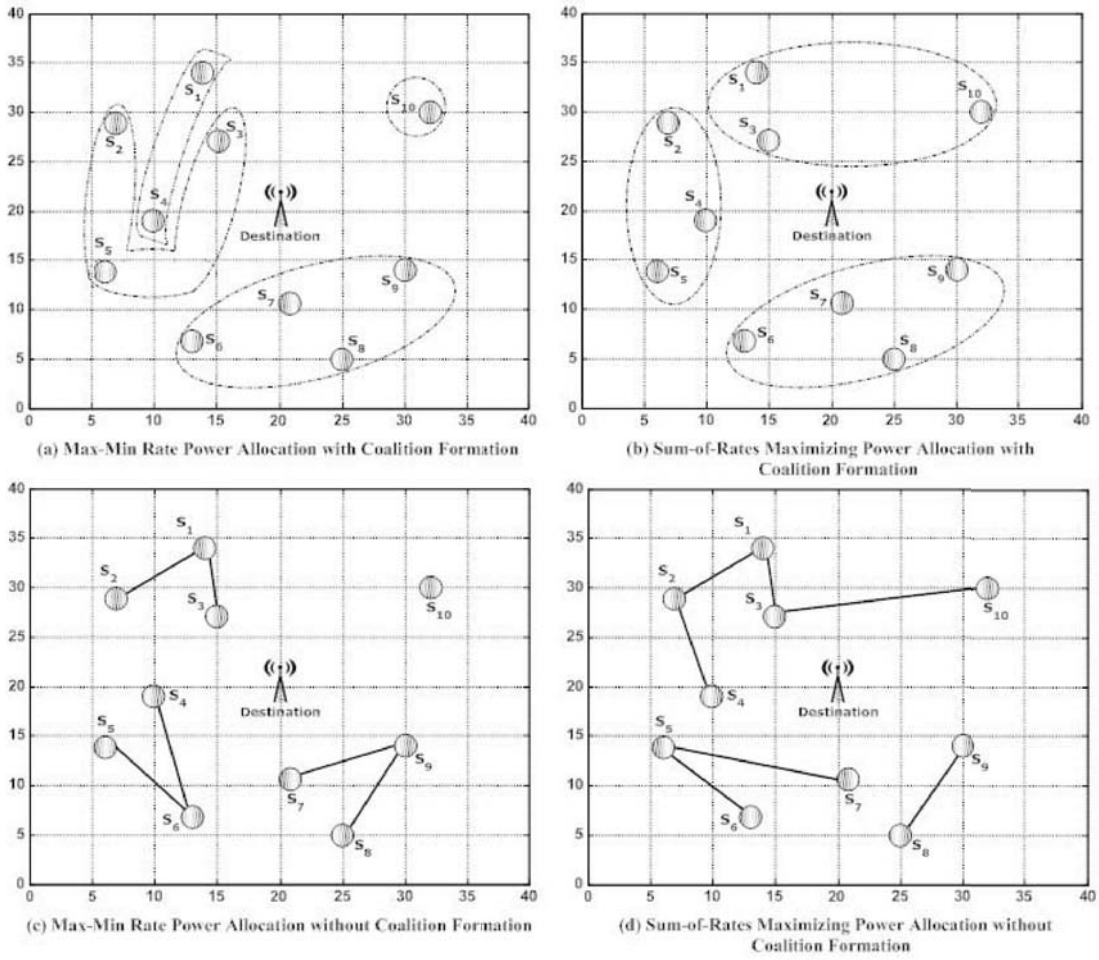

Figure 6.4: Resulting Network Partitions Under Different Power Allocation Obtained via the Centralized Algorithm

runs with the nodes randomly and uniformly distributed across the deployment area for different network densities, while the destination is always located at the center of the area.

It is evident from Fig. 6.5 that as the network density increases, the network sum-rate under the different distributed and centralized power allocation criteria also increases and is superior to that of the direct transmission[5]. This is because with the increase in network density for a fixed number of nodes, the deployment area decreases and the possibility of finding cooperative partners increases. Furthermore, the distributed SRM-PA algorithm achieves the highest sum-rate among the distributed algorithms. Also, the centralized SRM-PA algorithm without coalition formation achieves the highest network sum-rate among all distributed and centralized power allocation criteria. Moreover, the computational complexity of the centralized algorithms for network densities beyond 0.005 nodes/unit square area becomes extremely expensive.

[5]Direct transmission is performed over $N = 15$ time-slots without the cooperation phase.

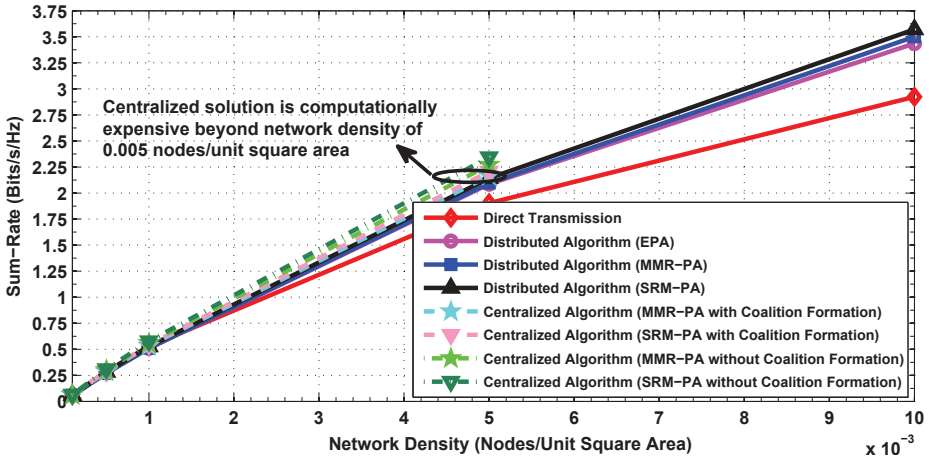

Figure 6.5: Network Sum-Rate of Different Power Allocation Criteria

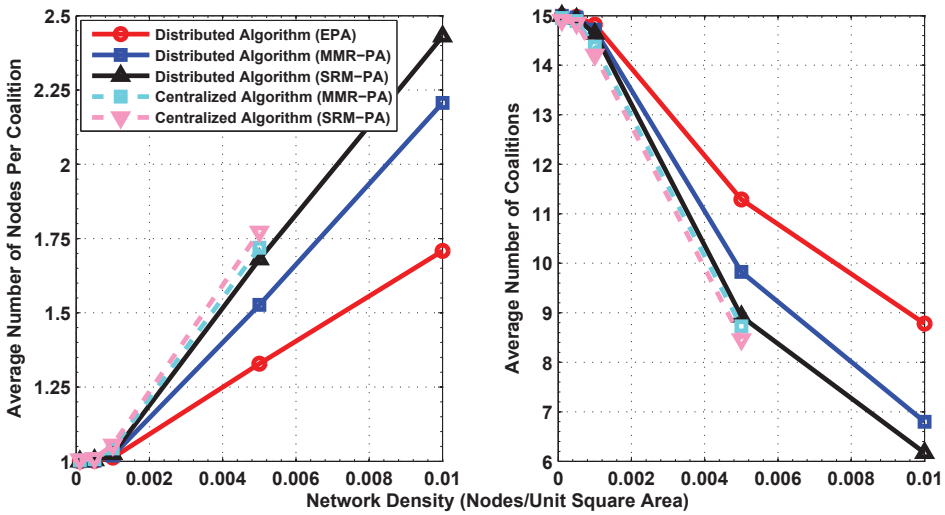

Figure 6.6: Average Number of Nodes Per Coalition and Number of Coalitions of Distributed and Centralized Algorithms

As can be seen from Fig. 6.6, the SRM-PA criterion results in the the highest average number of nodes per coalition. This is due to the altruistic coalition formation and the fact that the SRM-PA criterion yields the highest sum-rate. Hence, network nodes tend to form larger coalitions under the SRM-PA criterion to improve the sum-rate of the coalition, which in turn reduces the average number of coalitions formed.

In Fig. 6.7, the average number of iterations until convergence of the proposed distributed merge-and-split algorithm under the different power allocation criteria is shown. It can be seen that the SRM-PA criterion requires the largest number of iterations and this is because under this criterion, network nodes tend to form larger coalitions. Thus, in the proposed distributed merge-and-split algorithm, larger potential coalitions are formed and

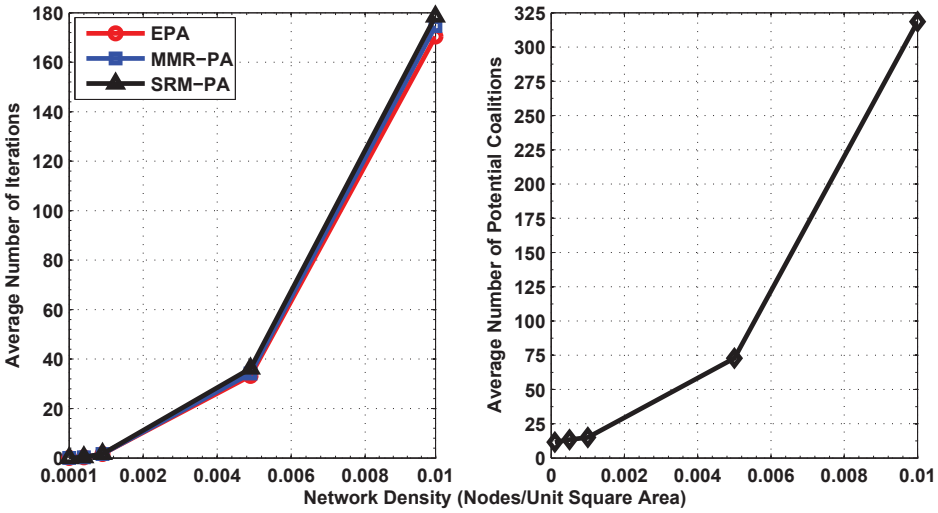

Figure 6.7: Average Number of Iterations and Potential Coalitions

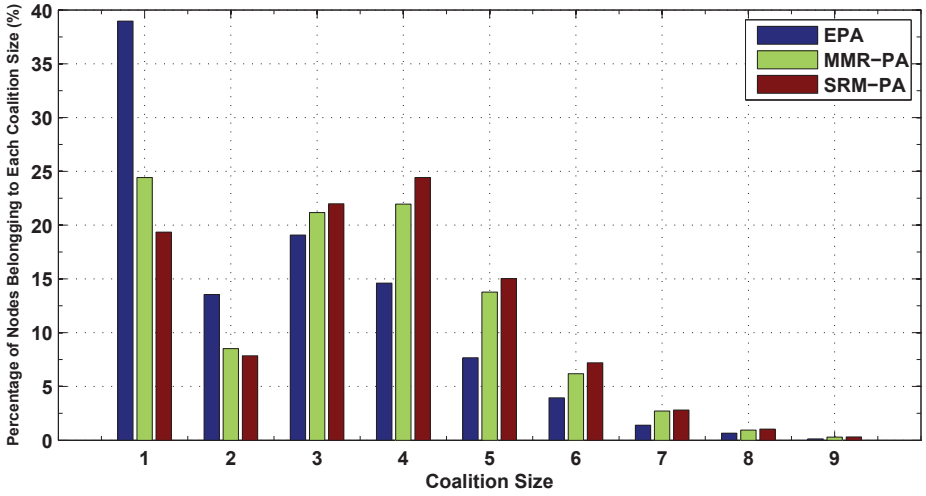

Figure 6.8: Percentage of Nodes Belonging to Each Coalition Size Under the Proposed Distributed Algorithm - Network Density = 0.01 Nodes/Unit Square Area

then possibly split, which in turn increases the number of iterations. Also shown in Fig. 6.7 is the average number of potential coalitions as a function of the network density, which is significantly smaller than $2^{15} - 1$ possible coalitions. This substantial reduction in the average number of potential coalitions is due to the initial neighbor discovery phase.

Based on the histogram shown in Fig. 6.8, it can be seen that a large portion of the nodes are participating in coalitions. Even for the EPA criterion, where singletons are most prevalent, more than half of the nodes are participating in coalitions of at least 2 nodes. As for the MMR-PA and SRM-PA criteria, more than half of the nodes are in coalitions of 3 or more nodes, with the SRM-PA criterion resulting in the largest coalitions.

When considering mobility, $N = 15$ nodes with density of 0.005 nodes/unit square area are assumed, and the network operation is observed over a period of 4 minutes. The pause and motion times of each node under the RWP mobility model are uniformly distributed between $[0, 8]$ s, and $[2, 10]$ s, respectively. Moreover, the speed is uniformly distributed between $s_{\min} = 0.1$ m/s and $s_{\max}$, as illustrated next[6]. As can be seen in Fig. 6.9, the average number of merge-and-split processes per minute increases with the increase in speed, as expected. This is because the higher is the speed, the more frequent are the network topology changes, which in turn triggers coalitions to either merge or split more often. Moreover, the SRM-PA criterion requires the highest average number of merge-and-split processes per minute. This is due to the fact that the SRM-PA criterion results in the highest number of coalitions among the different power allocation criteria and thus there is higher tendency to merge or split coalitions in response to network topology changes.

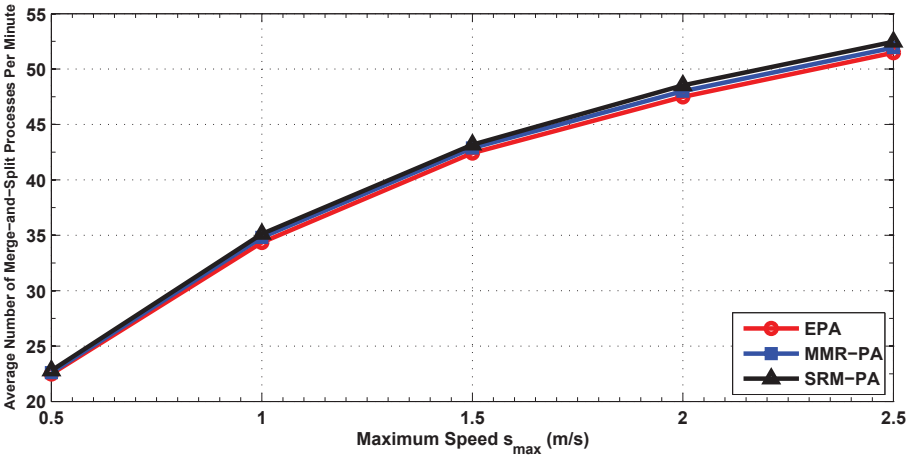

Figure 6.9: Average Number of Merge-and-Split Processes Under the Proposed Distributed Algorithm - Network Density = 0.005 Nodes/Unit Square Area - RWP Mobility Model

Fig. 6.10 illustrates the average number of coalitions and number of nodes per coalition as a function of time under the different power allocation criteria. As can be seen, the initial network structure starts with 15 singleton coalitions after which network nodes merge (or split) into larger (or smaller) coalitions. More importantly, the average number of coalitions and number of nodes per coalition agree with Fig. 6.6 (i.e. for the static network). This demonstrates that the proposed merge-and-split algorithm efficiently adapts to the nodes' mobility and topology changes.

Based on Fig. 6.7, the proposed merge-and-split algorithm converge—for instance—under the EPA criterion in about 170 iterations. To allow the proposed algorithm to converge faster and reduce the communication and computational complexities, especially under mobility, the algorithm time-index can be set to a maximum value of $\tau_{\max}$. Fig. 6.11 shows that by reducing the value of $\tau_{\max}$, the degradation in the sum-rate is insignificant, even for $\tau_{\max} = 50$ (which also reduces the number of nodes per coalition).

[6]It is noteworthy that the mobility of each node is sampled once every second.

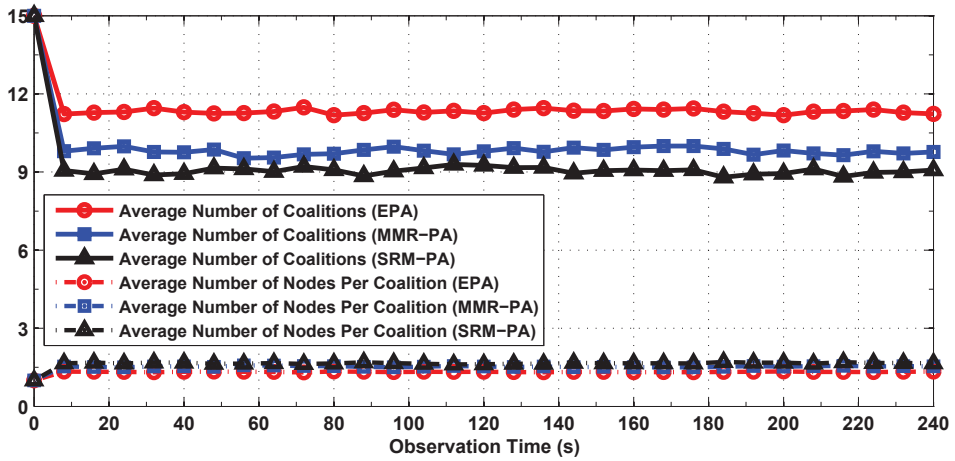

Figure 6.10: Average Number of Coalitions and Number of Nodes Per Coalition Under Proposed Distributed Algorithm - Network Density = 0.005 Nodes/Unit Square Area and Maximum Speed $s_{\max} = 1.5$ m/s - RWP Mobility Model

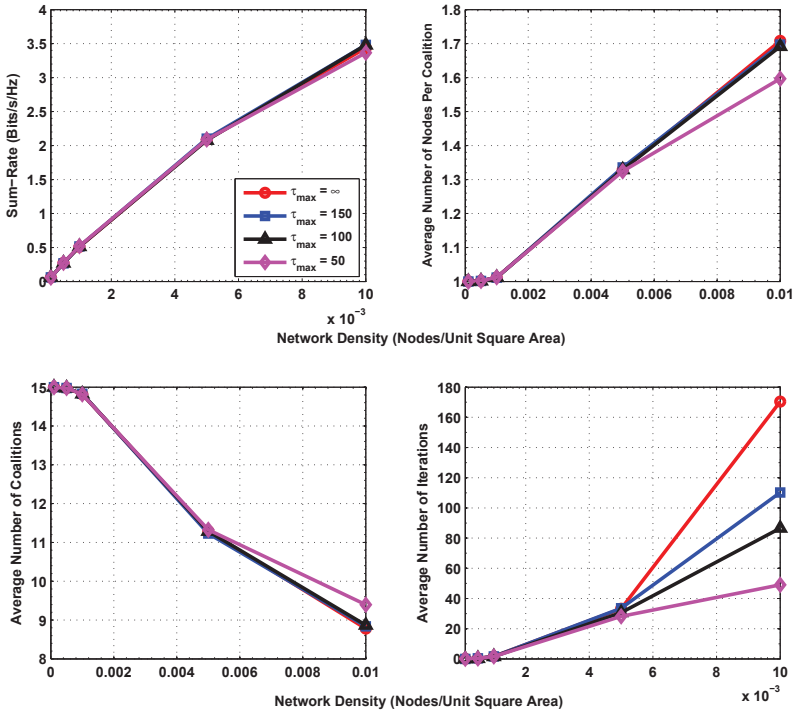

Figure 6.11: Network Sum-Rate and Number of Nodes Per Coalition, Coalitions and Iterations Under the Proposed Distributed Algorithm - EPA Criterion with $\tau_{\max}$

Fig. 6.12 shows the percentage of nodes belonging to each coalition size. Evidently, decreasing the value of $\tau_{\max}$ prevents large coalitions from forming, which increases the percentage of nodes remaining as singletons and decreases the percentage of nodes forming coalitions of larger sizes.

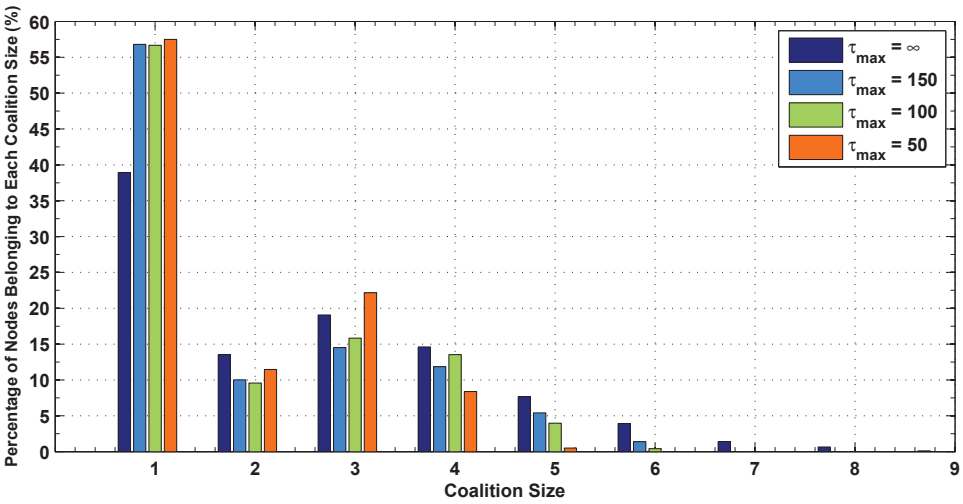

Figure 6.12: Percentage of Nodes Belonging to Each Coalition Size Under the Proposed Distributed Algorithm - EPA Criterion with $\tau_{\max}$ - Network Density = 0.01 Nodes/Unit Square Area

An alternative method to speed up the convergence of the proposed algorithm is to restrict the maximum coalition size to $C_{\max}$, as illustrated in Fig. 6.13. As before, when $C_{\max}$ decreases, the network sum-rate negligibly decreases but the average number of iterations decreases significantly. Finally, Fig. 6.14 demonstrates the percentage of nodes belonging to each coalition size. Clearly, as the value of $C_{\max}$ decreases, more than half of the nodes remain as singletons while the rest of the nodes mostly form coalitions of sizes 2 and 3.

6.10 Conclusions

In this chapter, the problem of altruistic coalition formation in cooperative ad-hoc wireless networks is investigated. In particular, a coalitional game-theoretic framework to the study of distributed altruistic coalition formations to improve the overall network sum-rate is applied. In turn, a distributed merge-and-split algorithm has been designed based on the utilitarian order and evaluated under different cooperative power allocation criteria. It has been shown that the proposed algorithm allows network nodes to self-organize into disjoint coalitions and that the sum-of-rates maximizing power allocation criterion results in the largest average coalition size and number of nodes per coalition, among the different power allocation criteria. Centralized power allocation and coalition formation are also investigated, where it shown that the proposed algorithm achieves a network sum-rate that is comparable with that of a centralized controller; however, with less computational complexity. Finally, the proposed algorithm has been shown to efficiently adapt to nodes' mobility and network topology changes.

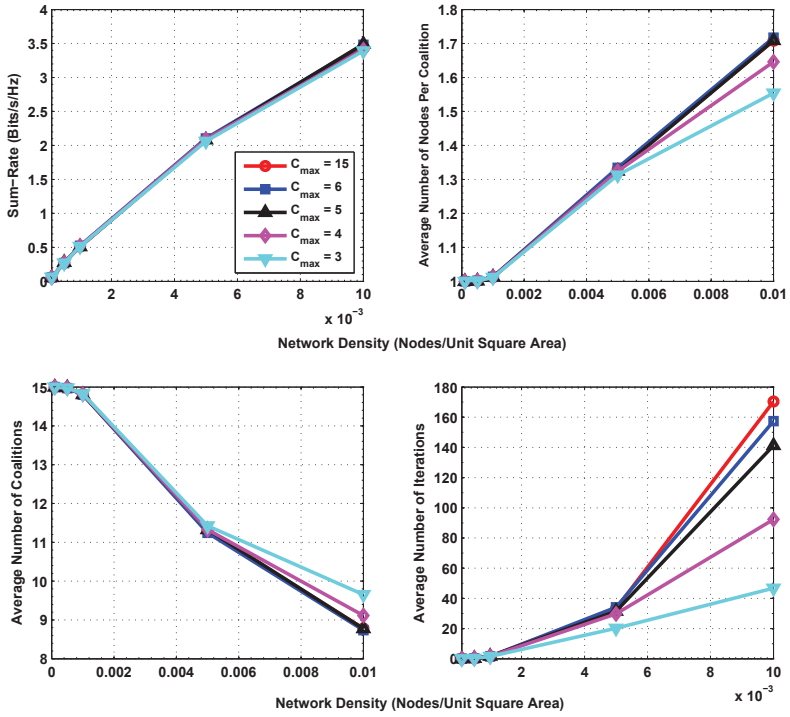

Figure 6.13: Network Sum-Rate and Number of Nodes Per Coalition, Coalitions and Iterations Under the Proposed Distributed Algorithm - EPA Criterion with $C_{\max}$

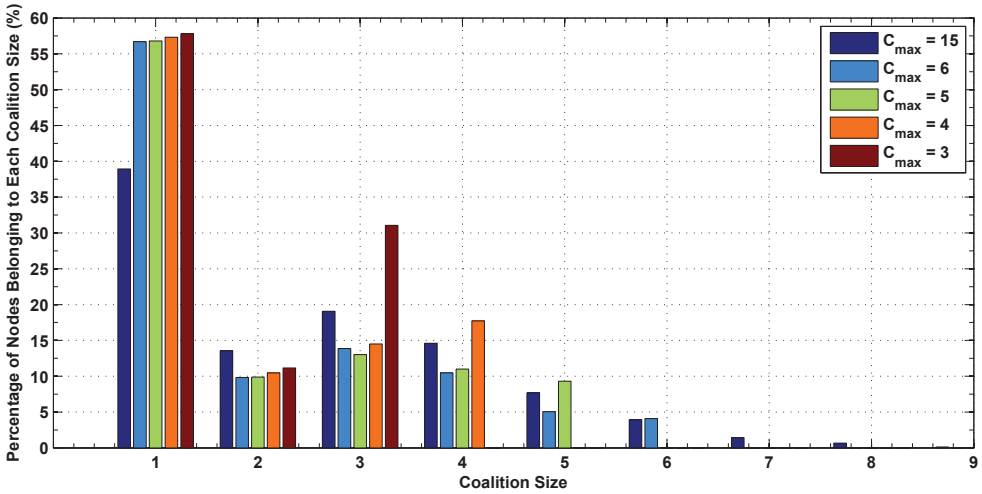

Figure 6.14: Percentage of Nodes Belonging to Each Coalition Size Under the Proposed Distributed Algorithm - EPA Criterion with $C_{\max}$ - Network Density = 0.01 Nodes/Unit Square Area

Chapter 7

Summary, Conclusions and Future Work

7.1 Summary and Conclusions

In this dissertation, the problems of efficient bandwidth utilization and optimal power control in cooperative wireless networks have been studied. In particular, the main focus has been on improving bandwidth utilization in multinode cooperative networks by means of wireless network coding and optimal node selection. As for power control, optimal power allocation has been formulated and computed via a centralized controller or distributively achieved via game-theoretic algorithm designs. More specifically, the research work in this dissertation has addressed the following problems.

In Chapter 2, bi-directional amplify-and-forward relay networks are studied. In the particular, the conventional time-division bi-directional amplify-and-forward (TD-BD-AF) scheme is compared with the multiple-access bi-directional amplify-and-forward (MA-BD-AF) scheme. It is shown that the MA-BD-AF scheme is more bandwidth efficient than the TD-BD-AF scheme; however, it requires stringent timing synchronization between the relay nodes. To further improve network bandwidth efficiency and mitigate the effect of timing synchronization errors, optimal-relay-selection bi-direction amplify-and-forward (ORS-BD-AF) is considered such that the relay that maximizes the sum-of-rates of the source nodes is selected. In addition, the suboptimal-relay-selection bi-directional amplify-and-forward (SRS-BD-AF) scheme the approximately maximizes the sum-of-rates is proposed and shown to be comparable to the ORS-BD-AF scheme and also achieve full diversity. More importantly, the SRS-BD-AF scheme is proven to outperform the TD-BD-AF and MA-BD-AF schemes in terms of the achievable rate, even with timing offsets and thus serves as a potential relaying scheme for bi-directional relay networks.

The multinode amplify-and-forward cooperative communication is studied in Chapter 3 through the novel concept of many-to-many space-time network coding (M2M-STNC).

Such a scheme is shown to allow N network nodes to communicate simultaneously over $2N$ time-slots; however, it requires perfect timing synchronization between the network nodes, which is extremely challenging in practice. In turn, the M2M-STNC with optimal-node-selection (i.e. M2M-STNC-ONS) scheme is proposed to maximize the sum-rate and achieve full diversity order; however, with less stringent timing synchronization requirement than the M2M-STNC scheme and more resistance to channel estimation errors.

Chapter 4 treats the problem of distributed power allocation in single-relay cooperative networks. In particular, the distributed power allocation is formulated as an ascending-clock auction and two algorithms are proposed, namely the conventional ascending-clock auction (C-ACA) and the alternative ascending-clock auction (A-ACA). It was proven that both the C-ACA and A-ACA algorithms converge in a finite number of time-steps and also maximize the social welfare. Furthermore, the A-ACA algorithm is shown to be superior to the C-ACA algorithm as its enforces truthful power demands and thus lends itself to practical implementation in ad-hoc wireless networks.

In Chapter 5, the multi-relay distributed power allocation problem is considered. Specifically, a distributed ascending-clock auction algorithm is proposed for efficient power allocation among multiple source nodes. It has been shown that the proposed algorithm enforces truthful power demands and converges in a finite number of time-steps to the Walrasian equilibrium allocation that maximizes the social welfare. Such an algorithm is demonstrated to yield performance that is closely comparable with that of a network with centralized control.

In Chapter 6, altruistic coalition formation for cooperative relay networks has been investigated. A distributed merge-and-split algorithm based on coalitional game theory has been proposed to allow network nodes to form disjoint independent coalitions. The impact of different cooperative power allocation criteria of coalition formations has also been considered. It has been shown that the sum-of-rates maximizing power allocation results in the largest average coalition size and number of nodes per coalition in comparison with the equal power allocation and the max-min rate power allocation criteria. Centralized power allocation and coalition formation have also been studied. Extensive simulations have shown that the proposed distributed algorithm—when compared with centralized algorithms—offers a good tradeoff between network sum-rate and computational complexity. Finally, the proposed algorithm has been shown to efficiently adapt to network topology changes.

7.2 Main Contributions of the Dissertation

The main contributions of this dissertation are summarized as follows:

- Proposed the SRS-BD-AF scheme which approximately maximizes the sum-of-rates in bi-directional relay networks. The proposed scheme is shown to be equivalent the suboptimal sum-of-rates maximizing power allocation under the multiple-access multi-relay bi-directional relaying scheme.

- Analytically characterized the approximate probability of relay selection as well as the SER performance of the proposed SRS-BD-AF scheme and provided diversity order analysis. Furthermore, the achievable rate of the proposed scheme is shown to be superior to the other bi-directional relaying schemes even with imperfect timing synchronization.

- Proposed the M2M-STNC scheme with optimal node selection (i.e. M2M-STNC-ONS) and analytically demonstrated that the conventional M2M-STNC scheme reduces to the M2M-STNC-ONS scheme under the sum-of-rates maximizing power allocation.

- Analyzed the SER performance of the proposed M2M-STNC-ONS scheme and its diversity order. Moreover, the M2M-STNC-ONS scheme is shown to be more resistant to timing offsets and channel estimation errors than its counterpart M2M-STNC scheme and outperforms it in terms of the SER performance as well as the achievable rate.

- Formulated the single-relay multi-source sum-of-rates maximizing power allocation as an auction game and proposed the C-ACA and A-ACA distributed algorithms. Furthermore, the A-ACA algorithm is proven to enforce truthful power demands and maximize the social welfare.

- Proposed a distributed ascending-clock auction-based algorithm for multi-source multi-relay sum-of-rates maximizing power allocation. Furthermore, the proposed algorithm is proved to converge to the Walrasian equilibrium, maximize the social welfare, enforce truthful power demands and yield good tradeoff between speed of convergence and social welfare.

- Proposed a distributed merge-and-split algorithm for altruistic coalition formation and analyzed the impact of different cooperative power allocation criteria on coalition formations and their stability.

- Formulated centralized max-min and sum-of-rates maximizing power allocation criteria with coalition formations as mixed integer nonlinear programming problems and showed that the proposed distributed merge-and-split algorithm results in good tradeoff between network sum-rate and computational complexity.

7.3 Publications

The following list summarizes the publications resulting from this dissertation:

- Journal papers:

  – **Mohammed W. Baidas** and Allen B. MacKenzie, "Analysis and Modeling of Coalition Formations in Cooperative Wireless Networks", *in preparation for submission to the IEEE Transactions on Wireless Communications.*

  - **Mohammed W. Baidas**, Allen B. MacKenzie and R. Michael Buehrer, "Network-Coded Bi-Directional Relaying for Amplify-and-Forward Cooperative Wireless Networks: A Comparative Study", *in preparation for submission to the IEEE Transactions on Signal Processing.*
  - **Mohammed W. Baidas** and Allen B. MacKenzie, "Many-to-Many Space-Time Network Coding for Amplify-and-Forward Cooperative Networks: Node Selection and Performance Analysis", *in preparation for submission to the IEEE Transactions on Wireless Communications.*
  - **Mohammed W. Baidas** and Allen B. MacKenzie, "An Auction Mechanism for Power Allocation in Multi-Source Multi-Relay Cooperative Wireless Networks", *IEEE Transactions on Wireless Communications*, submitted Sept. 2011, revised Jan. 2012.

- Conference papers:
  - **Mohammed W. Baidas** and Allen B. MacKenzie, "On the Impact of Power Allocation on Coalition Formation in Cooperative Wireless Networks", *in preparation for submission to the IEEE Global Communications Conference (GLOBECOM)*, March. 2012.
  - **Mohammed W. Baidas**, Allen B. MacKenzie and R. Michael Buehrer, "Performance Analysis of Network-Coded Bi-Directional Relaying for Amplify-and-Forward Cooperative Wireless Networks", *submitted to the IEEE 8th International Wireless Communications and Mobile Computing (IWCMC) Conference*, Jan. 2012.
  - **Mohammed W. Baidas** and Allen B. MacKenzie, "Auction-Based Power Allocation for Multi-Source Multi-Relay Cooperative Wireless Networks", *Proc. of IEEE Global Communications Conference (GLOBECOM)*, Dec. 2011.
  - **Mohammed W. Baidas** and Allen B. MacKenzie, "Auction-Based Power Allocation for Many-to-One Cooperative Wireless Networks", *Proc. of IEEE International Wireless Communications and Mobile Computing (IWCMC) Conference*, Jul. 2011.
  - **Mohammed W. Baidas** and Allen B. MacKenzie, "Space-time network coding with optimal node selection for amplify-and-forward cooperative networks", *Proc. of IEEE Consumer Communications and Networking Conference (CCNC)*, Jan. 2011.

7.4 Future Work

The future work based on this dissertation is detailed in the following subsections.

7.4.1 Reinforcement Learning and Cooperation Stimulation in Cooperative Wireless Networks

In ad-hoc wireless networks, users may communicate with each other by direct transmission or by cooperative relaying for each other without requiring centralized control or fixed network infrastructure. Moreover, network users typically do not belong to a single authority and may have different views of resource allocation and sharing. In such scenarios, assuming full cooperative behaviors is unwarranted. Also, users often encounter each other more than once and therefore must be able to adapt to each other's strategies and play optimally so as to maximize their individual utilities.

The future work in this direction considers the following two potential problems.

Reinforcement Learning

Most of the published research focuses on sharing transmission resource while assuming fully unselfish cooperative behavior from all the network users. However, in practical scenarios, network users may have non-stationary behavior that includes cooperation and/or defection. Therefore, the aim is to develop a game-theoretic framework with multinode reinforcement learning (RL) for the analysis of repeated interactions of network users [161]. This entails the design of an adaptive Q-learning RL algorithm that allows each node to interact optimally against a variety of known and unknown opponents and maximize their expected return value [162].

Cooperation Stimulation

Although rational network nodes are selfish by nature, they may be willing to share their resources with other nodes if doing so could indirectly improve their utility. In other words, a node could help relay other nodes' data and build good reputation such that other nodes may help it later. In turn, this incentivize nodes to share their resources and cooperate with each other so as to promote altruism. This requires the design of a reputation policy that takes into account the actions of the network nodes as well as an analysis of equilibrium and steady state conditions.

7.4.2 Node Selection for Energy-Efficient Distributed Detection in Wireless Sensor Networks

One of the key issues in designing wireless sensor networks is energy efficiency at each sensor node, such that the sensor network's lifetime is prolonged. In wireless sensor networks, a set of sensor nodes communicate their measurements to a sink (or equivalently, a fusion center) for data processing and decision-making. However, due to the density of such networks, sensor nodes are likely to capture spatio-temporally correlated measurements that are not necessarily very informative to the sink. In such a case, employing some of the

distributed nodes as relays could improve the reliability of communication and the detection error performance of the network. It has been established that less transmission energy and fewer sensor nodes are required in relay-based wireless sensor networks than in conventional sensor networks, due to the achievable diversity gains [163] [164].

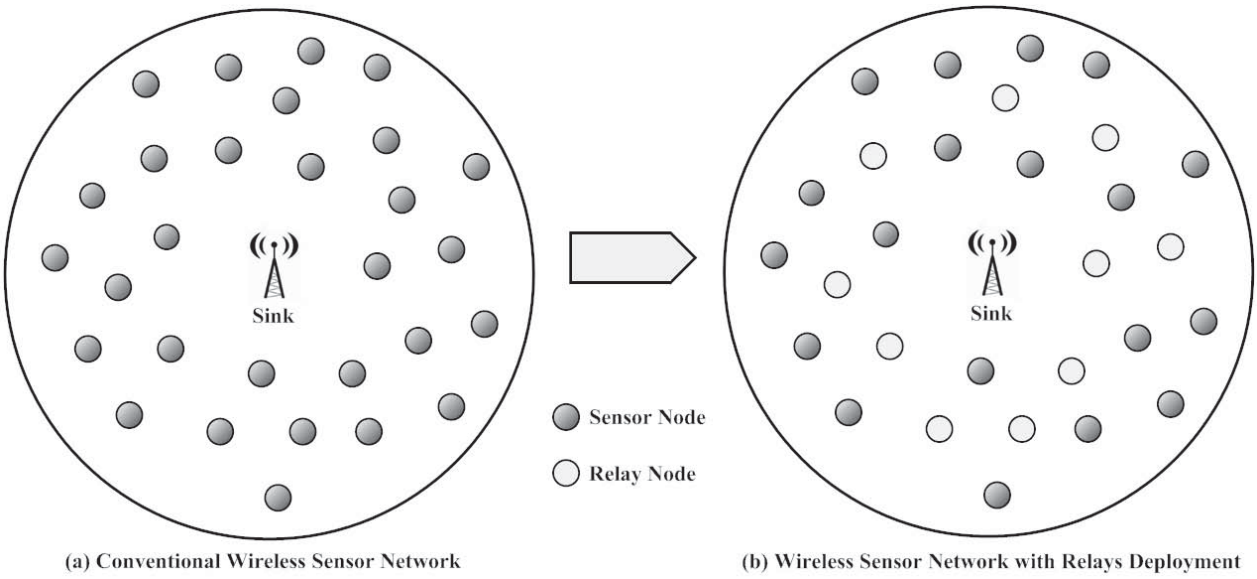

Figure 7.1: A Wireless Sensor Network

The future work in this direction aims at studying relay selection for energy-efficient distributed detection in wireless sensor networks (see Fig. 7.1). Specifically, the study involves formulating a binary hypothesis distributed detection problem and then deriving closed-form expressions for energy utilization per node as a function of the spatio-temporal correlation of the collected measurements, subject to a target probability of false alarm. After that, optimally activating some network nodes as sensors or relays is formulated as an mixed-integer programming (MIP) problem. As sensor networks are characterized by large numbers of deployed nodes, solving an MIP problem may be practically prohibitive as the complexity rises exponentially with the number of nodes. In turn, the design of an algorithm that offers reasonable tradeoff between optimality and complexity is highly desirable and is of ample importance.

Bibliography

[1] E. C. van der Meulen, "Three-terminal communication channels," *Advanced Applied Probability*, 1971.

[2] T. M. Cover and A. A. ElGamal, "Capacity theorems for the relay channel," *IEEE Trans. Information Theory*, vol. 25, no. 9, pp. 572–584, Sept. 1979.

[3] L. Sankaranarayanan, G. Kramer, and N. B. Mandayam, "Capacity theorems for the multiple-access relay channel," *Proc. of 42nd Annual Allerton Conference on Communication, Control and Computing*, Sept. 2004.

[4] C. T. K. Ng and A. J. Goldsmith, "Capacity gain from transmitter and receiver cooperation," *Proc. of IEEE Int. Symp. on Info. Theory (ISIT)*, Sept. 2005.

[5] A. Sendonaris, E. Erkip, and B. Aazhang, "User cooperation diversity, part I: System description," *IEEE Trans. on Comms.*, vol. 51, no. 11, pp. 1927–1938, Nov. 2003.

[6] ——, "User cooperation diversity, part II: Implementation aspects and performance analysis," *IEEE Trans. on Comms.*, vol. 51, no. 11, pp. 1939–1948, Nov. 2003.

[7] J. N. Laneman, D. N. Tse, and G. W. Wornell, "Cooperative diversity in wireless networks: Efficient protocols and outage behavior," *IEEE Trans. on Info. Theory*, vol. 50, pp. 3062–3080, Dec. 2004.

[8] J. N. Laneman and G. W. Wornell, "Distributed space-time coded protocols for exploiting cooperative diversity in wireless networks," *IEEE Trans. on Info. Theory*, vol. 49, no. 10, pp. 2415–2425, Oct. 2003.

[9] K. G. Seddik, A. K. Sadek, A. S. Ibrahim, and K. J. R. Liu, "Design criteria and performance analysis for disributed space-time coding," *IEEE Trans. on Veh. Tech.*, vol. 57, pp. 2280 – 2292, Jul. 2008.

[10] P. A. Anghel, G. Leus, and M. Kaveh, "Multi-user space-time coding in cooperative networks," *Proc. of IEEE International Conference on Acoustics, Speech and Signal Processing (ICASSP)*, vol. 6, pp. IV 73 – IV 76, Apr. 2003.

[11] Y. Jing and B. Hassibi, "Distributed space-time coding in wireless relay networks," *IEEE Trans. on Wireless Comms.*, vol. 5, no. 12, pp. 3524 – 3536, Dec. 2006.

[12] S. Barbarossa, L. Pescosolido, D. Ludovici, L. Barbetta, and G. Scutari, "Cooperative wireless networks based on distributed space-time coding," *Proc. of IEEE International Workshop on Wireless Ad-hoc Networks (IWWAN)*, pp. 30 – 34, Jun. 2004.

[13] W. Su, A. K. Sadek, and K. J. R. Liu, "SER performance analysis and optimum power allocation for decode-and-forward cooperation protocol in wireless networks," *Proc. of IEEE Wireless Communications and Networking Conference (WCNC)*, vol. 2, pp. 984 – 989, Mar. 2005.

[14] ——, "Cooperative communications in wireless networks: Performance analysis and optimum power allocation," *Wireless Personal Communications*, vol. 44, pp. 181–217, Aug. 2008.

[15] N. Yang, M. Elkashlan, and J. Yuan, "Symbol error rate of wireless multiuser relay networks in nakagami-m fading channels," *Proc. of IEEE International Conference on Communications (ICC)*, pp. 1 – 5, May 2010.

[16] P. A. Anghel and M. Kaveh, "Exact symbol error probability of a cooperative network in a Rayleigh-fading environment," *IEEE Trans. on Wireless Comms.*, vol. 3, pp. 1416 – 1421, Sept. 2004.

[17] A. Robeiro, X. Cai, and G. B. Giannakis, "Symbol error probabilities for general cooperative links," *IEEE Trans. on Wireless Comms.*, vol. 52, no. 10, pp. 1820–1830, Oct. 2004.

[18] A. K. Sadek, W. Su, and K. J. R. Liu, "Multi-node cooperative communications in wireless networks," *IEEE Trans. on Signal Processing*, vol. 55, pp. 341–355, Jan 2007.

[19] K. G. Seddik, A. K. Sadek, W. Su, and K. J. R. Liu, "Outage analysis and optimal power allocation for multinode relay networks," *IEEE Signal Processing Letters*, vol. 14, pp. 377–380, Jun. 2007.

[20] A. S. Ibrahim, A. K. Sadek, W. Su, and K. J. R. Liu, "Cooperative communications with relay-selection: When to cooperate and whom to cooperate with?" *IEEE Trans. on Wireless Comms.*, vol. 7, pp. 2814 – 2827, Jul. 2008.

[21] Z. Yi and I.-M. Kim, "Decode-and-forward cooperative networks with relay selection," *Proc. of IEEE 66th Vehicular Technology Conference (VTC)*, pp. 1167 – 1171, Sept. 2007.

[22] M. Torabi, W. Ajib, and D. Haccoun, "Performance analysis of amplify-and-forward cooperative networks with relay selection over rayleigh fading channels," *Proc. of IEEE 69th Vehicular Technology Conference (VTC)*, pp. 1 – 5, Apr. 2009.

[23] W. Su and X. Lin, "On optimum selection relaying protocols in cooperative wireless networks," *IEEE Trans. on Comms.*, vol. 58, pp. 52 – 57, Jan. 2010.

[24] Y. Zhao, R. Adve, and T. J. Lim, "Improving amplify-and-forward relay networks: Optimal power allocation versus selection," *IEEE Trans. on Wireless Comms.*, vol. 6, pp. 3114 – 3123, Aug. 2007.

[25] ——, "Symbol error rate of selection amplify-and-forward relay systems," *IEEE Communications Letters*, vol. 10, pp. 757–759, 2006.

[26] Y. Jing and H. Jafarkhani, "Single and multiple relay selection schemes and their achievable diversity orders," *IEEE Trans. in Wireless Comms.*, vol. 8, pp. 1414 – 1423, Mar. 2009.

[27] ——, "Single and multiple relay selection schemes and their diversity orders," *Proc. of IEEE International Conference on Communcations (ICC)*, vol. 1, pp. 349 – 353, 2008.

[28] V. Havary-Nassab, S. Shahbazpanahi, A. Grami, and Z.-Q. Luo, "Distributed beamforming for relay networks based on second-order statistics of the channel state information," *IEEE Trans. on Signal Processing*, vol. 56, pp. 4306–4316, 2008.

[29] R. Ahlswede, N. Cai, S.-Y. Li, and R. W. Yeung, "Network information flow," *IEEE Trans. on Info. Theory*, vol. 46, pp. 1204 – 1216, Jul. 2000.

[30] S.-Y. Li, R. W. Yeung, and N. Cai, "Linear network coding," *IEEE Trans. on Info. Theory*, vol. 49, pp. 371 – 381, Feb. 2003.

[31] L. Xiao, T. E. Fuja, J. Kliewer, and D. J. Costello, "A network coding approach to cooperative diversity," *IEEE Trans. on Info. Theory*, vol. 53, pp. 3714 – 3722, Jul. 2007.

[32] P. Popovski and H. Yomo, "Wireless network coding by amplify-and-forward for bidirectional traffic flows," *IEEE Communications Letters*, vol. 11, pp. 16 – 18, Jan. 2007.

[33] R. H. Y. Louie, Y. Li, and B. Vucetic, "Practical physical layer network coding for two-way relay channels: performance analysis and comparison," *IEEE Trans. on Wireless Comms.*, vol. 9, pp. 764 – 777, Feb. 2010.

[34] M. Riemensberger, Y. E. Sagduyu, M. L. Honig, and W. Utschick, "Comparison of analog and digital relay methods with network coding for wireless multicast," *Proc. of IEEE International Conference on Communications (ICC)*, May 2010.

[35] K.-S. Hwang, Y.-C. Ko, and M.-S. Alouini, "Performance analysis of two-way amplify and forward relaying with adaptive modulation over multiple relay network," *IEEE Trans. on Comms.*, vol. 59, pp. 402 – 406, Feb. 2011.

[36] Z. Ding, K. K. Leung, D. L. Goeckel, and D. Towsley, "On the study of network coding with diversity," *IEEE Trans. on Wireless Comms.*, vol. 8, pp. 1247 – 1259, Mar. 2009.

[37] H. Q. Lai, A. S. Ibrahim, and K. J. R. Liu, "Wireless network cocast: Location-aware cooperative communications using network coding," *IEEE Trans. on Wireless Comms.*, vol. 8, pp. 3844 – 3854, Jul. 2009.

[38] D. Fudenberg and J. Tirole, *Game Theory.* MIT Press, 1991.

[39] M. J. Osborne and A. Rubinstein, *A Course in Game Theory.* MIT Press, 1994.

[40] L. Lai and H. ElGamal, "On cooperation in energy effient wireless networks: the role of altruistic nodes," *IEEE Trans. on Wireless Comms.*, vol. 7, pp. 1868–1878, May 2008.

[41] Y. Chen and S. Kishore, "A game-threotic analysis of decode-and-forward user cooperation," *IEEE Trans. on Wireless Comms.*, vol. 7, pp. 1941–1951, May 2008.

[42] S.-K. Ng and W. K. G. Seah, "Game-theoretic approach for improving cooperation in wireless multihop networks," *IEEE Transactions on Systems, Man and Cybernetics - Part B: Cybernetics*, vol. 40, no. 3, pp. 559 – 574, Jun. 2010.

[43] V. Srivastava, J. Neel, A. Mackenzie, R. Menon, L. A. Dasilva, J. E. Hicks, J. H. Reed, and R. P. Gilles, "Using game theory to analyze wireless ad hoc networks," *IEEE Comms. Surveys and Tutorials*, vol. 7, pp. 46–56, 2006.

[44] A. B. MacKenzie and S. B. Wicker, "Game theory and the design of self-configuring, adaptive wireless networks," *IEEE Communications Magazine*, vol. 39, no. 11, pp. 126 – 131, Nov. 2001.

[45] G. Owen, *Game Theory, Third Edition.* Academic Press, London, 1995.

[46] G. Tian, "Lecture notes: Auction theory," *Department of Economics: Texas A&M University*, Oct. 2010.

[47] V. Krishna, *Auction Theory.* Academic Press, 2002.

[48] W. Vickrey, "Counterspeculation, auctions and competitive sealed tenders," *Journal of Finance*, vol. 16, no. 1, pp. 8 – 37, Mar. 1961.

[49] L. M. Ausubel, "An efficient ascending-bid auction for multiple objects," *Amer. Econ. Rev.*, vol. 94, pp. 1452–1475, 2004.

[50] P. Cramton, Y. Shoham, and R. Steinberg, *Combinatorial Auctions.* MIT Press, 2006.

[51] W. Saad, Z. Han, M. Debbah, A. Hjrungnes, and T. Basar, "Coalitional game theory for communication networks: A tutorial," *IEEE Signal Processing Magazine, Special Issue on Game Theory*, vol. 26, no. 5, pp. 77 – 97, Sept. 2009.

[52] R. Thrall and W. Lucas, "N-person games in partition function form," *Naval Research Logistics Quartely*, vol. 1, pp. 281–298, 1963.

[53] R. Myerson, "Graphs and cooperation in games," *Mathematics of Operations Research*, vol. 2, pp. 225–229, 1977.

[54] S. Mathur, L. Sankar, and N. B. Mandayam, "Coalitions in cooperative wireless networks," *IEEE Journal of Selected Areas in Comms.*, vol. 26, pp. 1104 – 1115, Sept. 2008.

[55] T. Sandholm, K. Larson, M. Anderson, O. Shehory, and F. Tohme, "Coalition structure generation with worst case guarantees," *Artificial Intelligence*, vol. 10, pp. 209 – 238, Jul. 1999.

[56] K. J. R. Liu, A. K. Sadek, W. Su, and A. Kwasinski, *Cooperative Communications and Networking*. Cambridge University Press, 2008.

[57] D. Tse and P. Viswanath, *Fundamentals of Wireless Communications*. Cambridge University Press, 2005.

[58] M. Engels, *Wireless* OFDM *Systems: How to Make Them Work?* Kluwer International Series in Engineering and Computer Science, 2002.

[59] R. van Nee and R. Prasad, OFDM *for Wireless Multimedia Communications*. Artech House Universal Personal Communications Library, 2000.

[60] O. Ami and M. Uysal, "Optimal bit and power loading for amplify-and-forward cooperative OFDM systems," *IEEE Trans. on Wireless Comms.*, vol. 10, no. 3, pp. 772 – 781, Mar. 2011.

[61] S. Lin and D. J. Costello, *Error Control Coding: Fundamentals and Applications*. Prentice Hall, 1983.

[62] L. H. C. Lee, *Convolutional Coding: Fundamentals and Applications*. Artech House Communications Library, 1997.

[63] A. J. Viterbi, "Error bounds for convolutional codes and an asymptotically optimum decoding algorithm," *IEEE Trans. on Info. Theory*, vol. 13, pp. 260–269, Apr. 1967.

[64] N. Chayat, "Tentative criteria for comparison of modulation methods," *IEEE P802.11-97/96*, Sept. 1997.

[65] P. Popovski and H. Yomo, "Bi-directional amplification of throughput in a wireless multi-hop network," *Proc. of IEEE 63rd Vehicular Technology Conference (VTC)*, vol. 2, pp. 588 – 593, 2006.

[66] M. Feng, X. She, and L. Chen, "Enhanced bidirectional relaying schemes for multi-hop communications," *IEEE Trans. on Veh. Tech.*, pp. 1 – 6, Nov. 2008.

[67] L. Lv, H. Yu, and J. Yang, "Opportunistic cooperative network-coding based on space-time coding for bi-directional traffic flows," *IEEE 4th Workshop on Network Coding, Theory and Applications*, vol. 1, pp. 1–6, 2008.

[68] P. Larsson, N. Johansson, and K.-E. Sunell, "Coded bi-directional relaying," *Proc. of IEEE 63rd Vehicular Technology Conference (VTC)*, vol. 2, pp. 851–855, 2006.

[69] S. J. Kim, N. Devroye, and V. Tarokh, "A class of bi-directional multi-relay protocols," *Proc. of IEEE International Symposium on Information Theory*, pp. 349 – 353, Jul. 2009.

[70] L. Song, Y. Li, A. Huang, B. Jiao, and A. V. Vasilakos, "Differential modulation for bidirectional relaying with analog network coding," *IEEE Trans. on Signal Processing*, vol. 58, pp. 3933 – 3938, Jul. 2010.

[71] Y. Jing, "A relay selection scheme for two-way amplify-and-forward relay networks," *Proc. of International Conference on Wireless Communications and Signal Processing (WCSP)*, pp. 1 – 5, Nov. 2009.

[72] L. Song, G. Hong, B. Jiao, and M. Debbah, "Joint relay selection and analog network coding using differential modulation in two-way relay channels," *IEEE Trans. on Veh. Tech.*, vol. 59, pp. 2932 – 2939, Jul. 2010.

[73] V. Havary-Nassab, S. Shahbazpanahi, and A. Grami, "Optimal distributed beamformig for two-way relay networks," *IEEE Trans. on Signal Processing*, vol. 58, pp. 1238 – 1250, Mar. 2010.

[74] S. Talwar, Y. Jing, and S. Shahbazpanahi, "Joint relay selection and power allocation for two-way relay networks," *IEEE Signal Processing Letters*, vol. 18, pp. 91 – 94, Feb. 2011.

[75] W. Yang, Y. Cai, J. Hu, and W. Yang, "Channel for two-way relay OFDM networks," *EURASIP Journal on Wireless Communications and Networking*, 2010.

[76] M. P. Wilson, K. Narayanan, H. D. Pfister, and A. Sprintson, "Joint physical layer coding and nerwork coding for bidirectional relaying," *IEEE Trans. on Info. Theory*, vol. 56, pp. 5641 – 5654, Nov. 2010.

[77] M. O. Hasna and M. S. Alouini, "End-to-end performance of transmission systems with relays over rayleigh fading channels," *IEEE Trans. on Wireless Comms.*, vol. 2, pp. 1126–1131, Nov. 2003.

[78] L. Song, "Relay selection for two-way relaying with amplify-and-forward protocols," *IEEE Trans. Veh. Tech.*, vol. 60, pp. 1954 – 1959, May 2011.

[79] A. W. Marshall, I. Olkin, and B. Arnold, *Inequalities: Theory of Majorization and Its Applications, 2nd Edition.* Springer Series in Statistics, 2011.

[80] I. S. Gradshteyn and I. M. Ryshik, *Table of Integrals, Series and Products, 7th. Edition.* New York: Academic Press, 2007.

[81] M.-S. Alouini, A. Abdi, and M. Kaveh, "Sum of gamma variates and performance of wireless communication systems over nakagami-fading channels," *IEEE Trans. on Veh. Tech.*, vol. 50, no. 6, pp. 1471 – 1480, Nov. 2001.

[82] M. Sommereder, *Modelling of Queueing Systems with Markov Chains.* Herstellung und Verlag: Books on Demand GmbH, 2011.

[83] M. K. Simon and M. S. Alouini, "A unified approach to the performance analysis of digital communications over generalized fading channels," *Proc. of IEEE*, vol. 86, no. 9, pp. 1860–1877, Sep. 1998.

[84] D. G. Brennan, "Linear diversity combining techniques," *Proc. of IEEE*, vol. 91, no. 2, pp. 331–356, Feb. 2003.

[85] K. T. Phan, L. B. Le, S. A. Vorobyov, and T. L. N. Ngoc, "Power allocation and admission control in multiuser relay networks via convex programming: Centralized and distributed schemes," *EURASIP Journal on Wireless Communications and Networking*, 2009.

[86] S. Schaible and J. Shi, "Fractional programming: the sum-of-ratios case," *Optimization Methods and Software*, vol. 18, no. 2, pp. 219 – 229, 2003.

[87] M. Avriel, W. E. Diewart, S. Schaible, and I. Zang, *Generalized Convexity.* Plenum Press, N. Y., 1988.

[88] M. S. Bazaraa, H. D. Sherali, and C. M. Shetty, *Nonlinear Programming: Theory and Algorithms, 3rd Edition.* Wiley and Sons, 2006.

[89] T. Kuno, "A branch-and-bound algorithm for maximizing the sum of several linear ratios," *Journal of Global Optimization*, vol. 22, pp. 155 – 174, Jan. 2002.

[90] H. P. Benson, "On the global optimization of sums of linear fractional functions over a convex set," *Journal of Optimization Theory and Applications*, vol. 121, no. 1, pp. 19 – 39, Apr. 2004.

[91] R. W. Freund and F. Jarre, "Solving the sum-of-ratios problem by an interior point method," *Journal of Global Optimization*, vol. 19, pp. 83 – 102, 2001.

[92] Y. Almogy and O. Levin, "A class of fractional programming problems," *Operations Research*, vol. 19, no. 1, pp. 57 – 67, Feb. 1971.

[93] B. D. Craven, *Fractional Programming*. Sigma Series in Applied Mathematics 4, Heldermann Verlag, 1988.

[94] S. Boyd and L. Vandenberghe, "Convex optimization," Cambridge University Press 2003.

[95] H. Mehrpouyan and S. D. Blostein, "Estimation, training and effect of timing offsets in distributed cooperative networks," *Proc. of IEEE Global Communications Conference (GLOBECOM)*, vol. 1, pp. 1 – 5, Dec. 2010.

[96] L. Hanzo, L. L. Yang, E. L. Kuan, and K. Yen, *Single and Multi-Carrier DS-CDMA: Multi-User Detection, Space-Time Spreading, Synchronisation, Networking and Standards*. Wiley-IEEE Press, 2003.

[97] H. Ge and Y. Bar-Ness, "Multi-shot approach to multiuser separation and interference separation in asynchronous CDMA," *Wireless Personal Communications*, vol. 12, no. 1, pp. 15 – 26, 2000.

[98] S. Verdu, *Multiuser Detection*. Cambridge University Press, 1998.

[99] K. S. Kim, I. Song, Y. H. Kim, Y. U. Lee, and J. Lee, "Analysis of quasi-ML multiuser detection of DS/CDMA systems in asynchronous channels," *IEEE Trans. on Comms.*, vol. 47, pp. 1875 – 1883, Dec. 1999.

[100] F. Swarts, P. van Rooyan, I. Oppermann, and M. P. Lotter, CDMA *Techniques for Third Generation Mobile Systems*. Kluwer Academic Publishers, 1999.

[101] T. Wang and G. B. Giannakis, "Complex field network coding for multisuer cooperative communications," *IEEE Journal of Selected Areas in Comms.*, vol. 26, pp. 561 – 571, Apr. 2008.

[102] H.-Q. Lai and K. J. R. Liu, "Space-time network coding," *IEEE Transactions on Signal Processing*, vol. 4, pp. 1706 – 1718, Apr. 2011.

[103] M. W. Baidas, H.-Q. Lai, and K. J. R. Liu, "Many-to-many communications via space-time network coding," *Proc. of IEEE Wireless Communcations and Networking Conference (WCNC)*, pp. 1 – 6, Apr. 2010.

[104] L. Venturino, X. Wang, and M. Lops, "Multiuser detection for cooperative networks and performance analysis," *IEEE Trans. on Signal Processing*, vol. 54, pp. 3315 – 3329, Sept. 2006.

[105] S. Wei, "Diversity-multiplexing tradeoff of asynchronous cooperative diversity in wireless networks," *IEEE Trans. on Info. Theory*, vol. 53, pp. 4150 – 4172, Nov. 2007.

[106] H. Adam, C. Bettstetter, and S. Senouci, "Adaptive relay selection in cooperative wireless networks," *Proc. of IEEE Personal, Indoor and Mobile Radio Communications (PIMRC)*, pp. 1–5, Sept. 2008.

[107] P. Gong, P. Xue, D. Park, and D. K. Kim, "Optimum power allocation in a nonorthognoal amplify-and-forward relay-assisted network," *IEEE Trans. on Veh. Tech.*, vol. 60, no. 3, pp. 890 – 900, Mar. 2011.

[108] A. S. Ibrahim and K. J. R. Liu, "Mitigating channel estimation error with timing synchronization tradeoff in cooperative communications," *IEEE Trans. on Signal Processing*, vol. 58, pp. 337 – 348, Jan. 2010.

[109] X. Li, Y.-C. Wu, and E. Serpedin, "Timing synchronization in decode-and-forward cooperative communication systems," *IEEE Trans. on Signal Processing*, vol. 57, pp. 1444 – 1455, Apr. 2009.

[110] S. Jagannathan, H. Aghajan, and A. Goldsmith, "The effect of time synchronization errors on the performance of cooperative miso systems," *Proc. of IEEE Global Communications Conference (GLOBECOM)*, vol. 57, pp. 102 – 107, Apr. 2004.

[111] H. Elders-Boll, H. D. Schotten, and A. Busboom, "Implementation of linear multiuser detectors for asynchronous CDMA system by linear interference cancellation algorithms," *Proc. of IEEE International Conference on Acoustics, Speech and Signal Processing (ICASSP)*, vol. 6, pp. 3225 – 3228, May 1998.

[112] S. Verdu, *Multiuser Detection*. Cambridge University Press, 1998.

[113] C. Sun, W. Zhang, and K. B. Letaief, "Cluster-based cooperative spectrum sensing in cognitive radio systems," *Proc. of IEEE International Conference on Communcations (ICC)*, pp. 2511 – 2515, Jun. 2007.

[114] Z. Zhou, S. Zhou, S. Cui, and J.-H. Cui, "Energy-efficient cooperative communication in a clustered wireless sensor network," *IEEE Trans. on Veh. Tech.*, vol. 57, pp. 3618 – 3628, Nov. 2008.

[115] A. Scaglione, D. Goeckel, and J. N. Laneman, "Cooperative communications in mobile ad-hoc networks: Rethinking the link abstraction," *IEEE Signal Processing Magazine: Special Issue on Signal Processing for Wireless Ad Hoc Communication Networks*, vol. 23, pp. 18–29, Sept. 2006.

[116] B. Wang, Z. Han, and K. J. R. Liu, "Distributed relay selection and power control for multiuser cooperative communication networks using Stackelberg game," *IEEE Transactions on Mobile Computing*, vol. 8, pp. 975–990, Jul. 2009.

[117] J. Huang, Z. Han, M. Chiang, and H. V. Poor, "Auction-based resource allocation for cooperative communications," *IEEE Journal on Selected Areas in Communications, Special Issue on Game Theory*, vol. 26, pp. 1226–1238, 2008.

[118] J. Sun, E. Modiano, and L. Zheng, "Wireless channel allocation using an auction algorithm," *IEEE Journal on Selected Areas in Comms.*, vol. 24, pp. 1085–1096, May 2006.

[119] Z. Han, G.-M. Su, H. Wang, S. Ci, and W. Su, "Auction-based resource allocation for cooperative video transmission protocols over wireless networks," *EURASIP Journal on Advances in Signal Processing*, 2009.

[120] M. W. Baidas and A. B. MacKenzie, "Space-time network coding with optimal node selection for amplify-and-forward cooperative networks," *Proc. of IEEE Consumer Communications and Networking Conference (CCNC)*, pp. 1202 – 1206, Jan. 2011.

[121] Y. Saez, D. Quintana, P. Isasi, and A. Mochon, "Effects of a rationing rule on the ausubel auction: A genetic algorithm implementation," *Computational Intelligence*, vol. 23, pp. 221–235, 2007.

[122] T. Cover and J. Thomas, *Elements of Information Theory.* John Wiley Inc., 1991.

[123] T. K. Forde and L. E. Doyle, "Combinatorial clock auction for OFDMA-based cognitive wireless networks," *Proc. of 3rd International Symposium on Wireless Pervasive Computing (ISWPC)*, pp. 329–333, May 2008.

[124] M. Xiao, N. B. Shroff, and E. K. P. Chong, "A utility-based power-control scheme in wireless cellular systems," *IEEE/ACM Trans. on Networking*, vol. 11, no. 2, pp. 210 – 221, Apr. 2003.

[125] M. Chiang, *Nonconvex Optimization for Communication Systems.* Advances in Mechs. and Maths., Springer, 2006.

[126] Y. Shi, J. Wang, K. B. Letaief, and R. Mallik, "A game-theoretic approach for distributed power control in interference relay channels," *IEEE Transaction on Wireless Communications*, vol. 8, pp. 3151 – 3161, Jun. 2009.

[127] G. Zhang, H. Zhang, L. Zhao, W. Wang, and L. Cong, "Fair resource sharing for cooperative relay networks using Nash bargaining solutions," *IEEE Communications Letters*, vol. 13, pp. 381 – 383, Jun. 2009.

[128] A. Mukherjee and H. M. Kwon, "General auction-theoretic strategies for distributed partner selection in cooperative wireless networks," *IEEE Trans. on Comms.*, vol. 58, pp. 2903 – 2915, Oct. 2010.

[129] L. M. Ausubel, "An efficient dynamic auction for heterogeneous commodities," *Amer. Econ. Rev.*, vol. 96, no. 3, 2000.

[130] P. Milgrom and B. Strulovici, "Substitute goods, auctions and equilibrium," *Journal of Economic Theory*, vol. 144, pp. 212 – 247, Jun. 2008.

[131] H. R. Varian, *Microeconomic Analysis, 3rd Edition.* W. W. Norton and Company, 1992.

[132] F. Gul and E. Stacchetti, "Walrasian equilibrium with gross substitutes," *Journal of Economic Theory*, vol. 87, no. 1, pp. 95 – 124, 1999.

[133] P. Samuelson, *Foundations and Economic Analysis.* Cambridge, MA: Harvard University Press, 1983.

[134] Y. Xie, B. Armbruster, and Y. Ye, "Dynamic spectrum management with the competitive market model," *IEEE Trans. on Signal Processing*, vol. 58, pp. 2442 – 2446, Apr. 2010.

[135] B. Codenotti, B. McCune, and K. Varadarajan, "Market equilibrium via the excess demand function," *Proc. 37th Annual ACM Symposium on Theory of Computing*, pp. 74–83, 2005.

[136] K. J. Arrow, H. D. Block, and L. Hurwics, "On the stability of the competitive equilibrium, II," *Econometrica*, vol. 27, pp. 82–109, 1959.

[137] H. Uzawa, "Walras' tâtonnement in the theory of exchange," *The Review of Economic Studies*, vol. 27, no. 3, pp. 182 – 194, 1960.

[138] A. Feldman, *Welfare economics and social choice theory.* Kluwer Academic Publishers, 1989.

[139] R. Shaffer, S. C. Deller, and D. W. Marcouiller, *Community economics: linking theory and practice, 2nd Edition.* Blackwell Publishing Professional, 2004.

[140] J. P. Sheu, C. M. Chao, W. K. Hu, and C. W. Sun, "A clock synchronization algorithm for multihop wireless ad-hoc networks," *Wireless Personal Communications*, vol. 43, pp. 185 – 200, 2006.

[141] C. H. Rentel and T. Kunz, "Network synchronization in wireless ad-hoc networks," *Carleton University, Technical Report SCE-04-08*, 2004.

[142] Mathworks, "Optimization toolbox: Constrained nonlinear optimization algorithms," Online: http://www.mathworks.com/help/toolbox/optim/ug/brnoxzl.html.

[143] E. Altman, K. Avrachenkov, and A. Garnaev, "Generalized alpha-fair resource allocation in wireless networks," *Proc. IEEE 47th Conference on Decision and Control*, Dec. 2008.

[144] M. Gast, *802.11 Wireless Networks: The Definite Guide.* O'Reilly Media, Apr. 2002.

[145] T. S. Rappaport, *Wireless Communications: Principles and Practice, 2nd Edition.* Prentice Hall, 2002.

[146] H. Manshaei, G. R. Cantieni, C. Barakat, and T. Turletti, "Performance analysis of the IEEE802.11 MAC and physical layer protocol," *Proc. of WoWMoM*, Jun. 2005.

[147] W. Saad, Z. Han, M. Debbah, and A. Hjorungnes, "A distributed coalition formation framework for fair user cooperation in wireless networks," *IEEE Trans. on Wireless Comms*, vol. 8, pp. 4580 – 4593, Sept. 2009.

[148] Z. Han and H. V. Poor, "Coalition games with cooperative transmission: A cure for the curse of boundary nodes in selfish packet-forwarding wireless networks," *IEEE Trans. on Comms.*, vol. 57, pp. 203 – 213, Jan. 2009.

[149] R. K. Guha, C. A. Sarkar, C. Singh, and A. Kumar, "Fair coalitions for power-aware routing in wireless networks," *IEEE Trans. on Mobile Computing*, vol. 6, pp. 206 – 220, Feb. 2007.

[150] A. Mukherjee and H. M. Kwon, "A coalition game framework for decode-and-forward relay networks," *Proc. of IEEE 70th Vehicular Technology Conference (VTC)*, pp. 1 – 5, Sept. 2009.

[151] H. Lai, Y. Chen, and K. J. R. Liu, "Coalition formation games for energy efficient wireless network cocast," *To appear, Proc. of IEEE Military Communications Conference (MILCOM)*, Nov. 2011.

[152] J. Luo, R. S. Blum, L. J. Cimini, L. J. Greenstein, and A. M. Haimovich, "Decode-and-forward cooperative diversity with power allocation in wireless networks," *IEEE Trans. on Wireless Comms.*, vol. 6, no. 3, pp. 793 – 799, Mar. 2007.

[153] K. Apt and A. Witzel, "A generic approach to coalition formation (extended version)," *Int. Game Theory Rev.*, vol. 11, no. 3, pp. 347 – 367, Mar. 2009.

[154] G. J. Woeginger, "Exact algorithms for NP-hard problems: A survey," *Combinatorial Optimization*, vol. 2570, pp. 185 – 207, 2003.

[155] P. Bonami, M. Kilinc, and J. Linderoth, "Algorithms and software for convex mixed integer nonlinear programs," *Technical Report # 1664, Computer Sciences Department, University of Wisconsin-Madison*, 2009.

[156] I. Nowak, *Relaxation and Decomposition Methods for Mixed Integer Nonlinear Programming.* Springer Scienece and Business Media - Birkhauser Verlag, Basel, 2005.

[157] K. Apt and T. Radzik, "Stable partitions in coalitional games," 2006, Online: http://arxiv.org/abs/cs.GT/0605132.

[158] D. Johnson and D. Maltz, *Dynamic Source Routing in Ad-Hoc Wireless Networks.* In T. Imelinsky and H. Korth, Editors - Mobile Computing, 1996.

[159] T. Camp, J. Boleng, and V. Davies, "A survey of mobility models for ad-hoc network research," *Proc. of Wireless Communications and Mobile Computing: Special Issue on Mobile Ad Hoc Networking: Research Trends and Applications*, vol. 2, no. 5, pp. 483 – 502, 2002.

[160] M. Schluter, M. Gerdts, and J. J. Ruckmann, "MIDACO: New global optimization software for MINLP," 2011, Online: http://http://www.midaco-solver.com/download_files/MIDACO_Paper.pdf.

[161] R. E. Bellman, *Dynamic Programming*. Princeton University Press, 1957.

[162] D. Bertsekas, *Dynamic Programming and Optimal Control*. Athena Scientific, 1995.

[163] M. W. Baidas, A. S. Ibrahim, K. G. Seddik, and K. J. R. Liu, "On the impact of correlation on distributed detection in wireless sensor networks with relays deployment," *Proc. IEEE International Conference on Communications (ICC)*, pp. 1 – 6, Jun. 2009.

[164] M. W. Baidas, A. A. ElSherif, and K. J. R. Liu, "Energy efficiency of cognitive cooperative distributed detection in wireless sensor networks," *Proc. of IEEE Wireless Communications and Networking Conference*, Apr. 2010.